Mathematical modelling for hybrid and nanoparticle imaging

Pierre Millien

Thèse de doctorat

En vue de l'obtention du grade de

Docteur
de l'École Normale Supérieure

École doctorale 386 de sciences mathématiques de Paris-Centre

Spécialité : Mathématiques Appliquées

Mathematical modelling for hybrid and nanoparticle imaging

Présentée et soutenue par:
Pierre Millien

Le 5 juin 2015 devant le jury composé de:

M. Habib AMMARI	*Directeur de thèse*
M. Josselin GARNIER	*Co-directeur de thèse*
M. Simon ARRIDGE	*Rapporteur*
M. Martin BURGER	*Rapporteur*
M. Matti LASSAS	*Rapporteur*
Mme Virginie BONNAILLIE-NOËL	*Examinatrice*
M. Stéphane MALLAT	*Examinateur*
M. Hoài-Minh NGUYÊN	*Examinateur*

À mes grand-parents: Marie-Juliette, Suzanne et Maurice.

Remerciements

J'ai la chance d'être extrêmement bien entouré et il est évident que l'aide et les encouragements que j'ai pu recevoir ont été absolument déterminants pour moi durant ces trois années. Je tiens à remercier ici mes collègues et mes proches qui m'ont accompagné durant ma thèse.

Mes premiers remerciements vont évidement à Habib Ammari qui m'a encadré durant ces trois ans de thèse. Sa disponibilité, sa gentillesse, ses encouragements et son sixième sens pour trouver des problèmes intéressants à résoudre m'ont permis de passer trois années formidables au DMA. Je tiens à le remercier de m'avoir permis de présenter nos résultats dans différentes conférences. J'espère que ces travaux ne sont que le début de notre collaboration. Cette thèse a été co-encadrée par Josselin Garnier, que je remercie pour tous ses conseils avisés et ses relectures attentives. C'est une grande chance d'avoir pu travailler avec quelqu'un d'aussi perspicace et rigoureux.

Je suis très heureux de pouvoir présenter ces résultats devant un jury si prestigieux. Je tiens donc à remercier chaleureusement Simon Arridge, Martin Burger et Matti Lassas d'avoir accepté de rapporter ce manuscrit, ainsi que Virginie Bonnaillie-Noël, Stéphane Mallat et Hoài-Minh Nguyen de faire partie de ce jury. Durant ces trois années, j'ai eu l'occasion de travailler avec Pol Grasland-Mongrain, Elie Bretin, Jin Keun Seo et Yojun Deng, qui ont co-signé les publications dont sont issus les chapitres de cette thèse. Je les remercie vivement pour toutes leurs bonnes idées sans lesquelles ces articles n'auraient pas la même portée. J'ai eu le plaisir de rencontrer de nombreux chercheurs, aussi bien en conférence qu'au DMA. Je voudrais ainsi remercier Claude

Boccara, Eric Bonnetier, Emmanuel Bossy, Charlie Demene, Amir Nahas et Faouzi Triki pour les échanges et discussions que nous avons pu avoir. Je tiens également à remercier Hyeonbae Kang pour l'accueil chaleureux en Corée, ainsi que William Lionheart et Kim Knudsen pour les invitations à venir exposer mes travaux. Il est difficile d'écrire une thèse de mathématiques sans une formation mathématique et je souhaiterais notamment remercier les professeurs qui m'ont donné envie de continuer dans cette voie, notement Mme Murat au lycée Condorcet, Arnaud Debussche, Michel Pierre, Gregory Vial à Ker Lann, et Nassif Ghoussoub à l'université de Colombie Britannique.

Le DMA est une petite structure et j'ai passé d'agréables moments en compagnie des autres doctorants. Merci à Cécile, Yannick, Quentin, Valentine, Ilaria pour les sympathiques pauses café. Je tiens aussi à remercier Bénédicte Auffray et Lara Morise pour leur bonne humeur et leur efficacité. J'ai une pensée particulièrement reconnaissante pour Zaina Elmir qui m'a énormément apporté aussi bien par sa connaissance du département que par sa compagnie et son écoute attentive. Enfin, je voudrais remercier les membres de l'équipe d'imagerie, Thomas, Han, Giovanni, Alden, Hai, Matias, Timothee, Wenlong pour les bons moments au quotidien et l'entraide scientifique. Je tiens à souligner le rôle que Laure et Laurent ont joué. Laure a été pour moi un soutien moral dont je n'aurais absolument pas pu me passer. Son humour, sa sagesse et son empathie ont rendu mes journées plus courtes. Enfin je ne peux qu'exprimer ma gratitude envers Laurent, qui était déjà mon acolyte en Bretagne. C'est grâce à lui que j'ai pu rencontrer Habib, et co-signer un article avec lui (le chapitre 1 du manuscrit) a été un vrai plaisir. Je tiens aussi à remercier Pierre et Annabelle que je côtoie depuis Rennes et dont l'enthousiasme et la gentillesse sont restés constants. Je ne peux évidement pas parler de Ker-Lann sans mentionner Xavier, dont la joie de vivre et le soutien infaillible me sont irremplaçables.

J'ai aussi des amis qui ont eu la présence d'esprit de ne pas s'engouffrer dans les mathématiques et je tiens à les remercier pour tous les moments de détente et leur indulgence envers mes mauvais pas de danse. Je pense notamment à Zara, Nicolas, Fayçal, Souhail, Guillaume, Thibaud, Florian, Arianne, Vincent, François, et les copains de Bastion. Un grand merci en particulier à Matthieu qui m'éclaire de sa sagesse quasi infinie (avant une heure du matin du moins), et m'inspire depuis de nombreuses années.

Je souhaiterais terminer en exprimant ma gratitude envers ma famille. À commencer par remercier Adriana, Marius, Livia et Matei qui m'ont accueilli depuis quelques années maintenant et ont su se rendre indispensables aussi bien par leur bonne humeur que leur soutien. Je pense aussi à François qui me rend un peu moins bête à chacune de

nos conversations, et à Julien qui par sa gentillesse et sa présence d'esprit est un modèle pour moi. Évidement je n'aurais jamais pu arriver ici sans les encouragements de mes parents, Anne et Jean-Claude. Merci de votre patience et de votre enthousiasme pour mes projets, même s'ils finissaient souvent avec une paire de béquilles et un abonnement chez le kiné. Les mots me manquent un peu pour remercier mon frère Thibault, grande source de rigolade et d'inspiration, "food for the soul". Enfin, je tiens à remercier Sînziana de tout mon cœur. C'est elle qui me donne une bonne raison de me lever tous les matins: lui apporter un café. Merci Sînziana, tu es la meilleure et j'espère rester ton réveil matin encore longtemps.

Contents

Introduction

This thesis aims at developing mathematical models and image reconstruction algorithms for imaging problems, particularly medical imaging problems. Medical imaging consists in mapping in-vivo some physical parameter p inside the body. The goal is to gain information on the internal structure and pathological state of an organ without using a surgical procedure. Most imaging procedures consist in probing a medium with some wave that will interact with the parameter of interest p, and then measuring the transmitted and reflected wave. The measurements are then analyzed and one needs to solve an inverse problem to gain information on p. The criterion of choice for p is contrast : it needs to offer contrast between tissue type to see the internal structure of the organ, and between pathological states to be able to detect a problem. The information we can hope to recover on p is determined by the type of wave used and by the mathematical nature of the inverse problem.

Table 1 Some physical parameters used in medical imaging, and the type of wave they interact with.

Physical parameter	Contrast in soft tissues	Type of wave
Acoustic impedance	Bad	High frequency sound waves
Density	Bad	X-rays
Electrical conductivity	Good	Electrical current
Shear modulus	Good	Low frequency elastic waves
Optical absorption	Good	Infrared light

The frequency also affects the resolution of the image because of the diffraction limit: one cannot hope to recover details that are smaller than half the wavelength of the probing wave. Waves can behave very differently depending on their type (acoustic, electromagnetic) and their frequency. As an example high frequency electromagnetic waves (like X-rays) propagate in a straight line and penetrate deeply whereas near infrared or visible light exhibit strong scattering and a lower penetration depth. Therefore the experimental apparatus and the parts of the body we can hope to image are

Table 2 Some medical imaging techniques

Imaging technique	Type of Wave	Resolution	Cost (€)	Side effects
Echography	High frequency sound waves	$\sim 0.5cm$	~ 10000	None
CT-scan	X-rays	$\sim 1mm$	~ 150000	Radiation exposition
Electrical impedance tomography	Electrical current	$\sim 1cm$	~ 10000	None

going to be totally different depending on the choice of the method. Table 1 gives a non-exhaustive list of parameters of clinical interest and the type of waves they interact with, while table 2 gives example of medical imaging techniques currently used by physicians.

It is then very easy to understand why the perfect imaging device does not exist : the parameters that are clinically the most interesting often affect low-frequency or highly scattering waves difficult to control, and the inverse problem associated to the image reconstruction are ill-posed.

To overcome the limitations of medical imaging, three different issues need to be addressed:

1. Improve the engineering of the transmitters, sensors
2. Image clinically interesting parameters like conductivity or shear modulus with high resolution
3. Improve the clinical interest of the parameters that interact with high frequency waves

Some of the limitations of medical imaging techniques can be fixed with technical improvements. A weak signal to noise ratio can be dealt with by using better sensors, and general technological improvements might drive the cost of the device down. Figure 0.0.1 shows an ultrasound image from 1965 and an image obtained with one of the latest ultrasound machine. Significant improvement can be made by engineering.

In this thesis we adress problems related to the other two issues.

To try to image parameters such as conductivity or shear modulus with a high resolution, one must find a coupling between some high frequency wave and the low frequency wave that is sensible to the parameter. This is called hybrid imaging.

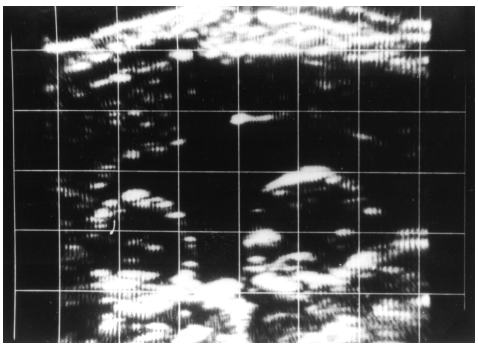

Figure 0.0.1 Twins in mother's womb, Figure 0.0.2 17 week old fetus, obtained obtained with Siemens' Vidoson, 1965 with Siemens' $S300$, 2014.

There are numerous hybrid imaging techniques such as magnetic resonnance electrical impedance tomography [126], opto-acoustic tomography [113]... Some of them are already used by physicians, as SuperSonic imagine's Aixplorer ultrasound device, which allows the mapping of the shear modulus by filming the propagation of a shear wave through the body with an ultra fast ultrasound device that captures around 1000 image per second [38]. The fact that shear waves propagate slowly becomes an advantage when coupled with high frequency sound waves. As hybrid imaging uses the interaction between different physical phenomenons the link between the measured signal and the parameter p might be complicated to quantify, and thus a precise physical and mathematical modeling is needed if one wants to quantitatively reconstruct the parameter. In the first part of this thesis we give a mathematical and numerical framework for three different hybrid techniques:

- Lorentz force imaging, a technique allowing conductivity imaging at ultrasound resolution by creating an electrical current using ultrasound pulse in a strong constant magnetic field.
- Magneto-acoustic tomography with magnetic induction, which exploits the same coupling as Lorentz force imaging, but the other way around : a time varying magnetic field is used to create an acoustic wave which can be measured, allowing for a reconstruction of the conductivity map.
- Optical coherent tomography elastography, which is a high resolution optical image of a sample is made before and after a mechanical perturbation, allowing to reconstruct the shear modulus inside the sample at a micro meter resolution.

Other emerging hybrid techniques for conductivity imaging have also been reported in [4, 6, 8, 12, 60, 122, 125, 126, 135].

The third approach to improve the specificity of imaging devices is to artificially improve the contrast between healthy and unhealthy tissue. This is particularly interesting in the context of cancer detection, when one wants to know weather there is a tumor, where it is, how big it is, without necessarily needing a full detailed image of the rest of the medium. This idea is already used in scintigraphy, where a radioactive agent agglomerates in tumors and emits radiations. Tracking the origin of the radiation allows for a tracking of the tumor. However scintigraphy yields a very poor resolution (see figure 0.0.3 for an example) and the use of radioactive material inside the human body is not the best option.

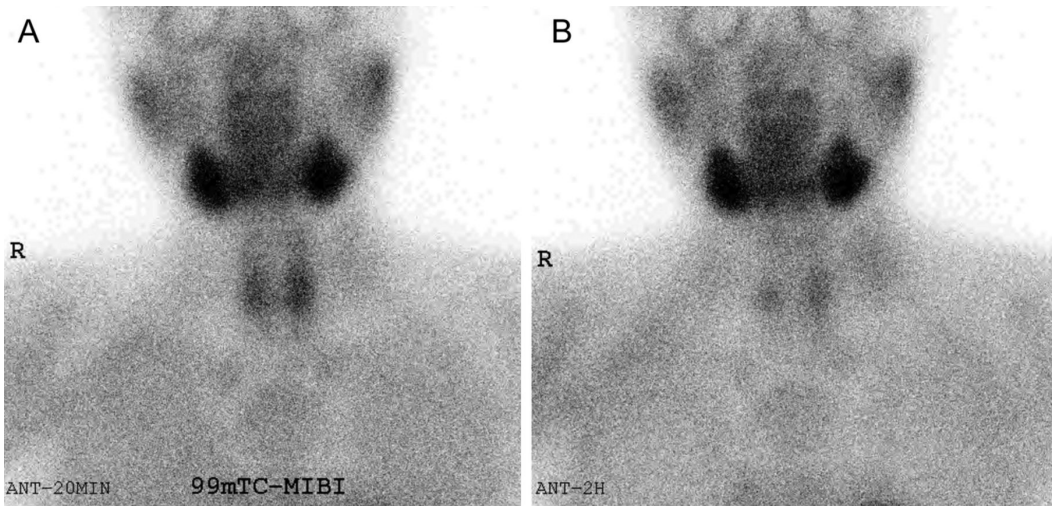

Figure 0.0.3 Scintigraphic image of the thyroid, 20 min and 2 hours after injection of the radioactive agent [81]. Images obtained by this method are not very detailed.

It has been shown that nanoparticles (particles whose size is between $1 \cdot 10^{-9}m$ and $100 \cdot 10^{-9}m$) will agglomerate in cancerous tissues [112] via a passive mechanism: the enhanced permeability and retention effect [90]. This is essentialy due to the fact that tumor tissue has a leaky vasculature, as shown on figure 0.0.4. Due to their small size, metallic nanoparticles interact with light differently from the bulk material they are made of. This is mainly due to the fact that there are a comparable number of atoms on the surface of the particle and inside the particle (the bulk), hence giving rise to "surface effects".

One of the most interesting properties of metallic nanoparticles is surface plasmon resonance. When exited at a specific frequency, some metallic nanoparticles exhibit strong absorption and scattering resulting from a local enhancement of the electric

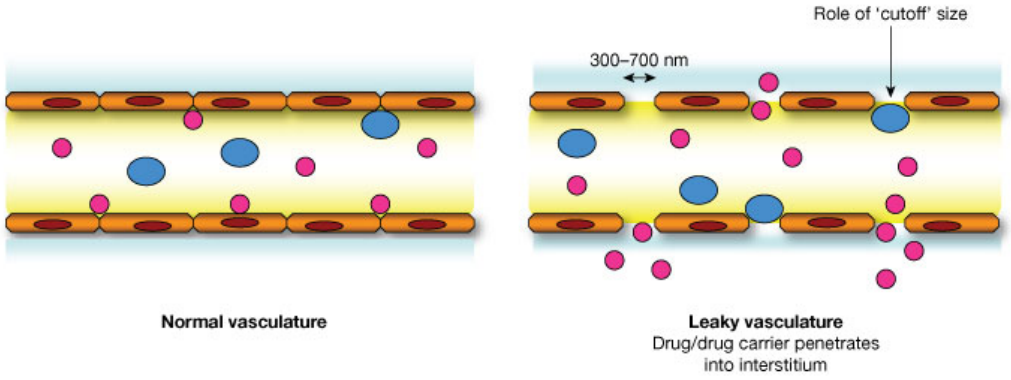

Figure 0.0.4 Enhanced permeability and retention effect in cancerous tissue [84]

field. The strong scattering allows the use of nanoparticles as contrast agents; and the absorption of light induces a raise in temperature around the nanoparticle. This raise is high enough to burn the surrounding tissues making them a potential therapeutic tool [112]. Theoretical explanations of surface plasmons resonance have been given in the case of a spherical nanoparticle within the quasi-static approximation, but the phenomenon is not well understood yet, and the only way to compute plasmon frequency for a given particle shape is to solve the full $3D$ Maxwell equation system. An exact understanding of these resonances is crucial in applications, as the increase of temperature around the particle is very hard to measure and has to be monitored precisely in order to burn only the unhealthy tissues and prevent the apparition of air bubbles in the blood. In this thesis we give a general definition of plasmon resonance as an eigenvalue problem and justify rigorously the quasi-static expression for surface plasmon from the full Maxwell equations for any particle with a C^1 shape, allowing a computation of a first order approximation of the plasmon frequency without solving the full $3D$ Maxwell system.

Nanoparticles also exhibit non linear optical behavior in the presence of strong oscillating fields, such as second harmonic generation, which is the coherent emission of a field oscillating at twice the frequency of the background field. Due to the coherent nature of the second harmonic signal, it is possible to use interferometric imaging techniques, such as holography to locate the particle. As most biological tissues do not produce a second harmonic signal, second harmonic imaging produces a precise image

of the nanoparticle, free from any scattering from the surrounding medium, contrarily to the fundamental frequency image where the signal measured is produced by both the particle and the medium. In the second chapter we show how one can use the nanoparticle as a probe and locate the nanoparticle in a strongly scattering medium using a back propagation algorithm (usually very sensitive to medium noise). We give an asymptotic formula for the second harmonic field and perform a statistical analysis, giving explicit expressions for the signal to noise ratio of the image obtained.

The results of chapter 1, 2, 3 are from [24] [9], and [11] respectively. The results of chapter 4 and 5 are from [15] and [22] respectively.

Part I

Hybrid methods in medical imaging

Chapter 1

Magneto-acoustic coupling : Lorentz force imaging

Contents

1.1 Introduction

In this chapter we provide a mathematical and numerical framework for Lorentz force imaging. This hybrid technique aims at combining ultrasonic imaging and conductivity imaging.

Ultrasonic imaging is currently used in a wide range of medical diagnostic applications. Its high spatial resolution, combined with a real-time imaging capability, lack of side effects, and relatively low cost makes it an attractive technique. However, it can be difficult to differentiate between soft tissues because acoustic impedance varies by less than 10% among muscle, fat, and blood [64]. In contrast, electrical conductivity varies widely among soft tissue types and pathological states [58, 106] and its measurement can provide information about the physiological and pathological condition of tissue [17]. Several techniques have been developed to map electrical conductivity. The most well known is electrical impedance tomography, in which electrodes are placed around the organ of interest, a voltage difference is applied, and the conductivity distribution can be reconstructed from the measurement of the induced current at the electrodes [6, 28, 47]. This technique is harmless to the patient if low currents are used. However, the ill-posed character of the inverse problem results in a lower spatial resolution than that achieved by ultrasound imaging, and any speckle information is lost.

The Lorentz force plays a key role in acousto-magnetic tomographic techniques [119]. Several approaches have been developed with the aim of providing electrical impedance information at a spatial resolution on the scale of ultrasound wavelengths [12, 65, 86, 94, 104, 119, 120, 134]. These include Hall effect imaging, magneto-acoustic current imaging, magneto-acoustic tomography with magnetic induction, and ultrasonically-induced Lorentz force imaging. Acousto-magnetic tomographic techniques have the potential to detect small conductivity inhomogeneities, enabling them to diagnose pathologies such as cancer by detecting tumorous tissues when other conductivity imaging techniques fail to do so.

In ultrasonically-induced Lorentz force method (experimental apparatus presented in Figure 1.1.1) an ultrasound pulse propagates through the medium to be imaged in the presence of a static magnetic field. The ultrasonic wave induces Lorentz' force on the ions in the medium, causing the negatively and positively charged ions to separate. This separation of charges acts as a source of electrical current and potential. Measurements of the induced current give information on the conductivity in the medium. A 1 *Tesla* magnetic field and a 1 *MPa* ultrasonic pulse induce current at the *nanoampere* scale. Stronger magnetic fields and ultrasonic beams can be used to enhance the signal-to-noise ratio [65].

We provide a physical model for ultrasonically-induced Lorentz force electrical impedance tomography, and develop two efficient methods for reconstructing the conductivity in the medium from the induced electrical current. As far as we know, this is the first mathematical and numerical modeling of the experiment conducted in [65] to illustrate the feasibility of ultrasonically-induced Lorentz force electrical impedance tomography. Earlier attempts to model mathematically this technique were made in [12, 82].

The chapter is organized as follows. We start by describing the ionic model of conductivity. From this model we derive the current density induced by an ultrasonic pulse in the presence of a static magnetic field. We then find an expression of the measured current. The inverse problem is to image the conductivity distribution from such measurements corresponding to different pulse sources and directions. A virtual potential used with simple integrations by parts can relate the measured current to the conductivity distribution and the velocity of the ultrasonic pulse. A Wiener deconvolution filter can then reduce the problem to imaging the conductivity from the internal electric current density. The internal electric current density corresponds to that which would be induced by a constant voltage difference between one electrode and another with zero potential. We introduce two reconstruction schemes for solving the imaging problem from the internal data. The first is an optimal control method; we also propose an alternative to this scheme via the use of a transport equation satisfied by the internal current density. The second algorithm is direct and can be viewed as a PDE-based reconstruction scheme. We prove that solving such a PDE yields to the true conductivity distribution as the regularization parameter tends to zero. In doing so, we prove the existence of the characteristic lines for the transport equation under some conditions on the conductivity distribution. We finally test numerically the two proposed schemes in the presence of measurement noise, and also quantify their stability and resolution.

The ultrasonically-induced Lorentz force electrical impedance tomography investigated here can be viewed as a new hybrid technique for conductivity imaging. It has been experimentally tested [65], and was reported to produce images of quality comparable to those of ultrasound images taken under similar conditions. Other emerging hybrid techniques for conductivity imaging have also been reported [8, 12, 18, 45, 60, 126, 135].

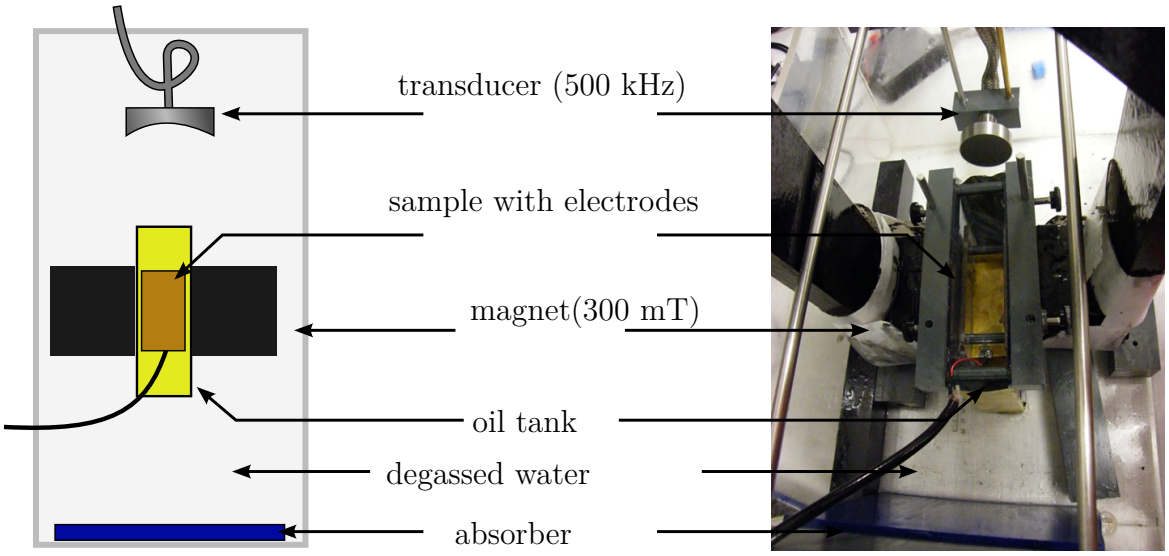

Figure 1.1.1 Example of the imaging device. A transducer is emitting ultrasound in a sample placed in a constant magnetic field. The induced electrical current is collected by two electrodes.

1.2 Electric measurements from acousto-magnetic coupling

Let a physical object to be imaged occupy a three-dimensional domain Ω with a smooth boundary $\partial\Omega$. Assume that this body is placed in a constant magnetic field B in the direction e_3 where $\{e_1, e_2, e_3\}$ denotes the standard orthonormal basis of $\mathbb{R}^3$. We are interested in recovering the electrical conductivity of this body $\sigma \in L^\infty(\Omega)$ with the known lower and upper bounds:

$$0 < \underline{\sigma} \leq \sigma \leq \overline{\sigma} < \infty.$$

An acoustic transducer sends a short acoustic pulse from $y \in \mathbb{R}^3$ in the direction $\xi \in S^2$, with S^2 being the unit sphere, such that $\xi \cdot e_3 = 0$. This pulse generates the velocity field $v(x,t)\xi$ with $v(x,t)$ taking the following form:

$$v(x,t) = w\Big(z - ct\Big)\ A\Big(z, |r|\Big), \tag{1.2.1}$$

where

$$z = (x-y)\cdot\xi \quad \text{and} \quad r = x - y - z\xi\ \in \Upsilon_\xi := \{\zeta \in \mathbb{R}^3\ :\ \zeta\cdot\xi = 0\}.$$

Here, $w \in \mathcal{C}_c^\infty\big(\mathbb{R}\big)$, supported in $]-\eta, 0[$, is the ultrasonic pulse profile; $A \in \mathcal{C}^\infty\big(\mathbb{R}\times\mathbb{R}^+\big)$, supported in $\mathbb{R}^+ \times [0, R]$, is the cylindrical profile distribution of the wave corresponding to the focus of the acoustic transducer; and R is the maximal radius of the acoustic beam.

1.2.1 The ionic model of conductivity

We describe here the electrical behavior of the medium as an electrolytic tissue composed of ions capable of motion in an aqueous tissue. We consider k types of ions in the medium with charges of q_i, $i \in \{1, \dots, k\}$. The corresponding volumetric density n_i is assumed to be constant. Neutrality in the medium is described as

$$\sum_i q_i n_i = 0. \tag{1.2.2}$$

The Kohlrausch law defines the conductivity of such a medium as a linear combination of the ionic concentrations

$$\sigma = e^+ \sum_i \mu_i q_i n_i, \tag{1.2.3}$$

where e^+ is the elementary charge, and the coefficients μ_i denote the ionic mobility of each ion i. See, for example, [104, 114].

1.2.2 Ion deviation by Lorentz force

We embed the medium in a constant magnetic field B with direction e_3, and perturb it mechanically using the short, focused, ultrasonic pulses v defined in (1.2.1). The motion of the charged particle i inside the medium is deviated by the Lorentz force

$$F_i = q_i v\xi \times B. \tag{1.2.4}$$

This force accelerates the ion in the orthogonal direction $\tau = \xi \times e_3$. Then, almost immediately, the ion reaches a constant speed given by

$$v_{\tau,i} = \mu_i |B| v$$

at the first order. See [104, 114] for more details. Finally, the ion i has a total velocity

$$v_i = v\xi + \mu_i |B| v\tau.$$

The current density generated by the displacement of charges can be described as follows:

$$j_S = \sum_i n_i q_i v_i = \left(\sum_i n_i q_i\right) v\xi + \left(\sum_i n_i \mu_i q_i\right) |B| v\tau.$$

Using the neutrality condition (1.2.2) and the definition of σ in (1.2.3), we get the following simple formula for j_S:

$$j_S = \frac{1}{e^+} |B| \sigma v \tau, \tag{1.2.5}$$

which is in accordance with the formula used in [12].

This electrolytic description of the tissue characterizes the interaction between the ultrasonic pulse and the magnetic field through a small deviation of the charged particles embedded in the tissue. This deviation generates a current density j_S orthogonal to ξ and to B, locally supported inside the domain. At a fixed time t, j_S is supported in the support of $x \mapsto v(x,t)$. This current is proportional to σ, and is the source of the current that we measure on the electrodes placed at $\partial\Omega$. In the next section, a formal link is substantiated between j_S and the measured current I.

1.2.3 Internal electrical potential

Because the characteristic time of the acoustic propagation is very long compared with the electromagnetic wave propagation characteristic time, we can adopt the electro-quasistatic frame. Consequently, the total current j in Ω at a fixed time t can be formulated as

$$j = j_S + \sigma \nabla u, \tag{1.2.6}$$

where u is the electrical potential. It satisfies

$$\nabla \cdot (j_S + \sigma \nabla u) = \nabla \cdot j = 0. \tag{1.2.7}$$

Figure 1.2.1 shows the configuration under consideration. Let Γ_1 and Γ_2 be portions of the boundary $\partial\Omega$ where two planner electrodes are placed. Denote $\Gamma_0 = \partial\Omega \setminus (\Gamma_1 \cup \Gamma_2)$.

As we measure the current between the two electrodes Γ_1 and Γ_2, the electrical potential is the same on both electrodes, and can be fixed to zero without loss of generality. Further, it is assumed that no current can leave from Γ_0. The potential u

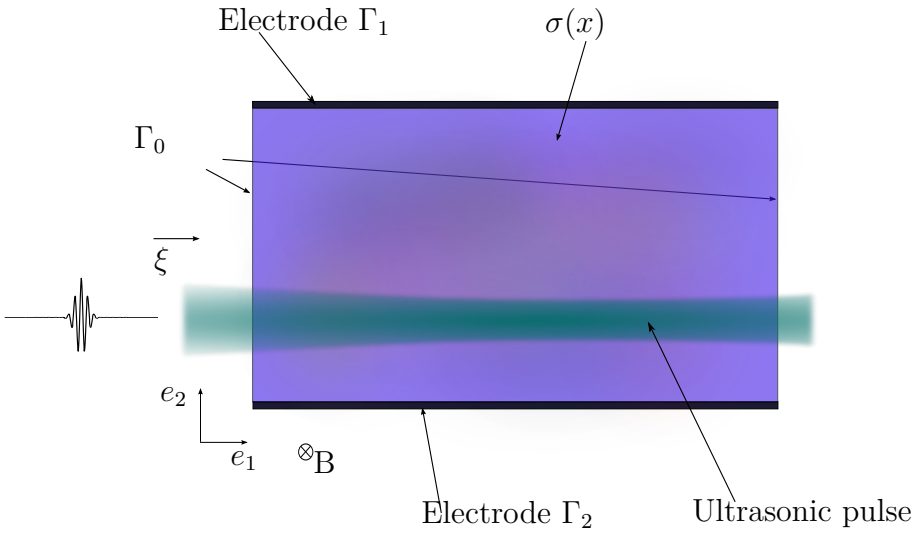

Figure 1.2.1 Imaging system configuration. An ultrasonic wave propagates in a medium of electrical conductivity σ between electrodes Γ_1 and Γ_2.

can then be defined as the unique solution in $H^1(\Omega)$ of the elliptic system

$$\begin{cases} -\nabla \cdot (\sigma \nabla u) = \nabla \cdot j_S & \text{in } \Omega, \\ u = 0 & \text{on } \Gamma_1 \cup \Gamma_2, \\ \partial_\nu u = 0 & \text{on } \Gamma_0. \end{cases} \tag{1.2.8}$$

Throughout this chapter ∂_ν denotes the normal derivative. Note that the source term j_S depends on the time $t > 0$, the position of the acoustic transducer $y \in \mathbb{R}^3$, and the direction $\xi \in S^2$. The electrical potential u also depends on these variables.

The measurable intensity I is the current flow through the electrodes. Integrating (1.2.8) by parts gives

$$\int_{\Gamma_1} \sigma \partial_\nu u + \int_{\Gamma_2} \sigma \partial_\nu u = 0,$$

which is the expression of current flow conservation. We define the intensity I by

$$I = \int_{\Gamma_2} \sigma \partial_\nu u. \tag{1.2.9}$$

1.2.4 Virtual potential

In order to link I to σ, we introduce a virtual potential $U \in H^1(\Omega)$ defined as the unique solution of

$$\begin{cases} -\nabla \cdot (\sigma \nabla U) = 0 & \text{in } \Omega, \\ U = 0 & \text{on } \Gamma_1, \\ U = 1 & \text{on } \Gamma_2, \\ \partial_\nu U = 0 & \text{on } \Gamma_0. \end{cases} \tag{1.2.10}$$

Then we multiply (1.2.8) by U and integrate by parts. Assuming that the support of v does not intersect the electrodes Γ_1 and Γ_2, we obtain

$$-\int_\Omega \sigma \nabla u \cdot \nabla U + \int_{\Gamma_2} \sigma \partial_\nu u = \int_\Omega j_S \cdot \nabla U.$$

From the property of U in (1.2.10) and the definition of I in (1.2.9), the above identity becomes

$$I = \int_\Omega j_S \cdot \nabla U.$$

The above identity links the measured intensity I to an internal information of σ using the expression of j_S in (1.2.5):

$$I = \frac{|B|}{e^+} \int_\Omega v(x,t)\sigma(x)\nabla U(x)dx \cdot \tau.$$

According to (1.2.1), v depends on y, ξ, and t, so does I. We define the measurement function as

$$M_{y,\xi}(z) = \int_\Omega v(x, z/c)\sigma(x)\nabla U(x)dx \cdot \tau(\xi) \tag{1.2.11}$$

for any $y \in \mathbb{R}^3$, $\xi \in S^2$ and $z > 0$. We assume the knowledge of this function in a certain subset of $\mathbb{R}^3 \times S^2 \times \mathbb{R}^+$ denoted by $Y \times \mathfrak{S} \times]0, z_{max}[$. We will discuss later the assumptions we have to impose on this subset in order to make the reconstruction accurate and stable.

1.3 Construction of the virtual current

For simplicity, let us restrict ourselves to the two dimensional case where both the conductivity σ and the virtual potential U do not change in e_3-direction. For convenience, the same notations will be used as in the three dimensional case.

In order to obtain the information of σ contained in $M_{y,\xi}$, we need to separate the contribution of the displacement term v from this measurement function. Using the cylindrical symmetry of this integration we write for any $z \in]0, z_{max}[$,

$$\begin{aligned} M_{y,\xi}(z) &= \int_{\mathbb{R}} \int_{\Upsilon_\xi} w(z-z')(\sigma \nabla U)(y+z'\xi+r) A(z',|r|) dr dz' \cdot \tau(\xi), \\ &= \int_{\mathbb{R}} w(z-z') \int_{\Upsilon_\xi} (\sigma \nabla U)(y+z'\xi+r) A(z',|r|) dr dz' \cdot \tau(\xi), \\ &= \left(W \star \Phi_{y,\xi}\right)(z) \cdot \tau(\xi), \end{aligned} \tag{1.3.1}$$

where $W(z) = w(-z)$, $\star$ denotes the convolution product, and

$$\Phi_{y,\xi}(z) = \int_{\Upsilon_\xi} \sigma(y+z\xi+r) A(z,|r|) \nabla U(y+z\xi+r) dr.$$

As will be shown in section 1.6, through a one dimensional deconvolution problem that can be stably solved using, for instance, a Wiener-type filtering method, we get access to the function $\Phi_{y,\xi} \cdot \tau(\xi)$. Now the question is about the reconstruction of σ from $\Phi_{y,\xi} \cdot \tau(\xi)$. We can notice that $\Phi_{y,\xi}$ is a weighted Radon transform applied to the virtual current field $\sigma \nabla U$. The weight $A(z,|r|)$ is critical for the choice of the method that we can use. Closer this weight is to a Dirac mass function, better is the stability of the reconstruction. In this case, if the field $\sigma \nabla U$ does not have too large variations, we can recover a first-order approximation; as discussed in the rest of this section.

In order to make the reconstruction accurate and stable, we make two assumptions on the set of parameters $Y \times D \times]0, z_{max}[$. For any $x \in \Omega$, we define

$$\mathfrak{S}_x = \left\{ \xi \in \mathfrak{S} \ : \ \xi = \frac{x-y}{|x-y|} \ \text{ for some } \ y \in Y \right\}.$$

The first assumption is

$$\text{(H1)} \quad \forall x \in \Omega, \ \ \exists \ \xi_1, \xi_2 \in \mathfrak{S}_x \quad \text{s.t.} \quad |\xi_1 \times \xi_2| \neq 0,$$

and the second one reads

$$\text{(H2)} \quad \forall x \in \Omega, \ \ \forall \xi \in \mathfrak{S}_x, \ \ \exists \text{ unique } \ y \in Y \quad \text{s.t.} \quad \xi = \frac{x-y}{|x-y|}.$$

From the assumption (H2), we can define a distance map $|x-y|$ as a function of x and ξ. We will denote $d_Y(x,\xi) = |x-y|$. By a change of variables, we rename our data function Σ as

$$\begin{aligned}\psi(x,\xi) &= \Phi_{y,\xi}\Big(d_Y(x,\xi)\Big)\cdot\tau(\xi)\\ &= \int_{\Upsilon_\xi}(\sigma\nabla U)(x+r)A\Big(d_Y(x,\xi),|r|\Big)dr\cdot\tau(\xi).\end{aligned} \tag{1.3.2}$$

Now if we denote by

$$\gamma(x,\xi) = \int_{\Upsilon_\xi} A\Big(d_Y(x,\xi),|r|\Big)dr\ \tau(\xi), \tag{1.3.3}$$

then we expect that

$$\psi(x,\xi) \approx (\sigma\nabla U)(x)\cdot\gamma(x,\xi),$$

provided the supp(A) is small enough and $\sigma\nabla U$ does not vary too much. The following lemma makes this statement precise.

Lemma 1.3.1. *Consider a fixed direction $\xi\in\mathfrak{S}$ and consider the domain covered by the pulses of direction ξ defined by $\Omega_\xi = \{x\in\Omega\ :\ \xi\in\mathfrak{S}_x\}$. Suppose that the virtual current $\sigma\nabla U$ has bounded variations, then*

$$\|\psi(\cdot,\xi)-\sigma\nabla U\cdot\gamma(\cdot,\xi)\|_{L^1(\Omega_\xi)} \le cR\|\sigma\nabla U\|_{TV(\Omega)^2},$$

where R is the maximum radius of the cylindrical support of the envelope A and $c>0$ depends on the shape of A. Here, $\|\ \|_{TV(\Omega)^2}$ denotes the total variation semi-norm.

Proof. For a.e. $x\in\Omega_\xi$, we have

$$\begin{aligned}&|\psi(x,\xi)-(\sigma\nabla U)(x)\cdot\gamma(x,\xi)| \le\\ &\int_{\Upsilon_\xi}|(\sigma\nabla U)(x+r)-(\sigma\nabla U)(x)|\,A\Big(d_Y(x,\xi),|r|\Big)dr,\end{aligned}$$

and so

$$\begin{aligned}&\|\psi(\cdot,\xi)-\sigma\nabla U\cdot\gamma(\cdot,\xi)\|_{L^1(\Omega_\xi)}\\ &\le\int_{\Upsilon_\xi}\int_{\Omega_\xi}|(\sigma\nabla U)(x+r)-(\sigma\nabla U)(x)|\,A\Big(d_Y(x,\xi),|r|\Big)dxdr\\ &\le\|\sigma\nabla U\|_{TV(\Omega)^2}\int_{\Upsilon_\xi}|r|\sup_{0<z<z_{max}}A(z,|r|)dr\\ &\le 2\pi R\|\sigma\nabla U\|_{TV(\Omega)^2}\int_{\mathbb{R}+}\sup_{0<z<z_{max}}A(z,\rho)d\rho.\end{aligned}$$

□

Note that in the most interesting cases, $\sigma\nabla U$ has bounded variations. For example, if σ has a piecewise $W^{1,\infty}$ smoothness on smooth inclusions, then $\sigma\nabla U$ has bounded variations. This also holds true for σ in some subclasses of functions of bounded variations. In the following, we make the assumption, as in Lemma 1.3.1, that $\sigma\nabla U$ has bounded variations.

In conclusion, our data approximates the quantity $(\sigma\nabla U)(x)\cdot\gamma(x,\xi)$ for any $x\in\Omega$, $\xi\in\mathfrak{S}_x$ where the vector $\gamma(x,\xi)$ is supposed to be known. To get the current $(\sigma\nabla U)(x)$, we simply consider data from two linearly independent directions. Using assumption (H1), for a fixed $x\in\Omega$, there exist $\xi_1,\xi_2\in\mathfrak{S}_x$ such that $\det(\xi_1,\xi_2)\neq 0$. We construct the 2×2 invertible matrix

$$\Gamma(x,\xi_1,\xi_2)=\begin{bmatrix}\gamma(x,\xi_1)^\perp\\ \gamma(x,\xi_2)^\perp\end{bmatrix},$$

and the data column vector

$$\Psi(x,\xi_1,\xi_2)=\begin{bmatrix}\psi(x,\xi_1)\\ \psi(x,\xi_2)\end{bmatrix}.$$

We approximate the current $\sigma\nabla U(x)$ by the vector field

$$V(x,\xi_1,\xi_2)=\Gamma(x,\xi_1,\xi_2)^{-1}\Psi(x,\xi_1,\xi_2).$$

Indeed, for any open set $\widetilde{\Omega}\subset\Omega_{\xi_1}\cap\Omega_{\xi_2}$, the following estimate holds:

$$\begin{aligned}&\|V(\cdot,\xi_1,\xi_2)-\sigma\nabla U\|_{L^1(\widetilde{\Omega})^2}\\ &\leq\sup_{x\in\widetilde{\Omega}}\left\|\Gamma(x,\xi_1,\xi_2)^{-1}\right\|_{\mathcal{L}(\mathbb{R}^2)}\left(\sum_{i=1}^{2}\|\psi(\cdot,\xi_i)-\sigma\nabla U\cdot\gamma(\cdot,\xi_i)\|_{L^1(\Omega_{\xi_i})}\right)^{1/2}\\ &\leq cR\|\sigma\nabla U\|_{TV(\Omega)^2}.\end{aligned}$$

It is worth mentioning that if more directions are available, then we can use them to enhance the stability of the reconstruction. The linear system becomes over-determined and we can get the optimal approximation by using a least-squares method.

1.4 Recovering the conductivity by optimal control

In this section we assume that, according to the previous one, we are in the situation where we know a good approximation of the virtual current $D := \sigma \nabla U$ in the sense of $L^1(\Omega)^2$. The objective here is to provide efficient methods for separating σ from D.

For $a < b$, let us denote by $L^\infty_{a,b}(\Omega) := \{f \in L^\infty(\Omega) \ : \ a < f < b\}$ and define the operator $\mathcal{F} : L^\infty_{\underline{\sigma},\overline{\sigma}}(\Omega) \longrightarrow H^1(\Omega)$ by

$$\mathcal{F}[\sigma] = U : \begin{cases} \nabla \cdot (\sigma \nabla U) = 0 & \text{in } \Omega, \\ U = 0 & \text{on } \Gamma_1, \\ U = 1 & \text{on } \Gamma_2, \\ \partial_\nu U = 0 & \text{on } \Gamma_0. \end{cases} \tag{1.4.1}$$

The following lemma holds.

Lemma 1.4.1. *Let $d\mathcal{F}$ be the Fréchet derivative of $\mathcal{F}$. For any $\sigma \in L^\infty_{\underline{\sigma},\overline{\sigma}}(\Omega)$ and $h \in L^\infty(\Omega)$ such that $\sigma + h \in L^\infty_{\underline{\sigma},\overline{\sigma}}(\Omega)$ we have*

$$d\mathcal{F}[\sigma](h) = v : \begin{cases} \nabla \cdot (\sigma \nabla v) = -\nabla \cdot (h \nabla \mathcal{F}[\sigma]) & \text{in } \Omega, \\ v = 0 & \text{on } \Gamma_1 \cup \Gamma_2, \\ \partial_\nu v = 0 & \text{on } \Gamma_0. \end{cases} \tag{1.4.2}$$

Proof. Let us denote by $w = \mathcal{F}[\sigma + h] - \mathcal{F}[\sigma] - v$. This function is in $H^1(\Omega)$ and satisfies the equation

$$\nabla \cdot (\sigma \nabla w) = -\nabla \cdot (h \nabla (\mathcal{F}[\sigma + h] - \mathcal{F}[\sigma]))$$

with the same boundary conditions as v. We have the elliptic global control:

$$\|\nabla w\|_{L^2(\Omega)} \leq \frac{1}{\underline{\sigma}} \|h\|_{L^\infty(\Omega)} \|\nabla (\mathcal{F}[\sigma + h] - \mathcal{F}[\sigma])\|_{L^2(\Omega)}.$$

Since

$$\nabla \cdot (\sigma \nabla (\mathcal{F}[\sigma + h] - \mathcal{F}[\sigma])) = -\nabla \cdot (h \nabla \mathcal{F}[\sigma + h]),$$

we can also control $\mathcal{F}[\sigma + h] - \mathcal{F}[\sigma]$ with

$$\|\nabla (\mathcal{F}[\sigma + h] - \mathcal{F}[\sigma])\|_{L^2(\Omega)} \leq \frac{1}{\sqrt{\underline{\sigma}}} \|h\|_{L^\infty(\Omega)} \|\nabla \mathcal{F}[\sigma + h]\|_{L^2(\Omega)}.$$

Then, there is a positive constant C depending only on Ω such that

$$\|\nabla \mathcal{F}[\sigma + h]\|_{L^2(\Omega)} \leq C\sqrt{\frac{\overline{\sigma}}{\underline{\sigma}}}.$$

Finally, we obtain

$$\|\nabla w\|_{L^2(\Omega)} \leq C\frac{\sqrt{\overline{\sigma}}}{\underline{\sigma}^2}\|h\|^2_{L^\infty(\Omega)}.$$

□

We look for the minimizer of the functional

$$J[\sigma] = \frac{1}{2}\int_\Omega |\sigma\nabla\mathcal{F}[\sigma] - D|^2. \tag{1.4.3}$$

In order to do so, we compute its gradient. The following lemma holds.

Lemma 1.4.2. *For any $\sigma \in L^\infty_{\underline{\sigma},\overline{\sigma}}(\Omega)$ and $h \in L^\infty(\Omega)$ such that $\sigma + h \in L^\infty_{\underline{\sigma},\overline{\sigma}}(\Omega)$,*

$$dJ[\sigma](h) = -\int_\Omega h\Big((\sigma\nabla\mathcal{F}[\sigma] - D - \nabla p)\cdot\nabla\mathcal{F}[\sigma]\Big),$$

where p is defined as the solution to the adjoint problem:

$$\begin{cases} \nabla\cdot(\sigma\nabla p) = \nabla\cdot(\sigma^2\nabla\mathcal{F}[\sigma] - \sigma D) & \text{in } \Omega, \\ p = 0 & \text{on } \Gamma_1\cup\Gamma_2, \\ \partial_\nu p = 0 & \text{on } \Gamma_0. \end{cases} \tag{1.4.4}$$

Proof. As $\mathcal{F}$ is Fréchet differentiable, so is J. For $\sigma \in L^\infty_{\underline{\sigma},\overline{\sigma}}(\Omega)$ and $h \in L^\infty(\Omega)$ such that $\sigma + h \in L^\infty_{\underline{\sigma},\overline{\sigma}}(\Omega)$, we have

$$dJ[\sigma](h) = \int_\Omega (\sigma\nabla\mathcal{F}[\sigma] - D)\cdot(h\nabla\mathcal{F}[\sigma] + \sigma\nabla d\mathcal{F}[\sigma](h)).$$

Now, multiplying (1.4.4) by $d\mathcal{F}[\sigma](h)$, we get

$$\int_\Omega \sigma\nabla p\cdot\nabla d\mathcal{F}[\sigma](h) = \int_\Omega (\sigma^2\nabla\mathcal{F}[\sigma] - \sigma D)\cdot\nabla d\mathcal{F}[\sigma](h).$$

On the other hand, multiplying (1.4.2) by p we arrive at

$$\int_\Omega \sigma\nabla p\cdot\nabla d\mathcal{F}[\sigma](h) = -\int_\Omega h\nabla\mathcal{F}[\sigma]\cdot\nabla p,$$

and therefore,

$$dJ[\sigma](h) = \int_\Omega h(\sigma\nabla\mathcal{F}[\sigma] - D - \nabla p)\cdot\nabla\mathcal{F}[\sigma].$$

□

Lemma 1.4.2 allows us to implement a numerical gradient descent method in order to find σ. A regularization term can also be added to $J[\sigma]$ in order to avoid instability. As we are seeking discontinuous σ with smooth variations out of the discontinuity set, a good choice would be the minimization of the regularized functional:

$$J_\varepsilon[\sigma] = \frac{1}{2}\int_\Omega |\sigma\nabla\mathcal{F}[\sigma] - D|^2 + \varepsilon||\sigma||_{TV(\Omega)}, \tag{1.4.5}$$

where $\varepsilon > 0$ is the regularization parameter.

1.5 The orthogonal field method

In this section, we present an alternative direct method to optimal control for reconstructing the conductivity σ from the internal data $\sigma\nabla U$. It is based on solving a transport equation. The following approach may be extended to the three dimensional case. However, several proofs would need to be revisited.

Given a vector field $D = \sigma\nabla U$ which is parallel to ∇U everywhere, we may construct the vectorial field $F = (D_2, -D_1)$ which is everywhere orthogonal to D. The flow of F may define the level sets of U. Assuming that the variations of the conductivity σ are far enough from Γ_0, we can assume that $U(x) = x_2$ on this boundary part. Then U is a solution of the following transport equation:

$$\begin{cases} F\cdot\nabla u = 0 & \text{in } \Omega, \\ u = x_2 & \text{on } \partial\Omega. \end{cases} \tag{1.5.1}$$

In the case where (1.5.1) is well posed and can be solved, we can reconstruct the virtual potential U. The conductivity σ is deduced from U and D by the following identity

$$\sigma = \frac{D\cdot\nabla U}{|D|^2}. \tag{1.5.2}$$

Despite to its very simple form, this first-order equation is really tricky. Existence and uniqueness are both difficult challenges in the general case. Our main difficulty here is due to the fact that F is discontinuous. As the function U that we are looking for is a

natural solution of this equation, we are only concerned here with the uniqueness of a solution to (1.5.1).

1.5.1 Uniqueness result for the transport equation

The uniqueness of a solution to (1.5.1) is directly linked to the existence of outgoing characteristics lines defined by the dynamic system:

$$\begin{cases} X'(t) = F(X(t)),\ t \geq 0, \\ X(0) = x,\ x \in \Omega, \end{cases} \tag{1.5.3}$$

which usually needs the continuity of F. As σ is in general not continuous, F is not continuous, which makes the classical existence results useless. Nevertheless, under some assumptions on σ, we can insure the existence of the characteristics lines.

Definition 1.5.1. *For any $k \in \mathbb{N}$, $\alpha \in]0,1[$, for any simple closed curve $\mathcal{C}$ of class $C^{1,\alpha}$ such that $\Omega \setminus \mathcal{C}$ is a union of connected domains $\Omega_i, i = 1, 2, \cdots n$, we define $C^{k,\alpha}_{\mathcal{C}}\left(\overline{\Omega}\right)$ to be the class of functions $f : \Omega \longrightarrow \mathbb{R}$ satisfying*

$$f|_{\Omega_i} \in C^{k,\alpha}\left(\overline{\Omega_i}\right) \quad \forall i = 1, \cdots n.$$

Definition 1.5.2. *A conductivity σ is said to be admissible if there exists a constant $\alpha \in]0,1[$ and a curve $\mathcal{C}$ of class $C^{1,\alpha}$ such that $\sigma \in C^{0,\alpha}_{\mathcal{C}}\left(\overline{\Omega}\right) \cap L^{\infty}_{\underline{\sigma},\overline{\sigma}}(\Omega)$ and*

$$\inf_{\Omega\setminus\mathcal{C}} \sigma \nabla \mathcal{F}[\sigma] \cdot e_2 \ > \ 0.$$

If σ is admissible and belongs to $C^{0,\alpha}_{\mathcal{C}}\left(\overline{\Omega}\right)$, then the solution U of (1.2.10) belongs to $C^{1,\alpha}_{\mathcal{C}}\left(\overline{\Omega}\right)$ and the field $F = (\sigma \nabla U)^{\perp}$ satisfies

$$F \in C^{0,\alpha}_{\mathcal{C}}\left(\overline{\Omega}\right) \quad \text{and} \quad \inf_{\Omega\setminus\mathcal{C}} F \cdot e_1 \ > \ 0.$$

Moreover, as F is orthogonal to $\sigma \nabla U$, we can describe the jump of F at the curve $\mathcal{C}$. Defining the normal and tangential unit vectors ν and τ and also the local sides (+) and (-) with respect to ν, we can write F on both sides as

$$F^+ = \sigma^+ \partial_\nu U^+ \tau + \sigma^+ \partial_\tau U^+ \nu,$$
$$F^- = \sigma^- \partial_\nu U^- \tau + \sigma^- \partial_\tau U^- \nu$$

with the transmission conditions, $\sigma^+\partial_\nu U^+ = \sigma^-\partial_\nu U^-$ and $\partial_\tau U^+ = \partial_\tau U^-$. Finally, we characterize the discontinuity of F by

$$[F] = [\sigma]\partial_\tau U\nu,$$

where $[\,]$ denotes the jump across $\mathcal{C}$.

With all of these properties for the field F, we can prove the existence of the characteristics lines for (1.5.3).

Theorem 1.5.1. *(Local existence of characteristics) Assume that $F \in C^{0,\alpha}_{\mathcal{C}}\left(\overline{\Omega}\right)$ with $\mathcal{C}$ of class $C^{1,\alpha}$ for $\alpha \in]0,1[$. Assume that the discontinuity of F on $\mathcal{C}$ satisfies*

$$F^+ = f\tau + \sigma^+ g\nu,$$
$$F^- = f\tau + \sigma^- g\nu$$

with $f, g, \sigma^+, \sigma^- \in C^{0,\alpha}(\mathcal{C})$ where σ^+, σ^- are positive and g is locally signed. Then, for any $x_0 \in \Omega$, there exists $T > 0$ and $X \in C^1\Big([0,T[,\Omega\Big)$ such that $t \mapsto F(X(t))$ is measurable and

$$X(t) = x_0 + \int_0^t F(X(s))ds, \quad \forall t \in [0,T[.$$

Proof. If $x_0 \notin \mathcal{C}$, then F is continuous in a neighborhood of x_0 and the Cauchy-Peano theorem can be applied.

If $x_0 \in \mathcal{C}$, then we choose a disk $B \subset \Omega$ centered at x_0. The oriented line $\mathcal{C}$ separates B in two simply connected open domains called B^+ and B^-. For ease of explanation, we may assume that $\mathcal{C} \cap B$ is straight line (since we can flatten the curve using a proper $C^{0,\alpha}$-diffeomorphism).

Assume that $g(x_0) > 0$. Up to rescaling B, we can assume that $g(x) > 0$ for all $x \in \mathcal{C} \cap B$. We extend $F|_{B^+}$ to a continuous field $\tilde{F} \in C^0(B)$ by even reflection. The Cauchy-Peano theorem insures the existence of $T > 0$ and $X \in C^1\Big([0,T[,\Omega\Big)$ such that $X(0) = x_0$ and $X'(t) = \tilde{F}(X(t))$ for all $t \in [0,T[$. As $g(x_0) > 0$, we have $X'(0) \cdot \nu(x_0) > 0$ and $X(t) \in \overline{B^+}$ in a neighborhood of 0. Thus, for a small enough t, $X'(t) = F(X(t))$. If $g(x_0) < 0$, then we apply the same argument by interchanging B^- and B^+.

Suppose now that $g(x_0) = 0$. The field F is now tangent to the discontinuity line. If $f(x_0) = 0$, then $X(t) = x_0$ is a solution. We assume here that $f(x_0) > 0$. As g is assumed to be locally signed, we can suppose that $g \geq 0$ in a small sub-curve of $\mathcal{C}$ satisfying $(x - x_0) \cdot \tau(x_0) > 0$. Again, we extend $F|_{B^+}$ to a continuous field $\tilde{F} \in C^0(B)$

by even reflection and use the Cauchy-Peano theorem to show that there exists $T > 0$ and $X \in C^1\Big([0,T[,\Omega\Big)$ such that $X(0) = x_0$ and $X'(t) = \tilde{F}(X(t))$ for all $t \in [0,T[$. In order to complete the proof, we should show that $X(t)$ belongs to $\overline{B^+}$ for t small enough. If not, there exists a sequence $t_n \searrow 0$ such that $X(t_n) \in B^-$. By the mean value theorem, there exists $\tilde{t}_n \in (0,t_n)$ such that $F(X(\tilde{t}_n)) \cdot \nu(x_0) = X'(\tilde{t}_n) \cdot \nu(x_0) < 0$. Thus, $X(t)$ belongs to $\overline{B^+}$ and $X'(t) = F(X(t))$ for t small enough.

Note that the local monotony of g is satisfied in many cases. For instance if $\mathcal{C}$ is analytic and σ is piecewise constant, then ∇U is analytic on $\mathcal{C}$ and hence, g is locally signed. □

It is worth mentioning that existence of a solution for the Cauchy problem (1.5.3) has been proved in [40] provided that $F \cdot \nu > 0$ on $\mathcal{C}$. Here, we have made a weaker assumption. In fact, we only need that $F \cdot \nu$ is locally signed.

Corollary 1.5.2. *(Existence of outgoing characteristics) Consider $F \in C^{0,\alpha}_{\mathcal{C}}(\Omega)$ satisfying the same conditions as in Theorem 1.5.1 and the condition*

$$\inf_{\Omega\setminus\mathcal{C}} F \cdot e_1 \geq c,$$

where c is a positive constant. Then for any $x_0 \in \Omega$ there exists $0 < T < T_{\max}$ where $T_{\max} = \dfrac{1}{c} diam(\Omega)$ and $X \in C^0\Big([0,T[,\Omega\Big)$ satisfying

$$\begin{aligned} &X(t) = x_0 + \int_0^t F(X(s))ds, \quad \forall t \in [0,T[, \\ &\lim_{t\to T} X(t) \in \partial\Omega. \end{aligned}$$

This result means that from any point $x_0 \in \Omega$, the characteristic line reaches $\partial\Omega$ in a finite time.

Proof. Let $x_0 \in \Omega$ and $X \in \mathcal{C}^0\Big([0,T[,\Omega\Big)$ a maximal solution of (1.5.3). Using $F \cdot e_1 \geq c$ we have that $X'(t) \cdot e_1 \geq c$ and so $X(t) \cdot e_1 \geq x_0 \cdot e_1 + ct$ and as $X(t) \in \Omega$ for all $t \in [0,T[$, it is necessary that $T < T_{\max}$. As $F \in C^{0,\alpha}_{\mathcal{C}}(\Omega)$, F is bounded, X is Lipschitz, and the limit of $X(t)$ when t goes to T exists in $\overline{\Omega}$ and is called $X(T)$. Let us show that $X(T) \in \partial\Omega$. Suppose that $X(T) \in \Omega$, then applying Theorem 1.5.1 at $X(T)$, we can continuously extend X on $[T, T+\varepsilon[$ for some positive ε which contradicts the fact that X is a maximal solution. □

Corollary 1.5.3. *(Uniqueness for the transport problem) Consider* $F \in C^{0,\alpha}_{\mathcal{C}}(\Omega)$ *satisfying the same conditions as in Corollary 1.5.2 and consider* $u \in C^0\Big(\overline{\Omega}\Big) \cap C^1_{\mathcal{C}}\Big(\overline{\Omega}\Big)$. *If* u *is a solution of the system*

$$\begin{cases} F \cdot \nabla u = 0 & \text{in } \Omega, \\ u = 0 & \text{on } \partial\Omega, \end{cases} \tag{1.5.4}$$

then $u = 0$ *in* Ω.

Proof. Consider $x_0 \in \Omega$ and a characteristic $X \in \mathcal{C}^0\Big([0,T[,\Omega\Big)$ satisfying

$$\begin{aligned} &X(t) = x_0 + \int_0^t F(X(s))ds, \quad \forall t \in [0,T[, \\ &\lim_{t\to T} X(t) \in \partial\Omega. \end{aligned}$$

We define $f \in C^0\Big([0,T],\mathbb{R}\Big)$ by $f(t) = u(X(t))$. We show that f is constant. Let us define $I = X^{-1}(\mathcal{C})$ then f is differentiable in $[0,T]\backslash I$ and $f'(t) = \nabla u(X(t))\cdot F(X(t)) = 0$. Let us take $t \in I$. If t is not isolated in I, using the fact that $\partial_\tau u^+$ and $\partial_\tau u^-$ are locally signed, $F(X(t))$ is parallel to $\mathcal{C}$ and for an $\varepsilon > 0$, $X(s) \in \overline{B^+}$ (or $\overline{B^-}$) for $s \in [t, t+\varepsilon[$. Then, $f(s) = u(x(s))$ is differentiable on $[t, t+\varepsilon[$ with $f'(s) = \nabla u^+(X(s)) \cdot F(X(s))$. This proves that f is right differentiable at t and $(f')^+(t) = 0$. By the same argument, f is left differentiable at t and $(f')^-(t) = 0$ and so f is differentiable at t with $f'(t) = 0$. Finally, except for a zero measure set of isolated points, f is differentiable on $[0,T]$ and $f' = 0$ almost everywhere. This is not enough to conclude because there exists continuous increasing functions whose derivative is zero almost everywhere. Since for all $t, s \in [0,T]$,

$$|f(t) - f(s)| \leq \sup|\nabla u||X(t) - X(s)| \leq \sup|\nabla U| \sup|F||t-s|,$$

f is Lipschitz and thus absolutely continuous which implies, since $f' = 0$ a.e., that f is constant on $[0,T]$. We finally have $u(x_0) = f(0) = f(T) = u(X(T)) = 0$. □

Hence we conclude that if σ is admissible, then U is the unique solution to (1.5.1) and we can recover σ by (1.5.2).

Remark 1.5.4. *The characteristic method can be used to solve the transport problem. However, it suffers from poor numerical stability which is exponentially growing with the distance to the boundary. To avoid this delicate numerical issue, we propose a*

regularized approach for solving (1.5.1). Our approach consists in forming from (1.5.1) a second-order PDE and adding to this PDE a small elliptic term of order two.

1.5.2 The viscosity-type regularization

In this subsection we introduce a viscosity approximation to (1.5.1). Let $\varepsilon > 0$. We regularize the transport equation (1.5.1) by considering the well-posed elliptic problem

$$\begin{cases} \nabla \cdot \left[\left(\varepsilon I + FF^T \right) \nabla u_\varepsilon \right] = 0 & \text{in } \Omega, \\ u_\varepsilon = x_2 & \text{on } \partial\Omega. \end{cases} \tag{1.5.5}$$

The main question is to understand the behavior of u_ε when ε goes to zero. Or more precisely, whether u_ε converges to the solution U of the transport equation (1.5.1) for a certain topology. The following result holds.

Theorem 1.5.5. *The sequence $(u_\varepsilon - U)_{\varepsilon>0}$ converges strongly to zero in $H_0^1(\Omega)$.*

Proof. We first prove that the sequence $(u_\varepsilon - U)_{\varepsilon>0}$ converges weakly to zero in $H_0^1(\Omega)$ when ε goes to zero. For any $\varepsilon > 0$, $\tilde{u}_\varepsilon := u_\varepsilon - U$ is in $H_0^1(\Omega)$ and satisfies

$$\nabla \cdot \left[\left(\varepsilon I + FF^T \right) \nabla \tilde{u}_\varepsilon \right] = -\varepsilon \triangle U \quad \text{in } \Omega. \tag{1.5.6}$$

Multiplying this equation by $\tilde{u}_\varepsilon$ and integrating by parts over Ω, we obtain

$$\varepsilon \int_\Omega |\nabla \tilde{u}_\varepsilon|^2 + \int_\Omega |F \cdot \nabla \tilde{u}_\varepsilon|^2 = -\varepsilon \int_\Omega \nabla U \cdot \nabla \tilde{u}_\varepsilon \tag{1.5.7}$$

and so,

$$\|\tilde{u}_\varepsilon\|^2_{H_0^1(\Omega)} \leq \int_\Omega |\nabla u \cdot \nabla \tilde{u}_\varepsilon| \leq \|U\|^1_H (\Omega) \, \|\tilde{u}_\varepsilon\|_{H_0^1(\Omega)}.$$

Then $\|\tilde{u}_\varepsilon\|_{H_0^1(\Omega)} \leq \|U\|^1_H (\Omega)$. The sequence $(u_\varepsilon)_{\varepsilon>0}$ is bounded in $H_0^1(\Omega)$ and so by Banach-Alaoglu's theorem, we can extract a subsequence which converges weakly to u^* in $H_0^1(\Omega)$. Multiplying (1.5.6) by u^* and integrating by parts, we get

$$\int_\Omega (F \cdot \nabla \tilde{u}_\varepsilon)(F \cdot \nabla u^*) = -\varepsilon \int_\Omega \nabla U \cdot \nabla u^* - \varepsilon \int_\Omega \nabla \tilde{u}_\varepsilon \cdot \nabla u^*.$$

Taking the limit when ε goes to zero,

$$\|F \cdot \nabla u^*\|_{L^2(\Omega)} = 0.$$

So u^* is a solution of the transport equation (1.5.4), and by Corollary 1.5.3, $u^* = 0$ in Ω. Since the limit u^* is independent of the subsequence, the convergence holds for u_ε.

Now, we are ready to prove the strong convergence. From (1.5.7) we get that

$$\int_\Omega |\nabla \tilde{u}_\varepsilon|^2 \leq -\int_\Omega \nabla U \cdot \nabla \tilde{u}_\varepsilon,$$

and as $\tilde{u}_\varepsilon \rightharpoonup 0$ in $H_0^1(\Omega)$, the term in the right-hand side goes to zero when ε goes to zero. Hence, $\|\tilde{u}_\varepsilon\|_{H_0^1(\Omega)} \to 0$. □

Finally, using Theorem 1.5.5 we define the approximate resistivity by

$$\frac{1}{\sigma_\varepsilon} = \frac{D \cdot \nabla u_\varepsilon}{|D|^2},$$

which strongly converges to $\dfrac{1}{\sigma}$ in $L^2(\Omega)$.

1.6 Numerical results

In this section we first discuss the deconvolution step. Then we test both the optimal control and the orthogonal field reconstruction schemes.

1.6.1 Deconvolution

In this subsection, we consider the problem of recovering $\Phi_{y,\xi}$ from the measurements $M_{y,\xi}$ in the presence of noise. From (1.3.1), it is easy to see that this can be done by deconvolution. However, deconvolution is a numerically very unstable process. In order to render stability we use a Wiener filter [91]. We assume that the signal $M_{y,\xi}(.)$ is perturbed by a random white noise:

$$\widetilde{M}_{y,\xi}(z) = M_{y,\xi}(z) + \mu(z), \tag{1.6.1}$$

where μ is a white Gaussian noise with variance ν^2. Equation (1.6.1) can be written as

$$\widetilde{M}_{y,\xi}(z) = (W \star \Phi_{y,\xi})(z) + \mu(z).$$

Denote by $S(\Sigma) = \int_{\mathbb{R}} |\mathcal{F}(\Phi_{y,\xi})(\omega)| d\omega$ the mean spectral density of Σ, where $\mathcal{F}$ is the Fourier transform. The Wiener deconvolution filter can be written in the frequency

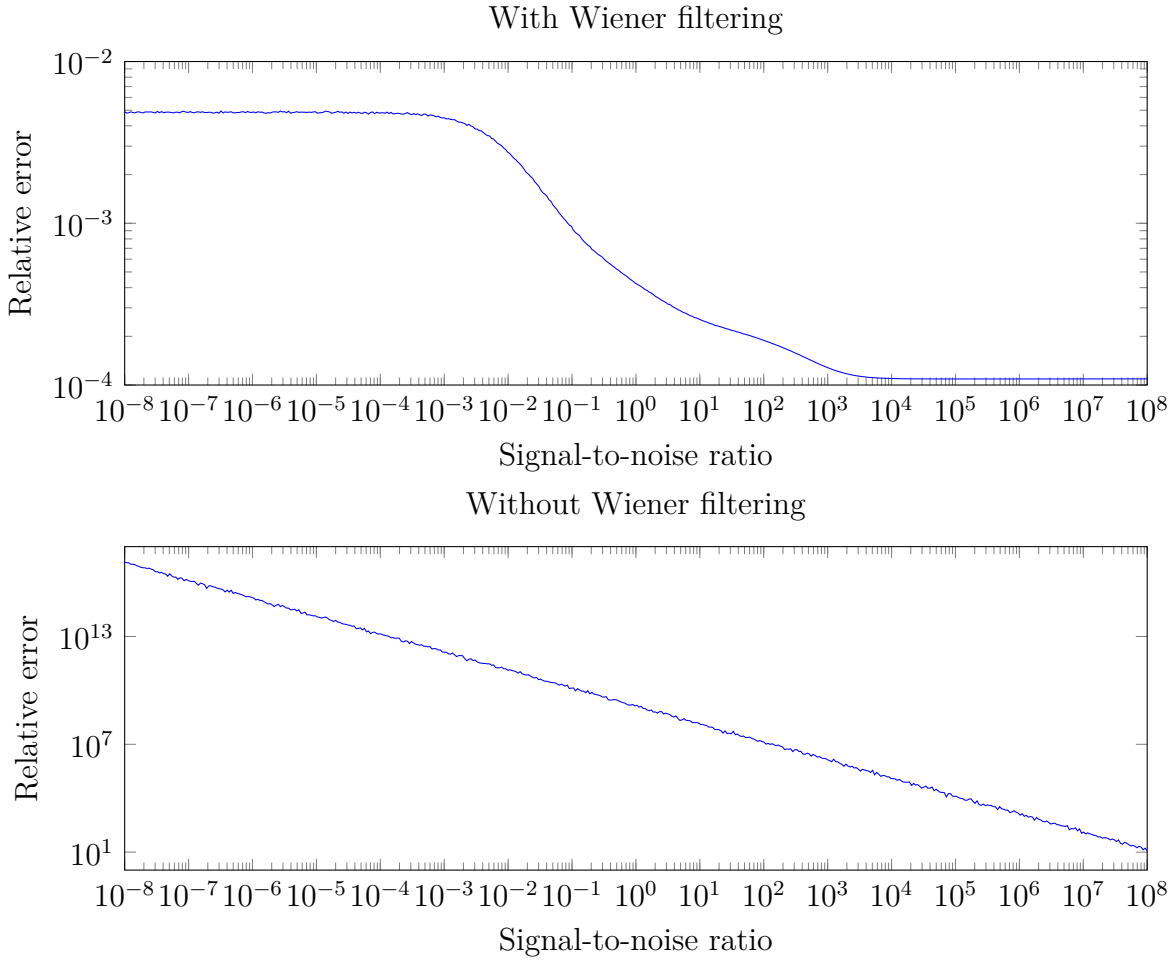

Figure 1.6.1 L^2 norm of the relative error $\frac{\|\Sigma-\widetilde{\Sigma}\|_2}{\|\Sigma\|_2}$ with respect to the signal-to-noise ratio.

domain as

$$\widehat{L}(\omega) = \frac{\overline{\mathcal{F}(W)}(\omega)}{|\mathcal{F}(W)|^2(\omega) + \frac{\nu}{S(\Sigma)}}.$$

The quotient $\nu/S(\Sigma)$ is the signal-to-noise ratio. So, in order to use the filter, we need to have an a priori estimate of the signal-to-noise ratio. We then recover Σ up to a small error by

$$\widetilde{\Sigma}_{y,\xi} = \mathcal{F}^{-1}\left(\mathcal{F}(\widetilde{M})\widehat{L}\right).$$

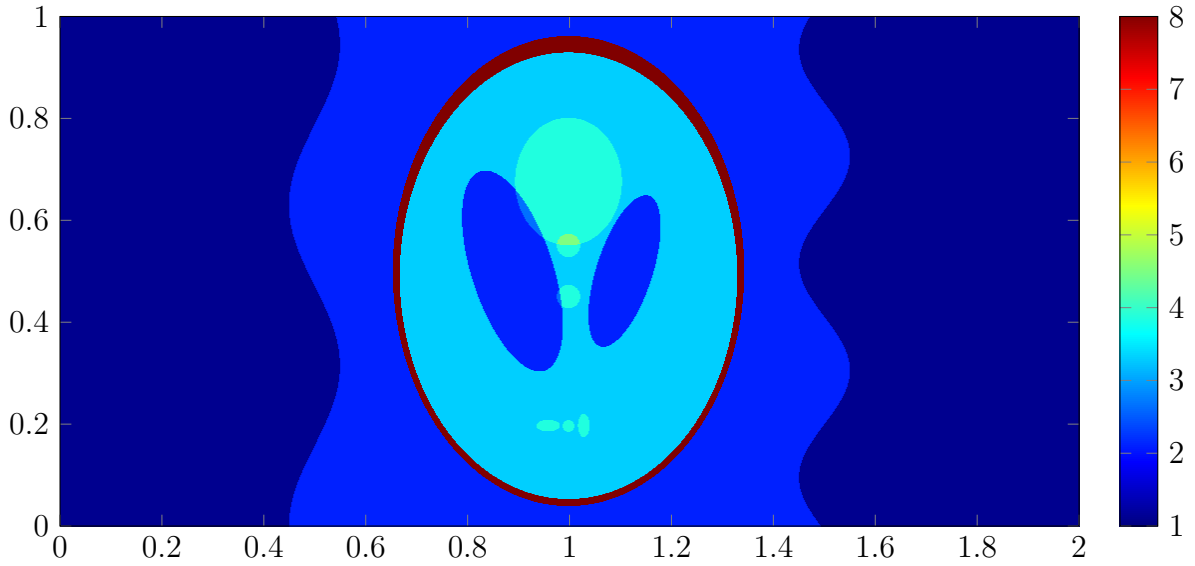

Figure 1.6.2 Conductivity map to be reconstructed.

1.6.2 Conductivity reconstructions

In the numerical simulations, we choose $\Omega =]0, 2[\times]0, 1[$. Figure 1.6.2 shows the true conductivity map in the medium. The simulations are done using a PDE solver. The data is simulated numerically on a fine mesh. For the orthogonal field method, in order to solve (1.5.5), we use a coarse mesh. Then we reconstruct an initial image of the conductivity. Based on the initial image, an adaptive mesh refinement for solving (1.5.5) yields a conductivity image of a better quality. Figure 1.6.3 shows the used meshes for solving the viscosity approximation.

The optimal control method

The minimization procedure gives a decent qualitative reconstruction. The main interfaces are easy to see, yet this method, due to its regularizing effect, fails to show details in weaker contrasts zones. Figures 1.6.4, 1.6.5, and 1.6.6 show the reconstruction obtained with different measurement noise levels.

The orthogonal field method

To find the solution of problem (1.5.5), we fix $\varepsilon = 10^{-3}$, and solve the equation on a uniform mesh on Ω using a finite element method. We reconstruct an approximation of σ, and adapt the mesh to this first reconstruction. We do this procedure a couple

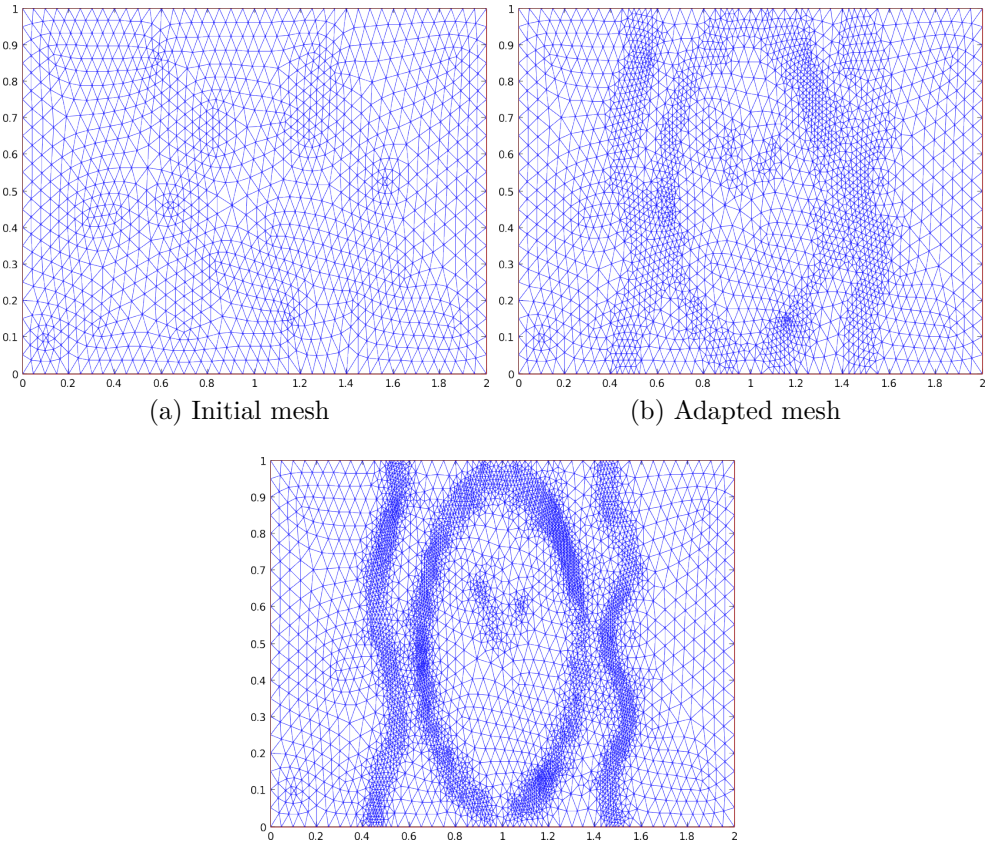

(a) Initial mesh (b) Adapted mesh

(c) Mesh used to generate the data

Figure 1.6.3 Mesh adaptation process

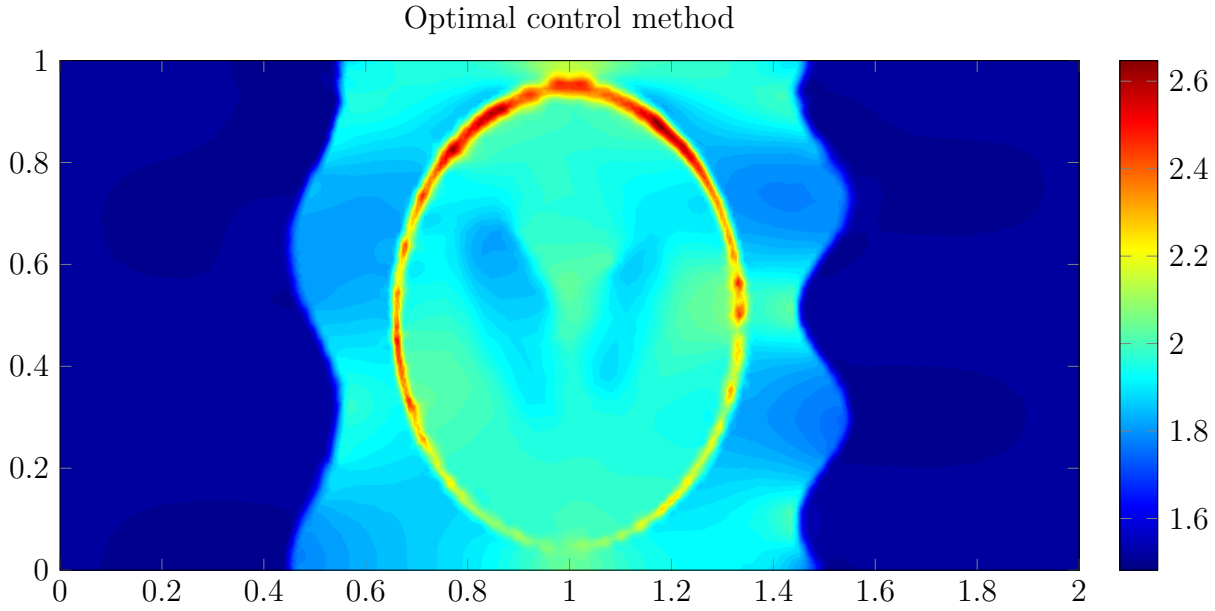

Figure 1.6.4 Reconstructed image without measurement noise.

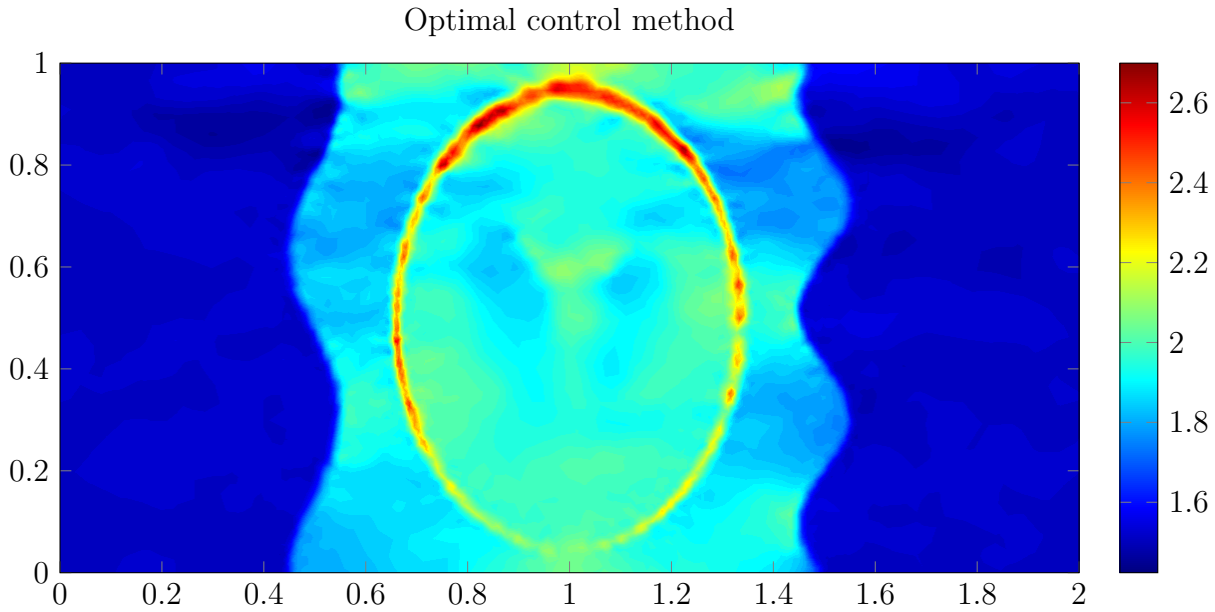

Figure 1.6.5 Reconstructed image with 2% measurement noise.

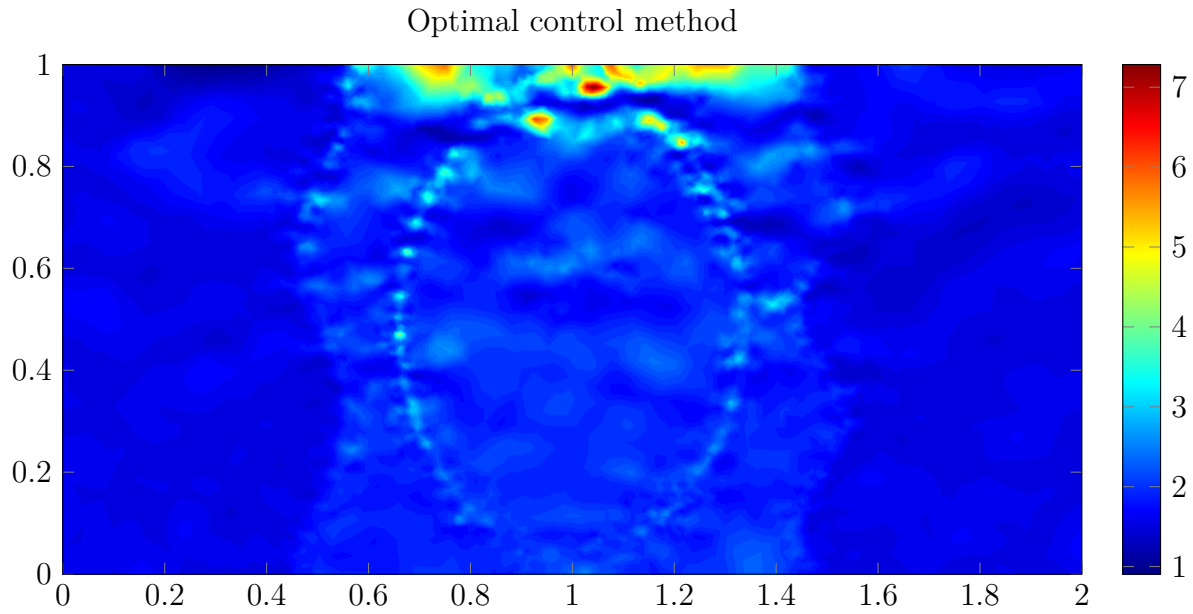

Figure 1.6.6 Reconstructed image with 20% measurement noise.

of times in order to get refined mesh near the conductivity jumps. We can see that besides being computationally lighter than the minimization method, the orthogonal field method allows a quantitative reconstruction of σ and shows details even in the low contrast zones. It is relatively stable with respect to measurement noise. Figures 1.6.7, 1.6.8, and 1.6.9 show the reconstruction with different measurement noise levels. Figure 1.6.10 shows the L^2 norm of the error with respect to measurement noise, with ε fixed at 10^{-3}. A smaller ε increases the noise sensibility at higher noise levels, but also improves the details and reduces the smoothing effect of the $\varepsilon\Delta$ term in (1.5.5).

1.7 Concluding remarks

In this chapter we have provided the mathematical basis of ultrasonically-induced Lorentz force electrical impedance tomography. The resolution of the reconstructed images is fixed by the ultrasound wavelength ,the width of the ultrasonic beam and the filter used in the deconvolution. It is possible, with this method, to get high resolution images of the electrical conductivity. We have designed two efficient algorithms for the reconstruction, and tested them numerically. The orthogonal field method performs much better than the optimization scheme in terms of both computational time and accuracy. In a forthcoming work, we intend to generalize our approach for imaging

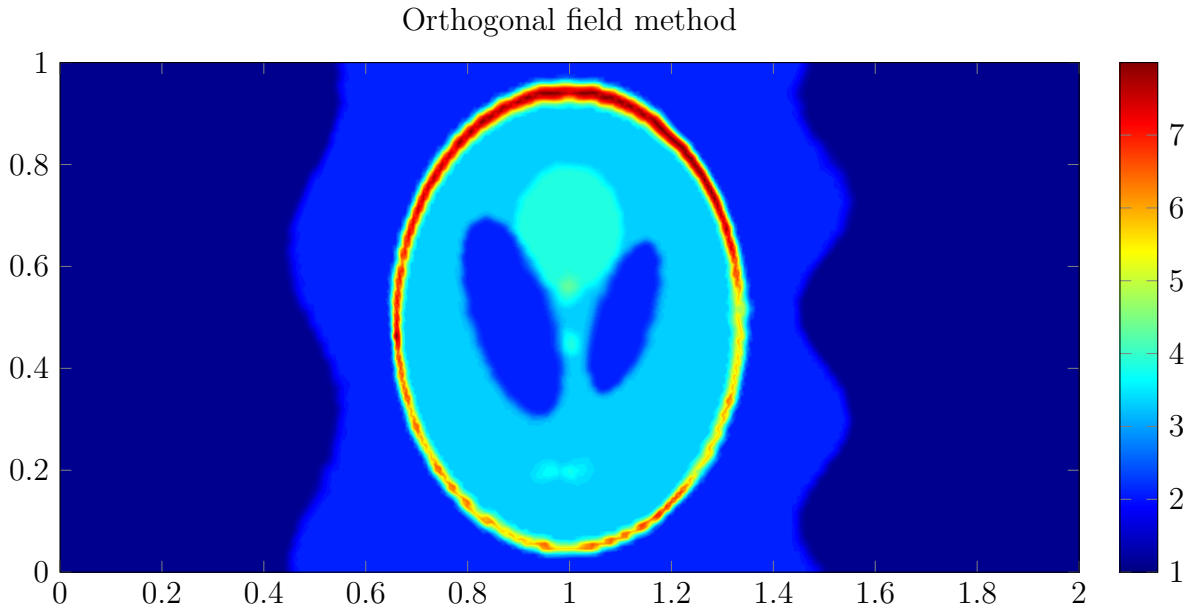

Figure 1.6.7 Reconstructed image without measurement noise.

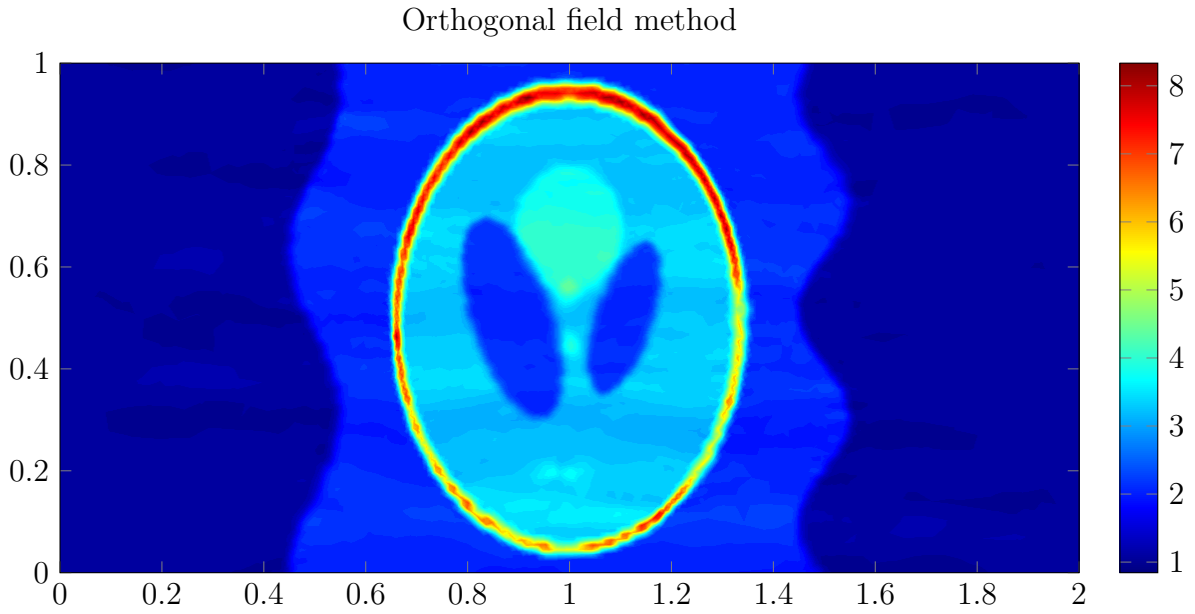

Figure 1.6.8 Reconstructed image with 2% measurement noise.

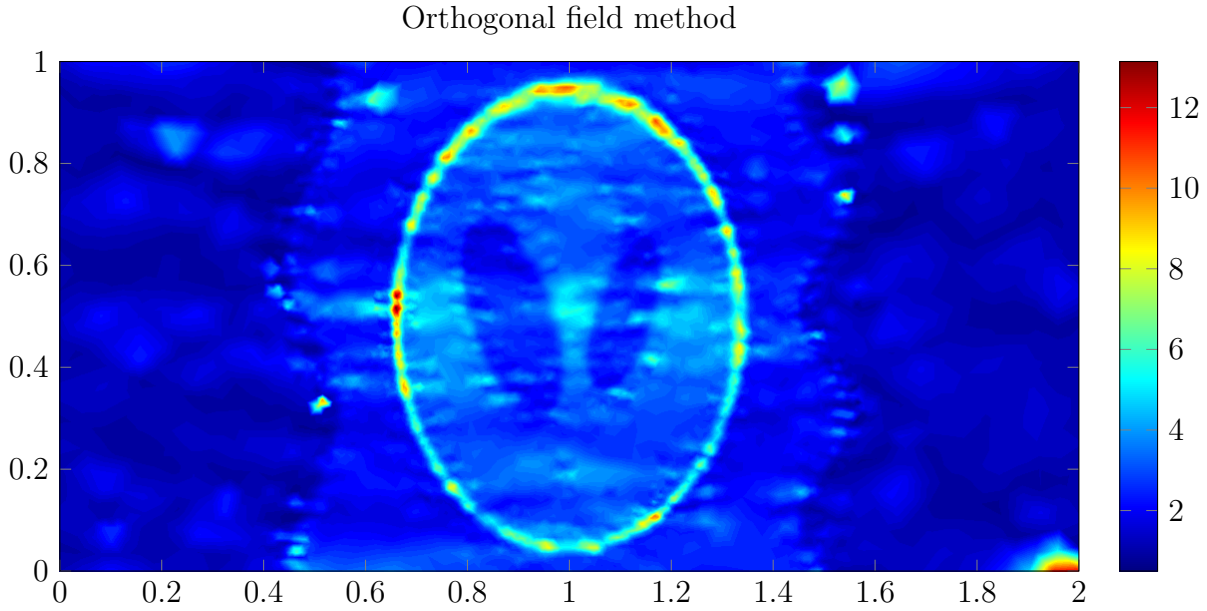

Figure 1.6.9 Reconstructed image with 20% measurement noise.

anisotropic conductivities by ultrasonically-induced Lorentz force [131]. We will also propose an algorithm to find $\sigma\nabla U$ from the data function ψ using (1.3.2) and correct the leading-order approximation (1.3.3). This will enhance the resolution of the reconstructed conductivity images. Another challenging problem under consideration is to interpret the high-frequency component of $M_{y,\xi}$ in terms of speckle conductivity contrasts.

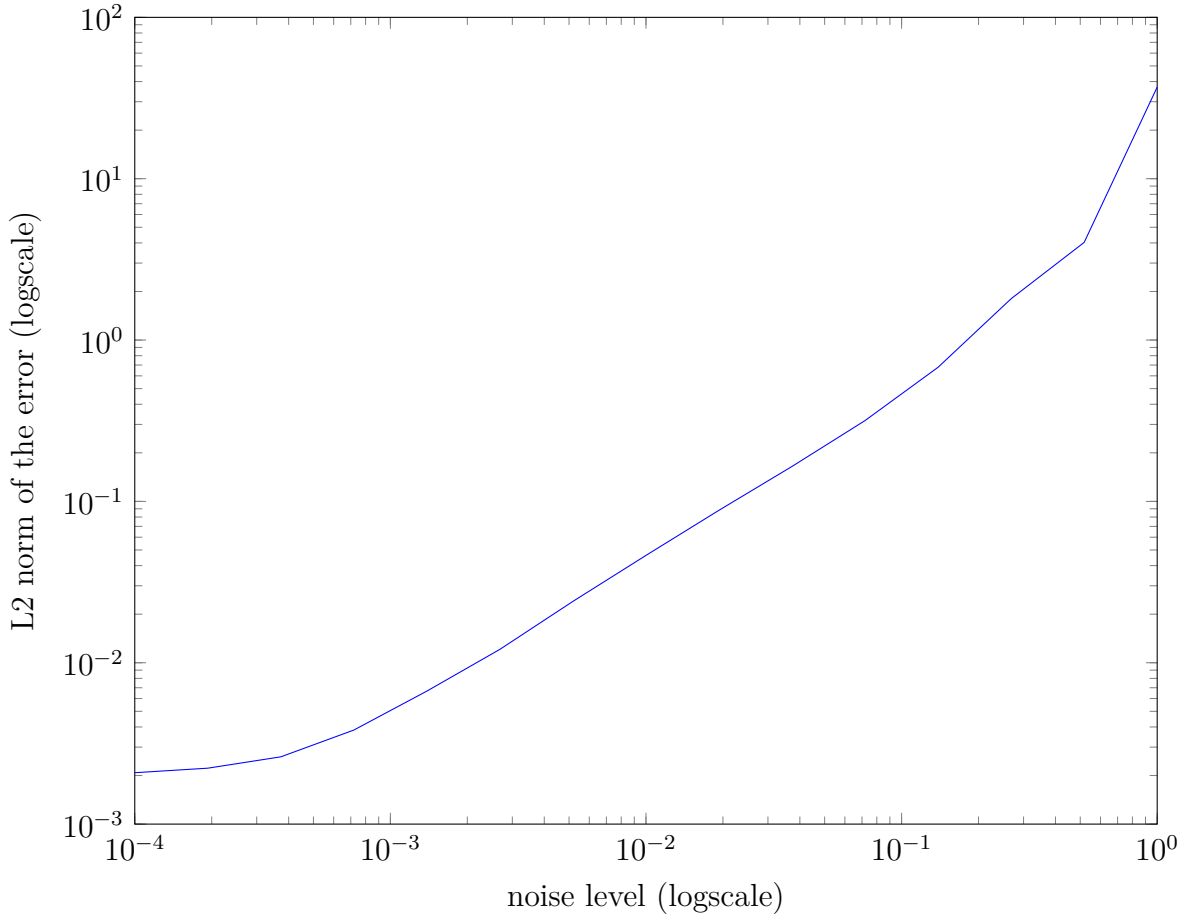

Figure 1.6.10 L^2 norm of the error with respect to the noise level

Chapter 2

Magneto-acoustic tomography with magnetic induction

Contents

2.1 Introduction

In this chapter we study a different technique based on the same acousto-magnetic coupling induced by Lorentz force we saw in chapter 1. However, the experimental apparatus is completely different.

In magnetoacoustic imaging with magnetic induction, magnetic fields are used to induce currents in the tissue. Ultrasound is generated by placing the tissue in a dynamic and static magnetic field. The dynamic field induces eddy currents and the static field leads to generation of acoustic vibration from Lorentz force on the induced currents. The divergence of the Lorentz force acts as acoustic source of propagating ultrasound waves that can be sensed by ultrasonic transducers placed around the tissue. The imaging problem is to obtain the conductivity distribution of the tissue from the acoustic source map; see [85, 86, 94, 95, 139].

We provide a rigorous mathematical and numerical framework for magnetoacoustic imaging with magnetic induction. We develop efficient methods for reconstructing the conductivity in the medium from the Lorentz force induced vibration. For doing so, we first estimate the electric current density in the tissue. Then we design efficient algorithms for reconstructing the heterogeneous conductivity map from the electric current density with the ultrasonic resolution.

The chapter is organized as follows. We start by describing the forward problem. Then we reconstruct from the acoustic measurements the divergence of the Lorentz force, which is acting as the source term in the acoustic wave equation. We recover the electric current density from the divergence of the Lorentz force, which reduces the problem to imaging the conductivity from the internal electric current density. We introduce three reconstruction schemes for solving the conductivity imaging problem from the internal electric current density. The first is an optimal control method. One of the contributions of this paper is the proof of convergence and stability of the optimal control approach provided that two magnetic excitation leading to nonparallel current densities are employed. Then we present a point fixed approach and prove that it convergences to the true conductivity image. Finally, we give an alternative to these iterative schemes via the use of a transport equation satisfied by the internal electric current density, similar to the one used in chapter 1. Our third algorithm is direct and can be viewed as a PDE-based reconstruction scheme. We test numerically the three proposed schemes in the presence of measurement noise, and also quantify their stability and resolution.

The feasibility of imaging of Lorentz-force-induced motion in conductive samples was shown in [36]. The magnetoacoustic tomography with magnetic induction in-

vestigated here was experimentally tested in [94, 95], and was reported to produce conductivity images of quality comparable to that of ultrasound images taken under similar conditions.

2.2 Forward problem description

2.2.1 Time scales involved

The forward problem in magnetoacoustic tomography with magnetic induction (MAT-MI) is multiscale in nature. The different phenomena involved in the experiment evolve on very different time scales. Precisely, there are three typical times that appear in the mathematical model for MAT-MI.

- The first one is the time needed for an electromagnetic wave to propagate in the medium and is denoted by τ_{em}. Typically, if the medium has a diameter of $1cm$, we have $\tau_{\text{em}} \sim 10^{-11}s$.
- The second characteristic time length, denoted by τ_{pulse} of the experiment is the time width of the magnetic pulse sent into the medium. Since, the time-varying magnetic field is generated by discharging a capacitor, τ_{pulse} is in fact the time needed to discharge the capacitor such that $\tau_{\text{pulse}} \sim 1\mu s$ [137].
- The third characteristic time, τ_{sound}, is the time consumed by the acoustic wave to propagate through the medium. The speed of sound is about $1.5 \cdot 10^3 m.s^{-1}$ so $\tau_{\text{sound}} \sim 6\mu s$ for a medium of $1cm$ diameter.

2.2.2 Electromagnetic model

Let $(\mathbf{e}_i)_{i=1,2,3}$ be an orthonormal basis of $\mathbb{R}^3$. Let Ω be a three-dimensional bounded $\mathcal{C}^1$ convex domain. The medium is assumed to be non magnetic, and its conductivity is given by σ (the question of the regularity of σ will arise later). Assume that the medium Ω is placed in a uniform, static magnetic field in the transverse direction $\mathbf{B}_0 = B_0\mathbf{e}_3$.

The magneto-quasistatic regime

At time $t = 0$ a second time varying magnetic field is applied in the medium. The time varying magnetic field has the form $\mathbf{B}_1(x,t) = B_1(x)u(t)\mathbf{e}_3$. B_1 is assumed to be a known smooth function and u is the shape of the stimulating pulse. The typical

width of the pulse is about $1\mu s$ so we are in presence of a slowly varying magnetic-field. This regime can be described by the magnetoquasistatic equations [83], where the propagation of the electrical currents is considered as instantaneous, but, the induction effects are not neglected. These governing equations in $\Omega \times \mathbb{R}_+$ are

$$\nabla \cdot \mathbf{B} = 0, \tag{2.2.1}$$

$$\nabla \times \mathbf{E} = -\frac{\partial \mathbf{B}}{\partial t}, \tag{2.2.2}$$

and

$$\nabla \cdot \mathbf{J} = 0, \tag{2.2.3}$$

where ε_0 is the permittivity of free space, $\mathbf{B}$ is the total magnetic field in the medium and $\mathbf{E}$ is the total electric field in the medium. Ohm's law is valid and is expressed as

$$\mathbf{J} = \sigma \mathbf{E} \quad \text{in } \Omega \times \mathbb{R}_+, \tag{2.2.4}$$

where σ is the electrical conductivity of the medium. For now on, we assume that $\sigma \in L^{\infty}_{a,b}(\Omega)$, where

$$L^{\infty}_{a,b}(\Omega) := \{f \in L^{\infty}(\Omega') : a < f < b \text{ in } \Omega', \quad f \equiv \sigma_0 \text{ in } \Omega \setminus \overline{\Omega'}\}$$

with σ_0, a, and b being three given positive constants, $0 < a < b$, and $\Omega' \Subset \Omega$.

As in [83], we use the Coulomb gauge ($\nabla \cdot \mathbf{A} = 0$) to express the potential representation of the fields $\mathbf{B}$ and $\mathbf{E}$. The magnetic field $\mathbf{B}$ is written as

$$\mathbf{B} = \nabla \times \mathbf{A}, \tag{2.2.5}$$

and the electric field $\mathbf{E}$ is then of the form

$$\mathbf{E} = -\nabla \widetilde{V} - \frac{\partial \mathbf{A}}{\partial t} \quad \text{in } \Omega \times \mathbb{R}_+, \tag{2.2.6}$$

where $\widetilde{V}$ is the electric potential. Writing $\mathbf{A}$ as follows:

$$\mathbf{A}(x,t) = \mathbf{A}_0(x) + \mathbf{A}_1(x)u(t),$$

where $\mathbf{A}_0$ and $\mathbf{A}_1$ are assumed to be smooth, we get from (2.2.3) and (2.2.6) that $\widetilde{V}(x,t) = V(x)u'(t)$ with V satisfying

$$\nabla \cdot \sigma \nabla V = -\nabla \cdot \sigma \mathbf{A}_1 \quad \text{in } \Omega \times \mathbb{R}_+.$$

The boundary condition on V can be set as a Neumann boundary condition. Since the medium Ω is usually embedded in a non-conductive medium (air), no currents leave the medium, i.e., $\mathbf{J} \cdot \boldsymbol{\nu} = 0$ on $\partial\Omega$, where $\boldsymbol{\nu}$ is the outward normal at $\partial\Omega$. To make sure that the boundary-value problem satisfied by V is well posed, we add the condition $\int_\Omega V = 0$. We have the following boundary value problem for V:

$$\begin{cases} \nabla \cdot \sigma \nabla V = -\nabla \cdot \sigma \mathbf{A}_1 & \text{in } \Omega, \\ \sigma \dfrac{\partial V}{\partial \nu} = -\sigma \mathbf{A}_1 \cdot \boldsymbol{\nu} & \text{on } \partial\Omega, \\ \displaystyle\int_\Omega V = 0. \end{cases} \tag{2.2.7}$$

2.2.3 The acoustic problem

Elasticity formulation

The eddy currents induced in the medium, combined with the magnetic field, create a Lorentz force based stress in the medium . The Lorentz force $\mathbf{f}$ is determined as

$$\mathbf{f} = \mathbf{J} \times \mathbf{B} \quad \text{in } \Omega \times \mathbb{R}_+. \tag{2.2.8}$$

Since the duration and the amplitude of the stimulation are both small, we assume that we can use the linear elasticity model. The displacements inside the medium can be described by the initial boundary-value problem for the Lamé system of equations

$$\begin{cases} \rho \partial_t^2 \mathbf{u} - \nabla \lambda \nabla \cdot \mathbf{u} - \nabla \cdot \mu \nabla^s \mathbf{u} = \mathbf{J} \times \mathbf{B} & \text{in } \Omega \times \mathbb{R}_+, \\ \dfrac{\partial \mathbf{u}}{\partial n} = 0 & \text{on } \partial\Omega \times \mathbb{R}_+, \\ \mathbf{u}(x,0) = \dfrac{\partial \mathbf{u}}{\partial t}(x,0) = 0 & \text{in } \Omega, \end{cases} \tag{2.2.9}$$

where λ and μ are the Lamé coefficients, ρ is the density of the medium at rest, and $\nabla^s \mathbf{u} = (\nabla \mathbf{u} + \nabla^T \mathbf{u})/2$ with the superscript T being the transpose. Here, $\partial/\partial n$ denotes

the co-normal derivative defined by

$$\frac{\partial \mathbf{u}}{\partial n} = \lambda(\nabla \cdot \mathbf{u})\boldsymbol{\nu} + 2\mu\nabla^s \mathbf{u}\,\boldsymbol{\nu} \quad \text{on } \partial\Omega,$$

where $\boldsymbol{\nu}$ is the outward normal at $\partial\Omega$. The functions λ, μ, and ρ are assumed to be positive, smooth functions on $\overline{\Omega}$.

The Neumann boundary condition, $\partial\mathbf{u}/\partial n = 0$ on $\partial\Omega$, comes from the fact that the sample is embedded in air and can move freely at the boundary.

The acoustic wave

Under some physical assumptions, the Lamé system of equations (2.2.9) can be reduced to an acoustic wave equation. For doing so, we neglect the shear effects in the medium by taking $\mu = 0$. The acoustic approximation says that the dominant wave type is a compressional wave. Equation (2.2.9) becomes

$$\begin{cases} \rho\partial_t^2 \mathbf{u} - \nabla\lambda\nabla\cdot\mathbf{u} = \mathbf{J}\times\mathbf{B} & \text{in } \Omega\times\mathbb{R}_+, \\ \dfrac{\partial \mathbf{u}}{\partial n} = 0 & \text{on } \partial\Omega\times\mathbb{R}_+, \\ \mathbf{u}(x,0) = \dfrac{\partial \mathbf{u}}{\partial t}(x,0) = 0 & \text{in } \Omega. \end{cases} \tag{2.2.10}$$

Introduce the pressure

$$p = \lambda\nabla\cdot\mathbf{u} \quad \text{in } \Omega\times\mathbb{R}_+.$$

Taking the divergence of (2.2.10) yields the acoustic wave equation

$$\begin{cases} \dfrac{1}{\lambda}\dfrac{\partial^2 p}{\partial t^2} - \nabla\cdot\dfrac{1}{\rho}\nabla p = \nabla\cdot\dfrac{1}{\rho}(\mathbf{J}\times\mathbf{B}) & \text{in } \Omega\times\mathbb{R}_+, \\ p = 0 & \text{on } \partial\Omega\times\mathbb{R}_+, \\ p(x,0) = \dfrac{\partial p}{\partial t}(x,0) = 0 & \text{in } \Omega. \end{cases} \tag{2.2.11}$$

We assume that the duration T_{pulse} of the electrical pulse sent into the medium is short enough so that p is the solution to

$$\begin{cases} \dfrac{1}{\lambda}\dfrac{\partial^2 p}{\partial t^2}(x,t) - \nabla\cdot\dfrac{1}{\rho}\nabla p(x,t) = f(x)\delta_{t=0} & \text{in } \Omega\times\mathbb{R}_+, \\ p = 0 & \text{on } \partial\Omega\times\mathbb{R}_+, \\ p(x,0) = \dfrac{\partial p}{\partial t}(x,0) = 0 & \text{in } \Omega, \end{cases} \tag{2.2.12}$$

where

$$f(x) = \int_0^{T_{\text{pulse}}} \nabla \cdot (\frac{1}{\rho}\mathbf{J}(x,t) \times \mathbf{B}(x,t))dt. \tag{2.2.13}$$

Note that acoustic wave reflection in soft tissue by an interface with air can be modeled well by a homogeneous Dirichlet boundary condition; see, for instance, [133].

Let

$$g(x,t) = \frac{\partial p}{\partial \nu}(x,t), \quad \forall (x,t) \in \partial\Omega \times \mathbb{R}_+.$$

In the next section, we aim at reconstructing the source term f from the data g.

2.3 Reconstruction of the acoustic source

In this subsection, we assume that $\lambda = \lambda_0 + \delta\lambda$ and $\rho = \rho_0 + \delta\rho$, where the functions $\delta\lambda$ and $\delta\rho$ are such that $||\delta\lambda||_{L^\infty(\Omega)} \ll \lambda_0$ and $||\delta\rho||_{L^\infty(\Omega)} \ll \rho_0$. We assume that λ, λ_0, ρ, and ρ_0 are known and denote by $c_0 = \sqrt{\frac{\lambda_0}{\rho_0}}$ the background acoustic speed.

We first consider the time-harmonic regime and define Γ^ω to be the outgoing fundamental solution to $\Delta + \frac{\omega^2}{c_0^2}$:

$$\left(\Delta_x + \frac{\omega^2}{c_0^2}\right)\Gamma^\omega(x,y) = \delta_y(x), \tag{2.3.1}$$

subject to the Sommerfeld radiation condition:

$$|x|^{\frac{1}{2}}\left(\frac{\partial}{\partial|x|}\Gamma^\omega(x,y) - i\frac{\omega}{c_0}\Gamma^\omega(x,y)\right) \longrightarrow 0, \quad |x| \to \infty.$$

We need the following integral operator $(\mathcal{K}_\Omega^\omega)^\star : L^2(\partial\Omega) \to L^2(\partial\Omega)$ given by

$$(\mathcal{K}_\Omega^\omega)^\star[\phi](x) = \int_{\partial\Omega} \frac{\partial\Gamma^\omega}{\partial\nu(x)}(x,y)\phi(y)\, ds(y).$$

Let G_Ω^ω be the Dirichlet Green function for $\Delta + \frac{\omega^2}{c_0^2}$ in Ω, i.e., for each $y \in \Omega$, $G_\Omega^\omega(x,y)$ is the solution to

$$\begin{cases} \left(\Delta_x + \frac{\omega^2}{c_0^2}\right) G_\Omega^\omega(x,y) = \delta_y(x), & x \in \Omega, \\ G_\Omega^\omega(x,y) = 0, & x \in \partial\Omega. \end{cases}$$

Let $\hat{p}$ denote the Fourier transform of the pressure p and $\hat{g}$ the Fourier transform of g. The function $\hat{p}$ is the solution to the Helmholtz equation:

$$\begin{cases} \dfrac{\omega^2}{\lambda(x)}\hat{p}(x,\omega) + \nabla \cdot \dfrac{1}{\rho(x)}\nabla\hat{p}(x,\omega) = f(x), & x \in \Omega, \\ \hat{p}(x,\omega) = 0, & x \in \partial\Omega. \end{cases}$$

Note that f is a real-valued function.

The Lippmann-Schwinger representation formula shows that

$$\begin{aligned} \hat{p}(x,\omega) = \int_\Omega (\frac{\rho_0}{\rho(y)} - 1)\nabla\hat{p}(y,\omega)\cdot\nabla G_\Omega^\omega(x,y)\,dy \\ - \omega^2 \int_\Omega (\frac{\rho_0}{\lambda(y)} - \frac{\rho_0}{\lambda_0})\hat{p}(y,\omega)G_\Omega^\omega(x,y)\,dy + \rho_0\int_\Omega f(y)G_\Omega^\omega(x,y)\,dy. \end{aligned}$$

Using the Born approximation , we obtain

$$\begin{aligned} \hat{p}(x,\omega) \;\approx\; & -\frac{1}{\rho_0}\int_\Omega \delta\rho(y)\nabla\hat{p}_0(y,\omega)\cdot\nabla G_\Omega^\omega(x,y)\,dy + \frac{\omega^2}{c_0^2}\int_\Omega \frac{\delta\lambda(y)}{\lambda_0}\hat{p}_0(y,\omega)G_\Omega^\omega(x,y)\,dy \\ & +\rho_0\int_\Omega f(y)G_\Omega^\omega(x,y)\,dy \end{aligned}$$

for $x \in \Omega$, where

$$\hat{p}_0(x,\omega) := \rho_0\int_\Omega f(y)G_\Omega^\omega(x,y)\,dy, \quad x \in \Omega.$$

Therefore, from the identity [26, Eq. (11.20)]

$$(\frac{1}{2}I + (\mathcal{K}_\Omega^\omega)^\star)\left[\frac{\partial G_\Omega^\omega}{\partial\nu_\cdot}(\cdot,y)\right](x) = \frac{\partial\Gamma^\omega}{\partial\nu(x)}(x,y), \quad x \in \partial\Omega, y \in \Omega,$$

it follows that

$$\begin{aligned} \left(\frac{1}{2}I + (\mathcal{K}_\Omega^\omega)^\star\right)[\hat{g}](x,\omega) \approx & -\frac{1}{\rho_0}\int_\Omega \delta\rho(y)\nabla\hat{p}_0(y,\omega)\cdot\nabla\frac{\partial\Gamma^\omega(x,y)}{\partial\nu(x)}\,dy \\ & + \frac{\omega^2}{c_0^2}\int_\Omega \frac{\delta\lambda(y)}{\lambda_0}\hat{p}_0(y,\omega)\frac{\partial\Gamma^\omega(x,y)}{\partial\nu(x)}\,dy + \rho_0\int_\Omega f(y)\frac{\partial\Gamma^\omega(x,y)}{\partial\nu(x)}\,dy \end{aligned}$$

for $x \in \partial\Omega$.

Introduce

$$I(z,\omega) := \int_{\partial\Omega}\left[\overline{\Gamma^\omega}(x,z)(\frac{1}{2}I + (\mathcal{K}_\Omega^\omega)^\star)[\hat{g}](x,\omega) - \Gamma^\omega(x,z)\overline{(\frac{1}{2}I + (\mathcal{K}_\Omega^\omega)^\star)[\hat{g}]}(x,\omega)\right]ds(x)$$

for $z \in \Omega$.

We recall the Helmholtz-Kirchoff identity [19, Lemma 2.32]

$$\int_{\partial\Omega} \left[\overline{\Gamma^\omega}(x,z) \frac{\partial \Gamma^\omega(x,y)}{\partial \nu(x)} - \Gamma^\omega(x,z) \overline{\frac{\partial \Gamma^\omega(x,y)}{\partial \nu(x)}} \right] ds(x) = 2i \Im m \Gamma^\omega(z,y).$$

We also recall that f is real-valued and write $f \approx f^{(0)} + \delta f$. Given $I(z,\omega)$ we solve the deconvolution problem

$$2i\rho_0 \int_\Omega \Im m \Gamma^\omega(z,y) f^{(0)}(y)\, dy = I(z,\omega), \quad z \in \Omega, \tag{2.3.2}$$

in order to reconstruct $f^{(0)}$ with a resolution limit determined by the Rayleigh criteria. Once $f^{(0)}$ is determined, we solve the second deconvolution problem (2.3.3)

$$2i\rho_0 \int_\Omega \Im m \Gamma^\omega(z,y) \delta f(y)\, dy = \delta I(z,\omega), \quad z \in \Omega, \tag{2.3.3}$$

to find the correction δf. Here,

$$\delta I(z,\omega) := \int_{\partial\Omega} \left[\overline{\Gamma^\omega}(x,z) \delta\hat{g}(x,\omega) \; - \Gamma^\omega(x,z) \overline{\delta\hat{g}}(x,\omega) \right] ds(x)$$

with

$$\delta\hat{g}(x,\omega) = \frac{1}{\rho_0} \int_\Omega \delta\rho(y) \nabla \hat{p}^{(0)}(y,\omega) \cdot \nabla \frac{\partial \Gamma^\omega(x,y)}{\partial \nu(x)}\, dy + \frac{\omega^2}{c_0^2} \int_\Omega \frac{\delta\lambda(y)}{\lambda_0} \hat{p}^{(0)}(y,\omega) \frac{\partial \Gamma^\omega(x,y)}{\partial \nu(x)}\, dy,$$

and

$$\hat{p}^{(0)}(x,\omega) := \rho_0 \int_\Omega f^{(0)}(y) G^\omega_\Omega(x,y)\, dy, \quad x \in \Omega.$$

Since by Fourier transform, $\hat{g}$ is known for all $\omega \in \mathbb{R}_+$, $I(z,\omega)$ can be computed for all $\omega \in \mathbb{R}_+$. Then from the identity [19, Eq. (1.35)]

$$\frac{2}{\pi} \int_{\mathbb{R}_+} \omega \Im m \Gamma^\omega(x,z)\, d\omega = -\delta_z(x),$$

where δ_z is the Dirac mass at z, it follows that

$$f^{(0)}(z) = \frac{1}{i\pi\rho_0} \int_{\mathbb{R}_+} \omega I(z,\omega)\, d\omega \quad \text{and } \delta f(z) = \frac{1}{i\pi\rho_0} \int_{\mathbb{R}_+} \omega \delta I(z,\omega)\, d\omega.$$

We refer to [33, 34] and the references therein for source reconstruction approaches with finite set of frequencies.

2.4 Reconstruction of the conductivity

We assume that we have reconstructed the pressure source f given by (2.2.13). We also assume that the sample Ω is thin and hence can be assimilated to a two dimensional domain. Further, we suppose that $\Omega \subset \text{vect}\,(\mathbf{e}_1, \mathbf{e}_2)$. Recall that the magnetic fields $\mathbf{B}_0$ and $\mathbf{B}_1$ are parallel to $\mathbf{e}_3$. We write $\mathbf{J}(x,t) = \mathbf{J}(x)u'(t)$. In order to recover the conductivity distribution, we start by reconstructing the vector field $\mathbf{J}(x)$ in Ω.

2.4.1 Reconstruction of the electric current density

Helmholtz decomposition

Let $H^1(\Omega) := \{v \in L^2(\Omega) : \nabla v \in L^2(\Omega)\}$. Let $H_0^1(\Omega)$ be the set of functions in $H^1(\Omega)$ with trace zero on $\partial\Omega$ and let $H^{-1}(\Omega)$ be the dual of $H_0^1(\Omega)$.

We need the following two classical results.

Lemma 2.4.1. *If $\sigma \in L^\infty_{a,b}(\Omega)$ then the solution V of (2.2.7) belongs to $H^1(\Omega)$ and hence, the electric current density $\mathbf{J}$ belongs to $L^2(\Omega)$.*

The following Helmholtz decomposition in two dimensions holds [128].

Lemma 2.4.2. *If $\mathbf{f}$ is a vector field in $L^2(\Omega)$, then there exist two functions $v \in H^1(\Omega)$ and $w \in H^1(\Omega)$ such that*

$$\mathbf{f} = \nabla v + \boldsymbol{curl}\; w. \tag{2.4.1}$$

*The differential operator **curl** is defined by **curl** $w = (-\partial_2 w, \partial_1 w)$. Furthermore, if $\nabla \cdot \mathbf{f} \in L^2(\Omega)$, then the potential v is a solution to*

$$\begin{cases} -\Delta v = \nabla \cdot \mathbf{f} & \text{in } \Omega, \\ \dfrac{\partial v}{\partial \nu} = \mathbf{f} \cdot \boldsymbol{\nu} & \text{on } \partial\Omega, \end{cases} \tag{2.4.2}$$

and w is the unique solution of

$$\int_\Omega \boldsymbol{curl}\; w \cdot \boldsymbol{curl}\; \phi = \int_\Omega (\mathbf{f} - \nabla v) \cdot \boldsymbol{curl}\; \phi, \quad \forall \phi \in H(\Omega), \tag{2.4.3}$$

where $H(\Omega) = \{\phi \in L^2(\Omega), \nabla \times \phi \in L^2(\Omega), \nabla \cdot \phi = 0\}$. The problem can be written in strong form in $H^{-1}(\Omega)$:

$$\begin{cases} -\Delta w = curl\, \mathbf{f} & \text{in } \Omega, \\ w = 0 & \text{on } \partial\Omega, \end{cases}$$

where the operator curl is defined on vector fields by curl $\mathbf{f} = -\partial_2 f_1 + \partial_1 f_2$.

We apply the Helmholtz decomposition (2.4.1) to the vector field $\mathbf{J} \in L^2(\Omega)$ and get the following proposition.

Proposition 2.4.3. *There exists a function $w \in H$ such that*

$$\mathbf{J} = \boldsymbol{curl}\ w, \tag{2.4.4}$$

and w is the unique solution of

$$\begin{cases} -\Delta w = curl\ \mathbf{J} & in\ \Omega, \\ w = 0 & on\ \partial\Omega. \end{cases} \tag{2.4.5}$$

Recall (2.2.3):

$$\nabla \cdot \mathbf{J} = 0,$$

together with the fact that no current leaves the medium

$$\mathbf{J} \cdot \boldsymbol{\nu} = 0 \quad \text{on } \partial\Omega,$$

we get that, since v is a solution to (2.2.7) v has to be constant: $v \in \mathbb{R}$. So, in order to reconstruct $\mathbf{J}$ one just needs to reconstruct w.

Recovery of J

Under the assumption $|\mathbf{B}_1| \ll |\mathbf{B}_0|$ in $\Omega \times \mathbb{R}_+$ and $|\delta\rho| \ll \rho_0$ in Ω, the pressure source term f defined by (2.2.13) can be approximated as follows:

$$f(x) \approx \frac{1}{\rho_0} \nabla \cdot (\mathbf{J}(x) \times \mathbf{B}_0)(u(T_{\text{pulse}}) - u(0)),$$

where we have used that $\mathbf{J}(x,t) = \mathbf{J}(x)u'(t)$.

Since $\mathbf{B}_0$ is constant we get

$$\nabla \cdot (\mathbf{J}(x) \times \mathbf{B}_0) = (\nabla \times \mathbf{J}) \cdot \mathbf{B}_0 = |\mathbf{B}_0| \text{curl } \mathbf{J}.$$

Now, since $\mathbf{B}_0$ is known, we can compute w as the unique solution of

$$\begin{cases} -\Delta w = \dfrac{\rho_0 f}{|\mathbf{B}_0|(u(T_{\text{pulse}}) - u(0))} & \text{in } \Omega, \\ w = 0 & \text{on } \partial\Omega, \end{cases}$$

and then, by Proposition 2.4.3, compute $\mathbf{J}$ by $\mathbf{J} = \mathbf{curl}\ w$.

Note that since the problem is reduced to the two dimensional case, $\mathbf{J}$ is then contained in the plane $\mathbf{B}_0^\top$ with $\top$ denoting the orthogonal.

2.4.2 Recovery of the conductivity from internal electric current density

In this subsection we denote by $\sigma_\star$ the true conductivity of the medium, and we assume that $\sigma_\star \in L^\infty_{a,b}(\Omega)$ with $0 < a < b$, i.e., it is bounded from below and above by positive known constants and is equal to some given positive constant σ_0 in a neighborhood of $\partial\Omega$.

Optimal control method

Recall that $\mathbf{A}_1$ is defined by $\nabla \cdot \mathbf{A}_1 = 0, B_1(x)\mathbf{e}_3 = \nabla \times \mathbf{A}_1(x)$. Define the following operator $\mathcal{F}$:

$$\begin{aligned} L^\infty_{a,b}(\Omega) &\longrightarrow H^1(\Omega) \\ \sigma &\longmapsto \mathcal{F}[\sigma] \end{aligned}$$

with

$$\mathcal{F}[\sigma] := U \begin{cases} \nabla \cdot \sigma \nabla U = -\nabla \cdot \sigma \mathbf{A}_1 & \text{in } \Omega, \\ \sigma \dfrac{\partial U}{\partial \nu} = -\sigma \mathbf{A}_1 \cdot \boldsymbol{\nu} & \text{on } \partial\Omega, \\ \displaystyle\int_\Omega U = 0. \end{cases} \tag{2.4.6}$$

The following lemma holds.

Lemma 2.4.4. *The operator $\mathcal{F}$ is Fréchet differentiable. For any $\sigma \in L^\infty_{a,b}(\Omega)$ and h such that $\sigma + h \in L^\infty_{a,b}(\Omega)$, we have*

$$d\mathcal{F}[\sigma](h) := q \begin{cases} \nabla \cdot \sigma \nabla q = -\nabla \cdot h\mathbf{A}_1 - \nabla \cdot h \nabla \mathcal{F}[\sigma] & \textit{in } \Omega, \\ \sigma \dfrac{\partial q}{\partial \nu} = 0 & \textit{on } \partial\Omega, \\ \displaystyle\int_\Omega q = 0. \end{cases} \tag{2.4.7}$$

Proof. Denote by r the function $\mathcal{F}[\sigma + h] - \mathcal{F}[\sigma] - q$. The function r belongs to $H^1(\Omega)$ and satisfies the following equation in Ω:

$$\nabla \cdot \sigma \nabla r = \nabla \cdot h \nabla \left(\mathcal{F}[\sigma] - \mathcal{F}[\sigma + h] \right),$$

together with the boundary condition

$$\frac{\partial r}{\partial \nu} = 0 \quad \text{on } \partial\Omega,$$

and the zero mean condition $\int_\Omega r = 0$. We have the following estimate:

$$\|\nabla r\|_{L^2(\Omega)} \leq \frac{1}{a}\|h\|_{L^\infty(\Omega)}\|\nabla\left(\mathcal{F}[\sigma] - \mathcal{F}[\sigma+h]\right)\|_{L^2(\Omega)}.$$

Since $\mathcal{F}[\sigma] - \mathcal{F}[\sigma+h]$ satisfies

$$\nabla\cdot\left(\sigma\nabla\left(\mathcal{F}[\sigma] - \mathcal{F}[\sigma+h]\right)\right) = -\nabla\cdot\left(h\nabla\mathcal{F}[\sigma+h]\right) + \nabla\cdot\left(h\mathbf{A}_1\right)$$

with the boundary condition

$$\frac{\partial}{\partial\nu}\left(\mathcal{F}[\sigma+h] - \mathcal{F}[\sigma]\right) = 0,$$

and the zero mean condition $\int_\Omega \left(\mathcal{F}[\sigma+h] - \mathcal{F}[\sigma]\right) = 0$. We can also estimate the L^2-norm of $\nabla\left(\mathcal{F}[\sigma+h] - \mathcal{F}[\sigma]\right)$ as follows:

$$\|\nabla\left(\mathcal{F}[\sigma+h] - \mathcal{F}[\sigma]\right)\|_{L^2(\Omega)} \leq \frac{1}{a}\|h\|_{L^\infty(\Omega)}\left(\|\nabla\mathcal{F}[\sigma+h]\|_{L^2(\Omega)} + \|\mathbf{A}_1\|_{L^2(\Omega)}\right).$$

Therefore, we can bound the H^1-norm of $\mathcal{F}[\sigma+h]$ independently of σ and h for $||h||_{L^\infty}$ small enough. There exists a constant C, depending only on Ω, a, b, and $\mathbf{A}_1$, such that

$$\|\nabla\mathcal{F}[\sigma+h]\|_{L^2(\Omega)} \leq C.$$

Hence, we get

$$\|\nabla\left(\mathcal{F}[\sigma+h] - \mathcal{F}[\sigma]\right)\|_{L^2(\Omega)} \leq \frac{1}{a}\|h\|_{L^\infty(\Omega)}\left(C + \|\mathbf{A}_1\|_{L^2(\Omega)}\right),$$

and therefore,

$$\|\nabla r\|_{L^2(\Omega)} \leq \widetilde{C}\|h\|^2_{L^\infty(\Omega)},$$

which shows the Fréchet differentiability of $\mathcal{F}$. □

Now, we introduce the misfit functional:

$$\begin{aligned} L^\infty_{a,b} &\longrightarrow \mathbb{R} \\ \sigma &\longmapsto \mathcal{J}[\sigma] = \frac{1}{2}\int_\Omega |\sigma\nabla\left(\mathcal{F}[\sigma] + \mathbf{A}_1\right) - \mathbf{J}|^2, \end{aligned} \tag{2.4.8}$$

Lemma 2.4.5. *The misfit functional $\mathcal{J}$ is Fréchet-differentiable. For any $\sigma \in L^\infty_{a,b}(\Omega)$, we have*

$$d\mathcal{J}[\sigma] = (\sigma\nabla\mathcal{F}[\sigma] + \sigma\mathbf{A}_1 - \mathbf{J}) \cdot (\nabla\mathcal{F}[\sigma] + \mathbf{A}_1) + \sigma\nabla s \cdot (\mathbf{A}_1 - \nabla\mathcal{F}[\sigma]),$$

where s is defined as the solution to the adjoint problem

$$\begin{cases} \nabla \cdot \sigma\nabla s = \nabla \cdot \left(\sigma^2\nabla\mathcal{F}[\sigma] + \sigma^2\mathbf{A}_1 - \sigma\mathbf{J}\right) & \text{in } \Omega, \\ \sigma\dfrac{\partial s}{\partial \nu} = 0 & \text{on } \partial\Omega, \\ \displaystyle\int_\Omega s = 0. \end{cases} \tag{2.4.9}$$

Proof. Since $\mathcal{F}$ is Fréchet-differentiable, so is $\mathcal{J}$. For any $\sigma \in L^\infty_{a,b}(\Omega)$ and h such that $\sigma + h \in L^\infty_{a,b}(\Omega)$, we have

$$d\mathcal{J}[\sigma](h) = \int_\Omega (\sigma\nabla\mathcal{F}[\sigma] + \sigma\mathbf{A}_1 - \mathbf{J}) \cdot (h\nabla(\mathcal{F}[\sigma] + \mathbf{A}_1) + \sigma\nabla(d\mathcal{F}[\sigma](h))).$$

Multiplying (2.4.9) by $d\mathcal{F}[\sigma](h)$ we get

$$\int_\Omega \sigma\,(\sigma\nabla\mathcal{F}[\sigma] + \sigma\mathbf{A}_1 - \mathbf{J}) \cdot \nabla d\mathcal{F}[\sigma](h) = \int_\Omega \sigma\nabla s \cdot \nabla d\mathcal{F}[\sigma](h).$$

On the other hand, multiplying (2.4.7) by s we obtain

$$\int_\Omega \sigma\nabla s \cdot \nabla d\mathcal{F}[\sigma](h) = \int_\Omega \sigma h\nabla s \cdot (\mathbf{A}_1 - \nabla\mathcal{F}[\sigma]).$$

So we have

$$d\mathcal{J}[\sigma](h) = \int_\Omega h\Big[(\sigma\nabla\mathcal{F}[\sigma] + \sigma\mathbf{A}_1 - \mathbf{J}) \cdot (\nabla\mathcal{F}[\sigma] + \mathbf{A}_1) + \sigma\nabla s \cdot (\mathbf{A}_1 - \nabla\mathcal{F}[\sigma]) \Big],$$

and the proof is complete. □

Lemma 2.4.5 allows us to apply the gradient descent method in order to minimize the discrepancy functional $\mathcal{J}$. Let $\sigma_{(0)}$ be an initial guess. We compute the iterates

$$\sigma_{(n+1)} = T[\sigma_{(n)}] - \mu d\mathcal{J}[T[\sigma_{(n)}]], \quad \forall n \in \mathbb{N}, \tag{2.4.10}$$

where $\mu > 0$ is the step size and $T[f] = \min\{\max\{f, a\}, b\}$.

In the sequel, we prove the convergence of (2.4.10) with two excitations. Let $\mathbf{J}^{(1)}$ and $\mathbf{J}^{(2)}$ correspond to two different excitations $\mathbf{A}_1^{(1)}$ and $\mathbf{A}_1^{(2)}$. Assume that $\mathbf{J}^{(1)} \times \mathbf{J}^{(2)} \neq 0$

in Ω. Let $\mathcal{G}^{(i)} : \sigma \mapsto \sigma\nabla\left(\mathcal{F}^{(i)}[\sigma] + \mathbf{A}_1^{(i)}\right) - \mathbf{J}_i$, where $\mathcal{F}^{(i)}$ is defined by (2.4.7) with $\mathbf{A}_1 = \mathbf{A}_1^{(i)}$ for $i = 1, 2$. The optimal control algorithm (2.4.10) with two excitations is equivalent to the following Landweber scheme given by

$$\sigma_{(n+1)} = T[\sigma_{(n)}] - \mu d\mathcal{G}^{\star}[\mathcal{G}[T[\sigma_{(n)}]]], \quad \forall n \in \mathbb{N}, \tag{2.4.11}$$

where $\mathcal{G}[\sigma] = (\mathcal{G}^{(1)}[\sigma], \mathcal{G}^{(2)}[\sigma])^T$.

Following [23], we prove the convergence and stability of (2.4.11) provided that two magnetic excitations leading to nonparallel current densities are employed.

Proposition 2.4.6. *Let $\mathbf{J}^{(1)}$ and $\mathbf{J}^{(2)}$ correspond to two different excitations. Assume that $\mathbf{J}^{(1)} \times \mathbf{J}^{(2)} \neq 0$ in Ω. Then there exists $\eta > 0$ such that if $||\sigma_{(0)} - \sigma_\star||_{H_0^1(\Omega)} \leq \eta$, then $||\sigma_{(n)} - \sigma_\star||_{H_0^1(\Omega)} \to 0$ as $n \to +\infty$.*

Proof. According to [23], it suffices to prove that there exists a positive constant C such that

$$||d\mathcal{G}[\sigma](h)||_{H^1(\Omega)} \geq C||h||_{H_0^1(\Omega)} \tag{2.4.12}$$

for all $h \in H_0^1(\Omega)$ such that $\sigma + h \in L_{a,b}^{\infty}(\Omega)$. We have

$$d\mathcal{G}^{(i)}[\sigma](h) = h\mathbf{J}^{(i)} + \sigma\nabla d\mathcal{F}^{(i)}[\sigma](h).$$

Therefore,

$$\nabla \cdot d\mathcal{G}^{(i)}[\sigma](h) = 0, \quad d\mathcal{G}^{(i)}[\sigma](h) \cdot \boldsymbol{\nu} = 0,$$

and

$$\nabla \times (\frac{1}{\sigma} d\mathcal{G}^{(i)}[\sigma](h)) = h\nabla \times (\frac{1}{\sigma}\mathbf{J}^{(i)}) + \sigma\nabla h \times \mathbf{J}^{(i)}.$$

Since $\nabla \times (\frac{1}{\sigma}\mathbf{J}^{(i)}) \times \mathbf{e}_3 = 0$ and $\mathbf{J}^{(1)} \times \mathbf{J}^{(2)} \neq 0$, it follows that

$$||h||_{H_0^1(\Omega)} \leq C \sum_{i=1}^{2} ||d\mathcal{G}^{(i)}[\sigma](h)||_{H^1(\Omega)},$$

which completes the proof. □

Let $\mathcal{F}[\sigma] = (\mathcal{F}^{(1)}[\sigma], \mathcal{F}^{(2)}[\sigma])^T$. Note that analogously to (2.4.12) there exists a positive constant C such that

$$||d\mathcal{F}[\sigma](h)||_{H^1(\Omega)} \geq C||h||_{H_0^1(\Omega)}$$

for all $h \in H_0^1(\Omega)$ such that $\sigma + h \in L_{a,b}^{\infty}(\Omega)$, provided that $\mathbf{J}^{(1)} \times \mathbf{J}^{(2)} \neq 0$ in Ω.

Fixed point method

In this subsection, we denote by $\sigma_\star$ the true conductivity inside the domain Ω. We also make the following assumptions:

- $\exists c > 0, \quad$ such that $|\mathbf{B}_1| > c \quad$ in Ω;
- $\sigma \in \mathcal{C}^{0,\alpha}(\overline{\Omega}), \quad \alpha \in]0,1[$;
- $\sigma_\star = \sigma_0$ in an open neighborhood of $\partial\Omega$.

From the unique continuation principle, the following lemma holds.

Lemma 2.4.7. *The set* $\{x \in \Omega, \mathbf{J}(x) = 0\}$ *is nowhere dense.*

The interior data is $\mathbf{J} = \sigma_\star [\nabla \mathcal{F}[\sigma_\star] + \mathbf{A}_1]$. One can only hope to recover $\sigma_\star$ at the points where $\mathbf{J} \neq 0$. Even then, we can expect any type of reconstruction to be numerically unstable in sets where $\mathbf{J}$ is very small. For every $\varepsilon > 0$, we define the set

$$\Omega_\varepsilon := \{x \in \Omega,\ |\mathbf{J}(x)| > \varepsilon\}.$$

One can assume that Ω_ε is a C^1 domain without loosing generality. (If it is not, just replace Ω_ε by a smooth domain contained in Ω_ε). Now, introduce the operator $\mathcal{F}_\varepsilon$:

$$\begin{aligned} L^\infty_{a,b}(\Omega_\varepsilon) &\longrightarrow H^1(\Omega_\varepsilon) \\ \sigma &\longmapsto \mathcal{F}_\varepsilon[\sigma] := V_\varepsilon, \end{aligned}$$

where V_ε satisfies the following equation:

$$\begin{cases} \nabla \cdot \sigma \nabla V_\varepsilon = -\nabla \cdot (\sigma \mathbf{A}_1) & \text{in } \Omega_\varepsilon, \\ \sigma \dfrac{\partial V_\varepsilon}{\partial \nu} = -\sigma \mathbf{A}_1 \cdot \boldsymbol{\nu} + \mathbf{J} \cdot \boldsymbol{\nu} & \text{on } \partial\Omega_\varepsilon, \\ \displaystyle\int_{\Omega_\varepsilon} V_\varepsilon = 0, \end{cases} \tag{2.4.13}$$

where $\boldsymbol{\nu}$ denotes the outward normal to $\partial\Omega_\varepsilon$. Note that $\int_{\partial\Omega_\varepsilon} \mathbf{J} \cdot \boldsymbol{\nu} = 0$ since $\nabla \cdot \mathbf{J} = 0$ in Ω_ε.

We also define the nonlinear operator $\mathcal{G}_\varepsilon$ by

$$\begin{aligned} L^\infty_{a,b}(\Omega_\varepsilon) &\longrightarrow L^\infty(\Omega_\varepsilon) \\ \sigma &\longmapsto \mathcal{G}_\varepsilon[\sigma] := \sigma \frac{(\sigma \nabla V_\varepsilon[\sigma] + \sigma \mathbf{A}_1) \cdot \mathbf{J}}{|\mathbf{J}|^2}. \end{aligned} \tag{2.4.14}$$

Lemma 2.4.8. *The restriction of $\sigma_\star$ on Ω_ε is a fixed point for the operator $\mathcal{G}_\varepsilon$.*

Proof. For the existence it suffices to prove that $\mathcal{F}_\varepsilon\left[\sigma_\star|_{\Omega_\varepsilon}\right] = \mathcal{F}[\sigma_\star]\Big|_{\Omega_\varepsilon}$. Denote by $V_\star = \mathcal{F}[\sigma_\star]$. We can see that $V_\star$ satisfies

$$\nabla \cdot \sigma_\star \nabla V_\star = -\nabla \cdot (\sigma \mathbf{A}_1) \quad \text{in } \Omega_\varepsilon.$$

Taking the normal derivative along the boundary of Ω_ε, we get

$$\sigma \frac{\partial V_\star}{\partial \nu} = -\sigma \mathbf{A}_1 \cdot \boldsymbol{\nu} + \mathbf{J} \cdot \boldsymbol{\nu} \quad \text{on } \partial\Omega_\varepsilon.$$

From the well posedness of (2.4.13), it follows that

$$V_\star\Big|_{\Omega_\varepsilon} = \mathcal{F}_\varepsilon[\sigma_\star\Big|_{\Omega_\varepsilon}] + c, \quad c \in \mathbb{R}.$$

So, we arrive at

$$\mathcal{G}_\varepsilon\left[\sigma_\star\Big|_{\Omega_\varepsilon}\right] = \sigma_\star\Big|_{\Omega_\varepsilon}.$$

□

We need the following lemma. We refer to [128] for its proof.

Lemma 2.4.9. *Let $\Omega \subset \mathbb{R}^2$ be a bounded domain with Lipschitz boundary. For each $g \in H^{-1}(\Omega)$ there exists at least one $\mathbf{v} \in L^2(\Omega)$ with $\nabla \cdot \mathbf{v} = g$ in the sense of the distributions and*

$$\|\mathbf{v}\|_{L^2(\Omega)} \leq C\|g\|_{H^{-1}(\Omega)}$$

with the constant C depending only on Ω.

The following result holds.

Lemma 2.4.10. *If $\|\mathbf{A}_1\|_{L^2(\Omega_\varepsilon)}$ is small enough, then the operator $\mathcal{G}_\varepsilon$ is a contraction.*

Proof. Take σ_1 and σ_2 in $L^\infty_{a,b}(\Omega)$. We have

$$\begin{aligned}|\mathcal{G}_\varepsilon[\sigma_1](x) - \mathcal{G}_\varepsilon[\sigma_2](x)| &= \frac{1}{|\mathbf{J}(x)|^2} \\ &\times \left|\left(\sigma_1^2(x)\nabla V_\varepsilon[\sigma_1](x) - \sigma_2^2(x)\nabla V_\varepsilon[\sigma_2](x) + \left(\sigma_1^2(x) - \sigma_2^2(x)\right)\mathbf{A}_1(x)\right) \cdot \mathbf{J}(x)\right|,\end{aligned}$$

which gives, using the Cauchy-Schwartz inequality:

$$|\mathcal{G}_\varepsilon[\sigma_1](x) - \mathcal{G}_\varepsilon[\sigma_2](x)| \leq \frac{1}{\varepsilon} \times \left|\left(\sigma_1^2(x)\nabla V_\varepsilon[\sigma_1](x) - \sigma_2^2(x)\nabla V_\varepsilon[\sigma_2](x) + \left(\sigma_1^2(x) - \sigma_2^2(x)\right)\mathbf{A}_1(x)\right)\right|.$$

The right-hand side can be rewritten using the fact that $|\sigma_i(x)| \leq b$ for $i = 1, 2$, and hence,

$$|\mathcal{G}_\varepsilon[\sigma_1](x) - \mathcal{G}_\varepsilon[\sigma_2](x)| \leq \frac{b}{\varepsilon} \times \left[|\sigma_1(x)\nabla V_\varepsilon[\sigma_1](x) - \sigma_2(x)\nabla V_\varepsilon[\sigma_2](x)| + |(\sigma_1(x) - \sigma_2(x))\,\mathbf{A}_1(x)|\right]. \quad (2.4.15)$$

Now, consider the function $\mathbf{v} = \sigma_1\nabla V_\varepsilon[\sigma_1] - \sigma_2\nabla V_\varepsilon[\sigma_2]$. We get

$$\nabla\cdot\mathbf{v} = -\nabla\cdot\left[(\sigma_1 - \sigma_2)\,\mathbf{A}_1\right] \quad \text{in } \partial\Omega_\varepsilon,$$

along with the boundary condition $\mathbf{v}\cdot\boldsymbol{\nu} = 0$ on $\partial\Omega_\varepsilon$. Using Lemma 2.4.9, there exists a constant C depending only on Ω_ε such that

$$\|\mathbf{v}\|_{L^2(\Omega_\varepsilon)} \leq C\|\nabla\cdot\left[(\sigma_1 - \sigma_2)\,\mathbf{A}_1\right]\|_{H^{-1}(\Omega_\varepsilon)},$$

which shows that

$$\|\mathbf{v}\|_{L^2(\Omega_\varepsilon)} \leq C\|\,(\sigma_1 - \sigma_2)\,\mathbf{A}_1\,\|_{L^2(\Omega_\varepsilon)}.$$

Using Cauchy-Schwartz inequality:

$$\|\mathbf{v}\|_{L^2(\Omega_\varepsilon)} \leq C\|\sigma_1 - \sigma_2\|_{L^2(\Omega_\varepsilon)}\|\mathbf{A}_1\,\|_{L^2(\Omega_\varepsilon)}. \quad (2.4.16)$$

Putting together (2.4.15) with (2.4.16), we arrive at

$$\|\mathcal{G}_\varepsilon[\sigma_1] - \mathcal{G}_\varepsilon[\sigma_2]\|_{L^2(\Omega_\varepsilon)} \leq (C+1)\frac{b}{\varepsilon}\|\mathbf{A}_1\|_{L^2(\Omega_\varepsilon)}\|\sigma_1 - \sigma_2\|_{L^2(\Omega_\varepsilon)}.$$

The proof is then complete.

□

The following proposition shows the convergence of the fixed point reconstruction algorithm.

Proposition 2.4.11. *Let $\sigma_{(n)} \in \left(L^2(\Omega_\varepsilon)\right)^{\mathbb{N}}$ be the sequence defined by*

$$\begin{aligned} &\sigma_{(0)} = 1, \\ &\sigma_{(n+1)} = \max\left(\min\left(\mathcal{G}_\varepsilon[\sigma_{(n)}], b\right), a\right), \quad \forall n \in \mathbb{N}. \end{aligned} \tag{2.4.17}$$

If $\|\mathbf{A}_1\|_{L^2(\Omega_\varepsilon)}$ is small enough, then the sequence is well defined and $\sigma_{(n)}$ converges to $\sigma_\star\Big|_{\Omega_\varepsilon}$ in $L^2(\Omega_\varepsilon)$.

Proof. Let $(X, d) = \left(L^\infty_{a,b}(\Omega_\varepsilon), \|\cdot\|_{L^2(\Omega_\varepsilon)}\right)$. Then, (X, d) is a complete, non empty metric space. Let T_ε be the map defined by

$$\begin{aligned} L^\infty_{a,b}(\Omega_\varepsilon) &\longrightarrow L^\infty_{a,b}(\Omega_\varepsilon) \\ \sigma &\longmapsto T_\varepsilon[\sigma] := \max\left(\min\left(\mathcal{G}_\varepsilon[\sigma], b\right), a\right). \end{aligned}$$

Using Lemma 2.4.10, we get that T_ε is a contraction, provided that $\|\mathbf{A}_1\|_{L^2(\Omega_\varepsilon)}$ is small enough. We already have the existence of a fixed point given by Lemma 2.4.8, and therefore, Banach's fixed point theorem gives the convergence of the sequence for the L^2 norm over Ω_ε, and the uniqueness of the fixed point. □

Orthogonal field method

In this section we present a non-iterative method to reconstruct the electrical conductivity from the electric current density. This direct method was first introduced in [10] and works with piecewise regularity for the true conductivity $\sigma_\star$ in the case of a Lorentz force electrical impedance tomography experiment. However, the practical conditions are a bit different here and we have to modify the method to make it work in the present case.

We assume in this section that $\sigma_\star \in \mathcal{C}^{0,\alpha}(\overline{\Omega}), \quad \alpha \in]0, 1]$. The fields $\mathbf{J} = (J_1, J_2)$ and $\mathbf{A}_1$ are assumed to be known in Ω. Our goal is to reconstruct $V_\star$ the solution of (2.2.7) in $H^1(\Omega)$. Then, computing $\frac{|\nabla V_\star + \mathbf{A}_1|}{|\mathbf{J}|}$ for $|\mathbf{J}|$ nonzero will give us $\frac{1}{\sigma_\star}$. Recall that $\mathbf{J} = \mathbf{curl}\ w$ where w is defined by equation (**??**).

Definition 2.4.1. *We say that the data f on the right hand side of (**??**) is admissible if $f > 0$ or $f < 0$ in Ω and if the critical points of w are isolated.*

Introduce $\mathbf{F} = (-J_2, J_1)^T$ the rotation of $\mathbf{J}$ by $\frac{\pi}{2}$. It is worth noticing that the true electrical potential $V_\star$ is a solution of

$$\begin{cases} \mathbf{F} \cdot \nabla V_\star = -\mathbf{F} \cdot \mathbf{A}_1 & \text{in } \Omega, \\ \dfrac{\partial V_\star}{\partial \nu} = 0 & \text{on } \partial\Omega, \\ \displaystyle\int_\Omega V_\star = 0. \end{cases} \tag{2.4.18}$$

Equation (2.4.18) has a unique solution in $H^1(\Omega)$, and this solution is the true potential $V_\star$.

The following uniqueness result holds.

Proposition 2.4.12. *If $U \in H^1(\Omega)$ is a solution of*

$$\begin{cases} \mathbf{F} \cdot \nabla U = 0 & \text{in } \Omega, \\ \dfrac{\partial U}{\partial \nu} = 0 & \text{on } \partial\Omega, \\ \displaystyle\int_\Omega U = 0, \end{cases} \tag{2.4.19}$$

then $U = 0$ in Ω.

Proof. We use the characteristic method (see, for instance, [57]) for solving (2.4.19). For any $x_0 \in \Omega$, consider the Cauchy problem:

$$\begin{cases} \dfrac{dX}{dt} = \mathbf{F}\left(X(t)\right), \quad t \in \mathbb{R}, \\ X(0) = x_0 \in \Omega. \end{cases} \tag{2.4.20}$$

We call the set $\{x(t), t \in \mathbb{R}\}$ the integral curve at x_0. Since $\sigma \in \mathcal{C}^{0,\alpha}(\Omega)$, $\mathbf{F} \in \mathcal{C}^{1,\alpha}(\Omega)$. We can apply the Cauchy-Lipschitz theorem and get global existence and uniqueness of a solution to (2.4.20). Now, assume that $U \in H^1(\Omega)$ is a solution of (2.4.19). Since $\mathbf{J} = \mathbf{curl}\ w$, $\mathbf{F}$ can be written as

$$\mathbf{F} = -\nabla w \quad \text{in } \Omega.$$

Equation (2.4.20) can be written as a gradient flow problem :

$$\begin{cases} \dfrac{dX}{dt} = -\nabla w\left(X(t)\right), \quad t \in \mathbb{R}, \\ X(0) = x_0 \in \Omega. \end{cases} \tag{2.4.21}$$

Using [**?**], we know that there are finitely many isolated critical points $p_1 \dots p_n$ for w on Ω. It is known (see [**?**], p.204) , since the sets $w^{-1}(]-\infty, c])$ are compact for every $c \in \mathbb{R}$, that $\lim_{t\to\infty} X(t)$ exists and equals one of the equilibrium points $p_1 \dots p_n$. Now, for every i, we define Ω_i the set of points $x_0 \in \Omega$ such that the solution of (2.4.21) converges to p_i. We have $\Omega = \cup_{i=1}^{n} \Omega_i$.

Now, for any i consider $x_0 \in \Omega_i$, and $X \in \mathcal{C}^1([0, T[, \Omega)$ the solution of (2.4.21). We define $f \in \mathcal{C}^0(\mathbb{R}^+, \mathbb{R})$ by $f(t) = U(X(t))$. The function f is differentiable on $\mathbb{R}^+$ and $f'(t) = \nabla U(X(t)) \cdot \mathbf{F}(X(t)) = 0$. Hence, f is constant. We have

$$U(x_0) = f(0) = \lim_{t\to\infty} f(t) = U(p_i) = c_i \in \mathbb{R}.$$

So, U is constant equal to c_i in Ω_i. The regularity of U implies that $\forall i, j \in [\![1, n]\!]$, $c_i = c_j$. Therefore U is constant on Ω and the zero integral condition gives:

$$U = 0 \text{ in } \Omega.$$

This yields the uniqueness of a solution to (2.4.19) and thus, concludes the proof. □

In order to solve numerically (2.4.18), we use a method of vanishing viscosity [24]. The field $\mathbf{A}_1$ is known and we can solve uniquely the following problem:

$$\begin{cases} \nabla \cdot \left[\left(\eta I + \mathbf{F}\mathbf{F}^T \right) \nabla U^{(\eta)} \right] = -\nabla \cdot \mathbf{F}\mathbf{F}^T \mathbf{A}_1 & \text{in } \Omega, \\ \dfrac{\partial U^{(\eta)}}{\partial \nu} = -\mathbf{A}_1 \cdot \boldsymbol{\nu} & \text{on } \partial\Omega, \\ \displaystyle\int_\Omega U^{(\eta)} = 0, \end{cases} \tag{2.4.22}$$

for some small $\eta > 0$. Here, I denotes the 2×2 identity matrix.

Proposition 2.4.13. *Let $\sigma_\star$ be the true conductivity. Let $V_\star$ be the solution to (2.4.6) with $\sigma = \sigma_\star$. The solution $U^{(\eta)}$ of (2.4.22) converges strongly to $V_\star$ in $H^1(\Omega)$ when η goes to zero.*

Proof. We can easily see that $\widetilde{U}^{(\eta)} = U^{(\eta)} - V_\star$ is the solution to

$$\begin{cases} \nabla \cdot \left[\left(\eta I + \mathbf{F}\mathbf{F}^T \right) \nabla \widetilde{U}^{(\eta)} \right] = -\eta \Delta V_\star & \text{in } \Omega, \\ \dfrac{\partial \widetilde{U}^{(\eta)}}{\partial \nu} = 0 & \text{on } \partial\Omega, \\ \displaystyle\int_\Omega \widetilde{U}^{(\eta)} = 0. \end{cases} \tag{2.4.23}$$

Multiplying (2.4.23) by $\widetilde{U}^{(\eta)}$ and integrating by parts over Ω, we find that

$$\eta \int_\Omega |\nabla \widetilde{U}^{(\eta)}|^2 + \int_\Omega |\mathbf{F} \cdot \nabla \widetilde{U}^{(\eta)}|^2 = \eta \int_\Omega \nabla \widetilde{U}^{(\eta)} \cdot \nabla V_\star + \eta \int_{\partial\Omega} \widetilde{U}^{(\eta)} \mathbf{A}_1 \cdot \boldsymbol{\nu}, \tag{2.4.24}$$

since $\dfrac{\partial \widetilde{U}^{(\eta)}}{\partial \nu} = 0$ and $\dfrac{\partial V_\star}{\partial \nu} = -\mathbf{A}_1 \cdot \boldsymbol{\nu}$. Therefore, we have

$$\|\widetilde{U}^{(\eta)}\|^2_{H^1(\Omega)} \leq \|\widetilde{U}^{(\eta)}\|_{H^1(\Omega)} \|V_\star\|_{H^1(\Omega)} + C \|\widetilde{U}^{(\eta)}\|_{H^1(\Omega)},$$

where C depends only on Ω and $\mathbf{A}_1$. This shows that the sequence $(\widetilde{U}^{(\eta)})_{\eta>0}$ is bounded in $H^1(\Omega)$. Using Banach-Alaoglu's theorem we can extract a subsequence which converges weakly to some u^* in $H^1(\Omega)$. We multiply (2.4.23) by u^* and integrate by parts over Ω to obtain

$$\int_\Omega \left(\mathbf{F} \cdot \nabla \widetilde{U}^{(\eta)}\right)\left(\mathbf{F} \cdot \nabla u^*\right) = \eta \left[\int_\Omega \nabla V_\star \cdot \nabla u^* - \int_\Omega \nabla \widetilde{U}^{(\eta)} \cdot \nabla u^* + \int_{\partial\Omega} u^* \mathbf{A}_1 \cdot \boldsymbol{\nu}\right].$$

Taking the limit when η goes to zero yields

$$\|\mathbf{F} \cdot \nabla u^*\|_{L^2(\Omega)} = 0.$$

Using Proposition 2.4.12, we have

$$u^* = 0 \text{ in } \Omega,$$

since u^* is a solution to (2.4.19).

Actually, we can see that there is no need for an extraction, since 0 is the only accumulation point for $\widetilde{U}^{(\eta)}$ with respect to the weak topology. If we consider a subsequence $\widetilde{U}^{(\phi(\eta))}$, it is still bounded in $H^1(\Omega)$ and therefore, using the same argument as above, zero is an accumulation point of this subsequence. For the strong convergence, we use (2.4.24) to get

$$\int_\Omega |\nabla \widetilde{U}^{(\eta)}|^2 \leq \int_\Omega \nabla \widetilde{U}^{(\eta)} \cdot \nabla V_\star + \int_{\partial\Omega} \widetilde{U}^{(\eta)} \mathbf{A}_1 \cdot \boldsymbol{\nu}. \tag{2.4.25}$$

Since $\widetilde{U}^{(\eta)} \rightharpoonup 0$, the right-hand side of (2.4.25) goes to zero when η goes to zero. Hence,

$$\|\widetilde{U}^{(\eta)}\|_{H^1(\Omega)} \longrightarrow 0 \quad \text{as } \eta \to 0.$$

□

Now, we take $U^{(\eta)}$ to be the solution of (2.4.22) and define the approximated resistivity (inverse of the conductivity) by

$$\frac{1}{\sigma_\eta} = \frac{|\nabla U^{(\eta)} + \mathbf{A}_1|}{|\mathbf{J}|}. \tag{2.4.26}$$

Since

$$\frac{1}{\sigma_\star} = \frac{|\nabla V_\star + \mathbf{A}_1|}{|\mathbf{J}|},$$

Proposition 2.4.13 shows that $\dfrac{1}{\sigma_\eta}$ is a good approximation for $\dfrac{1}{\sigma_\star}$ in the L^2-sense.

Proposition 2.4.14. *Let $\sigma_\star$ be the true conductivity and let σ_η be defined by (2.4.26). We have*

$$\left\| \frac{1}{\sigma_\eta} - \frac{1}{\sigma_\star} \right\|_{L^2(\Omega)} \longrightarrow 0 \quad \text{as } \eta \to 0.$$

2.5 Numerical illustrations

We set $\Omega = \left\{ (x,y) \in \mathbb{R}^2,\ \left(\frac{x}{2}\right)^2 + y^2 < 1 \right\}$. We take a conductivity $\sigma \in \mathcal{C}^{0,\alpha}(\Omega)$ as represented on Figure 2.5.1. The potential $\mathbf{A}_1$ is chosen as

$$\mathbf{A}_1(x) = 10^{-2} \left(\frac{y}{2} + 1; -\frac{x}{2} + 1 \right),$$

so that $\mathbf{B}_1$ is constant in space. The domain Ω is triangulated and equations are solved using the finite element method.

2.5.1 Optimal control

We use the algorithm presented in section 2.4.2. We set a step size equal to $8 \cdot 10^{-7}$ and $\sigma_{(0)} = 3$ as an initial guess. After 50 iterations, we get the reconstruction shown in Figure 2.5.2. The general shape of the conductivity is recovered but the conductivity contrast is not recovered. Moreover, the convergence is quite slow. It is worth mentioning that using two nonparallel electric current densities does not improve significantly the quality of the reconstruction.

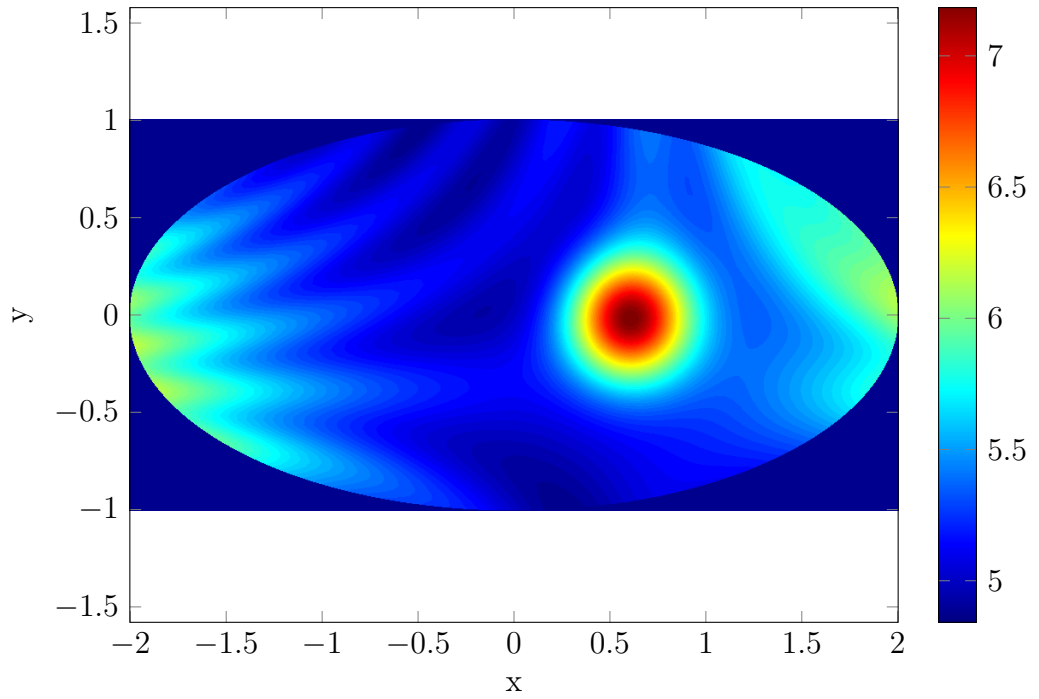

Figure 2.5.1 Conductivity to be reconstructed.

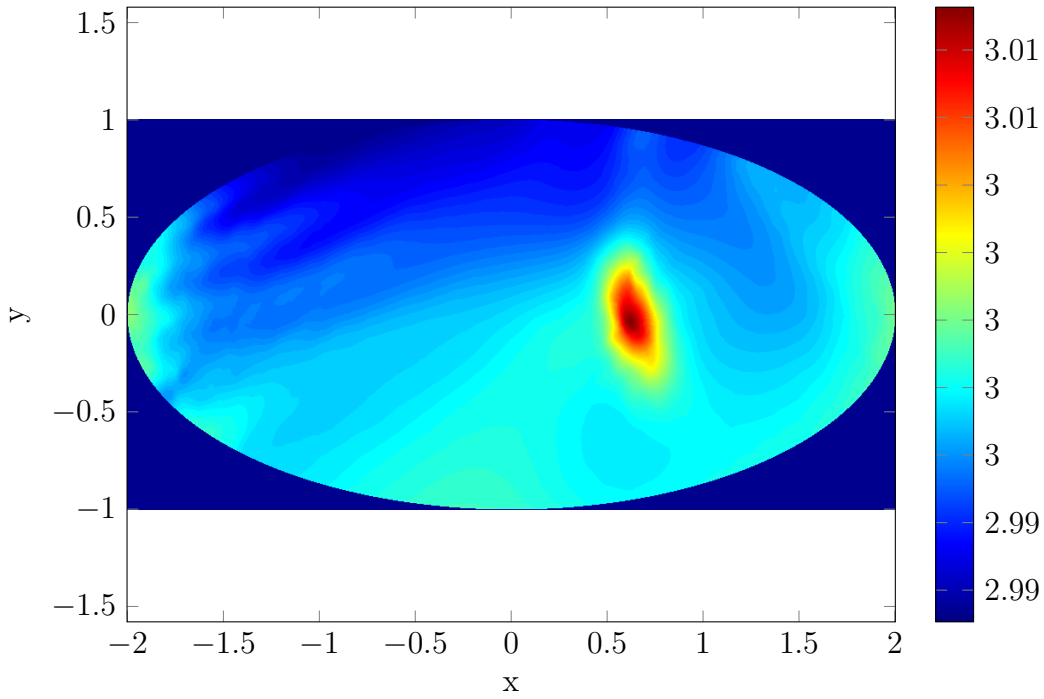

Figure 2.5.2 Conductivity reconstructed by the optimal control method.

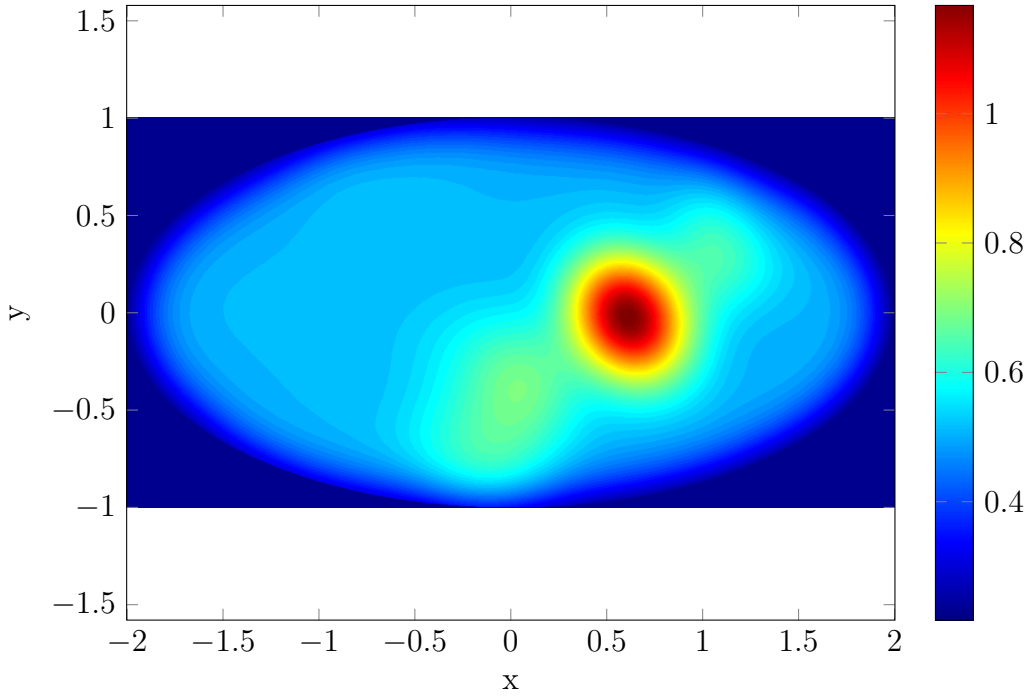

Figure 2.5.3 Conductivity reconstructed by the fixed point method.

2.5.2 Fixed-point method

We use the algorithm described in section 2.4.2, but slightly modified. The operator $\mathcal{G}$ defined by

$$\mathcal{G}[\sigma] := \sigma \frac{(\sigma \nabla V[\sigma] + \sigma \mathbf{A}_1) \cdot \mathbf{J}}{|\mathbf{J}|^2}$$

is replaced by

$$\widetilde{\mathcal{G}}[\sigma] := \frac{(\nabla V[\sigma] + \mathbf{A}_1) \cdot \mathbf{J}}{|\nabla V[\sigma] + \mathbf{A}_1|^2},$$

which is analytically the same but numerically is more stable. Since the term $|\nabla V[\sigma] + \mathbf{A}_1|^2$ can be small, we smooth out the reconstructed conductivity $\sigma_{(n)}$ at each step by convolving it with a Gaussian kernel. This makes the algorithm less unstable. The result after 9 iterations is shown in Figure 2.5.3. The convergence is faster than the gradient descent, but the algorithm still fails at recovering the exact values of the true conductivity.

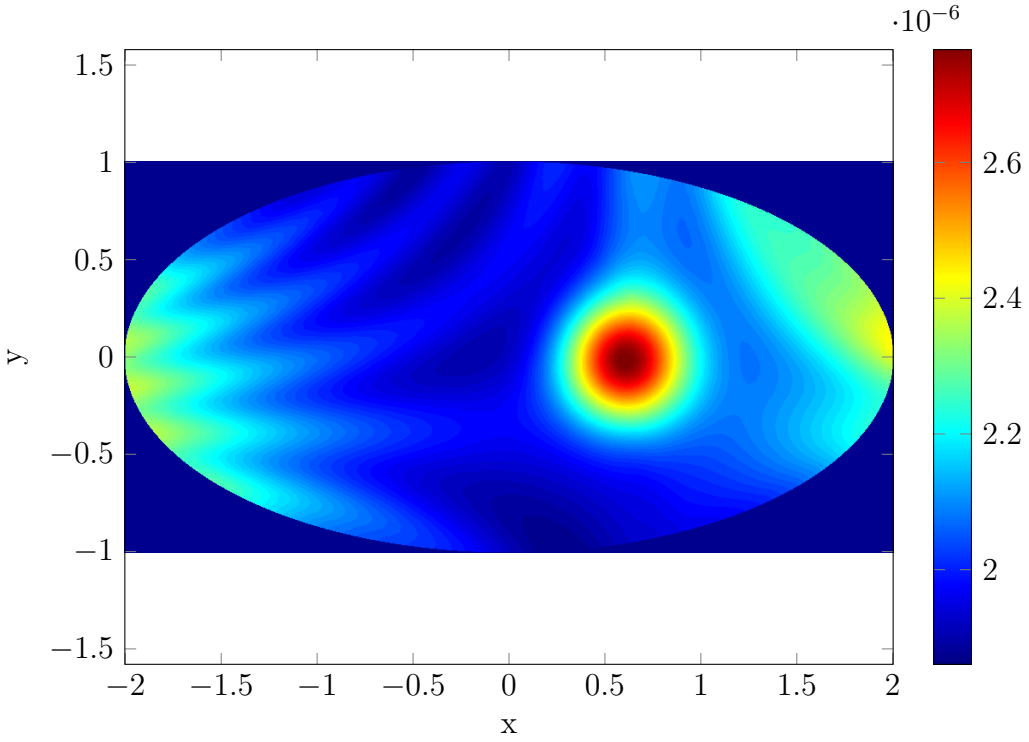

Figure 2.5.4 Conductivity recovered by the orthogonal field method before scaling.

2.5.3 Orthogonal field method

We set $\eta = 5 \cdot 10^{-4}$ and perform the computation described in section 2.4.2. The result we get is shown in Figure 2.5.4. It is a scaled version of the true conductivity $\sigma_\star$, which means that the contrast is recovered. So assuming we know the conductivity in a small region of Ω (or near the boundary $\partial\Omega$) we can re-scale the result, as shown in Figure 2.5.5. When η goes to zero, the solution of (2.4.22) converges to the true potential $V_\star$ up to a scaling factor which goes to infinity. When η is large, the scaling factor goes to one but the solution $U^{(\eta)}$ becomes a "smoothed out" version of $V_\star$. This method allows an accurate reconstruction of the conductivity by solving only one partial differential equation. It covers the contrast accurately, provided we have a little bit of a prior information on $\sigma_\star$.

Finally, we study the numerical stability with respect to measurement noise of the orthogonal field method. We compute the relative error defined by

$$e := \frac{\|\sigma_\eta - \sigma_\star\|_{L^2}}{\|\sigma_\star\|_{L^2}},$$

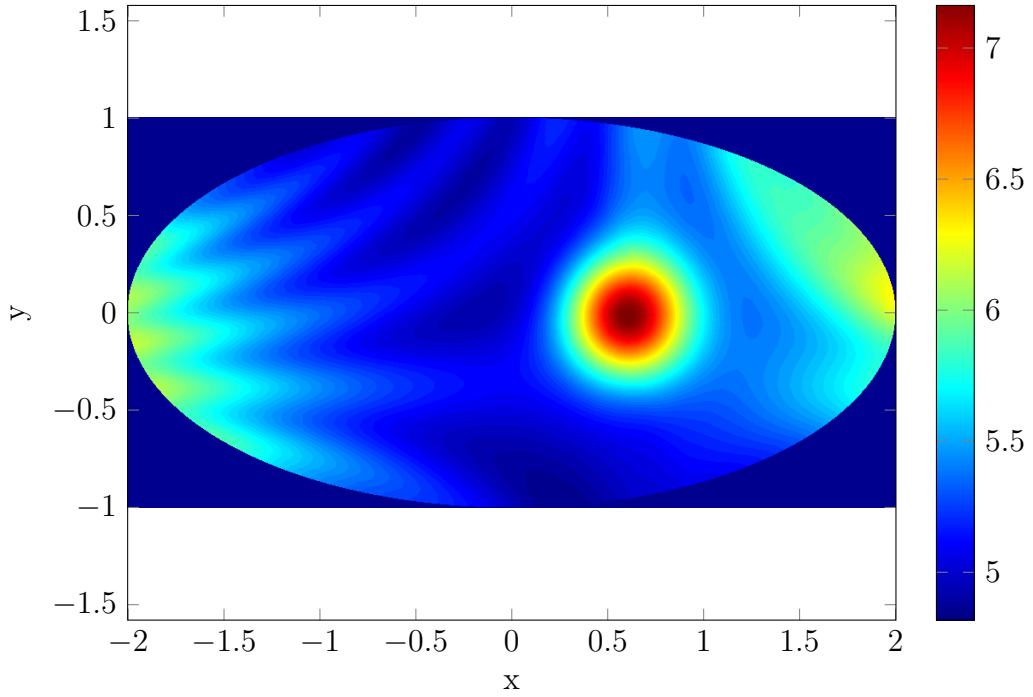

Figure 2.5.5 Conductivity recovered by the orthogonal field method after scaling.

averaged over 150 different realizations of measurement noise on $\mathbf{J}$. The results are shown in Figure 2.5.6. We show the results of a reconstruction with noise level of 2% (resp. 10%) in Figure 2.5.7 (resp. Figure 2.5.8). Clearly, the orthogonal method is quite robust with respect to measurement noise.

2.6 Concluding remarks

In this chapter we have presented a new mathematical and numerical framework for conductivity imaging using magnetoacoustic tomography with magnetic induction. We gave a new physical model for MAT-MI, and we developed three different algorithms for conductivity imaging from boundary measurements of the Lorentz force induced tissue vibration. We proved convergence and stability properties of the three algorithms and compared their performance. As in Chapter 1, the orthogonal field method performs much better than the optimization scheme and the fixed-point method in terms of both computational time and accuracy, since one needs to solve only one partial differential equation to recover the conductivity from the internal current. It is also robust with respect to measurement noise. In a forthcoming work, we intend to generalize our

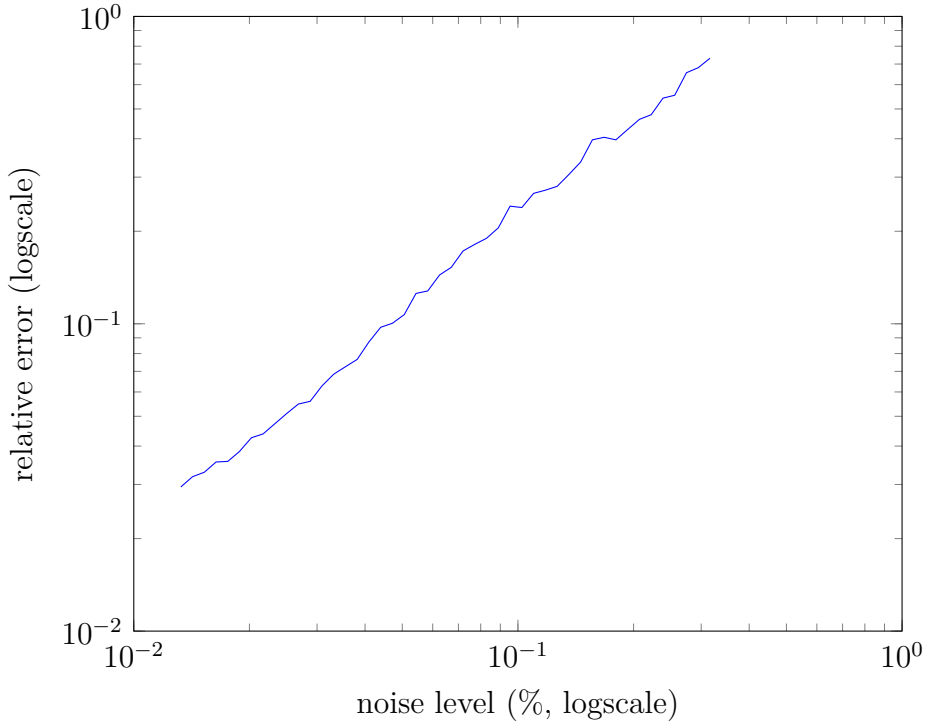

Figure 2.5.6 Relative error with respect to measurement noise.

approach for imaging anisotropic conductivities by magnetoacoustic tomography with magnetic induction.

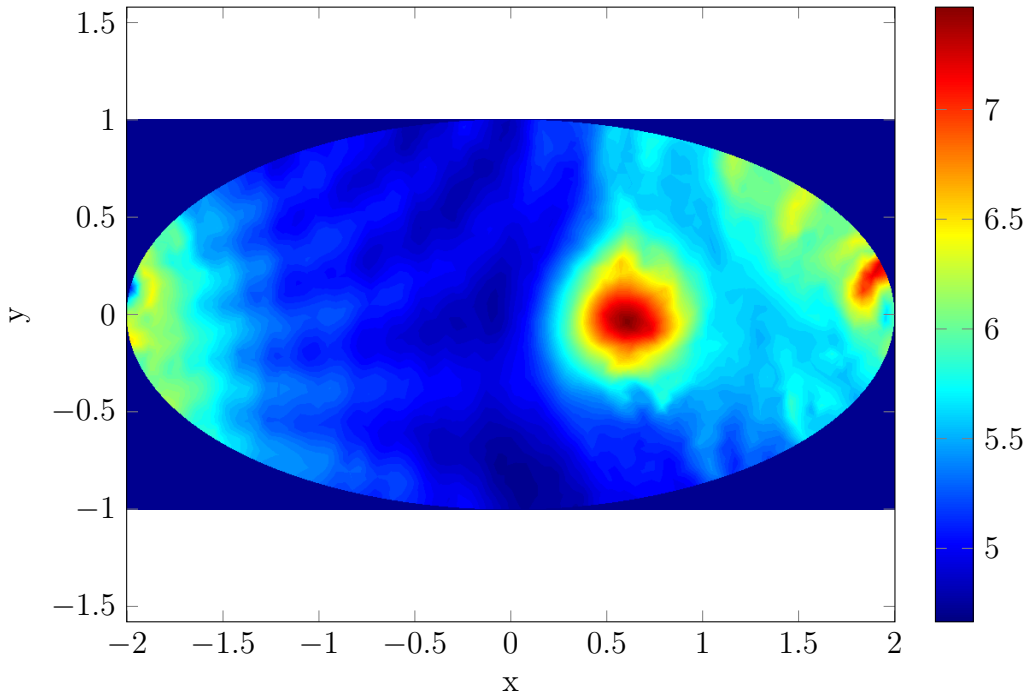

Figure 2.5.7 Reconstruction with the orthogonal field method with measurement noise level of 2%.

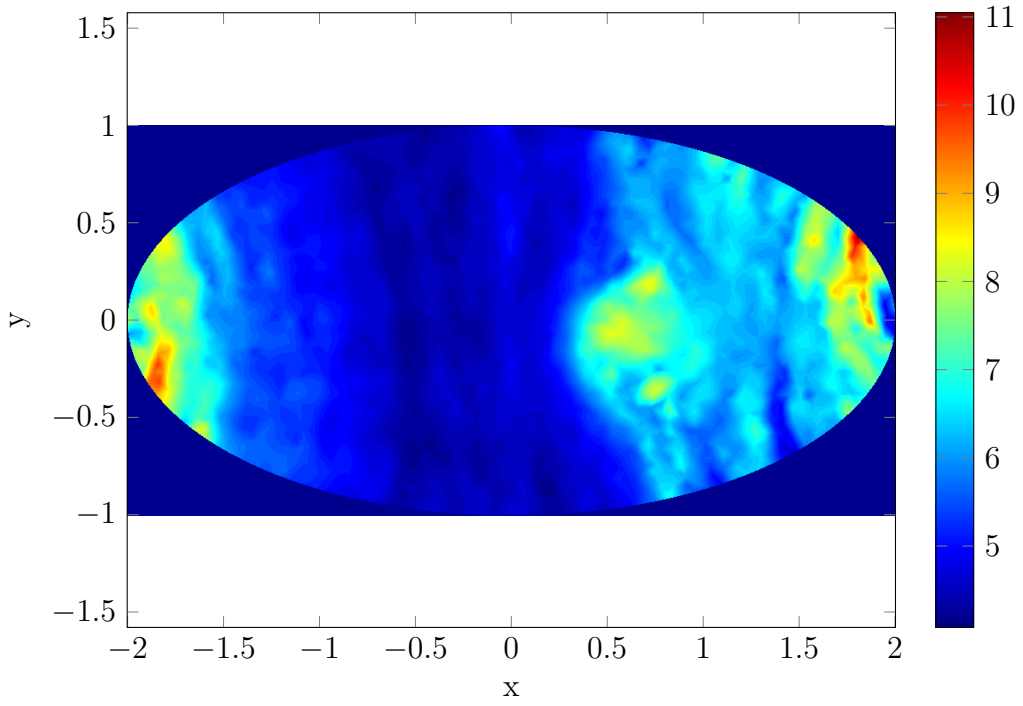

Figure 2.5.8 Reconstruction with the orthogonal field method with measurement noise level of 10%.

Chapter 3

Optical coherence tomography based elastography

Contents

3.1 Introduction

In this chapter we present a third hybrid technique aiming at imaging the elastic shear modulus of a sample with a micro-meter resolution.

Optical coherence tomography (OCT) is a non-invasive and a non-ionizing imaging technique that produces high-resolution images of biological tissues. It performs optical slicing in the sample, to allow three-dimensional reconstructions of internal structures. Conventional optical coherence time-domain and frequency-domain tomographies require transverse scanning of the illumination spot in one or two directions to obtain

cross-sectional or en face images, respectively. Full-field OCT allows OCT to be performed without transverse scanning; the tomographic images are obtained by combining interferometric images acquired in parallel using an image sensor. Both the transverse and the axial resolutions are of the order of 1μm; see [53, 54]. We refer to [56] for the mathematical modeling of OCT.

Elastography is an imaging-based technique for the estimation of the elastic properties of tissues. Given that the mechanical properties of tissues and cells are related to their structure and function, changes in those properties can reflect healthy or pathological states such as weakening of vessel walls or cirrhosis of the liver. Elastography can aid the identification of suspicious lesions, the diagnosis of various diseases and the monitoring of the effectiveness of treatments (see [92, 107]). Different imaging modalities (e.g., ultrasound and magnetic resonance imaging) can be used to measure tissue displacements and to estimate the resulting tissue stiffness and viscosity. Magnetic resonance elastography is relatively expensive, due to the high magnetic field environment, which requires specifically designed equipment. Several reconstruction approaches for elastography have been derived [6, 10, 16, 29, 30, 77, 98, 99, 125, 136].

In [109], elastographic contrast has been combined with full-field OCT with the aim of creating a virtual palpation map at the micrometer scale. The idea is to register a volumetric optical image before and after mechanical solicitation of the sample. Based on the assumption that the density of the optical scatterers is advected by the deformation, the displacement map can be first estimated. Then, using a quasi-incompressible model for the tissue elasticity, the shear modulus distribution can be reconstructed from the estimated displacement map.

The OCT elastography is able to perform displacement measurements with subcellular resolution. It enables a more precise characterization of tissues than that achieved using ultrasound or magnetic resonance elastography; therefore, it provides a more accurate assessment of microscale variations of elastic properties. A map of mechanical properties added as a supplementary contrast mechanism to morphological images could aid diagnosis. The technique costs less than other elastography techniques.

The mapping of mechanical properties was first introduced to OCT imaging by Schmitt [123], who measured displacements as small as a few micrometers in heterogeneous gelatin phantoms containing scattering particles in addition to living skin. Various subsequent applications have employed OCT methods in elastography; these include dynamic and full-field optical coherence elastography (see [88, 117, 118]).

In all of the aforementioned techniques, transforming the OCT images before and after the application of a load into quantitative maps of the shear modulus is a challenging problem.

In this paper we present a mathematical and numerical framework for the OCT-elastography experiment described in [109]. Using the set of images before and after mechanical solicitation we design a novel method to reconstruct the shear modulus distribution inside the sample.

To mathematically formulate the problem, let $\Omega_0 \subset \mathbb{R}^d, d = 2, 3$, and let ε_0 be the known piece-wise smooth optical image of the medium, and μ be its shear modulus. In this chapter we consider heterogeneous (unknown) shear modulus distributions. The medium is solicited mechanically. Since compression modulus of biological media is four order of magnitude larger than the shear modulus, it can be shown that the displacement map $\mathbf{u}$ obeys the linearized equations of incompressible fluids or the Stokes system [6, 10, 16]. The model problem is then the following Stokes system in a heteregeneous medium which reads:

$$\begin{cases} \nabla \cdot \left(\mu(\nabla \mathbf{u} + \nabla \mathbf{u}^T)\right) + \nabla p = 0 \quad \text{in} \ \ \Omega_0, \\ \nabla \cdot \mathbf{u} = 0 \quad \text{in} \ \ \Omega_0, \\ \mathbf{u} = \mathbf{f} \quad \text{on} \ \ \partial\Omega_0, \end{cases} \tag{3.1.1}$$

where superposed T denotes the transpose and the real-valued vector $\mathbf{f}$ satisfies the compatibility condition $\int_{\partial\Omega_0} \mathbf{f} \cdot \boldsymbol{\nu} = 0$ with $\boldsymbol{\nu}$ being the outward normal at $\partial\Omega_0$.

Throughout this chapter, we assume that $\mu \in \mathcal{C}^{0,1}(\overline{\Omega}_0)$ and $\mathbf{f} \in \mathcal{C}^2(\partial\Omega_0)^d$. From [46, 61, 87], (3.1.1) has a unique solution $\mathbf{u} \in \mathcal{C}^1(\overline{\Omega_0})^d$. Moreover, there exists a positive constant C depending only on μ and Ω_0 such that

$$||\mathbf{u}||_{\mathcal{C}^1(\overline{\Omega_0})^d} \leq C||\mathbf{f}||_{\mathcal{C}^2(\partial\Omega_0)^d}.$$

Using a second OCT scan, one has access to the optical image of the deformed medium $\varepsilon_u(\widetilde{\mathbf{x}}),\ \forall\, \widetilde{\mathbf{x}} \in \Omega_u$, where Ω_u is defined by

$$\Omega_u = \{\mathbf{x} + \mathbf{u}(\mathbf{x}),\ \mathbf{x} \in \Omega_0\}.$$

The new optical image is linked to the original one by

$$\varepsilon(\mathbf{x}) = \varepsilon_u\left(\mathbf{x} + \mathbf{u}(\mathbf{x})\right), \quad \forall\, \mathbf{x} \in \Omega_0. \tag{3.1.2}$$

The goal is to reconstruct the shear modulus map μ on Ω_0 from the functions ε and ε_u. We first prove that, in two dimensions, if the direction of $\dfrac{\nabla\varepsilon}{|\nabla\varepsilon|}$ is not constant in a neighborhood of $\mathbf{x}$, then the displacement field $\mathbf{u}$ at $\mathbf{x}$ can be approximately reconstructed. In three dimensions, one shall assume that the vectors $\dfrac{\nabla\varepsilon(\mathbf{y})}{|\nabla\varepsilon(\mathbf{y})|}$ are not coplanar for $\mathbf{y}$ a neighborhood of $\mathbf{x}$. Hence, the reconstructed value of $\mathbf{u}(\mathbf{x})$ serves as an initial guess for the minimization of the discrepancy between computed and measured changes in the optical image. Then, we compute an element of the subgradient [49] of the discrepancy functional. Finally, we implement a minimization scheme to retrieve the shear modulus map from the reconstructed displacements. Note that reconstructing the displacement field from $\varepsilon - \varepsilon_u$ is a registration problem and its linearization is an optical flow problem; see [71]. It is also worth mentioning that the approach developed in this paper applies to other speckle imaging modalities.

The chapter is organized as follows. Section 3.2 is devoted to some mathematical preliminaries. In section 3.3 we consider piecewise smooth ε functions and first derive a leading-order Taylor expansion of ε_u as $||\mathbf{u}||_{\mathcal{C}^1}$ goes to zero. Then we provide an initial guess by linearization. Finally, we prove the Fréchet differentiability of the discrepancy functional between the measured and the computed advected images. The displacement field inside the sample can be obtained as the minimizer of such functional. Section 3.4 is devoted to the reconstruction of the shear modulus from the displacement measurements. In section 3.5 we present some numerical results to highlight the viability and the performance of the proposed algorithm.

3.2 Preliminaries

Let Ω be a bounded smooth domain in $\mathbb{R}^d, d = 2, 3$. We start by defining a class of piecewise smooth functions.

Definition 3.2.1. *For any $k \in \mathbb{N}$, $\alpha \in]0,1[$, for any curve S of class $\mathcal{C}^{1,\alpha}$ for some $0 < \alpha < 1$ such that $\Omega \setminus S$ is a union of connected domains $\Omega_i, i = 1, 2, \cdots n$, we define $\mathcal{C}_S^{k,\alpha}\left(\overline{\Omega}\right)$ to be the class of functions $f : \Omega \to \mathbb{R}$ satisfying*

$$f|_{\Omega_i} \in \mathcal{C}_S^{k,\alpha}\left(\overline{\Omega}_i\right) \quad \forall\, i = 1, \cdots n. \tag{3.2.1}$$

Definition 3.2.2. *We define* $\mathrm{BV}(\Omega)$ *as the subspace of $L^1(\Omega)$ of all the functions f whose weak derivative Df is a finite Radon measure. In other terms, f satisfies*

$$\int_\Omega f \nabla \cdot \mathbf{F} \leq C \sup_{x\in\Omega} |\mathbf{F}|, \quad \forall\, \mathbf{F} \in \mathcal{C}_0^1(\Omega)^d$$

for some positive constant C with $\mathcal{C}_0^1(\Omega)$ being the set of compactly supported $\mathcal{C}^1$ functions.

The derivative of a function $f \in \mathrm{BV}(\Omega)$ can be decomposed as

$$Df = \nabla f \mathcal{H}^d + [f]\boldsymbol{\nu}_s \mathcal{H}_S^{d-1} + D_c f,$$

where $\mathcal{H}^d$ is the Lebesgue measure on Ω, $\mathcal{H}_S^{d-1}$ is the surface Hausdorff measure on a rectifiable surface S, $\boldsymbol{\nu}_S$ is a normal vector defined a.e. on S, $\nabla f \in L^1(\Omega)$ is the smooth derivative of f, $[f] \in L^1(S, \mathcal{H}_S^{d-1})$ is the jump of f across S and $D_c f$ is a vector measure supported on a set of Hausdorff dimension less than $(d-1)$, which means that its $(d-1)$-Hausdorff-measure is zero; see [5, 93].

Definition 3.2.3. *We define* $\mathrm{SBV}(\Omega)$ *as the subspace of* $\mathrm{BV}(\Omega)$ *of all the functions* f *satisfying* $D_c f = 0$.

Definition 3.2.4. *For any* $1 \leq p \leq +\infty$*, we define*

$$\mathrm{SBV}^p(\Omega) = \left\{ f \in \mathrm{SBV}(\Omega) \cap L^p(\Omega),\ \nabla f \in L^p(\Omega)^d \right\}.$$

Let $W^{1,p}(\Omega) = \{f \in L^p(\Omega),\ \nabla f \in L^p(\Omega)^d\}$ for $p \geq 1$. Roughly speaking, a function $u \in SBV^p(\Omega)$ is a function of class $W^{1,p}$ admitting surface discontinuities. Note also that $\mathcal{C}_S^{k,\alpha}\left(\overline{\Omega}\right) \subset \mathrm{SBV}^p(\Omega)$; see [5].

From now on, we assume that the optical image in the medium ε belongs to $\mathcal{C}_S^{k,\alpha}\left(\overline{\Omega}\right)$, which is a simple but good model for a discontinuous medium. Some of the following propositions are true for more general maps $\varepsilon \in \mathrm{SBV}(\Omega)$. In these propositions we only assume that ε is in $\mathrm{SBV}(\Omega)$.

3.3 Displacement field measurements

In this section we consider the problem of reconstructing the displacement $\mathbf{u}$ from the optical images before and after applying a load on the sample. Assuming that ε is piecewise smooth, we derive a leading-order Taylor expansion of ε_u as $||\mathbf{u}||_{\mathcal{C}^1}$ goes to zero. Then we provide an initial guess by linearization. Finally, we prove the Fréchet differentiability of the discrepancy functional I between the measured and the computed advected images provided that ε is smooth. If ε has jumps, then I has a nonempty subgradient. Therefore, in both cases, the displacement field $\mathbf{u}$ inside the sample can be obtained as the minimizer of such functional.

3.3.1 First order approximation

Let $\Omega \Subset (\Omega_0 \cap \Omega_u)$ be a smooth simply connected domain. On Ω, we have

$$\begin{aligned} \varepsilon_u = &\ \varepsilon \circ (\mathbb{I} + \mathbf{u})^{-1} \\ \varepsilon = &\ \varepsilon_u \circ (\mathbb{I} + \mathbf{u}), \end{aligned}$$

where $\mathbb{I}$ is the $d \times d$ identity matrix.

Proposition 3.3.1. *Let $\varepsilon \in \mathrm{BV}(\Omega)$ and let $\mathbf{u} \in \mathcal{C}^1(\overline{\Omega})^d$ be such that $\|\mathbf{u}\|_{\mathcal{C}^1(\overline{\Omega})^d} < 1$. Then, for any $\psi \in \mathcal{C}_0^1(\Omega)$, we have*

$$\left| \int_\Omega (\varepsilon - \varepsilon_u)\, \psi - \int_\Omega \psi \mathbf{u} \cdot D\varepsilon \right| \leq C \|\mathbf{u}\|_{\mathcal{C}^0(\overline{\Omega})^d} \|\mathbf{u}\|_{\mathcal{C}^1(\overline{\Omega})^d} \|\psi\|_{\mathcal{C}_0^1(\Omega)} |\varepsilon|_{\mathrm{TV}(\Omega)}, \tag{3.3.1}$$

where the constant C is independent of ψ and $|\ |_{\mathrm{TV}(\Omega)}$ denotes the total variation semi-norm. Estimate (3.3.1) yields that $\dfrac{\varepsilon_u - \varepsilon + \mathbf{u} \cdot D\varepsilon}{\|\mathbf{u}\|_{\mathcal{C}^0(\overline{\Omega})^d}}$ weakly converges to 0 in $\mathcal{C}_0^1(\Omega)$ when $\|\mathbf{u}\|_{\mathcal{C}^1(\overline{\Omega})^d}$ goes to 0.

Proof. For each $t \in [0,1]$, define ϕ_t by $\phi_t^{-1}(\mathbf{x}) = \mathbf{x} + t\mathbf{u}(\mathbf{x})$. Let $\eta > 0$ be a small parameter, and $\varepsilon^{(\eta)}$ be a smooth function such that $\|\varepsilon - \varepsilon^{(\eta)}\|_{L^1(\Omega)} \to 0$, and $|\varepsilon^{(\eta)}|_{\mathrm{TV}(\Omega)} \to |\varepsilon|_{\mathrm{TV}(\Omega)}$ as $\eta \to 0$. Analogously, we define $\varepsilon_u^{(\eta)}$ to be the smooth approximation of ε_u given by

$$\varepsilon_u^{(\eta)}(\mathbf{x}) = \varepsilon^{(\eta)} \circ \phi_1(\mathbf{x}).$$

From

$$\varepsilon_u^{(\eta)}(\mathbf{x}) - \varepsilon^{(\eta)}(\mathbf{x}) = \left(\varepsilon^{(\eta)} \circ \phi_1\right)(\mathbf{x}) - \left(\varepsilon^{(\eta)} \circ \phi_0\right)(\mathbf{x}), \quad \forall\, \mathbf{x} \in \Omega,$$

we have

$$\varepsilon_u^{(\eta)}(\mathbf{x}) - \varepsilon^{(\eta)}(\mathbf{x}) = \int_0^1 \nabla \varepsilon^{(\eta)}(\phi_t(\mathbf{x})) \cdot \partial_t \phi_t(\mathbf{x}) dt, \quad \forall\, \mathbf{x} \in \Omega.$$

Therefore, for $\psi \in C_0^\infty(\Omega)$ with $C_0^\infty(\Omega)$ being the set of compactly supported $\mathcal{C}^\infty$ functions,

$$\begin{aligned} &\int_\Omega \left[\varepsilon_u^{(\eta)}(\mathbf{x}) - \varepsilon^{(\eta)}(\mathbf{x}) + \nabla \varepsilon^{(\eta)}(\mathbf{x}) \cdot \mathbf{u}(x)\right] \psi(\mathbf{x}) d\mathbf{x} = \\ &\quad \int_\Omega \left[\int_0^1 \nabla \varepsilon^{(\eta)}(\phi_t(\mathbf{x})) \cdot \partial_t \phi_t(\mathbf{x}) dt\right] \psi(\mathbf{x}) d\mathbf{x} + \int_\Omega \nabla \varepsilon^{(\eta)}(\mathbf{x}) \cdot \mathbf{u}(\mathbf{x}) \psi(\mathbf{x}) d\mathbf{x}, \quad \forall\, \mathbf{x} \in \Omega. \end{aligned} \tag{3.3.2}$$

By a change of variables in the first integral and using the fact that

$$\partial_t \phi_t(\mathbf{x}) = -\partial_{\mathbf{x}} \phi_t(\mathbf{x}) \partial_t \phi_t^{-1}(\mathbf{y})|_{\mathbf{y}=\phi_t(\mathbf{x})},$$

we get, for all $\mathbf{x} \in \Omega$,

$$\int_0^1 \left[\int_\Omega \nabla \varepsilon^{(\eta)}(\phi_t(\mathbf{x})) \cdot \partial_t \phi_t(\mathbf{x}) \psi(\mathbf{x}) d\mathbf{x} \right] dt = \\ - \int_0^1 \int_\Omega \nabla \varepsilon^{(\eta)}(\mathbf{y}) \cdot \left[\partial_{\mathbf{x}} \phi_t(\phi_t^{-1}(\mathbf{y})) \partial_t \phi_t^{-1}(\mathbf{y}) \right] |\text{det } \partial_{\mathbf{x}} \phi_t^{-1}(\mathbf{y})| \psi \left(\phi_t^{-1}(\mathbf{y}) \right) d\mathbf{y} dt.$$

Here, det denotes the determinant of a matrix. Since

$$\forall\ (\mathbf{y}, t) \in \Omega \times [0,1], \quad \partial_t \phi_t^{-1}(\mathbf{y}) = \mathbf{u}(\mathbf{y}),$$

$$\partial_{\mathbf{y}} \phi_t^{-1}(\mathbf{y}) = \mathbb{I} + t \nabla \mathbf{u}(\mathbf{y}),$$

and

$$\partial_{\mathbf{x}} \phi_t(\phi_t^{-1}(\mathbf{y})) \partial_{\mathbf{y}} \phi_t^{-1}(\mathbf{y}) = \mathbb{I},$$

we can write

$$\int_0^1 \int_\Omega \left[\nabla \varepsilon^{(\eta)}(\phi_t(\mathbf{x})) \cdot \partial_t \phi_t(\mathbf{x}) \psi(\mathbf{x}) d\mathbf{x} \right] dt = \\ - \int_0^1 \int_\Omega \nabla \varepsilon^{(\eta)}(\mathbf{y}) \cdot \left[(\mathbb{I} + t \nabla \mathbf{u}(\mathbf{y}))^{-1} \mathbf{u}(\mathbf{y}) \right] |\text{det } \mathbb{I} + t \nabla \mathbf{u}(\mathbf{y})| \psi \left(\phi_t^{-1}(\mathbf{y}) \right) d\mathbf{y} dt,$$

and hence,

$$\int_\Omega \left[\varepsilon_u^{(\eta)}(\mathbf{x}) - \varepsilon^{(\eta)}(\mathbf{x}) + \nabla \varepsilon^{(\eta)}(\mathbf{x}) \cdot \mathbf{u}(\mathbf{x}) \right] \psi(\mathbf{x}) d\mathbf{x} = \\ \int_0^1 \int_\Omega \nabla \varepsilon^{(\eta)}(\mathbf{x}) \cdot \mathbf{u}(\mathbf{x}) \left[\psi(\mathbf{x}) - \psi \left(\phi_t^{-1}(\mathbf{x}) \right) \right] d\mathbf{x} dt \\ + \int_0^1 \int_\Omega \nabla \varepsilon^{(\eta)}(\mathbf{x}) \cdot \left(\left[(\mathbb{I} + t \nabla \mathbf{u}(\mathbf{x}))^{-1} |\text{det } \mathbb{I} + t \nabla \mathbf{u}(\mathbf{x})| - \mathbb{I} \right] \mathbf{u}(\mathbf{x}) \right) \psi \left(\phi_t^{-1}(\mathbf{x}) \right) d\mathbf{x} dt. \tag{3.3.3}$$

The first term in the right-hand side of (3.3.3) can be estimated as follows:

$$\left| \int_0^1 \int_\Omega \nabla \varepsilon^{(\eta)}(\mathbf{x}) \cdot \mathbf{u}(\mathbf{x}) \left[\psi(\mathbf{x}) - \psi \left(\phi_t^{-1}(\mathbf{x}) \right) \right] d\mathbf{x} dt \right| \leq \|\mathbf{u}\|^2_{\mathcal{C}^0(\overline{\Omega})^d} \|\nabla \varepsilon^{(\eta)}\|_{L^1(\Omega)^d} \|\nabla \psi\|_{\mathcal{C}^0(\Omega)^d}.$$

Let tr denote the trace of a matrix. Using the fact that

$$(\mathbb{I} + t\nabla\mathbf{u})^{-1} = \sum_{i=0}(-1)^i \left(t\nabla\mathbf{u}\right)^i,$$

which follows from $||\mathbf{u}||_{\mathcal{C}^1(\Omega)^d} < 1$, and

$$\det\ (\mathbb{I} + t\nabla\mathbf{u}) = \begin{cases} 1 - \text{tr } t\nabla\mathbf{u} + \det\ t\nabla\mathbf{u} & \text{if } d = 2, \\ 1 + \text{tr } t\nabla\mathbf{u} - \dfrac{1}{2}\left[(\text{tr } t\nabla\mathbf{u})^2 - \text{tr }\ (t\nabla\mathbf{u})^2\right] + \det\ t\nabla\mathbf{u} & \text{if } d = 3, \end{cases}$$

we get

$$\int_0^1 \int_\Omega \nabla\varepsilon^{(\eta)}(\mathbf{x}) \cdot \mathbf{u}(\mathbf{x}) \left[(\mathbb{I} + t\nabla\mathbf{u}(\mathbf{x}))^{-1} \left|\det\ \mathbb{I} + t\nabla\mathbf{u}(\mathbf{x})\right| - \mathbb{I}\right] \psi\left(\phi_t^{-1}(\mathbf{x})\right) dxdt$$
$$\leq \|\mathbf{u}\|_{\mathcal{C}^0(\overline{\Omega})^d} \|\mathbf{u}\|_{\mathcal{C}^1(\overline{\Omega})^d} \|\nabla\varepsilon^{(\eta)}\|_{L^1(\Omega)^d} \|\psi\|_{\mathcal{C}^0(\Omega)},$$

which is the desired estimate for the second term in the right-hand side of (3.3.3).

Now, we can deduce the final result by density when $\eta \to 0$. Since $\mathbf{u} \in \mathcal{C}^1(\Omega)^d$ and $\psi \in \mathcal{C}_0^1(\Omega)$, we can write

$$\int_\Omega \psi\mathbf{u} \cdot \nabla\varepsilon^{(\eta)} = -\int_\Omega \nabla \cdot (\psi\mathbf{u})\varepsilon^{(\eta)}.$$

Since $\|\varepsilon^{(\eta)} - \varepsilon\|_{L^1(\Omega)} \to 0$, we have

$$\int_\Omega \nabla \cdot (\psi\mathbf{u})\varepsilon^{(\eta)} \to \int_\Omega \nabla \cdot (\psi\mathbf{u})\varepsilon.$$

As $|\varepsilon^{(\eta)}|_{\text{TV}(\Omega)} \to |\varepsilon|_{\text{TV}(\Omega)}$, we arrive at (3.3.1) and the proof of the proposition is complete. □

3.3.2 Local recovery via linearization

Assuming that $\varepsilon \in \text{SBV}^2(\Omega)$, we can write

$$D\varepsilon = \nabla\varepsilon\mathcal{H}^d + [\varepsilon]_S \boldsymbol{\nu}_S \mathcal{H}_S^{d-1},$$

where $\boldsymbol{\nu}_S$ is the outward normal at the oriented surface S of discontinuity of ε.

The data consists of ε and ε_u on Ω. In order to reconstruct $\mathbf{u}$, we can use the first order approximation of $\varepsilon - \varepsilon_u$:

$$\varepsilon - \varepsilon_u \approx \mathbf{u} \cdot D\varepsilon,$$

given by Proposition 3.3.1. These data can be decomposed into two parts:

$$\mathbf{u} \cdot D\varepsilon(\cdot) = \mathbf{u} \cdot \nabla\varepsilon \mathcal{H}^d + [\varepsilon]_S \mathbf{u} \cdot \boldsymbol{\nu}_S \mathcal{H}_S^{d-1} = d_{\text{reg}} \mathcal{H}^d + d_{\text{sing}} \mathcal{H}_S^{d-1}.$$

Let w be a mollifier supported on $[-1, 1]$. For any $\delta > 0$, we define

$$w_\delta = \frac{1}{\delta^d} w\left(\frac{\cdot}{\delta}\right),$$

and introduce

$$\mathbf{u}_\delta(\mathbf{x}) = \int_\Omega \mathbf{u}(\mathbf{y}) w_\delta(|\mathbf{x} - \mathbf{y}|) d\mathbf{y}.$$

Since $\mathbf{u}$ is smooth, for any $\mathbf{x} \in \Omega$, $\mathbf{u}_\delta(\mathbf{x})$ is a good approximation of $\mathbf{u}$ on the ball with center $\mathbf{x}$ and radius δ.

We want to find an approximate value for $\mathbf{u}_\delta$ from the optical measurements and use it as an initial guess in an optimization procedure. For doing so, we introduce the functional $J_\mathbf{x} : \mathbb{R}^d \longrightarrow \mathbb{R}$ given by

$$\begin{aligned}\mathbf{u} \longmapsto J_\mathbf{x}(\mathbf{u}) = \int_\Omega |\nabla\varepsilon(\mathbf{y}) \cdot \mathbf{u} - d_{\text{reg}}(\mathbf{y})|^2 w_\delta(|\mathbf{x} - \mathbf{y}|) d\mathbf{y} \\ + \int_\Omega |[\varepsilon]_S \mathbf{u} \cdot \boldsymbol{\nu}_S - d_{\text{sing}}(\mathbf{y})|^2 w_\delta(|\mathbf{x} - \mathbf{y}|) d\mathbf{y},\end{aligned}$$

and look for minimizers of $J_\mathbf{x}$ in $\mathbb{R}^d$. The gradient of $J_\mathbf{x}$ can be explicitly computed as follows:

$$\begin{aligned}\nabla J_\mathbf{x}(\mathbf{u}) = 2 \int_\Omega \left(\nabla\varepsilon(y) \cdot \mathbf{u} - d_{\text{reg}}(\mathbf{y})\right) \nabla\varepsilon(\mathbf{y}) w_\delta(|\mathbf{x} - \mathbf{y}|) d\mathbf{y} \\ + 2 \int_\Omega \left([\varepsilon]_S(\mathbf{y}) \mathbf{u} \cdot \boldsymbol{\nu}(\mathbf{y}) - d_{\text{sing}}(\mathbf{y})\right) [\varepsilon]_S(\mathbf{y}) \boldsymbol{\nu}(\mathbf{y}) w_\delta(|\mathbf{x} - \mathbf{y}|) d\mathbf{y}.\end{aligned}$$

In the case where ε has no jumps, $J_\mathbf{x}$ is a quadratic functional and we have

$$\nabla J_\mathbf{x}(\mathbf{u}) = 0 \Leftrightarrow \mathbf{u}^T \left(\int_\Omega w_\delta(|\mathbf{x} - \mathbf{y}|) \nabla\varepsilon(\mathbf{y}) \nabla\varepsilon^T(\mathbf{y}) d\mathbf{y} \right) = \int_{\mathbf{x}+\delta B} d_{\text{reg}}(\mathbf{y}) w_\delta(|\mathbf{x} - \mathbf{y}|) \nabla\varepsilon(\mathbf{y}) d\mathbf{y}, \tag{3.3.4}$$

where B is the ball with center 0 and radius 1.

If the matrix $\int_\Omega w_\delta(|\mathbf{x}-\mathbf{y}|)\nabla\varepsilon(\mathbf{y})\nabla\varepsilon^T(\mathbf{y})$ is invertible, then the minimizer is given by

$$\mathbf{u}^T = \left(\int_\Omega w_\delta(|\mathbf{x}-\mathbf{y}|)\nabla\varepsilon(\mathbf{y})\nabla\varepsilon^T(\mathbf{y})d\mathbf{y}\right)^{-1}\int_{\mathbf{x}+\delta B} d_{\text{reg}}w_\delta(|\mathbf{x}-\mathbf{y}|)\nabla\varepsilon(\mathbf{y})d\mathbf{y}. \quad (3.3.5)$$

The following proposition gives a sufficient condition for the invertibilty of the matrix $\int_\Omega w_\delta(|\mathbf{x}-\mathbf{y}|)\nabla\varepsilon(\mathbf{y})\nabla\varepsilon^T(\mathbf{y})$.

Proposition 3.3.2. *Suppose that ε has no jumps and $d=2$. Assume $\mathbf{x}+\delta B\subset\Omega$. Then, if all vectors $\nabla\varepsilon$ in $\{\mathbf{y}\ :\ w_\delta(|\mathbf{y}-\mathbf{x}|)\neq 0\}$ are not collinear, then the matrix*

$$\int_\Omega w_\delta(|\mathbf{x}-\mathbf{y}|)\nabla\varepsilon(\mathbf{y})\nabla\varepsilon^T(\mathbf{y})d\mathbf{y}$$

is invertible.

Proof. Writing

$$\forall\ \mathbf{y}\in\mathbf{x}+\delta B,\quad \nabla\varepsilon(\mathbf{y}) = u(\mathbf{y})\mathbf{e}_1 + v(\mathbf{y})\mathbf{e}_2,$$

where $\{\mathbf{e}_1,\mathbf{e}_2\}$ is the cannonical basis of $\mathbb{R}^2$, it follows that

$$\nabla\varepsilon\nabla\varepsilon^T(\mathbf{y}) = u^2(\mathbf{y})\mathbf{e}_1\mathbf{e}_1^T + v^2(\mathbf{y})\mathbf{e}_2\mathbf{e}_2^T + u(\mathbf{y})v(\mathbf{y})\left(\mathbf{e}_1\mathbf{e}_2^T+\mathbf{e}_2\mathbf{e}_1^T\right),\quad \forall\ \mathbf{y}\in\mathbf{x}+\delta B.$$

Computing the convolution with respect to w_δ, we get

$$\begin{aligned}\int_\Omega w_\delta(|\mathbf{y}-\mathbf{y}|)\nabla\varepsilon(\mathbf{y})\nabla\varepsilon^T(\mathbf{y})d\mathbf{y} &= \left(\int_\Omega u^2(\mathbf{y})w_\delta(|\mathbf{y}-\mathbf{x}|)d\mathbf{y}\right)\mathbf{e}_1\mathbf{e}_1^T\\ &+\left(\int_\Omega v^2(\mathbf{y})w_\delta(|\mathbf{y}-\mathbf{x}|)d\mathbf{y}\right)\mathbf{e}_2\mathbf{e}_2^T + \left(\int_\Omega u(\mathbf{y})v(\mathbf{y})w_\delta^T(|\mathbf{y}-\mathbf{x}|)d\mathbf{y}\right)\left(\mathbf{e}_1\mathbf{e}_2^T+\mathbf{e}_2\mathbf{e}_1^T\right).\end{aligned}$$

This matrix is not invertible if and only if

$$\left(\int_\Omega u^2(\mathbf{y})w_\delta(|\mathbf{y}-\mathbf{x}|)d\mathbf{y}\right)\left(\int_\Omega v^2(\mathbf{y})w_\delta(|\mathbf{y}-\mathbf{x}|)d\mathbf{y}\right) = \left(\int_\Omega u(\mathbf{y})v(\mathbf{y})w_\delta(|\mathbf{y}-\mathbf{x}|)d\mathbf{y}\right)^2,$$

which is exactly the equality case in weighted Cauchy-Schwarz inequality. So, if there exist two points $\mathbf{y_1},\mathbf{y_2}\in\{\mathbf{y}:\ w_\delta(|\mathbf{y}-\mathbf{x}|)\neq 0\}$ such that $\nabla\varepsilon(\mathbf{y_1})\times\nabla\varepsilon(\mathbf{y_2})\neq 0$, then u is not proportional to v, and the matrix is invertible. □

Remark 3.3.3. *Assuming that* $\nabla\varepsilon(\mathbf{y}) \neq 0$ *for* $\mathbf{y} \in \mathbf{x} + \delta B \subset \Omega$*, Proposition 3.3.2 gives that the direction of* $\dfrac{\nabla\varepsilon}{|\nabla\varepsilon|}$ *in not constant in* $\mathbf{x} + \delta B \subset \Omega$ *if and only if*

$$\int_{\mathbf{x}+\delta B} \nabla\varepsilon(\mathbf{y})\nabla\varepsilon^T(\mathbf{y})d\mathbf{y} \quad \textit{is invertible.}$$

Hence, under the above condition on ε *in the neighborhood* $\mathbf{x} + \delta B$*, the displacement field* $\mathbf{u}$ *at* $\mathbf{x}$ *can be approximately reconstructed.*

Remark 3.3.4. *By exactly the same arguments as those in two dimensions, one can prove that in the three-dimensional case, if all vectors* $\nabla\varepsilon$ *in* $\{\mathbf{y} \ : \ w_\delta(|\mathbf{y} - \mathbf{x}|) \neq 0\}$ *are not coplanar, then the matrix*

$$\int_\Omega w_\delta(|\mathbf{x} - \mathbf{y}|)\nabla\varepsilon(\mathbf{y})\nabla\varepsilon^T(\mathbf{y})d\mathbf{y}$$

is invertible.

On the other hand, in the case where ε *is piecewise smooth, one can first detect the surface of jumps of* ε *using for example an edge detection algorithm [44, 108] and then apply the proposed local algorithm in order to have a good approximation of* $\mathbf{u}$ *in the domains where* ε *is smooth.*

3.3.3 Minimization of the discrepancy functional

Let $\varepsilon \in \mathcal{C}_S^{k,\alpha}\big(\overline{\Omega}\big)$, where S is the surface of discontinuity. For the sake of simplicity we assume that $\Omega \setminus S$ is the union of two connected domains $\Omega_1 \cup \Omega_2$. Therefore, ε can be written as

$$\varepsilon = \varepsilon_1\chi_{\Omega_1} + \varepsilon_2\chi_{\Omega_2} \tag{3.3.6}$$

with $\varepsilon_i \in \mathcal{C}^1(\overline{\Omega}_i)$, for $i = 1, 2$.

Denote $\mathbf{u}^*$ the applied (true) displacement on Ω (as defined in (3.1.1)) and $\tilde{\varepsilon}$ the measured deformed optical image given by

$$\tilde{\varepsilon} = \varepsilon \circ (\mathbb{I} + \mathbf{u}^*)^{-1}.$$

Recall that a non-differentiable functional $\mathbf{u} \mapsto I(\mathbf{u})$ has a nonempty subgradient if there exists $\boldsymbol{\xi}$ such that

$$I(\mathbf{u} + \mathbf{h}) - I(\mathbf{u}) \geq (\boldsymbol{\xi}, \mathbf{h}), \tag{3.3.7}$$

holds for $||\mathbf{h}||$ small enough, which means that $\boldsymbol{\xi} \in \partial I$ with ∂I being the subgradient of I. In order to minimize I, it is sufficient to find one $\boldsymbol{\xi} \in \partial I$; see [49].

The following result holds.

Proposition 3.3.5. *Let ε verify (3.3.6), $\mathbf{u}^* \in \mathcal{C}^1(\Omega)^d$ be the solution of (3.1.1), and $\tilde{\varepsilon} = \varepsilon \circ (\mathbb{I} + \mathbf{u}^*)^{-1}$. Suppose that $\Omega_2 \Subset \Omega$. Then, the functional I defined by*

$$\begin{aligned} I : \mathcal{C}^1(\Omega)^d &\longrightarrow \mathbb{R}, \\ \mathbf{u} &\longmapsto I(\mathbf{u}) = \int_\Omega |\widetilde{\varepsilon} \circ (\mathbb{I} + \mathbf{u}) - \varepsilon|^2 \, d\mathbf{x} \end{aligned} \tag{3.3.8}$$

has a nonempty subgradient. Let $\boldsymbol{\xi}$ in the dual of $\mathcal{C}^1(\Omega)^d$ be given by

$$\boldsymbol{\xi} : \mathbf{h} \mapsto 2 \int_\Omega [\tilde{\varepsilon}(\mathbf{x} + \mathbf{u}) - \varepsilon(\mathbf{x})] \mathbf{h}(\mathbf{x}) \cdot D\tilde{\varepsilon} \circ (\mathbb{I} + \mathbf{u})(\mathbf{x}) \, d\mathbf{x}. \tag{3.3.9}$$

For $||\mathbf{h}||_{\mathcal{C}^1(\Omega)^d}$ small enough, (3.3.7) holds with $(\ ,\ )$ being the duality product between $\mathcal{C}^1(\Omega)^d$ and its dual.

Remark 3.3.6. *It is worth emphasizing that if ε has no jump, then I is Fréchet differentiable and $\boldsymbol{\xi}$ is its Fréchet derivative.*

Remark 3.3.7. *Under the assumptions of Proposition 3.3.5, if $\mathbf{u}^*$ is small enough (in $\mathcal{C}^1$-norm), then $\tilde{\varepsilon} = \varepsilon \circ (\mathbb{I} + \mathbf{u}^*)^{-1}$ can be written as*

$$\tilde{\varepsilon} = \tilde{\varepsilon}_1 + \tilde{\varepsilon}_2 \chi_{\tilde{\Omega}_2}, \tag{3.3.10}$$

with $\tilde{\varepsilon}_1 \in \mathcal{C}^1(\overline{\Omega})$ and $\tilde{\varepsilon}_2 \in \mathcal{C}^1_0(\Omega)$. In the sequel, we shall define $\tilde{\Omega}_i = (\mathbb{I} + \mathbf{u}^*)(\Omega_i)$ and $\tilde{f}_i = \varepsilon_i \circ (\mathbb{I} + \mathbf{u}^*)^{-1}$. For doing so, we extend $\tilde{f}_1$ into a function $\tilde{\varepsilon}_1$ defined on the whole domain such that $\tilde{\varepsilon}_1 \in \mathcal{C}^1(\overline{\Omega})$ and $\tilde{\varepsilon}_1\big|_{\tilde{\Omega}_1} = \tilde{f}_1$. Then, we set $\tilde{\varepsilon}_2 = \tilde{f}_2 - \tilde{\varepsilon}_1$ on $\tilde{\Omega}_2$. Finally, we extend $\tilde{\varepsilon}_2$ into a compactly supported $\mathcal{C}^1$-function on the whole domain Ω.

We first prove the following lemma.

Lemma 3.3.8. *Let $\mathbf{u}, \mathbf{h} \in \mathcal{C}^1(\Omega)^d$ and let $\tilde{\varepsilon}$ be as in (3.3.10). Then, for $\|\mathbf{u} - \mathbf{u}^*\|_{\mathcal{C}^1(\Omega)^d}$ and $\|\mathbf{h}\|_{\mathcal{C}^1(\Omega)^d}$ small enough, we have*

$$\int_\Omega \left[\tilde{\varepsilon}(\mathbf{x} + \mathbf{u} + \mathbf{h}) - \tilde{\varepsilon}(\mathbf{x} + \mathbf{u})\right]^2 \, d\mathbf{x} = \int_\Omega \tilde{\varepsilon}_2^2(\mathbf{x} + \mathbf{u}) |\mathbf{h} \cdot \boldsymbol{\nu}| \delta_{\partial\tilde{\Omega}_2}(\mathbf{x} + \mathbf{u}) \, d\mathbf{x} + o(\|\mathbf{h}\|_{\mathcal{C}^1(\Omega)^d}), \tag{3.3.11}$$

where $\delta_{\partial\tilde{\Omega}_2}$ is the Dirac distribution on $\partial\tilde{\Omega}_2$ and $\tilde{\varepsilon}_2$ is defined in Remark 3.3.7.

Proof. We start by decomposing $\tilde{\varepsilon}$ as follows:

$$\int_\Omega \left[\tilde{\varepsilon}(\mathbf{x}+\mathbf{u}+\mathbf{h}) - \tilde{\varepsilon}(\mathbf{x}+\mathbf{u})\right]^2 d\mathbf{x} =$$
$$\int_\Omega \left[\Big(\tilde{\varepsilon}_1(\mathbf{x}+\mathbf{u}+\mathbf{h}) - \tilde{\varepsilon}_1(\mathbf{x}+\mathbf{u})\Big) + \Big(\tilde{\varepsilon}_2(\mathbf{x}+\mathbf{u}+\mathbf{h})\chi_{\tilde{\Omega}_2}(\mathbf{x}+\mathbf{u}+\mathbf{h}) - \tilde{\varepsilon}_2(\mathbf{x}+\mathbf{u})\chi_{\tilde{\Omega}_2}(\mathbf{x}+\mathbf{u})\Big)\right]^2 d\mathbf{x}.$$

Now, by developing the square, the first term can be estimated by

$$\left|\int_\Omega \Big(\tilde{\varepsilon}_1(\mathbf{x}+\mathbf{u}+\mathbf{h}) - \tilde{\varepsilon}_1(\mathbf{x}+\mathbf{u})\Big)^2 d\mathbf{x}\right| \leq \|\tilde{\varepsilon}_1\|^2_{\mathcal{C}^1(\Omega)} \|\mathbf{h}\|^2_{\mathcal{C}^1(\Omega)^d}.$$

Next, we write

$$\begin{aligned}\tilde{\varepsilon}_2(x+\mathbf{u}+\mathbf{h})\chi_{\tilde{\Omega}_2}(\mathbf{x}+\mathbf{u}+\mathbf{h}) - \tilde{\varepsilon}_2(\mathbf{x}+\mathbf{u})\chi_{\tilde{\Omega}_2}(\mathbf{x}+\mathbf{u}) &= \left[\tilde{\varepsilon}_2(\mathbf{x}+\mathbf{u}+\mathbf{h}) - \tilde{\varepsilon}_2(\mathbf{x}+\mathbf{u})\right]\chi_{\tilde{\Omega}_2}(\mathbf{x}+\mathbf{u}+\mathbf{h}) \\ &\quad + \Big[\chi_{\tilde{\Omega}_2}(\mathbf{x}+\mathbf{u}+\mathbf{h}) - \chi_{\tilde{\Omega}_2}(\mathbf{x}+\mathbf{u})\Big]\tilde{\varepsilon}_2(\mathbf{x}+\mathbf{u}).\end{aligned}$$

Since $\left(\tilde{\varepsilon}_1(\mathbf{x}+\mathbf{u}+\mathbf{h}) - \tilde{\varepsilon}_1(\mathbf{x}+\mathbf{u})\right)\tilde{\varepsilon}_2(\mathbf{x}+\mathbf{u}) \in \mathcal{C}^1_0(\Omega)$, Proposition 3.3.1 yields

$$\begin{aligned}&\left|\int_\Omega \Big[\tilde{\varepsilon}_1(\mathbf{x}+\mathbf{u}+\mathbf{h}) - \tilde{\varepsilon}_1(\mathbf{x}+\mathbf{u})\Big]\Big[\chi_{\tilde{\Omega}_2}(\mathbf{x}+\mathbf{u}+\mathbf{h}) - \chi_{\tilde{\Omega}_2}(\mathbf{x}+\mathbf{u})\Big]\tilde{\varepsilon}_2(\mathbf{x}+\mathbf{u})\,d\mathbf{x}\right| \\ &\leq C\left(\int_\Omega \left[\mathbf{h}\cdot\nabla\tilde{\varepsilon}_1(\mathbf{x}+\mathbf{u})\right]^2 d\mathbf{x}\right)^{1/2}\left(\left[\int_\Omega \left[\mathbf{h}\cdot\boldsymbol{\nu}\tilde{\varepsilon}_2(\mathbf{x}+\mathbf{u})\right]^2 \delta_{\partial\tilde{\Omega}_2}(\mathbf{x}+\mathbf{u})\,d\mathbf{x}\right] + o(\|\mathbf{h}\|_{\mathcal{C}^1(\Omega)^d})\right)^{1/2} \\ &\leq C\|\mathbf{h}\|^2_{\mathcal{C}^1(\Omega)^d}.\end{aligned}$$

We now need to handle the last term

$$\begin{aligned}&\int_\Omega \Big(\Big[\chi_{\tilde{\Omega}_2}(\mathbf{x}+\mathbf{u}+\mathbf{h}) - \chi_{\tilde{\Omega}_2}(\mathbf{x}+\mathbf{u})\Big]\tilde{\varepsilon}_2(\mathbf{x}+\mathbf{u})\Big)^2 d\mathbf{x} \\ &\qquad = \int_\Omega \Big|\chi_{\tilde{\Omega}_2}(\mathbf{x}+\mathbf{u}+\mathbf{h}) - \chi_{\tilde{\Omega}_2}(\mathbf{x}+\mathbf{u})\Big|\tilde{\varepsilon}_2(\mathbf{x}+\mathbf{u})^2\,d\mathbf{x}.\end{aligned}$$

Using Proposition 3.3.1, we obtain that

$$\int_\Omega \Big(\Big|\chi_{\tilde{\Omega}_2}(\mathbf{x}+\mathbf{u}+\mathbf{h}) - \chi_{\tilde{\Omega}_2}(\mathbf{x}+\mathbf{u})\Big|\tilde{\varepsilon}_2(\mathbf{x}+\mathbf{u})\Big)^2 d\mathbf{x} = \int_\Omega \tilde{\varepsilon}_2^2(\mathbf{x}+\mathbf{u})|\mathbf{h}\cdot\boldsymbol{\nu}|\delta_{\partial\tilde{\Omega}_2}(\mathbf{x}+\mathbf{u})\,d\mathbf{x} + o(\|\mathbf{h}\|_{\mathcal{C}^1(\Omega)^d}),$$

which completes the proof of the lemma. □

We are now ready to prove Proposition 3.3.5.

Proof. of Proposition 3.3.5. If $\mathbf{u} \in \mathcal{C}^1(\Omega)^2$ and $\mathbf{h} \in \mathcal{C}^1(\Omega)^2$, then we have

$$I(\mathbf{u}+\mathbf{h}) - I(\mathbf{u}) = \int_\Omega \left[\tilde{\varepsilon}(\mathbf{x}+\mathbf{u}+\mathbf{h}) + \tilde{\varepsilon}(\mathbf{x}+\mathbf{u}) - 2\varepsilon(\mathbf{x})\right]\left[\tilde{\varepsilon}(\mathbf{x}+\mathbf{u}+\mathbf{h}) - \tilde{\varepsilon}(\mathbf{x}+\mathbf{u})\right] d\mathbf{x},$$

and hence,

$$I(\mathbf{u}+\mathbf{h}) - I(\mathbf{u}) = \int_\Omega \left[\tilde{\varepsilon}(\mathbf{x}+\mathbf{u}+\mathbf{h}) - \tilde{\varepsilon}(\mathbf{x}+\mathbf{u})\right]^2 \, d\mathbf{x} \\ + 2\int_\Omega \left[\tilde{\varepsilon}(\mathbf{x}+\mathbf{u}) - \varepsilon(\mathbf{x})\right]\left[\tilde{\varepsilon}(\mathbf{x}+\mathbf{u}+\mathbf{h}) - \tilde{\varepsilon}(\mathbf{x}+\mathbf{u})\right] \, d\mathbf{x}.$$

For any $\eta > 0$, let $g^{(\eta)}$ be a smooth, compactly supported function such that

$$\|g^{(\eta)} - [\tilde{\varepsilon} \circ (\mathbb{I}+\mathbf{u}) - \varepsilon]\,\|_{L^2(\Omega)} < \eta \quad \text{and} \quad \left||g^{(\eta)}|_{\mathrm{TV}(\Omega)} - |\tilde{\varepsilon} \circ (\mathbb{I}+\mathbf{u}) - \varepsilon|_{\mathrm{TV}(\Omega)}\right| < \eta;$$

see [5].

Now, we write

$$\int_\Omega \left[\tilde{\varepsilon}(\mathbf{x}+\mathbf{u}) - \varepsilon(\mathbf{x})\right]\left[\tilde{\varepsilon}(\mathbf{x}+\mathbf{u}+\mathbf{h}) - \tilde{\varepsilon}(\mathbf{x}+\mathbf{u})\right] \, d\mathbf{x} = \int_\Omega g^\eta(\mathbf{x})\left[\tilde{\varepsilon}(\mathbf{x}+\mathbf{u}+\mathbf{h}) - \tilde{\varepsilon}(\mathbf{x}+\mathbf{u})\right] \, d\mathbf{x} \\ + \int_\Omega \left[\tilde{\varepsilon}(\mathbf{x}+\mathbf{u}) - \varepsilon(\mathbf{x}) - g^\eta(\mathbf{x})\right]\left[\tilde{\varepsilon}(\mathbf{x}+\mathbf{u}+\mathbf{h}) - \tilde{\varepsilon}(\mathbf{x}+\mathbf{u})\right] \, d\mathbf{x}.$$

Let $\tau_{\mathbf{h}}$ be the translation operator. Then, $\tau_{\mathbf{h}}$ satisfies, for any $\mathbf{h} \in \mathcal{C}^1(\Omega)^d$,

$$\|\tau_{\mathbf{h}}[f] - f\|_p \leq C(f)\|\mathbf{h}\|_{\mathcal{C}^1(\Omega)^d}, \quad \forall\, f \in \mathrm{SBV}^p(\Omega). \tag{3.3.12}$$

Using Cauchy-Schwartz' inequality, we get

$$\left| \int_\Omega \left[\tilde{\varepsilon}(\mathbf{x}+\mathbf{u}) - \varepsilon(\mathbf{x}) - g^\eta(\mathbf{x})\right]\left[\tilde{\varepsilon}(\mathbf{x}+\mathbf{u}+\mathbf{h}) - \tilde{\varepsilon}(\mathbf{x}+\mathbf{u})\right] \, d\mathbf{x} \right| \leq C\eta\|\mathbf{h}\|_{\mathcal{C}^1(\Omega)^d}, \tag{3.3.13}$$

where C is a constant depending on $\tilde{\varepsilon},\ \mathbf{u}$, and Ω.

We know that for a certain function ρ such that $\rho(s) \to 0$ when $s \to 0$:

$$\left| \int_\Omega g^\eta(\mathbf{x})\left[\tilde{\varepsilon}(\mathbf{x}+\mathbf{u}+\mathbf{h}) - \tilde{\varepsilon}(\mathbf{x}+\mathbf{u})\right] \, d\mathbf{x} - \int_\Omega g^\eta(\mathbf{x})\mathbf{h}(\mathbf{x}) \cdot D\left(\tilde{\varepsilon} \circ (\mathbb{I}+\mathbf{u})\right) \, d\mathbf{x} \right| \leq \|\mathbf{h}\|_{\mathcal{C}^1(\Omega)^d}\rho(\|\mathbf{h}\|_{\mathcal{C}^1(\Omega)^d}). \tag{3.3.14}$$

Now, we have the following estimate:

$$\left| \int_\Omega g^\eta(\mathbf{x})\mathbf{h}(\mathbf{x}) \cdot D\left(\tilde{\varepsilon} \circ (\mathbb{I}+\mathbf{u})\right) \, d\mathbf{x} - \int_\Omega [\tilde{\varepsilon}(\mathbf{x}+\mathbf{u}) - \varepsilon(\mathbf{x})]\mathbf{h}(\mathbf{x}) \cdot D\left(\tilde{\varepsilon} \circ (\mathbb{I}+\mathbf{u})\right) \, d\mathbf{x} \right| \leq C'\eta\|\mathbf{h}\|_{\mathcal{C}^1(\Omega)^d}. \tag{3.3.15}$$

Indeed, since $\tilde{\varepsilon} \in \mathcal{C}_S^{k,\alpha}\left(\overline{\Omega}\right) \subset \mathrm{SBV}(\Omega)$, $\tilde{\varepsilon} \circ (\mathbb{I}+\mathbf{u}) \in \mathrm{SBV}(\Omega)$ and we can write the following decomposition of $D\left(\tilde{\varepsilon} \circ (\mathbb{I}+\mathbf{u})\right)$ into a continuous part and a jump part on a

rectifiable surface S:

$$D\left(\tilde{\varepsilon}\circ(\mathbb{I}+\mathbf{u})\right)=\nabla\left(\tilde{\varepsilon}\circ(\mathbb{I}+\mathbf{u})\right)\mathcal{H}^d+[\tilde{\varepsilon}\circ(\mathbb{I}+\mathbf{u})]\boldsymbol{\nu}_S\mathcal{H}_S^{d-1},$$

we have that

$$\left|\int_\Omega\Big[g^\eta(\mathbf{x})-[\tilde{\varepsilon}(\mathbf{x}+\mathbf{u})-\varepsilon(\mathbf{x})]\Big]\mathbf{h}(\mathbf{x})\cdot\nabla\left(\tilde{\varepsilon}\circ(\mathbb{I}+\mathbf{u})\right)(\mathbf{x})\,d\mathbf{x}\right|\leq C_1\eta\|\mathbf{h}\|_{\mathcal{C}^1(\Omega)^d}.$$

For the jump part, since S is a rectifiable surface and the function $f^\eta=g^\eta-[\tilde{\varepsilon}\circ(\mathbb{I}+\mathbf{u})-\varepsilon]$ is piecewise continuous, it is possible to define a trace $f^\eta|_S$ on the surface S satisfying

$$\|f^\eta|_S\|_{L^1(S)}\leq C_2\|f^\eta\|_{L^1(\Omega)}$$

for some positive constant C_2 depending only on S and Ω. Then we get

$$\left|\int_S f^\eta\mathbf{h}(\mathbf{x})\cdot[\tilde{\varepsilon}\circ(\mathbb{I}+\mathbf{u})]\boldsymbol{\nu}_S\mathcal{H}_S^{d-1}\right|\leq C_3\eta\|\mathbf{h}\|_{\mathcal{C}^1(\Omega)^d}$$

for some positive constant C_3 independent of η and $\mathbf{h}$.

Now, the last term $\int_\Omega\left[\tilde{\varepsilon}(\mathbf{x}+\mathbf{u}+\mathbf{h})-\tilde{\varepsilon}(\mathbf{x}+\mathbf{u})\right]^2$ can be handled using Lemma 3.3.8. Doing so, we obtain

$$\int_\Omega\left[\tilde{\varepsilon}(\mathbf{x}+\mathbf{u}+\mathbf{h})-\tilde{\varepsilon}(\mathbf{x}+\mathbf{u})\right]^2=\int_\Omega\tilde{\varepsilon}_2^2(\mathbf{x}+\mathbf{u})|\mathbf{h}\cdot\boldsymbol{\nu}|\delta_{\partial\tilde{\Omega}_2}(\mathbf{x}+\mathbf{u})+o(\|\mathbf{h}\|_{\mathcal{C}^1(\Omega)^d}).\quad(3.3.16)$$

Combining (3.3.13), (3.3.14), (3.3.15), and (3.3.16), we get that for every $\eta>0$,

$$\left|I(\mathbf{u}+\mathbf{h})-I(\mathbf{u})-2\int_\Omega[\tilde{\varepsilon}(\mathbf{x}+\mathbf{u})-\varepsilon(\mathbf{x})]\mathbf{h}(\mathbf{x})\cdot D\tilde{\varepsilon}\circ(\mathbb{I}+\mathbf{u})(\mathbf{x})\,d\mathbf{x}-\int_\Omega\tilde{\varepsilon}_2^2(\mathbf{x}+\mathbf{u})|\mathbf{h}\cdot\boldsymbol{\nu}|\delta_{\partial\tilde{\Omega}_2}(\mathbf{x}+\mathbf{u})\,d\mathbf{x}\right|$$
$$\leq C_4\|\mathbf{h}\|_{\mathcal{C}^1(\Omega)^d}\Big(\rho(\|\mathbf{h}\|_{\mathcal{C}^1(\Omega)^d})+\eta\Big)$$

for some positive constant C_4 independent of $\mathbf{h}$ and η.

Finally, it follows that

$$I(\mathbf{u}+\mathbf{h})-I(\mathbf{u})=(\boldsymbol{\xi},\mathbf{h})+\int_\Omega\tilde{\varepsilon}_2^2(\mathbf{x}+\mathbf{u})|\mathbf{h}\cdot\boldsymbol{\nu}|\delta_{\partial\tilde{\Omega}_2}(\mathbf{x}+\mathbf{u})\,d\mathbf{x}+o(\|\mathbf{h}\|_{\mathcal{C}^1(\Omega)^d}),$$

where $\boldsymbol{\xi}$ is defined by (3.3.9). Hence, either $\int_\Omega\tilde{\varepsilon}_2^2(\mathbf{x}+\mathbf{u})|\mathbf{h}\cdot\boldsymbol{\nu}|\delta_{\partial\tilde{\Omega}_2}(\mathbf{x}+\mathbf{u})\,d\mathbf{x}$ is of order of $\|\mathbf{h}\|_{\mathcal{C}^1(\Omega)^d}$ and we get

$$I(\mathbf{u}+\mathbf{h})-I(\mathbf{u})\geq(\boldsymbol{\xi},\mathbf{h})$$

for $\|\mathbf{h}\|_{\mathcal{C}^1(\Omega)^d}$ small enough or $\int_\Omega \tilde{\varepsilon}_2^2(\mathbf{x}+\mathbf{u})|\mathbf{h}\cdot\boldsymbol{\nu}|\delta_{\partial\tilde{\Omega}_2}(\mathbf{x}+\mathbf{u})\,d\mathbf{x} = o(\|\mathbf{h}\|_{\mathcal{C}^1(\Omega)^d})$ and in this case, I is Fréchet differentiable and $\boldsymbol{\xi}$ is its Fréchet derivative. The proof of Proposition 3.3.5 is then complete. □

Remark 3.3.9. *The minimization of the functional I gives a reconstruction of $\mathbf{u}^*$ on a subdomain $\Omega \subset \Omega_0$. In practical conditions, since $\mathbf{u}^*$ is small Ω is almost the whole domain Ω_0. The values of $\mathbf{u}^*$ on the boundary are known and, since $\mathbf{u}^*$ is of class $\mathcal{C}^1$, it is possible to deduce the values of $\mathbf{u}^*$ on $\Omega_0 \setminus \Omega$ by interpolation.*

3.4 Reconstruction of the shear modulus

The problem is now to recover the function μ the reconstructed internal data $\mathbf{u}$. For doing so, we use the method described in [10]. We introduce the operator $\mathcal{F}$

$$\mathbf{u} = \mathcal{F}[\mu] = \begin{cases} \nabla\cdot\left(\mu(\nabla\mathbf{u}+\nabla\mathbf{u}^T)\right)+\nabla p = 0 & \text{in } \Omega_0, \\ \nabla\cdot\mathbf{u} = 0 & \text{in } \Omega_0, \\ \mathbf{u} = \mathbf{f} & \text{on } \partial\Omega_0, \end{cases}$$

and minimize the function $\mathcal{K}$ given by

$$\begin{aligned} \mathcal{C}^{0,1}(\overline{\Omega_0}) &\longrightarrow \mathbb{R} \\ \mu &\longmapsto \mathcal{K}[\mu] = \int_\Omega |\mathcal{F}[\mu]-\mathbf{u}|^2\,d\mathbf{x}. \end{aligned}$$

According to [10], $\mathcal{K}$ is Fréchet differentiable and its gradient can be explicitly computed. Let $\mathbf{v}$ be the solution of

$$\begin{cases} \nabla\cdot\left(\mu(\nabla\mathbf{v}+\nabla\mathbf{v}^T)\right)+\nabla q = (\mathcal{F}[\mu]-\mathbf{u}) & \text{in } \Omega_0, \\ \nabla\cdot\mathbf{v} = 0 & \text{in } \Omega_0, \\ \mathbf{v} = 0 & \text{on } \partial\Omega_0. \end{cases}$$

Then,

$$\nabla\mathcal{K}(\mu)[h] = \int_{\Omega_0} h(\nabla\mathbf{v}+\nabla\mathbf{v}^T):(\nabla\mathbf{u}+\nabla\mathbf{u}^T)\,d\mathbf{x}.$$

A gradient descent method can be applied in order to reconstruct μ from $\mathbf{u}$. We refer to [10] for more details.

3.5 Numerical experiments

We take $\Omega = [0,1]^2$ and discretize it on a 300×300 grid, and generate a random Gaussian process to model the optical image ε of the medium as shown in Figure 3.5.1. Given a shear modulus μ map on Ω; see Figure 3.5.5 (left), we solve (3.1.1) on Ω via a finite element method compute the displacement field $\mathbf{u}$. We then compute the displaced optical image ε_u by using a spline interpolation approach and proceed to recover the shear modulus from the data ε and ε_u on the grid by the method described in the paper.

Using (3.3.5), we first compute the initial guess $\mathbf{u}_\delta$ for the displacement field as the least-square solution to minimization of $J_{\mathbf{x}}$. Figure 3.5.2 shows the kernel w_δ used to compute $\mathbf{u}_\delta$. As one can see δ needs to be large enough so the matrix $w_\delta \star \left(\nabla\varepsilon\nabla\varepsilon^T\right)$ is invertible at each point $\mathbf{x}$, which is basically saying that δ must be bigger than the correlation length of ε. Figure 3.5.3 shows the conditioning of the matrix $w_\delta \star \left(\nabla\varepsilon\nabla\varepsilon^T\right)$. Figure 3.5.4 shows the true displacement $\mathbf{u}^*$, the result of the first order approximation (i.e., the initial guess) $\mathbf{u}_\delta$ and then the result of the optimization process using a gradient descent method to minimize the discrepancy functional I.

Once the displacement inside the domain is reconstructed, we can recover the shear modulus μ, as shown in Figure 3.5.5. We reconstruct μ by minimizing the functional $\mathcal{K}$ and using a gradient descent-type method. Note that gradient of $\mathcal{K}$ is computed with the adjoint state method, described previously. As it can be seen in Figure 3.5.5, the reconstruction is very accurate but not so perfect on the boundaries of Ω, which is due to the poor estimation of $\mathbf{u}$ on $\partial\Omega$.

3.6 Concluding remarks

In this chapter, we developed a novel algorithm which gives access not only to stiffness quantitative information of biological tissues but also opens the way to other contrasts such as mechanical anisotropy. In the heart, the muscle fibers have anisotropic mechanical properties. It would be very interesting to detect a change in fiber orientation using OCT elastographic tomography. The implementation of the gradient descent algorithm in the case where ε is not continuous is very challenging and requires some extra work.

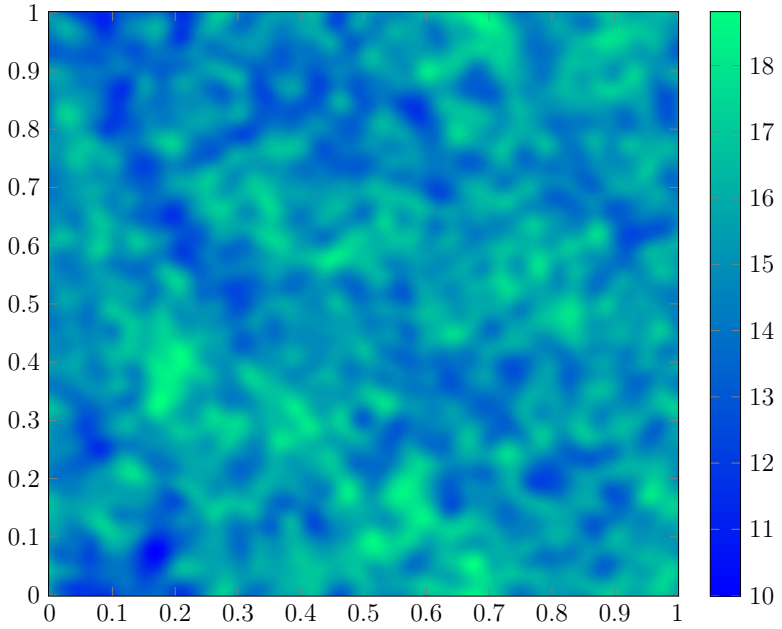

Figure 3.5.1 Optical image ε of the medium.

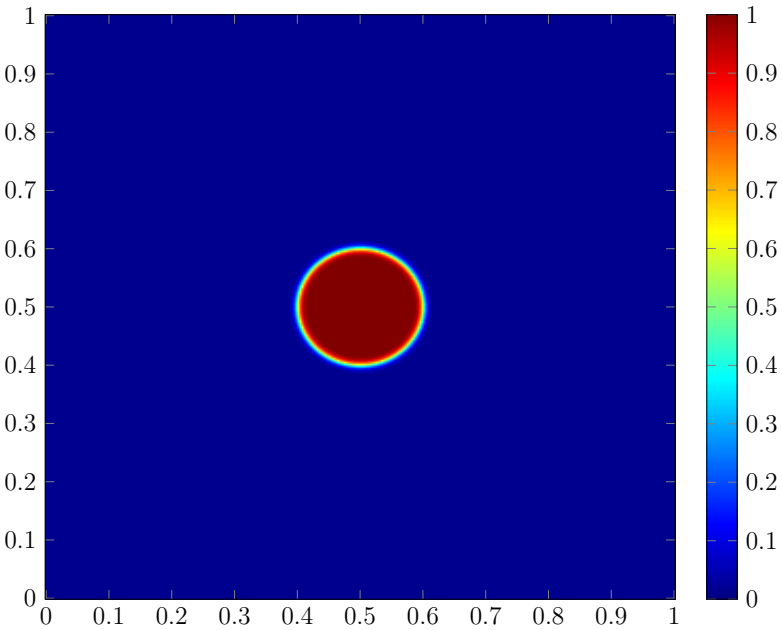

Figure 3.5.2 Averaging kernel w_δ.

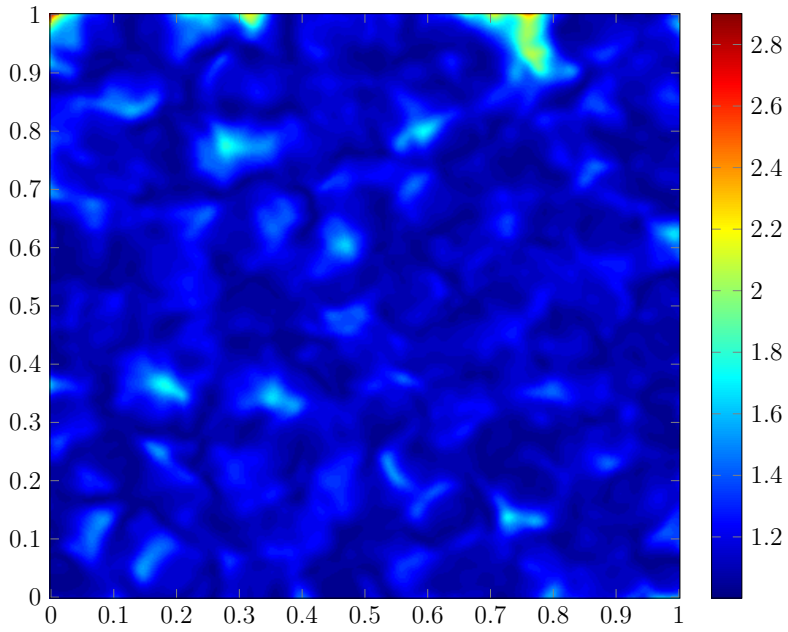

Figure 3.5.3 Conditioning of the matrix $w_\delta \star \nabla\varepsilon\nabla\varepsilon^T$.

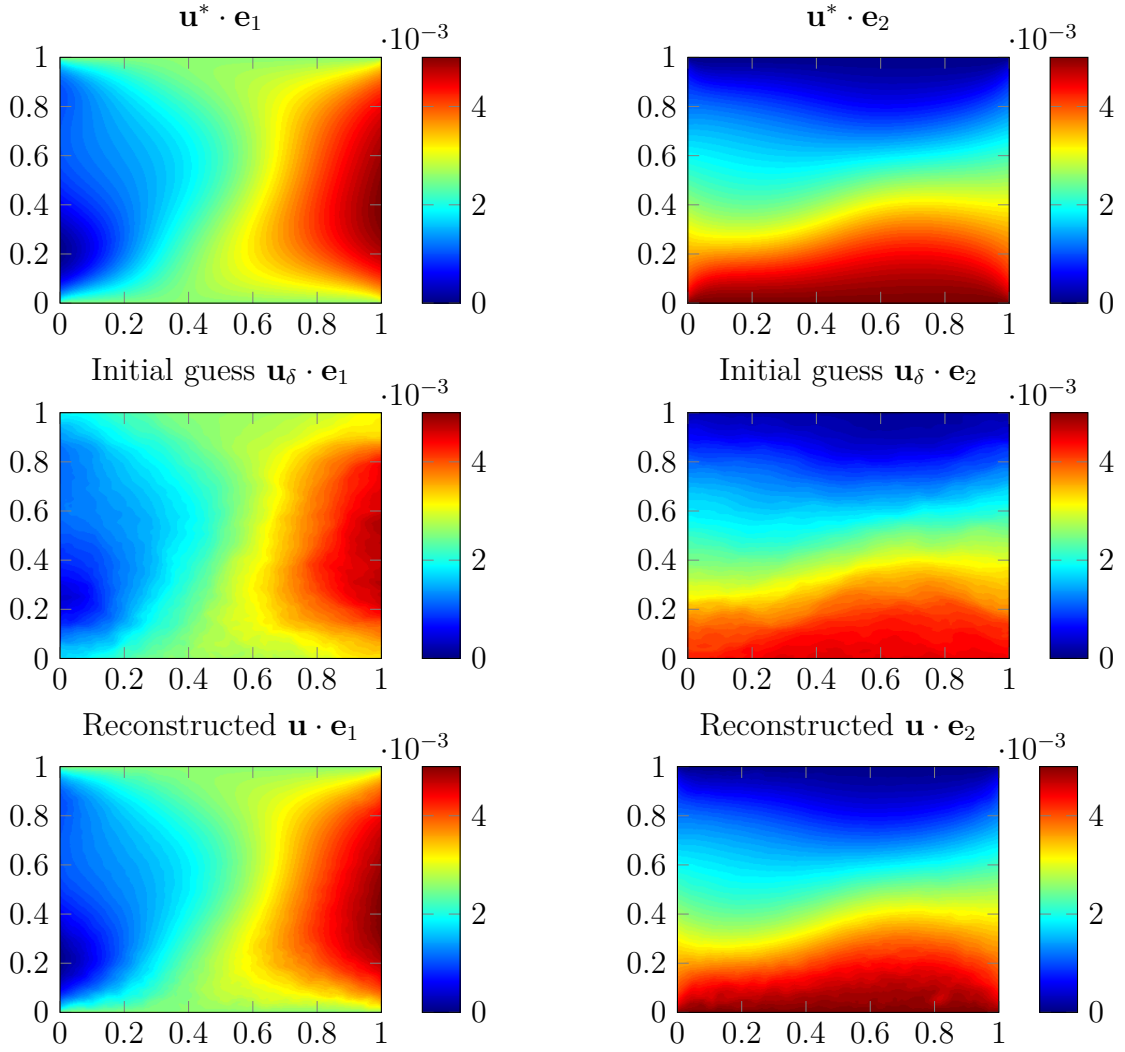

Figure 3.5.4 Displacement field and its reconstruction.

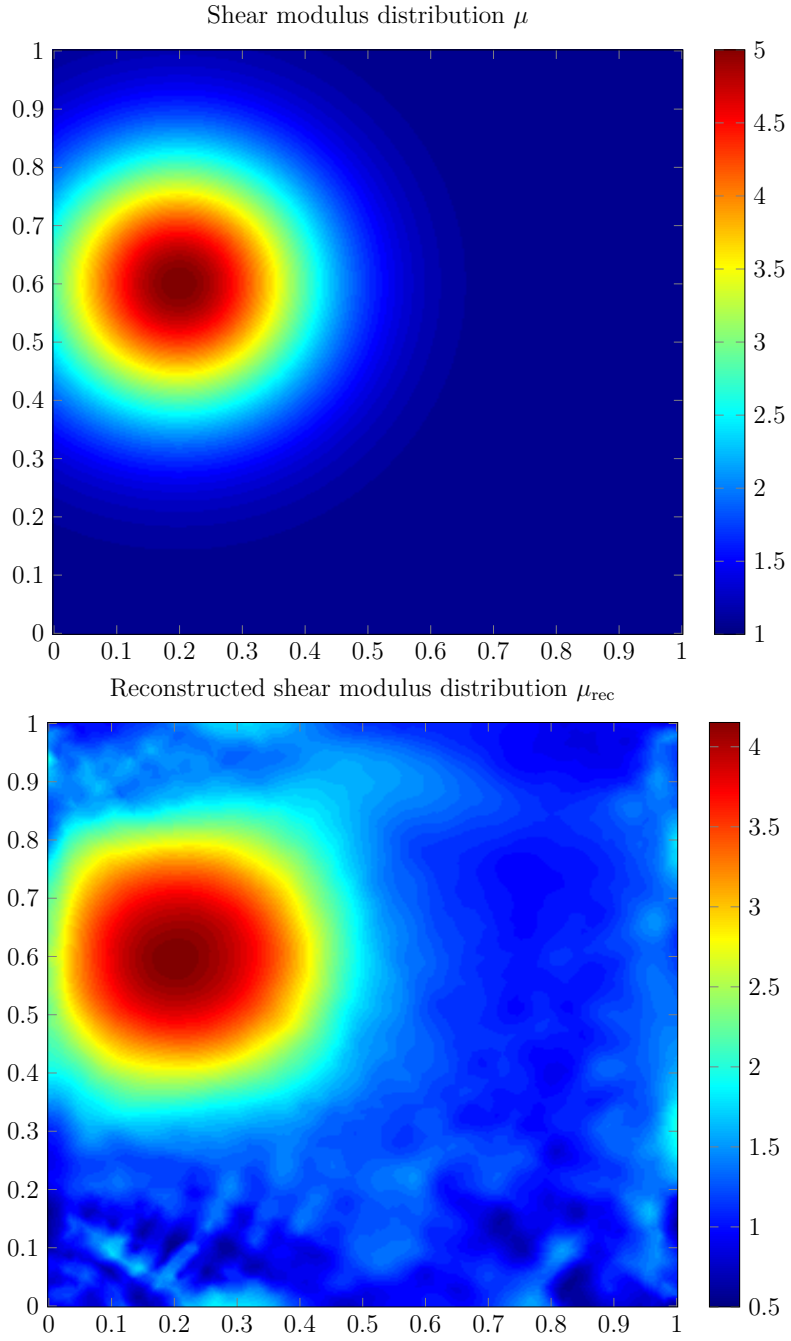

Figure 3.5.5 Shear modulus reconstruction

Part II

Nanoparticle Imaging

Chapter 4

Plasmonic nanoparticles

Contents

4.1 Introduction

In this chapter we deal with surface plasmon resonances of small nanoparticles. Localized surface plasmons are charge density oscillations confined to metallic nanoparticles. Excitation of localized surface plasmons by an electromagnetic field at an incident wavelength where resonance occurs results in a strong light scattering and an enhancement

of the local electromagnetic fields. Recently, the localized surface plasmon resonances of nanoparticles have received considerable attention for their application in biomedicine. They have enabled applications including sensing of cancer cells and their photothermal ablation. Plasmon resonant nanoparticles such as gold nanoparticles offer, in addition to their enhanced scattering and absorption, biocompatibility making them not only suitable for use as a contrast agent but also in therapeutic applications [76].

According to the quasi-static approximation for small particles, the surface plasmon resonance peak occurs when the particle's polarizability is maximized. Recently, it has been shown that plasmon resonances in nanoparticles can be treated as an eigenvalue problem for the Neumann-Poincaré operator, which leads to direct calculation of resonance values of permittivity and optimal design of nanoparticles that resonate at specified frequencies [13, 66, 97]. Classically, the frequency-dependent permittivity of metallic nanoparticles can be described by a Drude model which determines the material's dielectric and magnetic responses by considering the motion of the free electrons against a background of positive ion cores.

In this chapter, we provide a rigorous mathematical framework for localized surface plasmon resonances. We consider the full Maxwell equations. Using layer potential techniques, we derive the quasi-static limits of the electromagnetic fields in the presence of nanoparticles. We prove that the quasi-static limits are uniformly valid with respect to the nanoparticle's bulk electron relaxation rate. Note that uniform validity with respect to the contrast was proved in [111] in the context of small volume expansions for the conductivity problem. Then, we discuss the scattering and absorption enhancements by plasmon resonant nanoparticles. The nanoscale light concentration and near-field enhancement available to resonant metallic nanoparticles have been a driving force in nanoplasmonics. We first consider a single nanoparticle. Then we extend our approach to multiple nanoparticles. We study the influence of local environment on the near-field behavior of resonant nanoparticles. We simulate the localized surface plasmonic resonances associated to multiple particles in terms of their separation distance.

The chapter is organized as follows. In section 4.2, we introduce localized plasmonic resonances as the eigenvalues of the Neumann-Poincaré operator associated with the nanoparticle. In section 4.3 we describe a general model for the permittivity and permeability of nanoparticles as functions of the frequency. In section 4.4, we recall useful results on layer potential techniques for Maxwell's equations. Section 4.5 is devoted to the derivation of the uniform asymptotic expansions. We rigorously justify the quasi-static approximation for surface plasmon resonances. Our main results are

stated in Theorems 4.5.9 and 4.5.10. In section 4.6 we illustrate the validity of our results by a variety of numerical simulations. The chapter ends with a short discussion.

4.2 Plasmonic resonances

We first introduce the Neumann-Poincaré operator of an open connected domain D with $\mathcal{C}^{1,\eta}$ boundary in $\mathbb{R}^d$ $(d = 2, 3)$ for some $0 < \eta < 1$. Given such a domain D, we consider the following Neumann problem,

$$\Delta u = 0 \quad \text{in} \quad D\,; \qquad \frac{\partial u}{\partial \nu} = g \quad \text{on} \quad \partial D, \qquad \int_{\partial D} u \, d\sigma = 0, \tag{4.2.1}$$

where $g \in L^2_0(\partial D)$ with $L^2_0(\partial D)$ being the set of functions in $L^2(\partial D)$ with zero mean-value. In (4.2.1), $\partial/\partial\nu$ denotes the normal derivative. We note that the Neumann problem (4.2.1) can be rewritten as a boundary integral equation with the help of the single-layer potential. Given a density function $\varphi \in L^2(\partial D)$, the single-layer potential, $\mathcal{S}_D[\varphi]$, can be defined as follows,

$$\mathcal{S}_D[\varphi](x) := \int_{\partial D} \Gamma(x - y)\varphi(y) d\sigma(y) \tag{4.2.2}$$

for $x \in \mathbb{R}^d$, where Γ is the fundamental solution of the Laplacian in $\mathbb{R}^d$:

$$\Gamma(x - y) = \begin{cases} -\frac{1}{2\pi} \log |x - y| & \text{if } \ d = 2\,, \\ \frac{1}{(2-d)\omega_d} |x - y|^{2-d} & \text{if } \ d > 2\,, \end{cases} \tag{4.2.3}$$

where ω_d denotes the surface area of the unit sphere in $\mathbb{R}^d$. It is well-known that the single-layer potential satisfies the following jump condition on ∂D:

$$\frac{\partial}{\partial \nu} \left(\mathcal{S}_D[\varphi]\right)^{\pm} = (\pm\frac{1}{2} I + \mathcal{K}^*_D)[\varphi]\,, \tag{4.2.4}$$

where the superscripts $\pm$ indicate the limits from outside and inside D respectively, and $\mathcal{K}^*_D : L^2(\partial D) \to L^2(\partial D)$ is the Neumann-Poincaré operator defined by

$$\mathcal{K}^*_D[\varphi](x) := \frac{1}{\omega_d} \int_{\partial D} \frac{(x - y) \cdot \nu(x)}{|x - y|^d} \varphi(y) d\sigma(y)\,, \tag{4.2.5}$$

with $\nu(x)$ being the outward normal at $x \in \partial D$. We note that $\mathcal{K}^*_D$ maps $L^2_0(\partial D)$ onto itself.

With these notions, the Neumann problem (4.2.1) can then be formulated as

$$g = \frac{\partial}{\partial \nu} \left(\mathcal{S}_D[\varphi]\right)^- = (-\frac{1}{2} I + \mathcal{K}_D^*)[\varphi] \,. \tag{4.2.6}$$

Therefore, the solution to the Neumann problem (4.2.1) can be reformulated as a solution to the boundary integral equation with the Neumann-Poincaré operator $\mathcal{K}_D^*$.

The operator $\mathcal{K}_D^*$ arises not only in solving the Neumann problem for the Laplacian but also for representing the solution to the transmission problem as described below.

Consider an open connected domain D with $\mathcal{C}^2$ boundary in $\mathbb{R}^d$. Given a harmonic function u_0 in $\mathbb{R}^d$, we consider the following transmission problem in $\mathbb{R}^d$:

$$\begin{cases} \nabla \cdot (\varepsilon_D \nabla u) = 0 & \text{in } \mathbb{R}^d, \\ u - u_0 = O(|x|^{1-d}) & \text{as } |x| \to \infty, \end{cases} \tag{4.2.7}$$

where $\varepsilon_D = \varepsilon_c \chi(D) + \varepsilon_m \chi(\mathbb{R}^d \backslash \overline{D})$ with $\varepsilon_c, \varepsilon_m$ being two positive constants, and $\chi(\Omega)$ is the characteristic function of the domain $\Omega = D$ or $\mathbb{R}^d \backslash \overline{D}$. With the help of the single-layer potential, we can rewrite the perturbation $u - u_0$, which is due to the inclusion D, as

$$u - u_0 = \mathcal{S}_D[\varphi] \,, \tag{4.2.8}$$

where $\varphi \in L^2(\partial D)$ is an unknown density, and $\mathcal{S}_D[\varphi]$ is the refraction part of the potential in the presence of the inclusion. The transmission problem (4.2.7) can be rewritten as

$$\begin{cases} \Delta u = 0 & \text{in } D \bigcup (\mathbb{R}^d \backslash \overline{D}) \,, \\ u^+ = u^- & \text{on } \partial D \,, \\ \varepsilon_c \frac{\partial u^+}{\partial \nu} = \varepsilon_m \frac{\partial u^-}{\partial \nu} & \text{on } \partial D \,, \\ u - u_0 = O(|x|^{1-d}) & \text{as } |x| \to \infty \,. \end{cases} \tag{4.2.9}$$

With the help of the jump condition (4.2.4), solving the above system (4.2.9) can be regarded as solving the density function $\varphi \in L^2(\partial D)$ of the following integral equation

$$\frac{\partial u_0}{\partial \nu} = \left(\frac{\varepsilon_c + \varepsilon_m}{2(\varepsilon_c - \varepsilon_m)} I - \mathcal{K}_D^* \right) [\varphi] \,. \tag{4.2.10}$$

With the harmonic property of u_0, we can write

$$u_0(x) = \sum_{\alpha \in \mathbb{N}^d} \frac{1}{\alpha!} \partial^\alpha u_0(0) x^\alpha \tag{4.2.11}$$

with $\alpha = (\alpha_1, \ldots, \alpha_d) \in \mathbb{N}^d$, $\partial_\alpha = \partial_1^{\alpha_1} \ldots \partial_d^{\alpha_d}$ and $\alpha! = \alpha_1! \ldots \alpha_d!$.

Consider φ^α as the solution of the Neumann-Poincaré operator:

$$\frac{\partial x^\alpha}{\partial \nu} = \left(\frac{\varepsilon_c + \varepsilon_m}{2(\varepsilon_c - \varepsilon_m)} I - \mathcal{K}_D^* \right) [\varphi^\alpha] \,. \tag{4.2.12}$$

The invertibilities of the operator $(\frac{\varepsilon_c+\varepsilon_m}{2(\varepsilon_c-\varepsilon_m)} I - \mathcal{K}_D^*)$ from $L^2(\partial D)$ onto $L^2(\partial D)$ and from $L_0^2(\partial D)$ onto $L_0^2(\partial D)$ are proved, for example, in [27, 79], provided that $|\frac{\varepsilon_c+\varepsilon_m}{2(\varepsilon_c-\varepsilon_m)}| > 1/2$. We can substitute (4.2.11) and (4.2.12) back into (4.2.8) to get

$$u - u_0 = \sum_{|\alpha| \geq 1} \frac{1}{\alpha!} \partial^\alpha u_0(0) \mathcal{S}_D[\varphi^\alpha] = \sum_{|\alpha| \geq 1} \frac{1}{\alpha!} \partial^\alpha u_0(0) \int_{\partial D} \Gamma(x - y) \varphi^\alpha(y) d\sigma(y) \,. \tag{4.2.13}$$

Using the Taylor expansion,

$$\Gamma(x - y) = \Gamma(x) - y \cdot \nabla \Gamma(x) + O(\frac{1}{|x|^d}) \,, \tag{4.2.14}$$

which holds for all x such that $|x| \to \infty$ while y is bounded [27], we get the following result by substituting (4.2.14) into (4.2.13) that

$$(u - u_0)(x) = \nabla u_0(0) \cdot M(\lambda, D) \nabla \Gamma(x) + O(\frac{1}{|x|^d}) \quad \text{as} \quad |x| \to \infty, \tag{4.2.15}$$

where $M = (m_{ij})_{i,j=1}^d$ is the polarization tensor associated with the domain D and the contrast λ defined by

$$m_{ij}(\lambda, D) := \int_{\partial D} y_i (\lambda I - \mathcal{K}_D^*)^{-1} [\nu_j] (y) d\sigma(y) \,, \tag{4.2.16}$$

with

$$\lambda := \frac{\varepsilon_c + \varepsilon_m}{2(\varepsilon_c - \varepsilon_m)} \tag{4.2.17}$$

and ν_j being the j-th component of ν. Here we have used in (4.2.15) the fact that $\int_{\partial D} \nu \, d\sigma = 0$.

Typically the constants ε_c and ε_m are positive in order to make the system (4.2.9) physical. This corresponds to the situation with $|\lambda| > \frac{1}{2}$.

However, recent advances in nanotechnology make it possible to produce noble metal nanoparticles with negative permittivities at optical frequencies [76, 121]. Therefore, it is possible that for some frequencies, λ actually belongs to the spectrum of $\mathcal{K}_D^*$.

If this happens, the following integral equation

$$0 = (\lambda I - \mathcal{K}_D^*)[\varphi] \quad \text{on } \partial D \tag{4.2.18}$$

has non-trivial solutions $\varphi \in L^2(\partial D)$ and the nanoparticle resonates at those frequencies.

Therefore, we have to investigate the mapping properties of the Neumann-Poincaré operator. Assume that ∂D is of class $\mathcal{C}^{1,\eta}$, $0 < \eta < 1$. It is known that the operator $\mathcal{K}_D^* : L^2(\partial D) \to L^2(\partial D)$ is compact [79], and its spectrum is discrete and accumulates at zero. All the eigenvalues are real and bounded by $1/2$. Moreover, $1/2$ is always an eigenvalue and its associated eigenspace is of dimension one, which is nothing else but the kernel of the single-layer potential $\mathcal{S}_D$. In two dimensions, it can be proved that if $\lambda_i \neq 1/2$ is an eigenvalue of $\mathcal{K}_D^*$, then $-\lambda_i$ is an eigenvalue as well. This property is known as the twin spectrum property; see [96]. The Fredholm eigenvalues are the eigenvalues of $\mathcal{K}_D^*$. It is easy to see, from the properties of $\mathcal{K}_D^*$, that they are invariant with respect to rigid motions and scaling. They can be explicitly computed for ellipses and spheres. If a and b denote the semi-axis lengths of an ellipse then it can be shown that $\pm((a-b)/(a+b))^i$ are its Fredholm eigenvalues [80]. For the sphere, they are given by $1/(2(2i+1))$; see [78]. It is worth noticing that the convergence to zero of Fredholm eigenvalues is exponential for ellipses while it is algebraic for spheres.

Equation (4.2.18) corresponds to the case when plasmonic resonance occurs in D; see [66]. Given negative values of ε_c, the problem of designing a shape with prescribed plasmonic resonances is of great interest [13].

Finally, we briefly investigate the eigenvalue of the Neumann-Poincaré operator of multiple particles. Let D_1 and D_2 be two smooth bounded domains such that the distance $\operatorname{dist}(D_1, D_2)$ between D_1 and D_2 is positive. Let $\nu^{(1)}$ and $\nu^{(2)}$ denote the outward normal vectors at ∂D_1 and ∂D_2, respectively.

The Neumann-Poincaré operator $\mathbb{K}^*_{D_1 \cup D_2}$ associated with $D_1 \cup D_2$ is given by [14]

$$\mathbb{K}^*_{D_1 \cup D_2} := \begin{pmatrix} \mathcal{K}^*_{D_1} & \frac{\partial}{\partial \nu^{(1)}} \mathcal{S}_{D_2} \\ \frac{\partial}{\partial \nu^{(2)}} \mathcal{S}_{D_1} & \mathcal{K}^*_{D_2} \end{pmatrix}. \tag{4.2.19}$$

In section 4.6 we will be interested in how the eigenvalues of $\mathbb{K}^*_{D_1 \cup D_2}$ behave numerically as $\operatorname{dist}(D_1, D_2) \to 0$.

4.3 Drude's model for the electric permittivity and magnetic permeability

Let D be a simply connected bounded domain in $\mathbb{R}^d$ with $\mathcal{C}^{1,\eta}$ boundary for some $0 < \eta < 1$, and let (ε_m, μ_m) be the pair of electromagnetic parameters (electric permittivity and magnetic permeability) of $\mathbb{R}^d \setminus \overline{D}$ and (ε_c, μ_c) be that of D. We assume that ε_m and μ_m are real positive constants. We have

$$\varepsilon_D = \varepsilon_m \chi(\mathbb{R}^d \setminus \overline{D}) + \varepsilon_c \chi(D) \quad \text{and} \quad \mu_D = \mu_m \chi(\mathbb{R}^d \setminus \overline{D}) + \mu_c \chi(D).$$

Suppose that the electric permittivity ε_c and the magnetic permeability μ_c of the nanoparticle are changing with respect to the operating angular frequency ω while those of the surrounding medium, ε_m, μ_m, are independent of ω. Then we can write

$$\begin{aligned} \varepsilon_c(\omega) &= \varepsilon'(\omega) + i\varepsilon''(\omega), \\ \mu_c(\omega) &= \mu'(\omega) + i\mu''(\omega). \end{aligned} \tag{4.3.1}$$

Because of causality, the real and imaginary parts of ε_c and μ_c obey the following Kramer–Kronig relations:

$$\begin{aligned} \varepsilon'(\omega) &= -\frac{1}{\pi}\text{p.v.} \int_{-\infty}^{+\infty} \frac{1}{\omega - s}\varepsilon''(s)ds, \\ \varepsilon''(\omega) &= \frac{1}{\pi}\text{p.v.} \int_{-\infty}^{+\infty} \frac{1}{\omega - s}\varepsilon'(s)ds, \\ \mu''(\omega) &= -\frac{1}{\pi}\text{p.v.} \int_{-\infty}^{+\infty} \frac{1}{\omega - s}\mu'(s)ds, \\ \mu'(\omega) &= \frac{1}{\pi}\text{p.v.} \int_{-\infty}^{+\infty} \frac{1}{\omega - s}\mu''(s)ds, \end{aligned} \tag{4.3.2}$$

where p.v. denotes the principle value.

In the sequel, we set $k_c = \omega\sqrt{\varepsilon_c \mu_c}$ and $k_m = \omega\sqrt{\varepsilon_m \mu_m}$ and denote by

$$\lambda_\varepsilon(\omega) = \frac{\varepsilon_c(\omega) + \varepsilon_m}{2(\varepsilon_c(\omega) - \varepsilon_m)}, \quad \lambda_\mu(\omega) = \frac{\mu_c(\omega) + \mu_m}{2(\mu_c(\omega) - \mu_m)}. \tag{4.3.3}$$

We have

$$\lambda_\varepsilon(\omega) = \frac{(\varepsilon'(\omega))^2 - \varepsilon_m^2 + (\varepsilon''(\omega))^2}{2((\varepsilon'(\omega) - \varepsilon_m)^2 + (\varepsilon''(\omega))^2} - i\frac{\varepsilon'(\omega)\varepsilon''(\omega)}{2((\varepsilon'(\omega) - \varepsilon_m)^2 + (\varepsilon''(\omega))^2}.$$

A similar formula holds for $\lambda_\mu(\omega)$.

The electric permittivity $\varepsilon_c(\omega)$ and the magnetic permeability $\mu_c(\omega)$ can be described by the Drude model ; see, for instance, [121]. We have

$$\varepsilon_c(\omega) = \varepsilon_0(1 - \frac{\omega_p^2}{\omega(\omega + i\tau^{-1})}) \quad \text{and} \quad \mu_c(\omega) = \mu_0(1 - F\frac{\omega^2}{\omega^2 - \omega_0^2 + i\tau^{-1}\omega}),$$

or equivalently,

$$\varepsilon'(\omega) = \varepsilon_0\frac{\omega^2 + \tau^{-2} - \omega_p^2}{\omega^2 + \tau^{-2}}, \quad \varepsilon''(\omega) = \varepsilon_0\frac{\omega_p^2\tau^{-1}}{\omega(\omega^2 + \tau^{-2})},$$
$$\mu'(\omega) = \frac{\mu_0(\tau^{-2}\omega^2 + (\omega^2 - \omega_0^2)((1-F)\omega^2 - \omega_0^2)}{(\omega^2 - \omega_0^2)^2 + \tau^{-2}\omega^2}, \quad \mu''(\omega) = \frac{\mu_0 F\tau^{-1}\omega}{(\omega^2 - \omega_0^2)^2 + \tau^{-2}\omega^2},$$

where ω_p is the plasma frequency of the bulk material, $\tau > 0$ is the nanoparticle's bulk electron relaxation rate (τ^{-1} is the damping coefficient), F is a filling factor, and ω_0 is a localized plasmon resonant frequency.

When

$$\omega^2 + \tau^{-2} < \omega_p^2 \quad \text{and } (1-F)(\omega^2 - \omega_0^2)^2 - F\omega_0^2(\omega^2 - \omega_0^2) + \tau^{-2}\omega^2 < 0,$$

the real parts of $\varepsilon(\omega)$ and $\mu(\omega)$ are negative. Typical values are

- $\tau = 10^{-14}\, s$;
- $\omega = 10^{15}\, Hz$;
- $\varepsilon_0 = 9 \cdot 10^{-12} F\, m^{-1}$; $\varepsilon_m = (1.33)^2\varepsilon_0$;
- $\omega_p = 2 \cdot 10^{15} s^{-1}$ for a gold nanoparticle;

Using these values we find that $\lambda_\varepsilon \approx 0.495 - 0.005$.

It is interesting to have an idea on the size of $\Im m(\lambda_\varepsilon)$ (resp. $\Im m(\lambda_\mu)$) since it will be a lower bound for the distance $\text{dist}(\lambda_\varepsilon, \sigma(\mathcal{K}_D^*))$ (resp. $\text{dist}(\lambda_\mu, \sigma(\mathcal{K}_D^*))$) between λ_ε (resp. λ_μ) and the spectrum of the Neumann-Poincaré operator $\mathcal{K}_D^*$.

Finally, we define dielectric and magnetic plasmonic resonances. We say that ω is a dielectric plasmonic resonance if the real part of λ_ε is an eigenvalue of $\mathcal{K}_D^*$. Analogously, we say that ω is a magnetic plasmonic resonance if the real part of λ_μ is an eigenvalue of $\mathcal{K}_D^*$. Note that if ω is a dielectric (resp. magnetic) plasmonic resonance, then the polarization tensor $M(\lambda_\varepsilon(\omega), D)$ defined by (4.2.16) (resp. $M(\lambda_\mu(\omega), D)$) blows up.

In the case of two particles D_1 and D_2 with the same electromagnetic parameters, $\varepsilon_c(\omega)$ and $\mu_c(\omega)$, we say that ω is a dielectric (resp. magnetic) plasmonic resonance, if

the real part of λ_ε is an eigenvalue of $\mathbb{K}^*_{D_1\cup D_2}$. Analogously, we say that that ω is a magnetic plasmonic resonance if the real part of λ_μ is an eigenvalue of $\mathbb{K}^*_{D_1\cup D_2}$.

Let the polarization tensor $M(\lambda, D_1 \cup D_2) = (m_{ij})_{i,j=1}^d$ be defined by

$$\begin{aligned} m_{ij}(\lambda, D_1 \cup D_2) \;:=\; & \int_{\partial D_1} y_i \left[(\lambda I - \mathbb{K}_D^*)^{-1} \begin{bmatrix} \nu_j^{(1)} \\ \nu_j^{(2)} \end{bmatrix} (y) \right]_1 d\sigma(y) \\ & + \int_{\partial D_2} y_i \left[(\lambda I - \mathbb{K}_D^*)^{-1} \begin{bmatrix} \nu_j^{(1)} \\ \nu_j^{(2)} \end{bmatrix} (y) \right]_2 d\sigma(y)\,, \end{aligned} \tag{4.3.4}$$

where $\nu^{(l)} = (\nu_1^{(l)}, \dots, \nu_d^{(l)})$, $l = 1, 2$, and $[\,]_{l'}$ denotes the l'th component. As for single particles, $M(\lambda(\omega), D_1 \cup D_2) = (m_{ij})_{i,j=1}^d$ blows up for $\lambda(\omega)$ such that ω is a dielectric or magnetic plasmonic resonance.

4.4 Boundary integral operators

We start by recalling some well-known properties about boundary integral operators and proving a few technical lemmas that will be used in section 4.5 for deriving the asymptotic expansions of the electric and magnetic fields in the presence of nanoparticles. As will be shown in section 4.6, the plasmonic resonances for multiple identical particles are shifted from those of the single particle as the separating distance between the particles becomes comparable to their size.

4.4.1 Definitions

We first review commonly used function spaces. Let $\nabla_{\partial D}\cdot$ denote the surface divergence. Denote by $L^2_T(\partial D) := \{\boldsymbol{\phi} \in L^2(\partial D)^3, \boldsymbol{\nu}\cdot\boldsymbol{\phi} = 0\}$. Let $H^s(\partial D)$ be the usual Sobolev space of order s on ∂D. We also introduce the function spaces

$$\begin{aligned} \mathrm{TH}(\mathrm{div}, \partial D) :=& \Big\{ \phi \in L^2_T(\partial D) : \nabla_{\partial D}\cdot\phi \in L^2(\partial D) \Big\}, \\ \mathrm{TH}(\mathrm{curl}, \partial D) :=& \Big\{ \phi \in L^2_T(\partial D) : \nabla_{\partial D}\cdot(\phi\times\nu) \in L^2(\partial D) \Big\}, \end{aligned}$$

equipped with the norms

$$\begin{aligned} \|\phi\|_{\mathrm{TH}(\mathrm{div},\partial D)} &= \|\phi\|_{L^2(\partial D)} + \|\nabla_{\partial D}\cdot\phi\|_{L^2(\partial D)}, \\ \|\phi\|_{\mathrm{TH}(\mathrm{curl},\partial D)} &= \|\phi\|_{L^2(\partial D)} + \|\nabla_{\partial D}\cdot(\phi\times\nu)\|_{L^2(\partial D)}. \end{aligned}$$

We define the vectorial curl for $\varphi \in H^1(\partial D)$ by $\mathrm{curl}_{\partial D}\varphi = -\nu \times \nabla_{\partial D}\varphi$.

The following result from [42] will be useful.

Proposition 4.4.1. *The following Helmholtz decomposition holds:*

$$\mathrm{L}^2_T(\partial D) = \nabla_{\partial D}(H^1(\partial D)) \overset{\perp}{\oplus} \mathrm{curl}_{\partial D}(H^1(\partial D)). \tag{4.4.1}$$

Next, we recall that, for $k > 0$, the fundamental outgoing solution Γ_k to the Helmholtz operator $(\Delta + k^2)$ in $\mathbb{R}^3$ is given by

$$\Gamma_k(x) = -\frac{e^{ik|x|}}{4\pi|x|}. \tag{4.4.2}$$

For a density $\boldsymbol{\phi} \in \mathrm{TH}(\mathrm{div}, \partial D)$, we define the vectorial single layer potential associated with the fundamental solution Γ_k introduced in (4.4.2) by

$$\mathcal{A}^k_D[\boldsymbol{\phi}](x) := \int_{\partial D} \Gamma_k(x-y)\boldsymbol{\phi}(y)d\sigma(y), \quad x \in \mathbb{R}^3. \tag{4.4.3}$$

For a scalar density $\varphi \in L^2(\partial D)$, the single layer potential is defined similarly by

$$\mathcal{S}^k_D[\varphi](x) := \int_{\partial D} \Gamma_k(x-y)\varphi(y)d\sigma(y), \quad x \in \mathbb{R}^3. \tag{4.4.4}$$

We will also need the following boundary operators:

$$\begin{aligned} \mathcal{M}^k_D : \mathrm{L}^2_T(\partial D) &\longrightarrow \mathrm{L}^2_T(\partial D) \\ \boldsymbol{\phi} &\longmapsto \mathcal{M}^k_D[\boldsymbol{\phi}] = \boldsymbol{\nu}(x) \times \nabla \times \int_{\partial D} \Gamma^k(x,y)\boldsymbol{\nu}(y) \times \boldsymbol{\phi}(y)d\sigma(y), \end{aligned} \tag{4.4.5}$$

$$\begin{aligned} \mathcal{N}^k_D : \mathrm{TH}(\mathrm{curl}, \partial D) &\longrightarrow \mathrm{TH}(\mathrm{div}, \partial D) \\ \boldsymbol{\phi} &\longmapsto \mathcal{N}^k_D[\boldsymbol{\phi}] = 2\boldsymbol{\nu}(x) \times \nabla \times \nabla \times \int_{\partial D} \Gamma^k(x,y)\boldsymbol{\nu}(y) \times \boldsymbol{\phi}(y)d\sigma(y), \end{aligned} \tag{4.4.6}$$

$$\begin{aligned} \mathcal{L}^k_D : \mathrm{TH}(\mathrm{div}, \partial D) &\longrightarrow \mathrm{TH}(\mathrm{div}, \partial D) \\ \boldsymbol{\phi} &\longmapsto \mathcal{L}^k_D[\boldsymbol{\phi}] = \boldsymbol{\nu}(x) \times k^2\mathcal{A}^k_D[\boldsymbol{\phi}](x) + \nabla\mathcal{S}^k_D[\nabla_{\partial D} \cdot \boldsymbol{\phi}](x). \end{aligned} \tag{4.4.7}$$

In the following, we denote by $\mathcal{A}_D$, $\mathcal{S}_D$, $\mathcal{M}_D$, and $\mathcal{N}_D$ the operators $\mathcal{A}^0_D$, $\mathcal{S}^0_D$, $\mathcal{M}^0_D$, and $\mathcal{N}^0_D$ corresponding to $k = 0$, respectively.

4.4.2 Boundary integral identities

Let $\mathcal{K}_D$ be the L^2-adjoint of $\mathcal{K}_D^*$ defined in (4.2.5). Since $\mathcal{K}_D$ and

$$\mathcal{K}_D^* : L^2(\partial D) \to L^2(\partial D)$$

are compact, we have $\sigma(\mathcal{K}_D) = \sigma(\mathcal{K}_D^*)$.

We start with stating the following jump formula. We refer the reader to Appendix A for its proof.

Proposition 4.4.2. *Let $\boldsymbol{\phi} \in L_T^2(\partial D)$. Then $\mathcal{A}_D^k[\boldsymbol{\phi}]$ is continuous on $\mathbb{R}^3$ and its curl satisfies the following jump formula:*

$$\boldsymbol{\nu} \times \nabla \times \mathcal{A}_D^k[\boldsymbol{\phi}]\Big|_{\pm} = \mp\frac{\boldsymbol{\phi}}{2} + \mathcal{M}_D^k[\boldsymbol{\phi}] \quad \text{on } \partial D, \tag{4.4.8}$$

where

$$\forall x \in \partial D, \quad \boldsymbol{\nu}(x) \times \nabla \times \mathcal{A}_D^k[\boldsymbol{\phi}]\Big|_{\pm}(x) = \lim_{t \to 0^+} \boldsymbol{\nu}(x) \times \nabla \times \mathcal{A}_D^k[\boldsymbol{\phi}](x \pm t\boldsymbol{\nu}(x)).$$

Next, we prove the following integral identities.

Proposition 4.4.3. *We have*

$$\mathcal{M}_D^* = r\mathcal{M}_D r, \tag{4.4.9}$$

where r is defined by

$$r(\boldsymbol{\phi}) = \boldsymbol{\nu} \times \boldsymbol{\phi}, \quad \forall \boldsymbol{\phi} \in L_T^2(\partial D). \tag{4.4.10}$$

Moreover,

$$\nabla \cdot \mathcal{A}_D^k[\boldsymbol{\phi}] = \mathcal{S}_D^k[\nabla_{\partial D} \cdot \boldsymbol{\phi}] \quad \text{in } \mathbb{R}^3, \quad \forall \boldsymbol{\phi} \in TH\left(\mathrm{div}, \partial D\right). \tag{4.4.11}$$

$$\nabla_{\partial D} \cdot \mathcal{M}_D^k[\boldsymbol{\phi}] = -k^2 \nu \cdot \mathcal{A}_D^k[\boldsymbol{\phi}] - \left(\mathcal{K}_D^k\right)^* [\nabla_{\partial B} \cdot \boldsymbol{\phi}], \quad \forall \boldsymbol{\phi} \in TH\left(\mathrm{div}, \partial D\right). \tag{4.4.12}$$

Furthermore,

$$\nabla_{\partial D} \cdot \mathcal{M}_D[\boldsymbol{\phi}] = -\mathcal{K}_D^*[\nabla_{\partial D} \cdot \boldsymbol{\phi}], \quad \forall \boldsymbol{\phi} \in TH\left(\mathrm{div}, \partial D\right), \tag{4.4.13}$$

$$\mathcal{M}_D^*[\nabla_{\partial D}\phi] = -\nabla_{\partial D}\mathcal{K}_D[\phi], \tag{4.4.14}$$

and

$$\mathcal{M}_D[\mathrm{curl}_{\partial D}\varphi] = \mathrm{curl}_{\partial D}\mathcal{K}_D[\varphi], \quad \forall \varphi \in H^1(\partial D). \tag{4.4.15}$$

Proof. The proof of (4.4.11) can be found in [50]. We give it here for the sake of completeness. If $\boldsymbol{\phi} \in TH\,(\mathrm{div}, \partial D)$, then

$$\nabla \cdot \mathcal{A}_D^k[\boldsymbol{\phi}](x) = \int_{\partial D} \nabla_x \cdot \Big(\Gamma^k(x,y)\boldsymbol{\phi}(y)\Big)\, d\sigma(y), \quad x \in \mathbb{R}^3 \setminus \partial D.$$

Using the fact that

$$\nabla_x \cdot (\Gamma^k(x,y)\boldsymbol{\phi}(y)) = \boldsymbol{\phi}(y)\nabla_x\Gamma^k(x,y) = -\boldsymbol{\phi}(y)\nabla_y\Gamma^k(x,y),$$

and since

$$\nabla_y\Gamma^k(x,y) = \nabla_{\partial D}\Gamma^k(x,y) + \frac{\partial \Gamma^k}{\partial \nu(y)}(x,y),$$

we get

$$\nabla \cdot \mathcal{A}_D^k[\boldsymbol{\phi}](x) = -\int_{\partial D} \boldsymbol{\phi}(y) \cdot \nabla_{\partial D, y}\Gamma^k(x,y) d\sigma(y), \quad x \in \mathbb{R}^3 \setminus \partial D.$$

Using the fact that $-\nabla_{\partial D}$ is the adjoint of $\nabla_{\partial_D}\cdot$ we obtain

$$\nabla \cdot \mathcal{A}_D^k[\boldsymbol{\phi}](x) = \int_{\partial D} \Gamma^k(x,y)\nabla_{\partial D} \cdot \boldsymbol{\phi}(y) d\sigma(y), \quad x \in \mathbb{R}^3 \setminus \partial D.$$

Next, since $\mathcal{S}^k[\nabla_{\partial D}\boldsymbol{\phi}]$ is continuous across ∂D, the above relation can be extended to $\mathbb{R}^3$ and we get (4.4.11).

Now, in order to prove (4.4.12), we observe that, for any $\boldsymbol{\phi} \in TH\,(\mathrm{div}, \partial D)$,

$$\nabla \times \nabla \times \mathcal{A}_D^k[\boldsymbol{\phi}](x) = k^2\mathcal{A}_D^k[\boldsymbol{\phi}](x) + \nabla\mathcal{S}_D^k[\nabla_{\partial D} \cdot \boldsymbol{\phi}](x), \quad x \in \mathbb{R}^3 \setminus \partial D.$$

Using the jump relations on $\dfrac{\partial \mathcal{S}_D^k}{\partial \nu}$ we obtain that

$$2\nu \cdot \nabla \times \nabla \times \mathcal{A}_D^k[\boldsymbol{\phi}]\Big|_{\pm} = k^2\nu \cdot \mathcal{A}_D^k + (\mathcal{K}_D^k)^*[\nabla_{\partial D} \cdot \boldsymbol{\phi}] \mp \nabla_{\partial D} \cdot \boldsymbol{\phi} \quad \text{ on } \partial D.$$

Recall from [50, p.169] that if $\mathrm{f} \in \mathcal{C}^1(\mathbb{R}^3\setminus\overline{D}) \cap \mathcal{C}^0(\mathbb{R}^3\setminus D)$, then $\nabla_{\partial D}\cdot(\nu\times\mathrm{f}) = -\nu\cdot(\nabla\times\mathrm{f})$. Using the jump formula for $2\nu \times \nabla \times \mathcal{A}_D^k[\boldsymbol{\phi}]\Big|_{\pm} = \mathcal{M}_D^k[\boldsymbol{\phi}] \pm \boldsymbol{\phi}$, we arrive at (4.4.12). Setting $k = 0$ in (4.4.12) gives (4.4.13).

Identity (4.4.14) can be deduced from (4.4.13) by duality.

Now, we prove (4.4.15). Define $r(a) = \nu \times a$ for any smooth vector field a on ∂D. For $\varphi \in H^1(\partial D)$, we have

$$\mathcal{M}_D^*[\nabla_{\partial D}\varphi] = -\nabla_{\partial D}\mathcal{K}_D[\varphi].$$

Since $\mathcal{M}_D^* = r\mathcal{M}_D r$ (see [67]) and $\mathrm{curl}_{\partial D} = r(\nabla_{\partial D})$, it follows that

$$r\left(\mathcal{M}_D[\mathrm{curl}_{\partial D}\varphi]\right) = -\nabla_{\partial D}\mathcal{K}_D[\varphi].$$

Composing by $r^{-1} = -r$, we get

$$\mathcal{M}_D[\mathrm{curl}_{\partial D}\varphi] = \mathrm{curl}_{\partial D}\mathcal{K}_D[\varphi],$$

which completes the proof. □

Lemma 4.4.4. *The kernel of the operator $\mathcal{N}_D$ in $L_T^2(\partial D)$ is $\nabla_{\partial D}(H^1(\partial D))$.*

Proof. Take $\boldsymbol{\phi} = \mathrm{curl}_{\partial D}U$ with $U \in H^1(\partial D)$. From (4.4.11), it follows that

$$\mathcal{N}_D[\mathrm{curl}_{\partial D}U](x) = 2\boldsymbol{\nu}(x) \times \nabla\mathcal{S}_D[\nabla_{\partial D} \cdot \mathrm{curl}_{\partial D}U].$$

Since $\nabla_{\partial D} \cdot \mathrm{curl}_{\partial D}U = 0$, we have $\mathcal{N}_D[\boldsymbol{\phi}] = 0$. Now, take $\boldsymbol{\phi} \in L_T^2(\partial D)$ such that $\mathcal{N}_D[\boldsymbol{\phi}] = 0$. Then, on ∂D, we have

$$\begin{aligned} 2\boldsymbol{\nu}(x) \times \nabla\mathcal{S}_D[\nabla_{\partial D} \cdot \boldsymbol{\phi}] =& 2\boldsymbol{\nu}(x) \times \left(\nabla_{\partial D}\mathcal{S}_D[\nabla_{\partial D} \cdot r(\boldsymbol{\phi})] + \frac{\partial}{\partial \boldsymbol{\nu}}\mathcal{S}_D[\nabla_{\partial D} \cdot (r(\boldsymbol{\phi})]\right) \\ =& -2\mathrm{curl}_{\partial D}\mathcal{S}_D[\mathrm{curl}_{\partial D}\boldsymbol{\phi}]. \end{aligned}$$

Since $\mathrm{Ker}(\mathrm{curl}_{\partial D}) = \mathbb{R}$ (see [42]), we obtain that $\mathcal{S}_{\partial D}[\mathrm{curl}_{\partial D}\boldsymbol{\phi}] = c \in \mathbb{R}$. Then, $\mathrm{curl}_{\partial D}\boldsymbol{\phi} = 0$, which implies that $\boldsymbol{\phi} \in \nabla_{\partial D}H^1(\partial D)$ (see again [42]). □

Proposition 4.4.5. *We have the following Calderón type identity:*

$$\mathcal{N}_D\mathcal{M}_D^* = \mathcal{M}_D\mathcal{N}_D. \tag{4.4.16}$$

Proof. Let $\boldsymbol{\phi} \in H^{1/2}(\partial D)$. We have

$$\mathcal{M}_D\mathcal{N}_D[\boldsymbol{\phi}] = 2\mathcal{M}_D\Big[r\left(\nabla \times \nabla \times \mathcal{A}_D\Big[r(\boldsymbol{\phi})\Big]\right)\Big]$$

and

$$\mathcal{M}_D\mathcal{N}_D[\boldsymbol{\phi}] = 2\mathcal{M}_D^k\Big[r\left(\nabla\mathcal{S}_D^k\Big[\nabla_{\partial D} \cdot r(\boldsymbol{\phi})\Big]\right)\Big].$$

Since

$$\begin{aligned} r\Big(\nabla\mathcal{S}_D[\nabla_{\partial D}\cdot r(\boldsymbol{\phi})]\Big) =& \boldsymbol{\nu}\times\Big[\nabla_{\partial D}\mathcal{S}_D[\nabla_{\partial D}\cdot r(\boldsymbol{\phi})] + \frac{\partial}{\partial\boldsymbol{\nu}}\mathcal{S}_D[\nabla_{\partial D}\cdot r(\boldsymbol{\phi})]\boldsymbol{\nu}\Big] \\ =& -\operatorname{curl}_{\partial D}\mathcal{S}_D[\nabla_{\partial D}\cdot r(\boldsymbol{\phi})], \end{aligned}$$

we can deduce from (4.4.15) that

$$\mathcal{M}_D\mathcal{N}_D[\boldsymbol{\phi}] = -2\operatorname{curl}_{\partial D}\Big(\mathcal{K}_D\mathcal{S}_D\left[\nabla_{\partial D}\cdot r(\boldsymbol{\phi})\right]\Big).$$

Now, using the fact that $\mathcal{M}_D^* = r\mathcal{M}_D r$ and that $r^{-1} = -r$, we also have

$$\mathcal{N}_D\mathcal{M}_D^*[\boldsymbol{\phi}] = -2r\left(\nabla\times\nabla\times\mathcal{A}_D\mathcal{M}_D\Big[r(\boldsymbol{\phi})\Big]\right)$$

$$\mathcal{N}_D\mathcal{M}_D^*[\boldsymbol{\phi}] = -2r\Big(\nabla\mathcal{S}_D\left[\nabla_{\partial D}\cdot\mathcal{M}_D\Big[r(\boldsymbol{\phi})\Big]\right]\Big).$$

Moreover, (4.4.13) yields

$$\mathcal{N}_D\mathcal{M}_D^*[\boldsymbol{\phi}] = 2r\Big(\nabla\mathcal{S}_D\left[\mathcal{K}_D^*\Big[\nabla_{\partial D}\cdot r(\boldsymbol{\phi})\Big]\right]\Big).$$

Using Calderón's identity $\mathcal{S}_B\mathcal{K}_B^* = \mathcal{K}_B\mathcal{S}_B$ and the fact that

$$r(\nabla\mathcal{K}_D) = r(\nabla_{\partial D}\mathcal{K}_D) = -\operatorname{curl}_{\partial D}\mathcal{K}_D,$$

it follows that

$$\mathcal{N}_D\mathcal{M}_D^*[\boldsymbol{\phi}] = -2\operatorname{curl}_{\partial D}\left(\mathcal{K}_D\mathcal{S}_D\Big[\nabla_{\partial D}\cdot r(\boldsymbol{\phi})\Big]\right),$$

which completes the proof. □

4.4.3 Resolvent estimates

As seen in the section 4.2, we have to solve Fredholm type equations involving the resolvent of $\mathcal{K}_D$. We will also need to control the resolvent of $\mathcal{M}_D$. For doing so, the main difficulty is due to the fact that $\mathcal{K}_D$ and $\mathcal{M}_D$ are not self-adjoint. However, we will make use of a symmetrization technique in order to estimate the norms of the resolvents of $\mathcal{K}_D$ and $\mathcal{M}_D$.

The following result holds.

Proposition 4.4.6. *The operator $\mathcal{K}_D : L^2(\partial D) \longrightarrow L^2(\partial D)$ satisfies the following resolvent estimate*

$$\|(\lambda I - \mathcal{K}_D)^{-1}\|_{L^2(\partial D)} \leq \frac{c}{\operatorname{dist}(\lambda, \sigma(\mathcal{K}_D))},$$

where $\operatorname{dist}(\lambda, \sigma(\mathcal{K}_D))$ *is the distance between* λ *and the spectrum* $\sigma(\mathcal{K}_D)$ *of* $\mathcal{K}_D$ *and* c *is a constant depending only on* D*.*

Proof. We start from Calderón's identity

$$\forall \phi \in L^2(\partial D), \quad \mathcal{S}_D \mathcal{K}_D[\phi] = \mathcal{K}_D^* \mathcal{S}_D[\phi].$$

Since $\mathcal{S}_D : H^{-1/2}(\partial D) \longrightarrow H^{1/2}(\partial D)$ is a self-adjoint positive definite invertible operator in dimension three, we can define a new inner product on $L^2(\partial D)$. We denote $\mathcal{H}$ the Hilbert space $L^2(\partial D)$ equipped with the following inner product

$$\langle \phi, \psi \rangle_{\mathcal{H}} = \langle \mathcal{S}_D[\phi], \psi \rangle \quad \forall (\phi, \psi) \in \left(L^2(\partial D)\right)^2.$$

Since $\mathcal{S}_D$ is continuous and invertible, the norm associated with the inner product $\langle . \ , \ . \rangle_{\mathcal{H}}$ is equivalent to the $L^2(\partial D)$-norm. Now, $\mathcal{K}_D$ is a self-adjoint compact operator on $\mathcal{H}$. We can write [62]

$$\|(\lambda I - \mathcal{K}_D)^{-1}\|_{\mathcal{H}} \leq \frac{1}{\operatorname{dist}(\lambda, \sigma(\mathcal{K}_D))}.$$

Switching back to the original norm we get the desired result. □

Proposition 4.4.7. *We have* $-\sigma(\mathcal{M}_D) = \sigma(\mathcal{K}_D^*) \setminus \{\frac{1}{2}\}$.

Proof. First, we note that $-1/2$ is not an eigenvalue of $\mathcal{M}_D$; see [67, 103]. Let $\lambda \in \sigma(\mathcal{M}_D)$. Take $\phi \in L^2_T(\partial D)$ such that

$$(\lambda I - \mathcal{M}) [\boldsymbol{\phi}] = 0 \tag{4.4.17}$$

Using the Helmholtz decomposition (4.4.1), we write

$$\boldsymbol{\phi} = \nabla_{\partial D} U + \operatorname{curl}_{\partial D} V.$$

Equation (4.4.17) becomes

$$(\lambda I - \mathcal{M}_D) (\nabla_{\partial D} U + \operatorname{curl}_{\partial D} V) = 0, \tag{4.4.18}$$

which yields

$$\mathrm{curl}_{\partial D}\left(\lambda I - \mathcal{K}_D\right) V = -\left(\lambda I - \mathcal{M}_D\right) \nabla_{\partial D} U.$$

Taking the surface divergence we get

$$\lambda \Delta_{\partial D} U - \nabla_{\partial D} \cdot \mathcal{M}_D[\nabla_{\partial D} U] = 0,$$

and hence, by using (4.4.13),

$$\left(\lambda I + \mathcal{K}_D^*\right)[\Delta_{\partial D} U] = 0.$$

Therefore, either $-\lambda \in \sigma(\mathcal{K}_D^*)$ or $\Delta_{\partial D} U = 0$, which implies that U is constant and $\nabla_{\partial D} \cdot \phi = 0$. Now, we take the surface curl of (4.4.18) to get

$$-\lambda \Delta_{\partial D} V + \mathrm{curl}_{\partial D} \mathcal{M}_D\left[\mathrm{curl}_{\partial D} V\right] = 0.$$

Using (4.4.15), we obtain

$$\Delta_{\partial D}\left(\lambda I - \mathcal{K}_D\right)[V] = 0.$$

Then, $\lambda V - \mathcal{K}_D[V] = c$ for some constant c. By replacing V by $V' = V + \frac{c}{\lambda - 1/2}$ and using the fact that $\mathcal{K}_D[1] = 1/2$, we arrive at $\lambda V' - \mathcal{K}_D[V'] = 0$. If $\lambda \notin \sigma(\mathcal{K}_D)$, then $V' = 0$ thus V is constant and *phibf* is zero which yields a contradiction.

Now, let $\lambda \in \sigma(\mathcal{K}_D) \setminus \{1/2\}$ and let φ be an eigenvector associated with λ. From

$$\left(\lambda I - \mathcal{K}_D\right)[\phi] = 0,$$

Taking the surface curl and using (4.4.15) gives

$$\left(\lambda I - \mathcal{M}_D\right)[\mathrm{curl}_{\partial D} \varphi] = 0.$$

Either $\lambda \in \sigma(\mathcal{M}_D)$ or $\mathrm{curl}_{\partial D} \phi = 0$, which means that ϕ is constant ([42]). Since $\lambda \neq 1/2$, φ cannot be constant. □

Lemma 4.4.8. *Let* $\boldsymbol{\phi} \in \mathrm{H} := \mathrm{curl}_{\partial D}\left(H^1(\partial D)\right)$ *(*H *is the space of divergence free vectors in* L^2_T*). The following resolvent estimate holds:*

$$\left\| \left(\lambda I + \mathcal{M}_D\right)^{-1}[\boldsymbol{\phi}] \right\|_H \leq \frac{c}{\mathrm{dist}\left(\lambda, \sigma(\mathcal{K}_D)\right)}. \tag{4.4.19}$$

Proof. We proceed exactly as in the proof of Proposition 4.4.6. If we denote by $\langle ., . \rangle_{\mathrm{H}}$ the usual scalar product on H, then we introduce a new scalar product defined by

$$\forall \boldsymbol{\phi}, \boldsymbol{\psi} \in \mathrm{H} \times \mathrm{H}, \quad \langle \boldsymbol{\phi}, \boldsymbol{\psi} \rangle_{\mathcal{N}} = \langle \mathcal{N}_D[\boldsymbol{\phi}], \boldsymbol{\psi} \rangle_{\mathrm{H}},$$

where $\mathcal{N}_D\Big|_{\mathrm{H}}$ is the operator induced by $\mathcal{N}_D$ given in (4.4.6) on H. Then, we first prove that H is stable by $\mathcal{N}_D$. If $\boldsymbol{\phi} \in \mathrm{H}$, then $\mathcal{N}_D[\boldsymbol{\phi}] \in \mathrm{TH}(\mathrm{div}, \partial D)$ (see [50]) and, using the fact that for any $\mathrm{f} \in H(\mathrm{curl}, \Omega)$, $\nabla_{\partial D} \cdot (\boldsymbol{\nu} \times \mathrm{f}) = \boldsymbol{\nu} \cdot \nabla \times \mathrm{f}$, we get

$$\nabla_{\partial D} \cdot \mathcal{N}_D[\boldsymbol{\phi}] = \boldsymbol{\nu} \cdot \nabla \times \nabla \mathcal{S}_D[\nabla_{\partial D} \cdot (\boldsymbol{\nu} \times \boldsymbol{\phi})] = 0,$$

which means that $\mathcal{N}_D[\boldsymbol{\phi}] \in \mathrm{H}$. For the sake of simplicity we will denote by $\mathcal{N}_D$ the induced operator on H. It is easy to see that this bilinear operator is well defined, continuous and positive. Then, $\mathcal{N}_D$ is self-adjoint [50]. The bilinear form is positive since

$$\begin{aligned}
\langle \mathcal{N}[\boldsymbol{\phi}], \boldsymbol{\phi} \rangle_{\mathrm{H}} &= \int_{\partial D} \mathcal{N}[\boldsymbol{\phi}](x) \cdot \boldsymbol{\phi}(x) dx, \\
&= \int_{\partial D} \boldsymbol{\nu}(x) \times \nabla \mathcal{S}_D \left[\nabla_{\partial D} \cdot (\boldsymbol{\nu} \times \boldsymbol{\phi}) \right](x) \cdot \boldsymbol{\phi}(x) dx, \\
&= \int_{\partial D} -\mathrm{curl}_{\partial D} \mathcal{S}_D \left[\mathrm{curl}_{\partial D} \boldsymbol{\phi} \right](x) \cdot \boldsymbol{\phi}(x) dx, \\
&= -\int_{\partial D} \mathcal{S}_D \left[\mathrm{curl}_{\partial D} \boldsymbol{\phi} \right](x) \mathrm{curl}_{\partial D} \boldsymbol{\phi}(x) dx, \\
&= -\langle \mathcal{S}_D \left[\mathrm{curl}_{\partial D} \boldsymbol{\phi} \right], \mathrm{curl}_{\partial D} \boldsymbol{\phi} \rangle_{L^2(\partial D)}.
\end{aligned}$$

If we equip H with this new scalar product, then we can see by using Proposition 4.4.16 that $\mathcal{M}_D$ is self-adjoint and therefore,

$$\forall \boldsymbol{\phi} \in \mathrm{H}, \quad \| \left(\lambda I - \mathcal{M}_D \right)^{-1} [\boldsymbol{\phi}] \|_{\mathcal{N}} \leq \frac{1}{\mathrm{dist}\left(\lambda, \sigma(\mathcal{M}_D) \right)} \| \boldsymbol{\phi} \|_{\mathrm{H}}.$$

Using the fact that $\mathcal{N}_D$ is injective and continuous on H, we can go back to the original norm to have

$$\forall \boldsymbol{\phi} \in \mathrm{H}, \quad \| \left(\lambda I - \mathcal{M}_D \right)^{-1} [\boldsymbol{\phi}] \| \leq \frac{C}{\mathrm{dist}\left(\lambda, \sigma(\mathcal{M}_D) \right)} \| \boldsymbol{\phi} \|_{\mathrm{H}},$$

which completes the proof. □

Proposition 4.4.9. *Let $\lambda \in \mathbb{C} \setminus [-\frac{1}{2}, \frac{1}{2}]$. There exists a positive constant C such that*

$$\forall \boldsymbol{\phi} \in L^2_T(\partial D), \quad \| \left(\lambda I - \mathcal{M}_D \right)^{-1} [\boldsymbol{\phi}] \|_{L^2_T(\partial D)} \leq \frac{C}{\mathrm{dist}(\lambda, \sigma(\mathcal{M}_D))} \| \boldsymbol{\phi} \|_{L^2_T(\partial D)}. \quad (4.4.20)$$

Proof. Let $\boldsymbol{\psi}, \boldsymbol{\phi} \in \left(L_T^2(\partial D)\right)^2$ be such that

$$\left(\lambda I - \mathcal{M}_D\right)[\boldsymbol{\psi}] = \boldsymbol{\phi}. \tag{4.4.21}$$

Using Helmholtz decomposition (4.4.1), we can write

$$\boldsymbol{\psi} = \nabla_{\partial D} U + \mathrm{curl}_{\partial D} V,$$

with $U \in H^1(\partial D)$ and $V \in H^{1/2}(\partial D)$. Taking the surface divergence of (4.4.21), together with using (4.4.13), (4.4.15), and the fact that $\nabla_{\partial D} \cdot \mathrm{curl}_{\partial D} f = 0,\ \forall f$, yields

$$\left(\lambda I - \mathcal{K}_D^*\right)[\Delta_{\partial D} U] = \nabla_{\partial D} \cdot \boldsymbol{\phi},$$

which can be written as

$$\Delta_{\partial D} U = \left(\lambda I - \mathcal{K}_D^*\right)^{-1}\left[\nabla_{\partial D} \boldsymbol{\phi}\right]. \tag{4.4.22}$$

Now we deal with the curl part. If we apply $\mathcal{N}_D$ on (4.4.21) we get by using (4.4.16) together with Lemma 4.4.4 that

$$\left(\lambda I - \mathcal{M}_D^*\right)\mathcal{N}_D \mathrm{curl}_{\partial D} V = \mathcal{N}_D \boldsymbol{\phi},$$

or equivalently,

$$\mathcal{N}_D \mathrm{curl}_{\partial D} V = \left(\lambda I - \mathcal{M}_D^*\right)^{-1} \mathcal{N}_D \boldsymbol{\phi}. \tag{4.4.23}$$

From the Helmholtz decomposition of $\boldsymbol{\phi}$: $\boldsymbol{\phi} = \nabla_{\partial D} \boldsymbol{\phi}_1 + \mathrm{curl}_{\partial D} \boldsymbol{\phi}_2$, (4.4.23) becomes

$$\mathcal{N}_D \mathrm{curl}_{\partial D} V = \left(\lambda I - \mathcal{M}_D^*\right)^{-1} \mathcal{N}_D \left[\mathrm{curl}_{\partial D} \boldsymbol{\phi}_2\right]. \tag{4.4.24}$$

Now, we can work in the function space $\mathrm{H} = \mathrm{curl}_{\partial D} H^{1/2}(\partial D)$. We denote by $\tilde{\mathcal{N}}_D$ the operator induced by $\mathcal{N}_D$ on H and by $R(\tilde{\mathcal{N}}_D) \subset \mathrm{H}$ the range of the induced operator. $\mathcal{M}_D$ also induces an operator $\tilde{\mathcal{M}}_D$ on H; see the proof of (4.4.16).

Next, we want to make sure that $\left(\lambda I - \tilde{\mathcal{M}}_D^*\right)^{-1} \tilde{\mathcal{N}}_D \mathrm{curl}_{\partial D} V$ belongs to $R(\tilde{\mathcal{N}}_D)$ so that we can apply $\tilde{\mathcal{N}}_D$'s left inverse (recall from Lemma 4.4.4 that $\tilde{\mathcal{N}}_D$ is injective). For doing so, we show that the range of $\tilde{\mathcal{N}}_D$ is stable by $\left(\lambda I - \tilde{\mathcal{M}}_D^*\right)^{-1}$. Take $f = \tilde{\mathcal{N}}_D[g] \in$

$R(\tilde{\mathcal{N}}_D)$. Then,

$$\begin{aligned}
\left(\lambda I - \tilde{\mathcal{M}}_D^*\right)^{-1}[f] \in R(\tilde{\mathcal{N}}_D) &\Leftrightarrow \exists h \in \mathrm{H}, \quad \left(\lambda I - \tilde{\mathcal{M}}_D^*\right)^{-1} \tilde{\mathcal{N}}_D[g] = \tilde{\mathcal{N}}_D[h] \\
&\Leftrightarrow \exists h \in \mathrm{H}, \quad \tilde{\mathcal{N}}_D[g] = \left(\lambda I - \tilde{\mathcal{M}}_D^*\right) \tilde{\mathcal{N}}_D[h] \\
&\Leftrightarrow \exists h \in \mathrm{H}, \quad \tilde{\mathcal{N}}_D[g] = \tilde{\mathcal{N}}_D \left(\lambda I - \tilde{\mathcal{M}}_D\right)[h] \\
&\Leftrightarrow \exists h \in \mathrm{H}, \quad g = \left(\lambda I - \tilde{\mathcal{M}}_D\right)[h] \quad (\text{ by injectivity of } \tilde{\mathcal{N}}_D) \\
&\Leftrightarrow \exists h \in \mathrm{H}, \quad \left(\lambda I - \tilde{\mathcal{M}}_D\right)^{-1}[g] = h.
\end{aligned}$$

So we have the stability of $R(\tilde{\mathcal{N}}_D)$ by $\tilde{\mathcal{M}}_D$ and

$$\tilde{\mathcal{N}}_D^{-1} \left(\lambda I - \tilde{\mathcal{M}}_D^*\right)^{-1} \tilde{\mathcal{N}}_D = \left(\lambda I - \tilde{\mathcal{M}}_D\right)^{-1}. \tag{4.4.25}$$

Applying this to (4.4.24) we get

$$\mathrm{curl}_{\partial D} V = \left(\lambda I + \tilde{\mathcal{M}}_D\right)^{-1} \mathrm{curl}_{\partial D} \boldsymbol{\phi}_2.$$

Using Lemma 4.4.8 we get the desired result. □

4.5 Small volume expansion

The aim of this section is to prove Theorems 4.5.9 and 4.5.10.

4.5.1 Layer potential formulation

For a given plane wave solution (E^i, H^i) to the Maxwell equations

$$\begin{cases} \nabla \times E^i = i\omega\mu_m H^i & \text{in } \mathbb{R}^3, \\ \nabla \times H^i = -i\omega\varepsilon_m E^i & \text{in } \mathbb{R}^3, \end{cases}$$

let (E, H) be the solution to the following Maxwell equations

$$\begin{cases} \nabla \times E = i\omega\mu H & \text{in} \quad \mathbb{R}^3 \setminus \partial D, \\ \nabla \times H = -i\omega\varepsilon E & \text{in} \quad \mathbb{R}^3 \setminus \partial D, \\ [\nu \times E] = [\nu \times H] = 0 & \text{on} \quad \partial D, \end{cases} \tag{4.5.1}$$

subject to the Silver-Müller radiation condition:

$$\lim_{|x|\to\infty} |x|(\sqrt{\mu}(H-H^i)\times\hat{x}-\sqrt{\varepsilon}(E-E^i))=0,$$

where $\hat{x}=x/|x|$. Here, $[\boldsymbol{\nu}\times E]$ and $[\boldsymbol{\nu}\times H]$ denote the jump of $\boldsymbol{\nu}\times E$ and $\boldsymbol{\nu}\times H$ along ∂D, namely,

$$[\boldsymbol{\nu}\times E]=(\boldsymbol{\nu}\times E)\Big|_+-(\boldsymbol{\nu}\times E)\Big|_-,\quad [\boldsymbol{\nu}\times H]=(\boldsymbol{\nu}\times H)\Big|_+-(\boldsymbol{\nu}\times H)\Big|_-.$$

Using the layer potentials defined in section 4.4, the solution to (4.5.1) can be represented as:

$$E(x)=\begin{cases} E^i(x)+\mu_m\nabla\times\mathcal{A}_D^{k_m}[\boldsymbol{\phi}](x)+\nabla\times\nabla\times\mathcal{A}_D^{k_m}[\boldsymbol{\psi}](x), & x\in\mathbb{R}^3\setminus\overline{D},\\ \mu_c\nabla\times\mathcal{A}_D^{k_c}[\boldsymbol{\phi}](x)+\nabla\times\nabla\times\mathcal{A}_D^{k_c}[\boldsymbol{\psi}](x), & x\in D,\end{cases} \tag{4.5.2}$$

and

$$H(x)=-\frac{i}{\omega\mu}\Big(\nabla\times E\Big)(x),\quad x\in\mathbb{R}^3\setminus\partial D, \tag{4.5.3}$$

where the pair $(\boldsymbol{\phi},\boldsymbol{\psi})\in TH(\mathrm{div},\partial D)\times TH(\mathrm{div},\partial D)$ is the unique solution to

$$\begin{bmatrix}\frac{\mu_c+\mu_m}{2}I+\mu_c\mathcal{M}_D^{k_c}-\mu_m\mathcal{M}_D^{k_m} & \mathcal{L}_D^{k_c}-\mathcal{L}_D^{k_m}\\ \mathcal{L}_D^{k_c}-\mathcal{L}_D^{k_m} & \left(\frac{k_c^2}{2\mu_c}+\frac{k_m^2}{2\mu_m}\right)I+\frac{k_c^2}{\mu_c}\mathcal{M}_D^{k_c}-\frac{k_m^2}{\mu_m}\mathcal{M}_D^{k_m}\end{bmatrix}\begin{bmatrix}\boldsymbol{\phi}\\ \boldsymbol{\psi}\end{bmatrix}=\begin{bmatrix}\nu\times E^i\\ i\omega\nu\times H^i\end{bmatrix}\Big|_{\partial D}. \tag{4.5.4}$$

The invertibility of the system of equations (4.5.4) on $TH(\mathrm{div},\partial D)\times TH(\mathrm{div},\partial D)$ was proved in [130]. Moreover, there exists a constant $C=C(\varepsilon,\mu,\omega)$ such that

$$\|\boldsymbol{\phi}\|_{TH(\mathrm{div},\partial D)}+\|\boldsymbol{\psi}\|_{TH(\mathrm{div},\partial D)}\leq C\Big(\|E^i\times\nu\|_{TH(\mathrm{div},\partial D)}+\|H^i\times\nu\|_{TH(\mathrm{div},\partial D)}\Big). \tag{4.5.5}$$

4.5.2 Derivation of the asymptotic formula

We will need the following notation. For a multi-index $\alpha\in\mathbb{N}^3$, let $x^\alpha=x_1^{\alpha_1}x_2^{\alpha_2}x_3^{\alpha_3}$, $\partial^\alpha=\partial_1^{\alpha_1}\partial_2^{\alpha_2}\partial_3^{\alpha_3}$, with $\partial_j=\partial/\partial x_j$.

Let $D=\delta B+z$, where B is a $\mathcal{C}^{1,\eta}$ $(0<\eta<1)$ domain containing the origin. For any $y\in\partial D$, let $\tilde{y}=\frac{y-z}{\delta}\in\partial B$. Denote by $\tilde{\boldsymbol{\phi}}(\tilde{y})=\boldsymbol{\phi}(y)$ and $\tilde{\boldsymbol{\psi}}(\tilde{y})=\boldsymbol{\psi}(y)$.

Asymptotics for the operators

We have the following expansions for $\mathcal{M}_D^k$ and $\mathcal{L}_D^k$.

Proposition 4.5.1. *Let $\boldsymbol{\phi} \in L^2_T(\partial D)$. As $\delta \to 0$, we have*

$$\mathcal{M}^k_D[\boldsymbol{\phi}](x) = \mathcal{M}_B[\tilde{\boldsymbol{\phi}}](\tilde{x}) + O(\delta^2). \tag{4.5.6}$$

Proof. Let $x \in \partial D$, and write $\tilde{x} = \frac{x-z}{\delta}$. We have

$$\mathcal{M}^k_D[\boldsymbol{\phi}](\delta\tilde{x}+z) = -\frac{1}{4\pi\delta}\int_{\partial D} \boldsymbol{\nu}_D(\delta\tilde{x}+z) \times \left(\nabla_{\tilde{x}} \times \left(\frac{e^{ik|\delta\tilde{x}+z-y|}}{|\delta\tilde{x}+z-y|}\boldsymbol{\phi}(y)\right)\right) d\sigma(y).$$

Changing y by $\tilde{y} = \frac{y-z}{\delta}$ in the integral we get

$$\mathcal{M}^k_D[\boldsymbol{\phi}](\delta\tilde{x}+z) = -\frac{1}{4\pi\delta}\int_{\partial B} \boldsymbol{\nu}_D(\delta\tilde{x}+z) \times \left(\nabla_{\tilde{x}} \times \left(\frac{e^{ik\delta|\tilde{x}-\tilde{y}|}}{\delta|\tilde{x}-\tilde{y}|}\tilde{\boldsymbol{\phi}}(\tilde{y})\right)\right) \delta^2 d\sigma(\tilde{y}).$$

Since $\forall x \in \partial D, \boldsymbol{\nu}_D(x) = \boldsymbol{\nu}_B(\frac{x-z}{\delta})$,

$$\mathcal{M}^k_D[\boldsymbol{\phi}](x) = \mathcal{M}^{\delta k}_B[\tilde{\boldsymbol{\phi}}](\tilde{x}).$$

For any $\tilde{x} \in \delta B$, it follows that

$$\mathcal{M}^{\delta k}_B[\tilde{\boldsymbol{\phi}}](\tilde{x}) = \mathcal{M}_B[\tilde{\boldsymbol{\phi}}](\tilde{x}) + \int_{\partial B} \boldsymbol{\nu}_B(\tilde{x}) \times (\nabla_{\tilde{x}} \times (ik\delta)) + O\left(\delta^2\right),$$

which gives the result. □

Proposition 4.5.2. *Let $\boldsymbol{\phi} \in TH(\mathrm{div}, \partial\mathrm{D})$. For any $y \in \partial D$, we have*

$$\begin{aligned}&\mathcal{L}^{k_m}_D[\boldsymbol{\phi}](y) - \mathcal{L}^{k_c}_D[\boldsymbol{\phi}](y) = \\ &\delta(k_m^2 - k_c^2)\boldsymbol{\nu}_B(\tilde{y}) \times \left(\mathcal{A}_B[\tilde{\phi}](\tilde{y}) + \frac{1}{8\pi}\int_{\partial B} \frac{\tilde{y}-\tilde{y}'}{|\tilde{y}-\tilde{y}'|}\left(\nabla_{\partial B}\cdot\tilde{\boldsymbol{\phi}}(\tilde{y}')\right) d\sigma(\tilde{y}')\right) + O\left(\delta^2\right).\end{aligned} \tag{4.5.7}$$

Proof. Note that, for $y \in \partial D$,

$$\mathcal{A}^k_D[\phi](y) = \delta\mathcal{A}^{\delta k}_B[\tilde{\phi}](\tilde{y})$$

and

$$\nabla_{\partial D}\mathcal{S}^k_D[\nabla_{\partial B}\cdot\boldsymbol{\phi}](y) = \frac{1}{\delta}\nabla_{\partial B}\mathcal{S}^{\delta k}_B[\nabla_{\partial B}\cdot\tilde{\boldsymbol{\phi}}](\tilde{y}).$$

We can expand

$$\mathcal{A}^{\delta k}_B[\tilde{\boldsymbol{\phi}}](\tilde{y}) = \mathcal{A}_B[\tilde{\boldsymbol{\phi}}](\tilde{y}) + O(\delta).$$

We also have

$$\nabla_{\partial B}\mathcal{S}_B^{\delta k}[\nabla_{\partial B}\cdot\tilde{\boldsymbol{\phi}}](\tilde{y}) = -\frac{1}{4\pi}$$
$$\times\nabla_{\partial B}\int_{\partial B}\frac{1}{|\tilde{y}-\tilde{y}'|}\left(1+k\delta|\tilde{y}-\tilde{y}'|-\frac{1}{2}k^2\delta^2|\tilde{y}-\tilde{y}'|^2+O(\delta^3|\tilde{y}-\tilde{y}'|^3)\right)\nabla_{\partial B}\cdot\tilde{\boldsymbol{\phi}}(\tilde{y}')d\sigma(\tilde{y}')$$

and

$$\nabla_{\partial B}\mathcal{S}_B^{\delta k}[\nabla_{\partial B}\cdot\tilde{\boldsymbol{\phi}}](\tilde{y}) = -\frac{1}{4\pi}\nabla_{\partial B}\int_{\partial B}\frac{1}{|\tilde{y}-\tilde{y}'|}\nabla_{\partial B}\cdot\tilde{\boldsymbol{\phi}}(\tilde{y}')d\sigma(\tilde{y}')$$
$$-\frac{1}{2}\nabla_{\partial B}\int_{\partial B}|\tilde{y}-\tilde{y}'|\nabla_{\partial B}\cdot\tilde{\boldsymbol{\phi}}(\tilde{y}')+O(\delta^3).$$

Now, since $\forall f\in L^2(\partial B),\ \mathcal{S}_B[f]\big|_{\overline{B}}\in\mathcal{C}^1(\overline{B}),\ \mathcal{S}_B[f]\big|_{\mathbb{R}^3\setminus B}\in\mathcal{C}^1(\mathbb{R}^3\setminus B)$ and the tangential component of the gradient of $\mathcal{S}[f]$ is continuous across ∂B, we can state that

$$\forall\tilde{y}\in\partial B,\ \boldsymbol{\nu}_B(\tilde{y})\times\nabla_{\partial B}\mathcal{S}_B[f]\big|_{\partial B}(\tilde{y})=\boldsymbol{\nu}_D(\tilde{y})\times\nabla\mathcal{S}_B[f]\big|_{\mathbb{R}^3\setminus B}(\tilde{y})=\boldsymbol{\nu}_D(\tilde{y})\times\nabla\mathcal{S}_B[f]\big|_{\overline{B}}(\tilde{y}).$$

Then we can write

$$\forall\tilde{y}\in\partial B,\ \boldsymbol{\nu}_B(\tilde{y})\times\nabla_{\partial B}\mathcal{S}_B^{\delta k}[\nabla_{\partial B}\cdot\tilde{\boldsymbol{\phi}}](\tilde{y}) = -\frac{1}{4\pi}\boldsymbol{\nu}_B(\tilde{y})\times\left[\nabla_{\partial B}\int_{\partial B}\frac{1}{|\tilde{y}-\tilde{y}'|}\nabla_{\partial B}\cdot\tilde{\boldsymbol{\phi}}(\tilde{y}')d\sigma(\tilde{y}')\right.$$
$$\left.-\frac{1}{2}\int_{\partial B}\frac{\tilde{y}-\tilde{y}'}{|\tilde{y}-\tilde{y}'|}\nabla_{\partial B}\cdot\tilde{\boldsymbol{\phi}}(\tilde{y}')d\sigma(\tilde{y})+O(k^3\delta^3)\right].$$

The proof is then complete. □

Far-field expansion

Define $\tilde{\boldsymbol{\phi}}_\beta$ and $\tilde{\boldsymbol{\psi}}_\beta$ for every $\beta\in\mathbb{N}^3$ by

$$\mathcal{W}_B^\delta\begin{bmatrix}\tilde{\boldsymbol{\phi}}_\beta\\ \tilde{\boldsymbol{\psi}}_\beta\end{bmatrix}=\begin{bmatrix}\nu(\tilde{y})\times(\tilde{y}^\beta\partial^\beta E^i(z))\\ i\omega\nu(\tilde{y})\times(\tilde{y}^\beta\partial^\beta H^i(z))\end{bmatrix}\tag{4.5.8}$$

with

$$\mathcal{W}_B^\delta=\begin{bmatrix}\frac{\mu_m+\mu_c}{2}I+\mu_c\mathcal{M}_B^{\delta k_c}-\mu_m\mathcal{M}_B^{\delta k_m} & \mathcal{L}_{B,\delta}^{k_c}-\mathcal{L}_{B,\delta}^{k_m}\\ \mathcal{L}_{B,\delta}^{k_c}-\mathcal{L}_{B,\delta}^{k_m} & \omega^2(\frac{\varepsilon_m+\varepsilon_c}{2}I+\varepsilon_c\mathcal{M}_B^{\delta k_c}-\varepsilon_m\mathcal{M}_B^{\delta k_m})\end{bmatrix}.\tag{4.5.9}$$

Using (4.5.2) we have the following expansion for $E(x)$ for x far away from z:

$$E(x) = E^i(x) + \sum_{|\alpha|=0}^{\infty}\sum_{|\beta|=0}^{\infty} \delta^{2+|\alpha|+|\beta|}\frac{(-1)^{|\alpha|}}{\alpha!\beta!}\Big(\mu_m \nabla\partial^\alpha \Gamma_{k_m}(x-z)\times \int_{\partial B}\tilde{y}^\alpha \tilde{\boldsymbol{\phi}}_\beta(\tilde{y})d\sigma(\tilde{y}) \\ + \nabla\times\nabla\partial^\alpha\Gamma_{k_m}(x-z)\times\int_{\partial B}\tilde{y}^\alpha\tilde{\boldsymbol{\psi}}_\beta(\tilde{y})d\sigma(\tilde{y})\Big). \quad (4.5.10)$$

For $\beta\in\mathbb{N}^3$, define the tensors by

$$\mathrm{M}^e_{\alpha,\beta} := \int_{\partial B}\tilde{y}^\alpha\tilde{\boldsymbol{\psi}}_\beta d\sigma(\tilde{y}) \quad \text{and} \quad \mathrm{M}^h_{\alpha,\beta} := \int_{\partial B}\tilde{y}^\alpha\tilde{\boldsymbol{\phi}}_\beta d\sigma(\tilde{y}). \quad (4.5.11)$$

The following lemma holds.

Lemma 4.5.3. *For $x\in\mathbb{R}^3\setminus\overline{D}$, we have*

$$E(x) = E^i(x) + \sum_{|\alpha|=0}^{\infty}\sum_{|\beta|=0}^{\infty} \delta^{2+|\alpha|+|\beta|}\frac{(-1)^{|\alpha|}}{\alpha!\beta!}\Big(\mu_m \nabla\partial^\alpha \Gamma_{k_m}(x-z)\times \mathrm{M}^h_{\alpha,\beta} \\ + \nabla\times\nabla\partial^\alpha\Gamma_{k_m}(x-z)\times\mathrm{M}^e_{\alpha,\beta}\Big). \quad (4.5.12)$$

Asymptotics for the potentials

Proposition 4.5.4. *Let $\beta\in\mathbb{N}^3$. We can write the following expansions for $\tilde{\boldsymbol{\phi}}_\beta$ and $\tilde{\boldsymbol{\psi}}_\beta$:*

$$\tilde{\boldsymbol{\phi}}_\beta = \sum_{n=0}^{\infty}\delta^n\tilde{\boldsymbol{\phi}}_{\beta,n}, \qquad \tilde{\boldsymbol{\psi}}_\beta = \sum_{n=0}^{\infty}\delta^n\tilde{\boldsymbol{\psi}}_{\beta,n}.$$

Moreover, there exists a $C\geq 0$ depending on B, β, E, and H such that

$$\begin{aligned}
\forall n\in\mathbb{N}, \|\tilde{\boldsymbol{\phi}}_{\beta,n}\|_{\mathrm{TH}(\mathrm{div},\partial B)} \leq & C^{(n+1)}\left(\frac{1}{\mathrm{dist}(\lambda_\mu,\sigma(\mathcal{M}_B))}\right)^{\lfloor n/2\rfloor+1}\left(\frac{1}{\mathrm{dist}(\lambda_\varepsilon,\sigma(\mathcal{M}_B))}\right)^{\lfloor n/2+1\rfloor}, \\
\forall n\in\mathbb{N}, \|\tilde{\boldsymbol{\psi}}_{\beta,n}\|_{\mathrm{TH}(\mathrm{div},\partial B)} \leq & C^{(n+1)}\left(\frac{1}{\mathrm{dist}(\lambda_\varepsilon,\sigma(\mathcal{M}_B))}\right)^{\lfloor n/2\rfloor+1}\left(\frac{1}{\mathrm{dist}(\lambda_\mu,\sigma(\mathcal{M}_B))}\right)^{\lfloor n/2+1\rfloor}.
\end{aligned} \quad (4.5.13)$$

Proof. We proceed by induction. Using Propositions 4.5.1 and 4.5.2 we find that

$$\begin{aligned}
\tilde{\boldsymbol{\phi}}_{\beta,0} &= (\mu_c-\mu_m)^{-1}(\lambda_\mu I+\mathcal{M}_B)^{-1}\left[\boldsymbol{\nu}(\tilde{y})\times(\tilde{y}^\beta\partial^\beta E(z)\right], \\
\tilde{\boldsymbol{\psi}}_{\beta,0} &= i\omega^{-1}(\varepsilon_c-\varepsilon_m)^{-1}(\lambda_\varepsilon I+\mathcal{M}_B)^{-1}\left[\boldsymbol{\nu}(\tilde{y})\times(\tilde{y}^\beta\partial^\beta H(z)\right].
\end{aligned} \quad (4.5.14)$$

Note that $\nabla_{\partial B}\cdot\tilde{\boldsymbol{\phi}}_{\beta,0}=0$. Indeed,

$$\nabla_{\partial B}\cdot\tilde{\boldsymbol{\phi}}=(\mu_c-\mu_m)^{-1}(\lambda_\mu I-\mathcal{K}_B^*)^{-1}\left[\nabla_{\partial B}\cdot\Big(\boldsymbol{\nu}(\tilde{y})\times(\tilde{y}^\beta\partial^\beta E(z)\Big)\right],$$

and

$$\begin{aligned}\nabla_{\partial B}\cdot(\boldsymbol{\nu}(\tilde{y})\times\Big(\tilde{y}^\beta\partial^\beta E(z)\Big)=&\boldsymbol{\nu}(\tilde{y})\cdot\Big(\nabla\times[\tilde{y}^\beta E(z)]\Big)\\ =&0.\end{aligned}$$

In the same way we have $\nabla_{\partial B}\cdot\tilde{\boldsymbol{\psi}}_{\beta,0}=0$. Using Proposition 4.4.9, we get the result.

For the first-orders the equations satisfied by $\tilde{\boldsymbol{\phi}}_{\beta,1}$ and $\tilde{\boldsymbol{\psi}}_{\beta,1}$ are

$$\begin{aligned}(\mu_c-\mu_m)(\lambda_\mu I+\mathcal{M}_B)[\tilde{\boldsymbol{\phi}}_{\beta,1}]+(k_c^2-k_m^2)\boldsymbol{\nu}(\tilde{y})\times\mathcal{A}_B[\tilde{\boldsymbol{\psi}}_{\beta,0}]=0,\\ \omega^2(\varepsilon_c-\varepsilon_m)(\lambda_\varepsilon I+\mathcal{M}_B)[\tilde{\boldsymbol{\psi}}_{\beta,1}]+(k_c^2-k_m^2)\boldsymbol{\nu}(\tilde{y})\times\mathcal{A}_B[\tilde{\boldsymbol{\phi}}_{\beta,0}]=0.\end{aligned}\tag{4.5.15}$$

The fact that $\mathcal{A}_B$ is bounded together with Proposition 4.4.9 gives the estimate of $\|\tilde{\boldsymbol{\phi}}_{\beta,1}\|_{L^2_T(\partial B)}$ and $\|\tilde{\boldsymbol{\phi}}_{\beta,1}\|_{L^2_T(\partial B)}$. If we take the surface divergence of (4.5.15), we get

$$\begin{aligned}(\mu_c-\mu_m)(\lambda_\mu I-\mathcal{K}_B^*)[\nabla_{\partial B}\cdot\tilde{\boldsymbol{\phi}}_{\beta,1}]+(k_c^2-k_m^2)\nabla_{\partial B}\cdot\Big(\boldsymbol{\nu}(\tilde{y})\times\mathcal{A}_B[\tilde{\boldsymbol{\psi}}_{\beta,0}]\Big)=0,\\ \omega^2(\varepsilon_c-\varepsilon_m)(\lambda_\varepsilon I-\mathcal{K}_B^*)[\nabla_{\partial B}\cdot\tilde{\boldsymbol{\psi}}_{\beta,1}]+(k_c^2-k_m^2)\nabla_{\partial B}\cdot\Big(\boldsymbol{\nu}(\tilde{y})\times\mathcal{A}_B[\tilde{\boldsymbol{\phi}}_{\beta,0}]\Big)=0.\end{aligned}$$

Since $\nabla_{\partial B}\cdot\Big(\boldsymbol{\nu}(\tilde{y})\times\mathcal{A}_B[\tilde{\boldsymbol{\psi}}_{\beta,0}]\Big)=\boldsymbol{\nu}(\tilde{y})\cdot\Big(\nabla\times\mathcal{A}_B[\tilde{\boldsymbol{\phi}}_{\beta,0}]\Big)$ and $f\mapsto\boldsymbol{\nu}\cdot\nabla\times\mathcal{A}_B[f]$ is bounded from $L^2_T(\partial B)$ into $L^2(\partial B)$, we can estimate the L^2 norm of $\nabla_{\partial B}\cdot\tilde{\boldsymbol{\phi}}_{\beta,1}$ as follows

$$\left\|\frac{1}{\mu_c-\mu_m}\left(\lambda_\mu-\mathcal{K}_B^*\right)^{-1}\left[\boldsymbol{\nu}(\tilde{y})\cdot\Big(\nabla\times\mathcal{A}_B[\tilde{\boldsymbol{\phi}}_{\beta,0}]\Big)\right]\right\|_{L^2(\partial B)}\leq\frac{c}{\operatorname{dist}(\lambda_\mu,\sigma(\mathcal{K}_B))}\|\tilde{\boldsymbol{\phi}}_{\beta,0}\|_{L^2_T}.$$

Since $\sigma(\mathcal{M}_B)=\sigma(\mathcal{K}_D)$ (see Proposition 4.4.7) we get the result. The estimate for $\|\nabla_{\partial B}\cdot\tilde{\boldsymbol{\psi}}_{\beta,1}\|_{L^2}$ is obtained in the same way.

Now, fix $n\in\mathbb{N}^*$; $\tilde{\boldsymbol{\phi}}_{\beta,n+1}$ and $\tilde{\boldsymbol{\psi}}_{\beta,n+1}$ satisfy the following system:

$$\begin{aligned}(\mu_c-\mu_m)(\lambda_\mu I+\mathcal{M}_B)[\tilde{\boldsymbol{\phi}}_{\beta,i+1}]+(k_c^2-k_m^2)\boldsymbol{\nu}(\tilde{y})\times\Big(\mathcal{A}_B[\tilde{\boldsymbol{\psi}}_{\beta,i}]+\mathcal{B}_B[\tilde{\boldsymbol{\psi}}_{\beta,i}]\Big)=0,\\ \omega^2(\varepsilon_c-\varepsilon_m)(\lambda_\varepsilon I+\mathcal{M}_B)[\tilde{\boldsymbol{\psi}}_{\beta,0}]+(k_c^2-k_m^2)\boldsymbol{\nu}(\tilde{y})\times\Big(\mathcal{A}_B[\tilde{\boldsymbol{\phi}}_{\beta,i}]+\mathcal{B}_B[\tilde{\boldsymbol{\phi}}_{\beta,i}]\Big)=0,\end{aligned}$$

where the operator $\mathcal{B}_D$ is defined by

$$\begin{aligned}\mathrm{TH}(\operatorname{div},\partial B)\longrightarrow&\mathrm{TH}(\operatorname{div},\partial B)\\ f\longmapsto&\frac{1}{8\pi}\int_{\partial B}\frac{\tilde{y}-\tilde{y}'}{|\tilde{y}-\tilde{y}'|}\left(\nabla_{\partial B}\cdot f(\tilde{y}')\right)d\sigma(\tilde{y}').\end{aligned}$$

The operator $\mathcal{B}_B$ is bounded, and we can get the norm estimates for $\tilde{\boldsymbol{\phi}}_{\beta,n+1}$, $\tilde{\boldsymbol{\psi}}_{\beta,n+1}$, $\nabla_{\partial B}\cdot\tilde{\boldsymbol{\phi}}_{\beta,n+1}$ and $\nabla_{\partial B}\cdot\tilde{\boldsymbol{\psi}}_{\beta,n+1}$, as before. □

Derivation of the leading-order tensors

By Lemma 4.5.3, for $x\in\mathbb{R}^3\setminus\overline{D}$,

$$\begin{aligned}E(x) = E^i(x) &+ \delta^2\Big(\mu_m\nabla\Gamma_{k_m}(x-z)\times \mathrm{M}^h_{0,0} + \nabla\times\nabla\Gamma_{k_m}(x-z)\times \mathrm{M}^e_{0,0}\Big)\\ &+ \delta^3\Big(\mu_m\nabla\Gamma_{k_m}(x-z)\times \sum_{j=1}^3 \mathrm{M}^h_{0,j} + \nabla\times\nabla\Gamma_{k_m}(x-z)\times \sum_{j=1}^3 \mathrm{M}^e_{0,j}\Big)\\ &- \delta^3\Big(\mu_m\sum_{j=1}^3\nabla\partial_j\Gamma_{k_m}(x-z)\times \mathrm{M}^h_{j,0} + \nabla\times\sum_{j=1}^3\nabla\partial_j\Gamma_{k_m}(x-z)\times \mathrm{M}^e_{j,0}\Big)\\ &+ O(\delta^4).\end{aligned} \tag{4.5.16}$$

We start by computing $\mathrm{M}^h_{0,0}$:

$$\begin{aligned}\mathrm{M}^h_{0,0} &= \int_{\partial B}\tilde{\boldsymbol{\phi}}_0(\tilde{y})d\sigma(\tilde{y}),\\ \mathrm{M}^h_{0,0} &= \int_{\partial B}\tilde{\boldsymbol{\phi}}_0(\tilde{y})\nabla\tilde{y}d\sigma(\tilde{y}),\\ \mathrm{M}^h_{0,0} &= \int_{\partial B}\tilde{y}\nabla_{\partial B}\cdot\tilde{\boldsymbol{\phi}}_0(\tilde{y})d\sigma(\tilde{y}).\end{aligned}$$

Now, using the expansion of $\tilde{\boldsymbol{\phi}}$ given in Proposition 4.5.4 we have

$$\mathrm{M}^h_{0,0} = \int_{\partial B}\tilde{y}\nabla_{\partial B}\cdot\tilde{\boldsymbol{\phi}}_{0,0}(\tilde{y})d\sigma(\tilde{y}) + \int_{\partial B}\tilde{y}\nabla_{\partial B}\cdot\tilde{\boldsymbol{\phi}}_{0,1}(\tilde{y})d\sigma(\tilde{y}) + O(\delta^2).$$

Recall (4.5.14) for $\beta=0$:

$$\begin{aligned}\tilde{\boldsymbol{\phi}}_{0,0} &= (\mu_c-\mu_m)^{-1}(\lambda_\mu I+\mathcal{M}_B)^{-1}\left[\boldsymbol{\nu}(\tilde{y})\times E(z)\right]\\ \tilde{\boldsymbol{\psi}}_{0,0} &= i\omega^{-1}(\varepsilon_c-\varepsilon_m)^{-1}(\lambda_\varepsilon I+\mathcal{M}_B)^{-1}\left[\boldsymbol{\nu}(\tilde{y})\times H(z)\right].\end{aligned}$$

We can see, using (4.4.13) and the fact that

$$\nabla_{\partial B}\cdot\Big(E^i(z)\times\boldsymbol{\nu}(\tilde{y})\Big) = \nabla_{\partial B}\cdot\Big(H^i(z)\times\boldsymbol{\nu}(\tilde{y})\Big) = 0,$$

that

$$\nabla_{\partial B}\cdot\tilde{\boldsymbol{\phi}}_{0,0} = \nabla_{\partial B}\cdot\tilde{\boldsymbol{\psi}}_{0,0} = 0.$$

Now, taking the surface divergence of (4.5.15) for $\beta = 0$, it follows that

$$\begin{aligned}(\mu_c - \mu_m)(\lambda_\mu I - \mathcal{K}_B^*)[\nabla_{\partial B} \cdot \tilde{\boldsymbol{\phi}}_{0,1}] + (k_c^2 - k_m^2)\nabla_{\partial B} \cdot \left(\boldsymbol{\nu}(\tilde{y}) \times \mathcal{A}_B[\tilde{\boldsymbol{\psi}}_{0,0}]\right) = 0,\\ \omega^2(\varepsilon_c - \varepsilon_m)(\lambda_\varepsilon I - \mathcal{K}_B^*)[\nabla_{\partial B} \cdot \tilde{\boldsymbol{\psi}}_{0,1}] + (k_c^2 - k_m^2)\nabla_{\partial B} \cdot \left(\boldsymbol{\nu}(\tilde{y}) \times \mathcal{A}_B[\tilde{\boldsymbol{\phi}}_{0,0}]\right) = 0.\end{aligned} \tag{4.5.17}$$

Since $\nabla_{\partial B} \cdot (\boldsymbol{\nu} \times \acute{\mathrm{L}}) = \boldsymbol{\nu} \cdot (\nabla \times \acute{\mathrm{L}})$ we need to study the quantities

$$\boldsymbol{\nu} \cdot \nabla \times \mathcal{A}_B[\tilde{\boldsymbol{\phi}}_{0,0}]$$

and

$$\boldsymbol{\nu} \cdot \nabla \times \mathcal{A}_B[\tilde{\boldsymbol{\psi}}_{0,0}].$$

The following lemma holds.

Lemma 4.5.5. *We have*

$$\nabla \times \mathcal{A}_B[\tilde{\phi}_{0,0}] = \begin{cases} \dfrac{1}{\mu_c - \mu_m} \nabla \mathcal{S}_B \left(\lambda_\mu I + \mathcal{K}_B^*\right)^{-1} [\nu \cdot E^i(z)] & \text{in} \quad \mathbb{R}^3 \setminus \overline{B}, \\ \dfrac{1}{\mu_c} E^i(z) + \dfrac{\mu_m}{\mu_c^2 - \mu_m \mu_c} \nabla \mathcal{S}_B \left(\lambda_\mu I + \mathcal{K}_B^*\right)^{-1} [\nu \cdot E^i(z)] & \text{in} \quad B, \end{cases} \tag{4.5.18}$$

and

$$\nabla \times \mathcal{A}_B[\tilde{\psi}_{0,0}] = \begin{cases} \frac{i}{\omega(\varepsilon_c - \varepsilon_m)} \nabla \mathcal{S}_B \left(\lambda_\varepsilon I + \mathcal{K}_B^*\right)^{-1} [\nu \cdot H^i(z)] & \text{in} \quad \mathbb{R}^3 \setminus \overline{B}, \\ \dfrac{i}{\omega \varepsilon_c} H^i(z) + \dfrac{i\varepsilon_m}{\omega(\varepsilon_c^2 - \varepsilon_m \varepsilon_c)} \nabla \mathcal{S}_B \left(\lambda_\varepsilon I + \mathcal{K}_B^*\right)^{-1} [\nu \cdot H^i(z)] & \text{in} \quad B. \end{cases} \tag{4.5.19}$$

Proof. We only prove (4.5.18). We shall consider the solution to the following system

$$\begin{cases} \Delta u = 0 & \text{in} \quad \mathbb{R}^3, \\ \boldsymbol{\nu} \cdot \nabla u|_- = \boldsymbol{\nu} \cdot \nabla u|_+ & \text{on} \quad \partial B, \\ \mu_c \nu \times \nabla u|_- - \mu_m \nu \times \nabla u|_+ = \boldsymbol{\nu} \times E^i(z) & \text{on} \quad \partial B, \\ u = O(|x|^{-1}) & |x| \to \infty. \end{cases} \tag{4.5.20}$$

We can see that both the left-hand side and the right-hand side of (4.5.18) are divergence free. We want to prove that they are both equal to the field ∇u in $\mathbb{R}^3$. First we check that they satisfy the jump relations. We already have the continuity of the

normal part of the curl of a vectorial single layer potential [51]. Recall that

$$\tilde{\boldsymbol{\phi}}_{0,0} = (\mu_c - \mu_m)^{-1}(\lambda_\mu I + \mathcal{M}_B)^{-1}[\boldsymbol{\nu}(\tilde{y}) \times E^i(z)].$$

Then,

$$\boldsymbol{\nu} \times \nabla \times \mathcal{A}_D[\tilde{\boldsymbol{\phi}}_{0,0}]|_\pm = \frac{1}{\mu_c - \mu_m}\left(\mp\frac{I}{2} + \mathcal{M}_B\right)(\lambda I + \mathcal{M}_B)^{-1}\left[\boldsymbol{\nu}(\tilde{y}) \times E^i(z)\right],$$

so we have

$$\mu_c \boldsymbol{\nu} \times \nabla \times \mathcal{A}_D[\tilde{\boldsymbol{\phi}}_{0,0}]|_- - \mu_m \boldsymbol{\nu} \times \nabla \times \mathcal{A}_D[\tilde{\boldsymbol{\phi}}_{0,0}]|_+ = \boldsymbol{\nu}(\tilde{y}) \times E^i(z).$$

The continuity of the tangential derivative of a scalar single layer potential gives

$$\begin{aligned}\mu_c \boldsymbol{\nu} \times \left(\frac{1}{\mu_c - \mu_m}\nabla \mathcal{S}_B\left(\lambda_\mu I + \mathcal{K}_B^*\right)^{-1}\left[\nu \cdot E^i(z)\right]\Big|_-\right) = \mu_m \boldsymbol{\nu} \times \Bigg(&\frac{1}{\mu_c} E^i(z) \\ &+ \frac{\mu_m}{\mu_c^2 - \mu_m \mu_c}\nabla \mathcal{S}_B\left(\lambda_\mu I + \mathcal{K}_B^*\right)^{-1}\left[\nu \cdot E^i(z)\right]\Big|_+\Bigg),\end{aligned}$$

and the jump of the normal derivative of a scalar single layer potential can be written as follows

$$\boldsymbol{\nu} \cdot \nabla \mathcal{S}_B\left(\lambda_\mu I + \mathcal{K}_B^*\right)^{-1}\left[\nu \cdot E^i(z)\right]\Big|_\pm = \left(\mp\frac{I}{2} + \mathcal{K}_B^*\right)\left(\lambda_\mu I + \mathcal{K}_B^*\right)^{-1}\left[\nu \cdot E^i(z)\right],$$

which gives the correct jump relation for the normal derivative.

The only problem left is to prove the uniqueness of the system. Now let $\tilde{u}$ be the solution to (4.5.20) with the term $\boldsymbol{\nu} \times E^i(z)$ replaced by vector 0 on ∂B. Note that $\mu_c \nu \times \nabla \tilde{u}|_- = \mu_m \nu \times \nabla \tilde{u}|_+$ is equivalent to

$$\mu_c \frac{\partial \tilde{u}}{\partial T}\Big|_- = \mu_m \frac{\partial \tilde{u}}{\partial T}\Big|_+,$$

where T is any tangential direction on ∂B. Then by choosing any test function in $H^1(\partial B)$ and integrating by parts we can get $\mu_c \tilde{u}|_- = \mu_m \tilde{u}|_+$ on ∂B. Thus,

$$0 \leq \int_{\mathbb{R}^3} \mu |\nabla \tilde{u}|^2 dx = -\int_{\partial B} \mu_m \frac{\partial \tilde{u}}{\partial \boldsymbol{\nu}}\Big|_+ \tilde{u}|_+ + \int_{\partial B} \mu_c \frac{\partial \tilde{u}}{\partial \boldsymbol{\nu}}\Big|_- \tilde{u}|_- = 0,$$

which proves $\tilde{u} = 0$ and completes the proof. □

It is worth mentioning that it was proved in [67] that

$$\nabla \times \mathcal{A}_B(\frac{1}{2}I + \mathcal{M}_B)^{-1}[\nu \times E^i(z)] = E^i(z) \quad \text{in} \quad B,$$

which, by taking $\mu_m = 0$ (or let $\mu_c = \infty$), can be seen as the extreme case in (4.5.18).

Now that we have a better understanding of $\boldsymbol{\nu} \times \nabla \times \mathcal{A}_D[\tilde{\boldsymbol{\phi}}_{0,0}]$, by Lemma 4.5.5, we can introduce the unique solutions $u^e, u^h \in H^1(B)$ up to constants such that $\nabla u^e = \nabla \times \mathcal{A}_B[\tilde{\phi}_{0,0}]$, $\nabla u^h = \nabla \times \mathcal{A}_B[\tilde{\psi}_{0,0}]$ with u^e, u^h satisfying

$$\begin{cases} \Delta u^e = 0 & \text{in} \quad B, \\ \nu \cdot \nabla u^e|_- = \nu \cdot (\nabla \times \mathcal{A}_B[\tilde{\phi}_{0,0}]) & \text{on} \quad \partial B, \end{cases} \tag{4.5.21}$$

and

$$\begin{cases} \Delta u^h = 0 & \text{in} \quad B, \\ \nu \cdot \nabla u^h|_- = \nu \cdot (\nabla \times \mathcal{A}_B[\tilde{\psi}_{0,0}]) & \text{on} \quad \partial B. \end{cases} \tag{4.5.22}$$

The expressions of ∇u^e and ∇u^h are given by Lemma 4.5.5. Now, by using equation (4.5.17), we can compute the surface divergence of $\tilde{\phi}_{0,1}$ and $\tilde{\psi}_{0,1}$:

$$\begin{aligned} \nabla_{\partial B} \cdot \tilde{\phi}_{0,1} &= \frac{k_c^2 - k_m^2}{\mu_c - \mu_m}(\lambda_\mu I - \mathcal{K}_B^*)^{-1}\Big[\frac{\partial u^h}{\partial \nu}\Big|_-\Big], \\ \nabla_{\partial B} \cdot \tilde{\psi}_{0,1} &= \frac{k_c^2 - k_m^2}{\omega^2(\varepsilon_c - \varepsilon_m)}(\lambda_\varepsilon I - \mathcal{K}_B^*)^{-1}\Big[\frac{\partial u^e}{\partial \nu}\Big|_-\Big]. \end{aligned}$$

Then we have the following lemma.

Lemma 4.5.6. *Let v^e be the solution to*

$$\begin{cases} \Delta v^e = 0 & x \in \mathbb{R}^3 \setminus \partial B, \\ v^e|_+ - v^e|_- = 0 & x \in \partial B, \\ \varepsilon_m \frac{\partial v^e}{\partial \nu}\Big|_+ - \varepsilon_c \frac{\partial v^e}{\partial \nu}\Big|_- = (\varepsilon_c - \varepsilon_m)\nabla u^e \cdot \nu\Big|_- & x \in \partial B, \\ v^e \to 0 & |x| \to \infty, \end{cases} \tag{4.5.23}$$

and let v^h be the solution to

$$\begin{cases} \Delta v^h = 0 & x \in \mathbb{R}^3 \setminus \partial B, \\ v^h|_+ - v^h|_- = 0 & x \in \partial B, \\ \mu_m \frac{\partial v^h}{\partial \nu}\Big|_+ - \mu_c \frac{\partial v^h}{\partial \nu}\Big|_- = (\mu_c - \mu_m)\nabla u^h \cdot \nu\Big|_- & x \in \partial B, \\ v^h \to 0 & |x| \to \infty. \end{cases} \tag{4.5.24}$$

Then the following asymptotic expansions hold:

$$\mathrm{M}^e_{0,0} = \delta \frac{k_m^2 - k_c^2}{\omega^2 \varepsilon_m} \int_B \nabla(u^e + v^e) + O(\delta^2),$$
$$\mathrm{M}^h_{0,0} = \delta \frac{k_m^2 - k_c^2}{\mu_m} \int_B \nabla(u^h + v^h) + O(\delta^2).$$

Proof. By Proposition 4.5.4, we have

$$\begin{aligned}
\mathrm{M}^h_{0,0} &= \int_{\partial B} \tilde{\phi}_0 d\sigma(\tilde{y}) = \delta \int_{\partial B} \tilde{\phi}_{0,1} d\sigma(\tilde{y}) + O(\delta^2) \\
&= -\delta \int_{\partial B} \tilde{y} \nabla_{\partial B} \cdot \tilde{\phi}_{0,1} d\sigma(\tilde{y}) + O(\delta^2) \\
&= \delta \frac{k_m^2 - k_c^2}{\mu_c - \mu_m} \int_{\partial B} \tilde{y} (\lambda_\mu I - \mathcal{K}_B^*)^{-1} \Big[\frac{\partial u^h}{\partial \nu} \Big|_- \Big] d\sigma(\tilde{y}) + O(\delta^2).
\end{aligned}$$

Using the fact that

$$\lambda_\mu = \frac{1}{2} + \frac{\mu_m}{\mu_c - \mu_m},$$

we get that for $f \in L^2(\partial B)$,

$$f = \frac{\mu_c - \mu_m}{\mu_m} \left[(\lambda_\mu I - \mathcal{K}_B^*)[f] + \left(-\frac{I}{2} + \mathcal{K}_D^* \right)[f] \right].$$

Then,

$$\mathrm{M}^h_{0,0} = \delta \frac{k_m^2 - k_c^2}{\mu_m} \Big(\int_{\partial B} \tilde{y} \frac{\partial u^h}{\partial \nu} \Big|_- d\sigma(\tilde{y}) + \int_{\partial B} \tilde{y} (-\frac{I}{2} + \mathcal{K}_B^*)(\lambda_\mu I - \mathcal{K}_B^*)^{-1} \Big[\frac{\partial u^h}{\partial \nu} \Big|_- \Big] d\sigma(\tilde{y}) \Big) + O(\delta^2).$$

An integration by parts gives

$$\int_{\partial B} \tilde{y} \frac{\partial u^h}{\partial \nu} \Big|_- d\sigma(\tilde{y}) = \int_B \nabla u^h dx.$$

We now take a look at the transmission problem (4.5.24) solved by v^h. Using the jump relation of the normal derivative of the scalar single layer potential we find that, writing $v^h = \mathcal{S}_B[f]$ with f being such that $(\lambda_\mu I - \mathcal{K}^*)[f] = \dfrac{\partial u^h}{\partial \nu}$ gives

$$\left(-\frac{I}{2} + \mathcal{K}_B^* \right)[f] = \frac{\partial v^h}{\partial \boldsymbol{\nu}} \Big|_-,$$

and hence,

$$(-\frac{I}{2} + \mathcal{K}_B^*)(\lambda_\mu I - \mathcal{K}_B^*)^{-1} \Big[\frac{\partial u^h}{\partial \nu} \Big|_- \Big] = \frac{\partial v^h}{\partial \boldsymbol{\nu}} \Big|_-.$$

Integrating by parts we get

$$\mathrm{M}^h_{0,0} = \delta \frac{k_m^2 - k_c^2}{\mu_m} \Big(\int_B \nabla u^h dx + \int_B \nabla v^h dx \Big) + O(\delta^2).$$

The evaluation for $\mathrm{M}^e_{0,0}$ can be done in exactly the same way. □

Derivation of the leading-order tensors

Lemma 4.5.7. *We have*

$$\mathrm{M}^e_{\alpha,\beta} = \frac{i}{\omega \varepsilon_m} \Big(\int_B \nabla (x^\alpha x^\beta) \times \partial^\beta H^i(z) + i\omega(\varepsilon_c - \varepsilon_m) \int_B \nabla \times (x^\alpha \nabla \times \mathcal{A}_B[\tilde{\psi}_{\beta,0}]) \Big) + O(\delta), \tag{4.5.25}$$

$$\mathrm{M}^h_{\alpha,\beta} = \frac{1}{\mu_m} \Big(\int_B \nabla (x^\alpha x^\beta) \times \partial^\beta E^i(z) - (\mu_c - \mu_m) \int_B \nabla \times (x^\alpha \nabla \times \mathcal{A}_B[\tilde{\phi}_{\beta,0}]) \Big) + O(\delta). \tag{4.5.26}$$

In particular, we have

$$\mathrm{M}^e_{j,0} = \frac{i}{\omega \varepsilon_m} |B| e_j \times H^i(z) - \frac{\varepsilon_c - \varepsilon_m}{\varepsilon_m} e_j \times \int_B \nabla u^h + O(\delta), \tag{4.5.27}$$

$$\mathrm{M}^h_{j,0} = \frac{1}{\mu_m} |B| e_j \times E^i(z) - \frac{\mu_c - \mu_m}{\mu_m} e_j \times \int_B \nabla u^e + O(\delta), \tag{4.5.28}$$

$$\mathrm{M}^e_{0,j} = \frac{i}{\omega \varepsilon_m} |B| e_j \times \partial_j H^i(z) - \frac{\varepsilon_c - \varepsilon_m}{\varepsilon_m} \int_B \nabla \mathcal{S}_B[\nabla_{\partial B} \cdot \tilde{\psi}_{j,0}] + O(\delta), \tag{4.5.29}$$

$$\mathrm{M}^h_{0,j} = \frac{1}{\mu_m} |B| e_j \times \partial_j E^i(z) - \frac{\mu_c - \mu_m}{\mu_m} \int_B \nabla \mathcal{S}_B[\nabla_{\partial B} \cdot \tilde{\phi}_{j,0}] + O(\delta), \tag{4.5.30}$$

where (e_1, e_2, e_3) *is an orthonormal basis of* $\mathbb{R}^3$.

Proof. We shall only consider $\mathrm{M}^h_{\alpha,\beta}$. $\mathrm{M}^e_{\alpha,\beta}$ can be calculated in exactly the same way. We have

$$\mathrm{M}^h_{\alpha,\beta} = \mathrm{M}^{h,0}_{\alpha,\beta} + O(\delta),$$

where $\mathrm{M}^{h,0}_{\alpha,\beta}$ is given by

$$\mathrm{M}^{h,0}_{\alpha,\beta} = \int_{\partial B} \tilde{y}^\alpha \tilde{\phi}_{\beta,0} d\sigma(\tilde{y}).$$

Since $\lambda_\mu = \dfrac{1}{2} + \dfrac{\mu_m}{\mu_c - \mu_m}$ we have that for any $f \in L^2_T(\partial B)$,

$$(\lambda_\mu I + \mathcal{M}_B)[f] - \Big(\frac{I}{2} + \mathcal{M}_B \Big)[f] = \frac{\mu_m}{\mu_c - \mu_m} f.$$

By applying Lemma 4.5.4, it follows that

$$\mathrm{M}^{h,0}_{\alpha,\beta} = \frac{1}{\mu_m}\int_{\partial B}\tilde{y}^\alpha \nu(\tilde{y}) \times (\tilde{y}^\beta \partial^\beta E^i(z))d\sigma(\tilde{y}) \\ - \frac{1}{\mu_m}\int_{\partial B}\tilde{y}^\alpha (\frac{I}{2} + \mathcal{M}_B)(\lambda_\mu I + \mathcal{M}_B)^{-1}[\nu(\tilde{y}) \times \tilde{y}^\beta \partial^\beta E^i(z)]d\sigma(\tilde{y}).$$

Using the jump relations on $\mathcal{M}_B$ and the fact that

$$\tilde{\boldsymbol{\phi}}_{\beta,0} = \frac{1}{\mu_c - \mu_m}\left(\lambda_\mu I + \mathcal{M}_B\right)^{-1}[\nu(\tilde{y}) \times \tilde{y}^\beta \partial^\beta],$$

we can write

$$\mathrm{M}^{h,0}_{\alpha,\beta} = \frac{1}{\mu_m}\int_{\partial B}\tilde{y}^\alpha \nu(\tilde{y}) \times (\tilde{y}^\beta \partial^\beta E^i(z))d\sigma(\tilde{y}) \\ - \frac{\mu_c - \mu_m}{\mu_m}\int_{\partial B}\tilde{y}^\alpha \nu(\tilde{y}) \times \nabla \times \mathcal{S}_B[\tilde{\phi}_{\beta,0}]\Big|_- d\sigma(\tilde{y}).$$

The curl theorem yields

$$\mathrm{M}^{h,0}_{\alpha,\beta} = \frac{1}{\mu_m}\int_B \nabla(x^\alpha x^\beta) \times \partial^\beta E^i(z)dx - \frac{\mu_c - \mu_m}{\mu_m}\int_B \nabla \times (x^\alpha \nabla \times \mathcal{S}_B[\tilde{\phi}_{\beta,0}])dx,$$

and thus (4.5.26) holds. By using the definition of u^e and u^h we get the case where $|\alpha| = 1$, $|\beta| = 0$. □

Derivation of the polarization tensor

Denote by $G(x,z)$ the matrix valued function (Dyadic Green function)

$$G(x,z) = \varepsilon_m(\Gamma_{k_m}(x-z)I + \frac{1}{k_m^2}D_x^2\Gamma_{k_m}(x-z)).$$

It can be seen that $G(x,z)$ satisfies

$$\nabla_x \times \frac{1}{\varepsilon_m}\nabla_x \times G(x,z) - \omega^2\mu_m G(x,z) = -\delta_z I.$$

We can also easily check that

$$\nabla \times G(x,z) = \varepsilon_m \nabla \times (\Gamma_{k_m}(x-z)I) = \varepsilon_m \nabla\Gamma_{k_m}(x-z) \times I.$$

Theorem 4.5.8. *Define the polarization tensors*

$$M^e := \int_{\partial B} \tilde{y}(\lambda_\varepsilon I - \mathcal{K}_B^*)^{-1}[\nu]d\sigma(\tilde{y}) \quad \textit{and} \quad M^h := \int_{\partial B} \tilde{y}(\lambda_\mu I - \mathcal{K}_B^*)^{-1}[\nu]d\sigma(\tilde{y}). \tag{4.5.31}$$

Then the following far-field expansion holds:

$$E(x) - E^i(x) = -\delta^3\omega^2\mu_m G(x,z)M^e E^i(z) - \delta^3\frac{i\omega\mu_m}{\varepsilon_m}\nabla \times G(x,z)M^h H^i(z) + O(\delta^4). \tag{4.5.32}$$

Before we proceed, we stress that the polarization tensors M^e, M^h defined above are matrix with each entry m_{ij}^e and m_{ij}^h, $i,j = 1,2,3$, defined by (4.2.16) with $\lambda = \lambda_\varepsilon$ and $\lambda = \lambda_\mu$, respectively.

They are different from the vector valued tensors we defined in equation (4.5.11).

Proof. We shall give the analysis term by term in (4.5.16). It is easy to check that

$$\sum_{j=1}^3 e_j \times \partial_j E^i(z) = i\omega\mu_m H^i(z) \quad \text{and} \quad \sum_{j=1}^3 e_j \times \partial_j H^i(z) = -i\omega\varepsilon_m E^i(z)$$

and

$$\sum_{j=1}^3 \nabla\partial_j\Gamma_{k_m}(x-z) \times e_j \times E^i(z) = \omega^2\mu_m G(x,z)E^i(z).$$

Then by Lemma 4.5.7 it follows that

$$\nabla \times \sum_{j=1}^3 \nabla\partial_j\Gamma_{k_m}(x-z) \times \mathrm{M}_{j,0}^e = \omega^2\mu_m\nabla \times G(x,z)\Big(\frac{i}{\omega\varepsilon_m}|B|H^i(z) - \frac{\varepsilon_c - \varepsilon_m}{\varepsilon_m}\int_B \nabla u^h\Big) + O(\delta),$$

and

$$\mu_m\sum_{j=1}^3 \nabla\partial_j\Gamma_{k_m}(x-z) \times \mathrm{M}_{j,0}^h = \omega^2\mu_m G(x,z)\Big(|B|E^i(z) - (\mu_c - \mu_m)\int_B \nabla u^e\Big) + O(\delta).$$

Furthermore, we obtain from Lemma 4.5.4 that

$$\sum_{j=1}^{3} \nabla_{\partial B} \cdot \tilde{\phi}_{j,0} = \frac{1}{\mu_c - \mu_m} (\lambda_\mu I - \mathcal{K}_B^*)^{-1} \left[\sum_{j=1}^{3} \nabla_{\partial B} \cdot \Big(\boldsymbol{\nu}(\tilde{y}) \times (\tilde{y}_j \partial_j E^i(z)) \Big) \right],$$
$$\sum_{j=1}^{3} \nabla_{\partial B} \cdot \tilde{\phi}_{j,0} = \frac{1}{\mu_c - \mu_m} (\lambda_\mu I - \mathcal{K}_B^*)^{-1} \left[\sum_{j=1}^{3} \boldsymbol{\nu}(\tilde{y}) \cdot \Big(\nabla \times (\tilde{y}_j \partial_j E^i(z)) \Big) \right],$$

which gives

$$\sum_{j=1}^{3} \nabla_{\partial B} \cdot \tilde{\phi}_{j,0} = -\frac{i\omega\mu_m}{\mu_c - \mu_m} (\lambda_\mu I - \mathcal{K}_B^*)^{-1} [\nu \cdot H^i(z)].$$

Similarly, we have

$$\sum_{j=1}^{3} \nabla_{\partial B} \cdot \tilde{\psi}_{j,0} = -\frac{\varepsilon_m}{\varepsilon_c - \varepsilon_m} (\lambda_\mu I - \mathcal{K}_B^*)^{-1} [\nu \cdot E^i(z)].$$

Recall from (4.5.29) that

$$\mathrm{M}_{0,j}^e = \frac{i}{\omega\varepsilon_m} |B| e_j \times \partial_j H^i(z) - \frac{\varepsilon_c - \varepsilon_m}{\varepsilon_m} \int_B \nabla \mathcal{S}_B[\nabla_{\partial B} \cdot \tilde{\psi}_{j,0}] + O(\delta).$$

Summing over j gives

$$\begin{aligned}
\nabla \times \nabla\Gamma_{k_m}(x-z) \times \sum_{j=1}^{3} \frac{i}{\omega\varepsilon_m} |B| e_j \times \partial_j H^i(z) =& \nabla \times \nabla\Gamma_{k_m}(x-z) \times \left(\frac{i}{\omega\varepsilon_m} |B| \nabla_z \times H^i(z) \right) \\
=& - \nabla \times \nabla\Gamma_{k_m}(x-z) \times |B| E^i(z) \\
=& - \nabla \times \nabla \times G(x,z) |B| E^i(z) \\
=& \omega^2 \mu_m G(x,z) |B| E^i(z).
\end{aligned}$$

Hence, we can deduce that

$$\nabla \times \nabla\Gamma_{k_m}(x-z) \times \sum_{j=1}^{3} \mathrm{M}_{0,j}^e = \omega^2 \mu_m G(x,z) \left(|B| E^i(z + \int_B \nabla \mathcal{S}_B[\boldsymbol{\nu} \cdot H^i(z)] \right) + O(\delta).$$

A similar computation yields

$$\begin{aligned}
&\mu_m \nabla\Gamma_{k_m}(x-z) \times \sum_{j=1}^{3} \mathrm{M}_{0,j}^h = \\
&\qquad i\omega\mu_m \nabla\Gamma_{k_m}(x-z) \times \left(|B| H^i(z) + \int_B \nabla \mathcal{S}_B (\lambda_\mu I - \mathcal{K}_B^*)^{-1} [\nu \cdot H^i(z)] \right) + O(\delta),
\end{aligned}$$

and therefore,

$$\mu_m \nabla\Gamma_{k_m}(x-z) \times \sum_{j=1}^{3} \mathrm{M}_{0,j}^h = \\ i\omega \frac{\mu_m}{\varepsilon_m} \nabla \times G(x-z)\Big(|B| H^i(z) + \int_B \nabla \mathcal{S}_B (\lambda_\mu I - \mathcal{K}_B^*)^{-1} [\nu \cdot H^i(z)] \Big) + O(\delta).$$

Moreover, Lemma 4.5.6 gives

$$\nabla \times \nabla\Gamma_{k_m}(x-z) \times \mathrm{M}_{0,0}^e = \delta \frac{\mu_m}{\varepsilon_m} (k_m^2 - k_c^2) G(x,z) \int_B \nabla(u^e + v^e) + O(\delta^2)$$
$$\mu_m \nabla\Gamma_{k_m}(x-z) \times \mathrm{M}_{0,0}^h = \delta \frac{(k_m^2 - k_c^2)}{\varepsilon_m} \nabla \times G(x,z) \int_B \nabla(u^h + v^h) + O(\delta^2).$$

Combining the previous asymptotic expansions we arrive at

$$E(x) - E^i(x) = \delta^3 \frac{1}{\varepsilon_m} G(x,z) \Big(\mu_m (k_m^2 - k_c^2) \int_B \nabla(u^e + v^e) \\ + (\mu_c - \mu_m) k_m^2 \int_B \nabla u^e \quad + k_m^2 \int_B \nabla \mathcal{S}_B (\lambda_\varepsilon I - \mathcal{K}_B^*)^{-1} [\nu \cdot E^i(z)] \Big) \\ + \delta^3 \frac{1}{\varepsilon_m} \nabla \times G(x,z) \Big((k_m^2 - k_c^2) \int_B \nabla(u^h + v^h) + \omega^2 \mu_m (\varepsilon_c - \varepsilon_m) \int_B \nabla u^h \\ + i\omega\mu_m \int_B \nabla \mathcal{S}_B (\lambda_\mu I - \mathcal{K}_B^*)^{-1} [\nu \cdot H^i(z)] \Big) + O(\delta^4). \quad (4.5.33)$$

The proof is then complete. □

We shall analyze further (4.5.33). Recall that, from the proof of Lemma 4.5.6, we have

$$\int_B \nabla(u^e + v^e) dx = \frac{\varepsilon_m}{\varepsilon_c - \varepsilon_m} \int_{\partial B} \tilde{y} (\lambda_\varepsilon I - \mathcal{K}_B^*)^{-1} \Big[\frac{\partial u^e}{\partial \nu} \Big|_- \Big] d\sigma(x)$$

and

$$\int_B \nabla(u^h + v^h) dx = \frac{\mu_m}{\mu_c - \mu_m} \int_{\partial B} \tilde{y} (\lambda_\mu I - \mathcal{K}_B^*)^{-1} \Big[\frac{\partial u^h}{\partial \nu} \Big|_- \Big] d\sigma(x).$$

Noticing that

$$\mu_m (k_m^2 - k_c^2) = (\mu_c - \mu_m) k_m^2 \frac{\mu_m \varepsilon_m - \mu_c \varepsilon_c}{(\mu_c - \mu_m)(\varepsilon_c - \varepsilon_m)},$$

we get

$$\mu_m (k_m^2 - k_c^2) \int_B \nabla(u^e + v^e) + (\mu_c - \mu_m) k_m^2 \int_B \nabla u^e = \\ (\mu_c - \mu_m) k_m^2 \left(\frac{\mu_m \varepsilon_m - \mu_c \varepsilon_c}{(\mu_c - \mu_m)(\varepsilon_c - \varepsilon_m)} \int_{\partial B} \tilde{y} (\lambda_\varepsilon I - \mathcal{K}_B^*)^{-1} \Big[\frac{\partial u^e}{\partial \nu} \Big|_- \Big] + \int_{\partial B} \tilde{y} \frac{\partial u^e}{\partial \nu} \Big|_- \right).$$

Moreover, for any f, we have

$$\frac{\mu_m\varepsilon_m - \mu_c\varepsilon_c}{(\mu_c-\mu_m)(\varepsilon_c-\varepsilon_m)}\left(\lambda_\varepsilon I - \mathcal{K}_B^*\right)^{-1}[f] + f = \\ \frac{\mu_m\varepsilon_m - \mu_c\varepsilon_c}{(\mu_c-\mu_m)(\varepsilon_c-\varepsilon_m)}\left(\lambda_\varepsilon I - \mathcal{K}_B^*\right)^{-1}[f] + \left(\lambda_\varepsilon I - \mathcal{K}^*\right)\left(\lambda_\varepsilon I - \mathcal{K}_B^*\right)^{-1}[f].$$

so that

$$\frac{\mu_m\varepsilon_m - \mu_c\varepsilon_c}{(\mu_c-\mu_m)(\varepsilon_c-\varepsilon_m)}\left(\lambda_\varepsilon I - \mathcal{K}_B^*\right)^{-1}[f] + f = (\lambda_\mu I + \mathcal{K}_B^*)(\lambda_\varepsilon I - \mathcal{K}_B^*)^{-1}[f]$$

We can then write

$$\mu_m(k_m^2-k_c^2)\int_B \nabla(u^e+v^e) + (\mu_c-\mu_m)k_m^2\int_B \nabla u^e = \\ -(\mu_c-\mu_m)k_m^2\int_{\partial B}\tilde{y}(\lambda_\mu I + \mathcal{K}_B^*)(\lambda_\varepsilon I - \mathcal{K}_B^*)^{-1}\Big[\frac{\partial u^e}{\partial \nu}\Big|_-\Big].$$

Recall that by definition,

$$\frac{\partial u^e}{\partial \boldsymbol{\nu}}\Big|_- = \boldsymbol{\nu}\cdot\nabla\times\mathcal{A}_B[\tilde{\boldsymbol{\phi}}_{0,0}].$$

Then, by using Lemma 4.5.5, we obtain

$$\boldsymbol{\nu}\cdot\nabla\times\mathcal{A}_B[\tilde{\boldsymbol{\phi}}_{0,0}] = \frac{1}{\mu_c}\boldsymbol{\nu}\cdot E^i(z) + \frac{\mu_m}{\mu_c^2-\mu_m\mu_c}\boldsymbol{\nu}\cdot\nabla\mathcal{S}_B\left(\lambda_\mu I + \mathcal{K}_B^*\right)^{-1}[\nu\cdot E^i(z)]\Big|_-,$$

which together with the jump relations for the normal derivative of the scalar layer potential yields

$$\mu_m(k_m^2-k_c^2)\int_B \nabla(u^e+v^e) + (\mu_c-\mu_m)k_m^2\int_B \nabla u^e = \\ -\frac{\mu_c-\mu_m}{\mu_c}k_m^2\int_{.B}\tilde{y}(\lambda_\mu I + \mathcal{K}_B^*)(\lambda_\varepsilon I - \mathcal{K}_B^*)^{-1}[\nu\cdot E^i(z)] \\ -\frac{\mu_m}{\mu_c}k_m^2\int_{\partial B}\tilde{y}(\lambda_\mu I + \mathcal{K}_B^*)(\lambda_\varepsilon I - \mathcal{K}_B^*)^{-1}(-\frac{1}{2}I + \mathcal{K}_B^*)(\lambda_\mu I + \mathcal{K}_B^*)^{-1}[\nu\cdot E^i(z)].$$

If we set $\lambda_\varepsilon = -\frac{1}{2} + \frac{\varepsilon_c}{\varepsilon_c-\varepsilon_m}$, then we can write

$$-\frac{\mu_m}{\mu_c}\left(\lambda_\varepsilon I - \mathcal{K}_B^*\right)^{-1}\left(-\frac{1}{2}I + \mathcal{K}_B^*\right)[\boldsymbol{\nu}\cdot E^i(z)] = -\frac{\mu_m}{\mu_c}\left(\lambda_\varepsilon I - \mathcal{K}_B^*\right)^{-1}\left(-\frac{\varepsilon_c}{\varepsilon_c-\varepsilon_m}I + \mathcal{K}_B^*\right)[\boldsymbol{\nu}\cdot E^i(z)],$$

or equivalently,

$$-\frac{\mu_m}{\mu_c}\left(\lambda_\varepsilon I-\mathcal{K}_B^*\right)^{-1}\left(-\frac{1}{2}I+\mathcal{K}_B^*\right)[\boldsymbol{\nu}\cdot E^i(z)]= \\ -\frac{\mu_m}{\mu_c}\boldsymbol{\nu}\cdot E^i(z)+\frac{\varepsilon_c\mu_m}{\mu_c(\varepsilon_c-\varepsilon_m)}\left(\lambda_\varepsilon I-\mathcal{K}_B^*\right)^{-1}[\boldsymbol{\nu}\cdot E^i(z)].$$

Then, since

$$-\frac{\mu_c-\mu_m}{\mu_c}\left(\lambda_\mu I+\mathcal{K}_B^*\right)\left(\lambda_\varepsilon I-\mathcal{K}_B^*\right)^{-1}[\boldsymbol{\nu}\cdot E^i(z)]= \\ \frac{\mu_c-\mu_m}{\mu_c}\boldsymbol{\nu}\cdot E^i(z)-\frac{\mu_c-\mu_m}{\mu_c}(\lambda_\mu-\lambda_\varepsilon)\left(\lambda_\varepsilon I-\mathcal{K}_B^*\right)^{-1}[\boldsymbol{\nu}\cdot E^i(z)],$$

we can write

$$-\frac{\mu_c-\mu_m}{\mu_c}\left(\lambda_\mu I+\mathcal{K}_B^*\right)\left(\lambda_\varepsilon I-\mathcal{K}_B^*\right)^{-1}[\boldsymbol{\nu}\cdot E^i(z)] \\ -\frac{\mu_m}{\mu_c}\left(\lambda_\varepsilon I-\mathcal{K}_B^*\right)^{-1}\left(-\frac{1}{2}I+\mathcal{K}_B^*\right)[\boldsymbol{\nu}\cdot E^i(z)] \\ =\boldsymbol{\nu}\cdot E^i(z)+\left(\frac{\varepsilon_c\mu_m}{\mu_c(\varepsilon_c-\varepsilon_m)}-\frac{\mu_c-\mu_m}{\mu_c}(\lambda_\mu-\lambda_\varepsilon)\right)\left(\lambda_\varepsilon I-\mathcal{K}_B^*\right)^{-1}[\boldsymbol{\nu}\cdot E^i(z)].$$

A direct computation gives

$$\frac{\varepsilon_c\mu_m}{\mu_c(\varepsilon_c-\varepsilon_m)}-\frac{\mu_c-\mu_m}{\mu_c}(\lambda_\mu-\lambda_\varepsilon)=\frac{1}{2}+\lambda_\varepsilon,$$

and therefore,

$$\mu_m(k_m^2-k_c^2)\int_B\nabla(u^e+v^e)+(\mu_c-\mu_m)k_m^2\int_B\nabla u^e= \\ k_m^2\int_{\partial B}\tilde{y}\boldsymbol{\nu}\cdot E^i(z)d\sigma(\tilde{y})-k_m^2\left(\frac{1}{2}+\lambda_\varepsilon\right)\int_{\partial B}\tilde{y}\left(\lambda_\varepsilon I-\mathcal{K}_B^*\right)^{-1}[\boldsymbol{\nu}\cdot E^i(z)]d\sigma(\tilde{y}).$$

A similar computation yields

$$(k_m^2-k_c^2)\int_B\nabla(u^h+v^h)+\omega^2\mu_m(\varepsilon_c-\varepsilon_m)\int_B\nabla u^h= \\ i\omega\mu_m\int_{\partial B}\tilde{y}\boldsymbol{\nu}\cdot H^i(z)d\sigma(\tilde{y})-i\omega\mu_m\left(\frac{1}{2}+\lambda_\mu\right)\int_{\partial B}\tilde{y}\left(\lambda_\varepsilon I-\mathcal{K}_B^*\right)^{-1}[\boldsymbol{\nu}\cdot H^i(z)]d\sigma(\tilde{y}).$$

Now it remains to compute the last term in (4.5.33) which is

$$k_m^2 \int_B \nabla \mathcal{S}_B(\lambda_\varepsilon I - \mathcal{K}_B^*)^{-1}[\nu \cdot E^i(z)]d\tilde{y} = k_m^2 \int_{\partial B} \tilde{y} \frac{\partial}{\partial \boldsymbol{\nu}} \mathcal{S}_B\Big|_- (\lambda_\varepsilon I - \mathcal{K}_B^*)^{-1} [\boldsymbol{\nu} \cdot E^i(z)]d\sigma(\tilde{y}).$$

Writing that $\lambda_\varepsilon = \dfrac{1}{2} + \dfrac{\varepsilon_m}{\varepsilon_c + \varepsilon_m}$ together with the fact that $\dfrac{\partial}{\partial \boldsymbol{\nu}} \mathcal{S}_B\Big|_- = \left(-\dfrac{1}{2} I + \mathcal{K}_B^*\right)$, we obtain

$$\frac{\partial}{\partial \boldsymbol{\nu}} \mathcal{S}_B \left(\lambda_\varepsilon I - \mathcal{K}_B^*\right)^{-1} [\boldsymbol{\nu} \cdot E^i(z)] = -\boldsymbol{\nu} \cdot E^i(z) + \frac{\varepsilon_m}{\varepsilon_c + \varepsilon_m} \left(\lambda_\varepsilon I - \mathcal{K}_B^*\right)^{-1} [\boldsymbol{\nu} \cdot E^i(z)].$$

Hence,

$$\begin{aligned} k_m^2 \int_B \nabla \mathcal{S}_B(\lambda_\varepsilon I - \mathcal{K}_B^*)^{-1}[\nu \cdot E^i(z)]d\tilde{y} = -k_m^2 \int_{\partial B} \tilde{y} \boldsymbol{\nu} \cdot E^i(z)]d\sigma(\tilde{y}) \\ + k_m^2 \left(\lambda_\varepsilon - \frac{1}{2}\right) \int_{\partial B} \tilde{y} \left(\lambda_\varepsilon I - \mathcal{K}_B^*\right)^{-1} [\boldsymbol{\nu} \cdot E^i(z)]d\sigma(\tilde{y}). \end{aligned}$$

Similarly, we have

$$\begin{aligned} i\omega\mu_m \int_B \nabla \mathcal{S}_B(\lambda_\mu I - \mathcal{K}_B^*)^{-1}[\nu \cdot H^i(z)] = i\omega\mu_m \int_{\partial B} \tilde{y} \boldsymbol{\nu} \cdot H^i(z)d\sigma(\tilde{y}) \\ + i\omega\mu_m \left(\lambda_\mu - \frac{1}{2}\right) \int_{\partial B} \tilde{y} \left(\lambda_\varepsilon I - \mathcal{K}_B^*\right)^{-1} [\boldsymbol{\nu} \cdot H^i(z)]d\sigma(\tilde{y}). \end{aligned}$$

Finally, we arrive at

$$\begin{aligned} E(x) - E^i(x) = -\delta^3 \omega^2 \mu_m G(x,z) \int_{.B} \tilde{y} (\lambda_\varepsilon I - \mathcal{K}_B^*)^{-1}[\nu \cdot E^i(z)] \\ - \delta^3 \frac{i\omega\mu_m}{\varepsilon_m} \nabla \times G(x,z) \int_{.B} \tilde{y} (\lambda_\mu I - \mathcal{K}_B^*)^{-1}[\nu \cdot H^i(z)] + O(\delta^4). \end{aligned}$$

When a plasmonic resonance occurs, the term $\lambda_\varepsilon = \frac{\varepsilon_c + \varepsilon_m}{2(\varepsilon_c - \varepsilon_m)}$ can have a real part that is lower than $\frac{1}{2}$, and become close to an eigenvalue of the operator $\mathcal{K}_B^*$.

Using Lemma 4.5.4 we can easily see that each of the potentials $\boldsymbol{\phi}_{\beta,n}$ and $\boldsymbol{\psi}_{\beta,n}$ are controlled in norm by powers of $\frac{1}{d_\sigma}$, where d_σ is the distance of λ_ε to the spectrum $\sigma(\mathcal{M}_B) = -\sigma(\mathcal{K}_B^*) \setminus \{-1/2\}$. So the asymptotic development given by Theorem 4.5.8 is valid when $\delta/d_\sigma << 1$, which ensures that the reminder of the asymptotic expansion is still small compared to the first-order term.

The following results are our main results in this chapter.

Theorem 4.5.9. *Let* $d_\sigma := \min\{\text{dist}\,(\lambda_\varepsilon, \sigma(\mathcal{K}_B^*))\,, \text{dist}\,(\lambda_\mu, \sigma(\mathcal{K}_B^*))\}$. *The following uniform far-field expansion holds:*

$$\begin{aligned} E(x) - E^i(x) &= -\delta^3\omega^2\mu_m G(x,z)M^e E^i(z) - \delta^3\frac{i\omega\mu_m}{\varepsilon_m}\nabla\times G(x,z)M^h H^i(z) \\ &\quad +O(\frac{\delta^4}{d_\sigma}), \end{aligned} \tag{4.5.34}$$

where M^e *and* M^h *are defined by (4.5.31).*

The above theorem can be generalized to the case of multiple particles.

Theorem 4.5.10. *Let* M^e *and* M^h *be the polarization tensors associated with* $D_1 \cup D_2$ *and* λ_ε *and* λ_μ, *respectively. Let* $d_\sigma := \min\{\text{dist}(\lambda_\varepsilon, \sigma(\mathbb{K}_B^*)), \text{dist}(\lambda_\mu, \sigma(\mathbb{K}_B^*))\}$. *Then the following uniform far-field expansion holds:*

$$\begin{aligned} E(x) - E^i(x) &= -\delta^3\omega^2\mu_m G(x,z)M^e E^i(z) - \delta^3\frac{i\omega\mu_m}{\varepsilon_m}\nabla\times G(x,z)M^h H^i(z) \\ &\quad +O(\frac{\delta^4}{d_\sigma}), \end{aligned} \tag{4.5.35}$$

where M^e *and* M^h *are defined by (4.3.4) with* $\lambda = \lambda_\varepsilon$ *and* $\lambda = \lambda_\mu$, *respectively.*

Theorems 4.5.9 and 4.5.10 show the uniform validity with respect to the nanoparticle's bulk electron relaxation rate of the quasi-static approximation of the Maxwell's equations.

Finally, two more remarks are in order. First, in view of Theorems 4.5.9 and 4.5.10 and the blow up of the polarization tensors, it is clear that at plasmonic resonances the scattered electric field is enhanced. Secondly, from the representation formula (4.5.2) for the electric field in D and the estimates of the densities, it can be seen that the electric field inside the particle is enhanced as well and therefore, the absorbed energy, given by $\varepsilon'' \int_D |E|^2(y)\,dy$, is enhanced at dielectric plasmonic resonances. Note that the scattering enhancement when the particles are illuminated at their plasmonic resonances can be used for nano-resolved imaging from the far-field data while the absorption enhancement for thermotherapy applications as well as for photoacoustic imaging to remotely measure and control the local temperature within a medium [132].

4.6 Numerical illustrations

We illustrate the plasmon phenomenon numerically by computing the polarization tensor M^e for some different two-dimensional shapes. We use the values for the

parameters given in section 4.6. The wavelength of the incoming plane wave c/ω, where $c = 3.10^8$ is the speed of light, belongs to $[80, 1100].10^{-9}\, m$. Figures 4.6.1 and 4.6.2 show respectively the values of real and imaginary parts of ε_c and λ_ε as a function of the wavelength.

Then we compute the matrix M^e defined by (4.2.16) with $\lambda = \lambda_\varepsilon$. We plot the value of its norm with respect to the incoming wavelength. Figure 4.6.3 shows that if the shape B is a disk, then one has a resonant peak. This peak corresponds to $\lambda_\varepsilon = 0$. Figure 4.6.4 shows that for an ellipse, one can observe two resonant frequencies, one corresponding to each axis. This was experimentally observed in [55] for elongated particles. The two peaks correspond to $\lambda_\varepsilon = (a-b)/(a+b) \approx 0.33$ and $\lambda_\varepsilon = ((a-b)/(a+b))^2 \approx 0.11$, where $a = 1, b = 1/2$ are the semi-axis lengths of the ellipse. Figure 4.6.5 gives the norm of the polarization tensor for a star-shaped particle. One can observe that there are many resonant frequencies. This observation is also in agreement with the experimental results published in [69].

Finally, it is shown in Figure 4.6.7 that when two disks are close to each other, a strong interaction occurs and the plasmonic resonance frequencies are close to those of an equivalent ellipse.

4.7 Concluding remarks

In this chapter, we have provided a mathematical framework for localized plasmon resonance of nanoparticles. We have derived a uniform small volume expansion for the solution to Maxwell's equations in the presence of nanoparticles excited at their plasmonic resonances. We have presented a variety of numerical results to illustrate our main findings. As the particle size increases and moves away from the quasi-static approximation, high-order polarization tensors [27] should be included in order to compute the plasmonic resonances, which become size-dependent [76]. This would be the subject of a forthcoming work. We hope to be able to compute size-dependant plasmonic frequency for a given particle without solving the full 3D Maxwell system. Our approach in this chapter opens also a door for a numerical and mathematical framework for optimal shape design of resonant nanoparticles and their super resolved imaging [25].

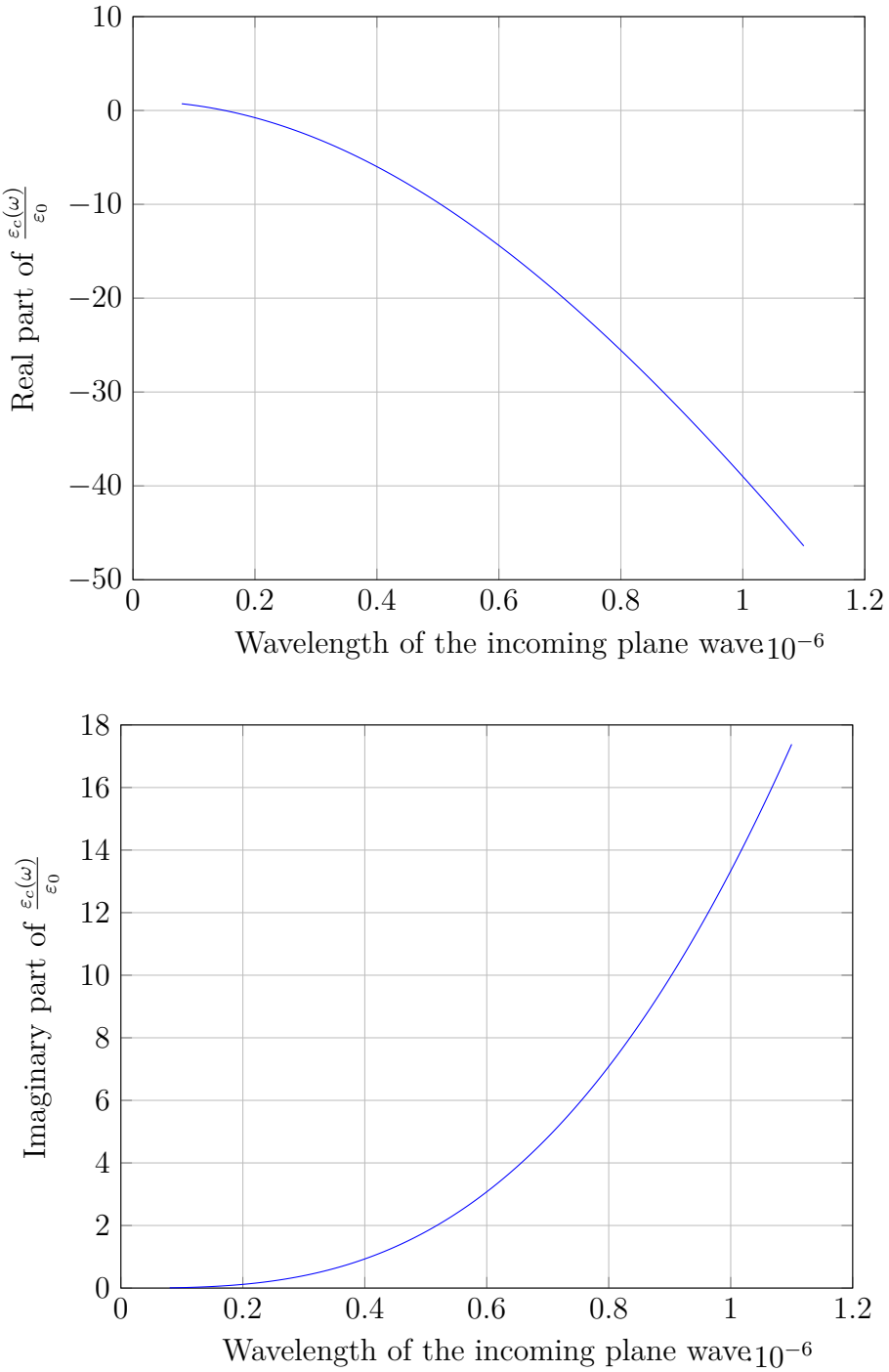

Figure 4.6.1 Values of the parameter $\varepsilon(\omega)$.

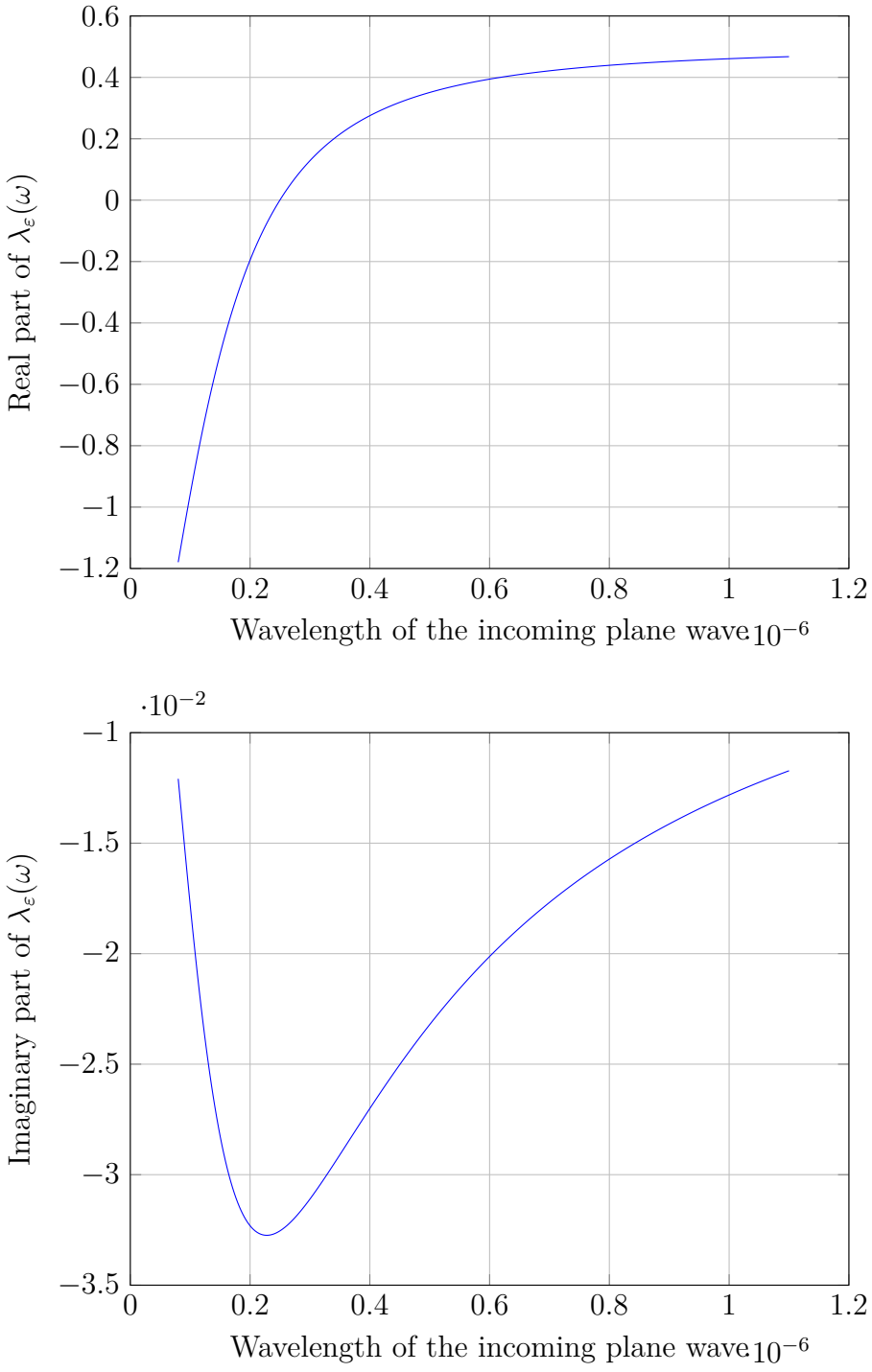

Figure 4.6.2 Values of the parameter $\lambda_\varepsilon(\omega)$.

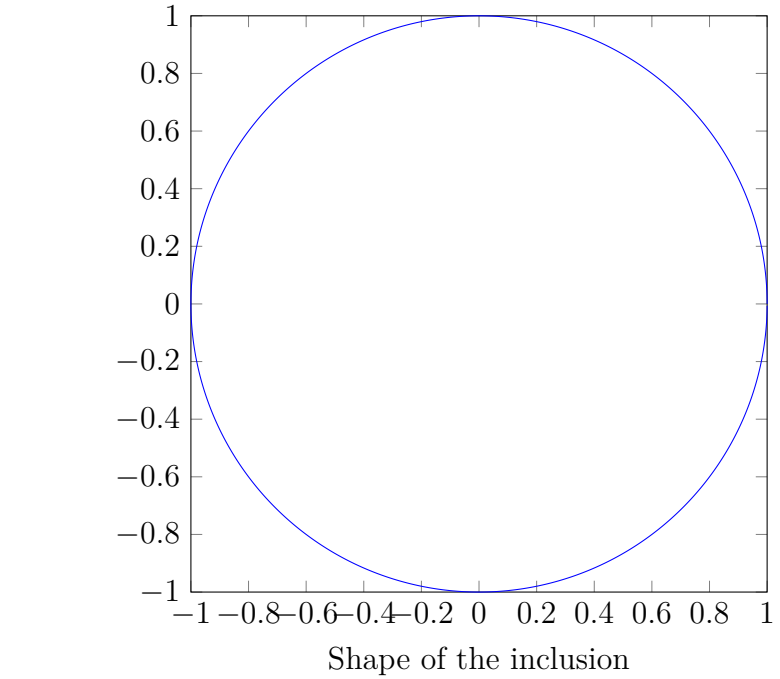

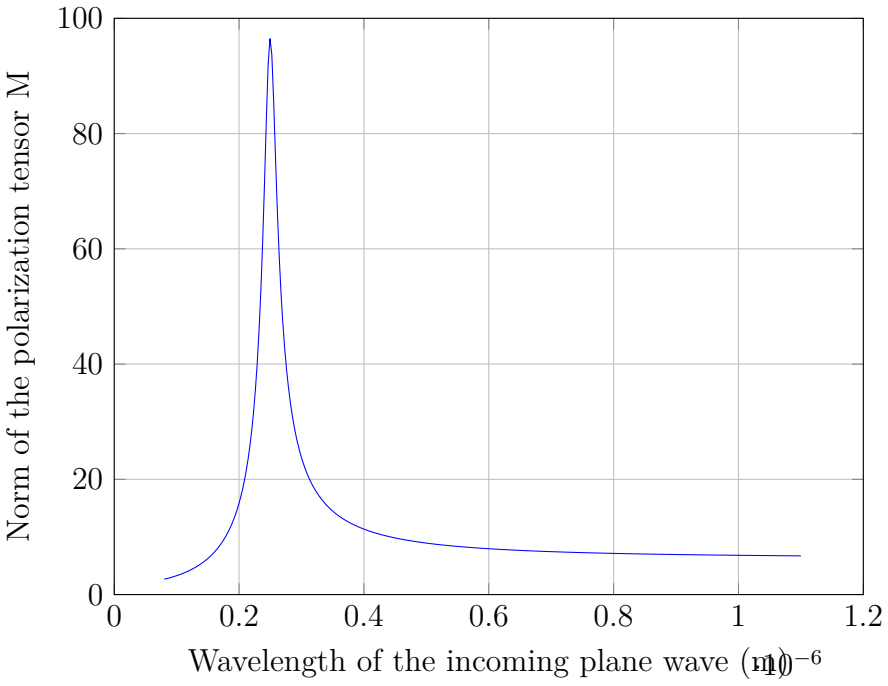

Figure 4.6.3 Norm of the polarization tensor for a circular inclusion.

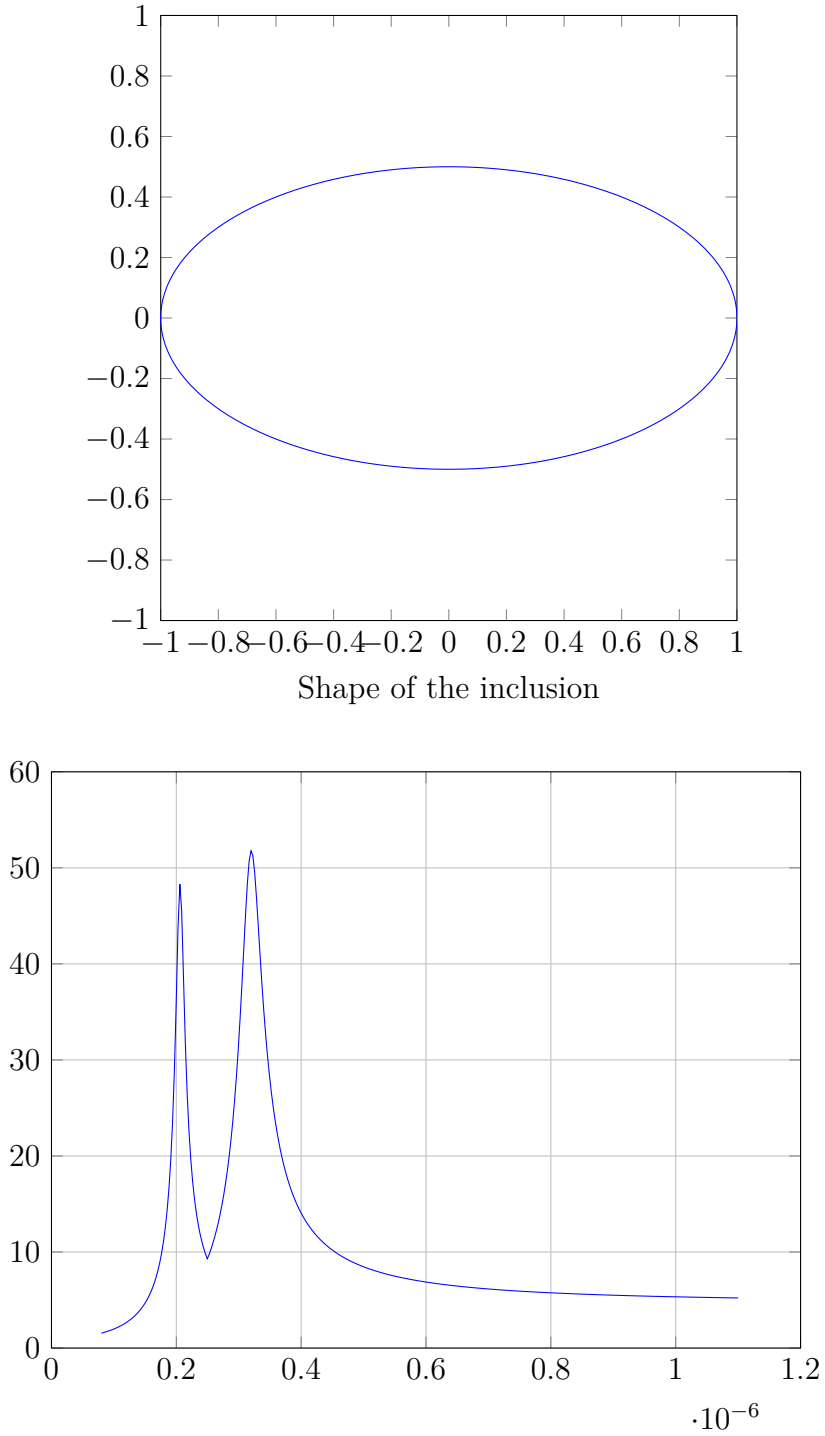

Figure 4.6.4 Norm of the polarization tensor for an elliptic inclusion.

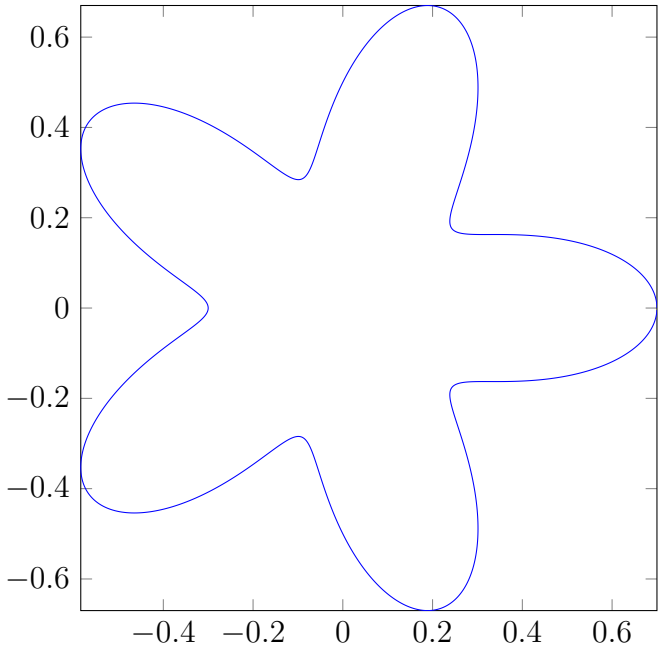

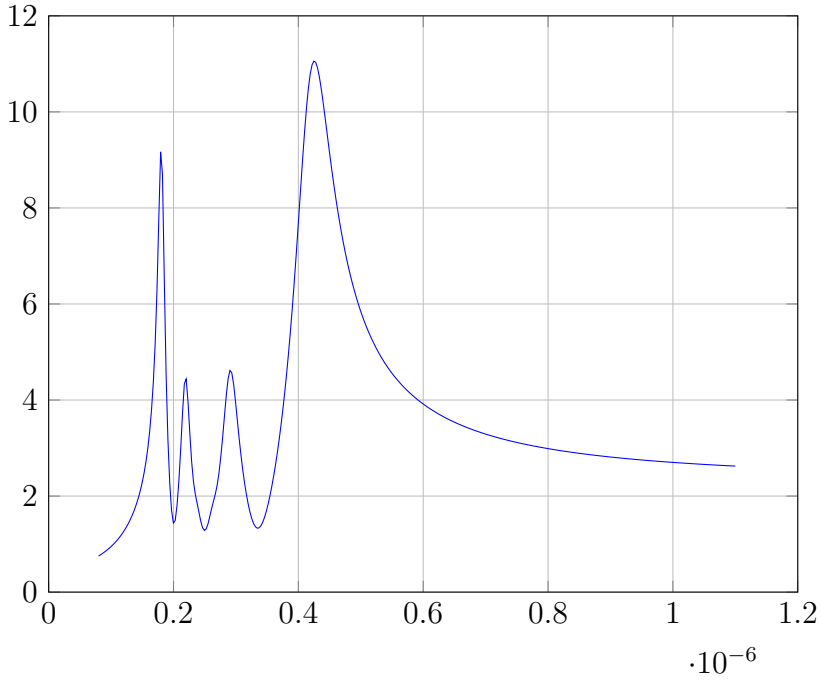

Figure 4.6.5 Norm of the polarization tensor for a flower-shaped inclusion.

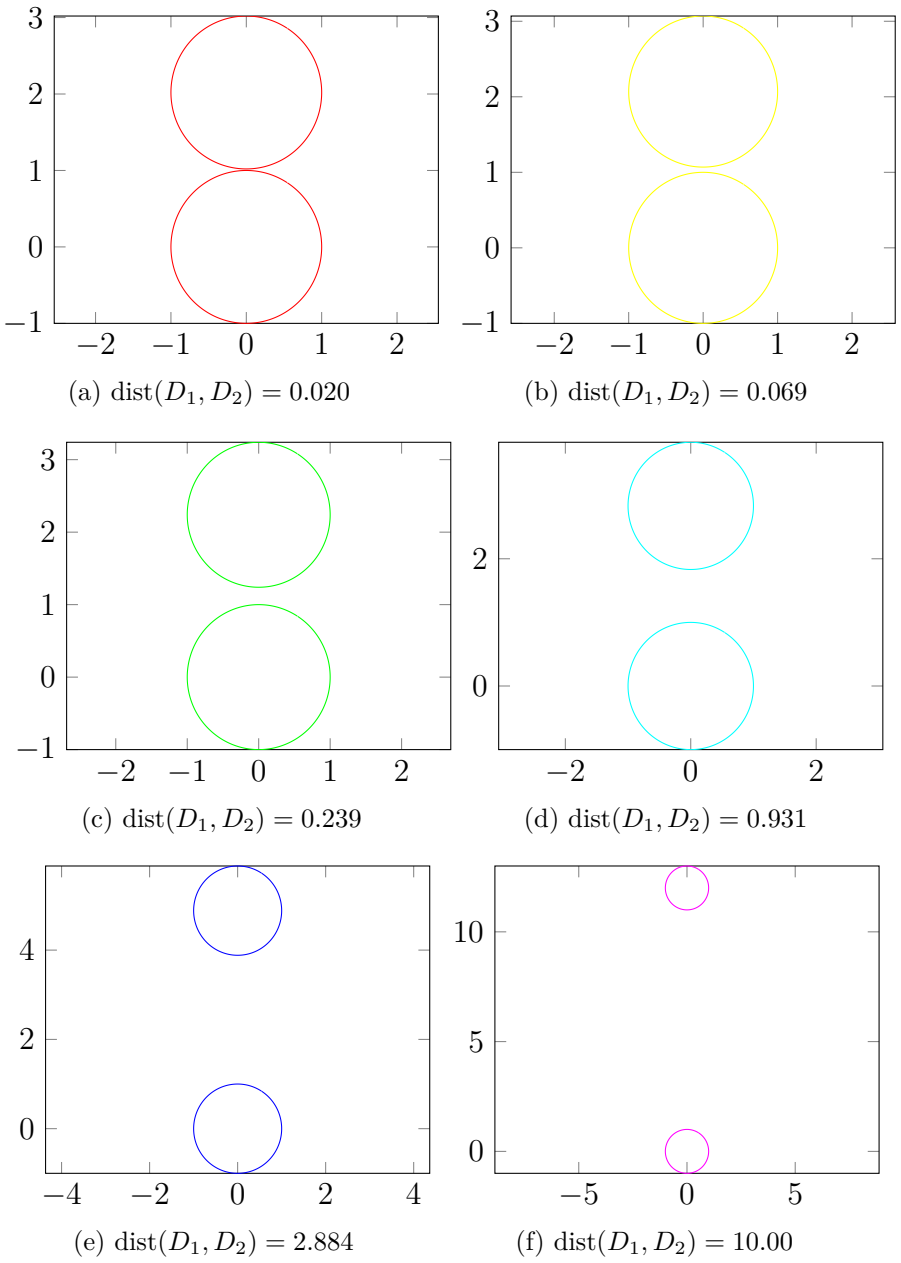

(a) $\mathrm{dist}(D_1, D_2) = 0.020$ (b) $\mathrm{dist}(D_1, D_2) = 0.069$

(c) $\mathrm{dist}(D_1, D_2) = 0.239$ (d) $\mathrm{dist}(D_1, D_2) = 0.931$

(e) $\mathrm{dist}(D_1, D_2) = 2.884$ (f) $\mathrm{dist}(D_1, D_2) = 10.00$

Figure 4.6.6 Different couplings between two disks.

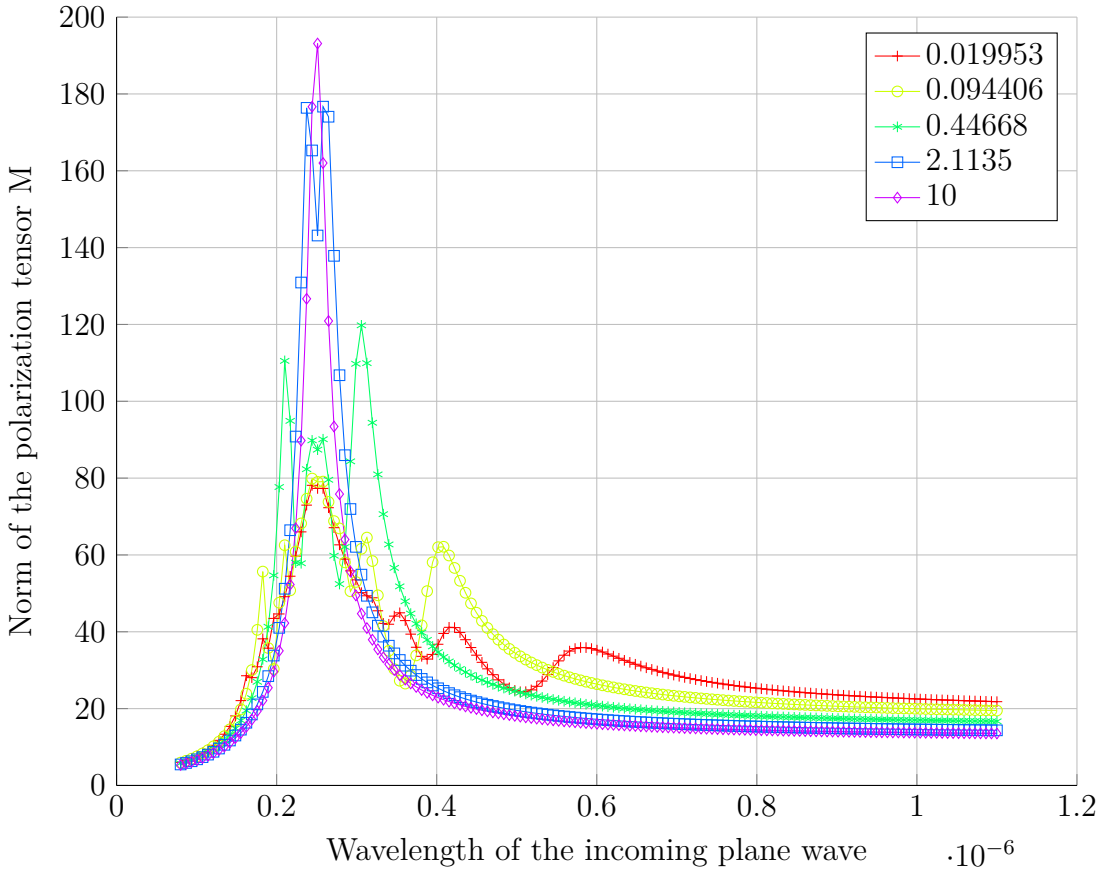

Figure 4.6.7 Norm of the polarization tensor for multiple disks for various separating distances.

Chapter 5

Second-harmonic generation

Contents

5.1 Introduction

Second-harmonic microscopy is a promising imaging technique based on a phenomenon called second-harmonic generation (SHG) or frequency-doubling. SHG requires an intense laser beam passing through a material with non vanishing second-order susceptibility [68]. A second electromagnetic field is emitted at exactly twice the frequency of the incoming field. Roughly speaking,

$$\mathbf{E}_{2\omega} \sim \mathbf{E}_{\omega}\chi^{(2)}\mathbf{E}_{\omega}, \tag{5.1.1}$$

where $\chi^{(2)}$ is the second-order susceptibility tensor. A condition for an object to have non vanishing second-order susceptibility tensor is to have a noncentrosymmetric structure. Thus SHG only occurs in a few types of physical bodies: crystals [102], interfaces like cell membranes [43, 70, 105], nanoparticle [75, 138], and natural structures like collagen or neurons [41, 100]. This makes SHG a very good contrast mechanism for microscopy, and has been used in biomedical imaging. SHG signals have a very low intensity because the coefficients in $\chi^{(2)}$ have a typical size of picometer $/V$ [48]. This is the reason why a high intensity laser beam is required in order to produce a second-harmonic field that is large enough to be detected by the microscope. Second-harmonic microscopy has several advantages. Among others, the fact that the technique does not involve excitation of molecules so it is not subject to phototoxicity effect or photobleaching. The excitation uses near infrared light which has a very good penetration capacity, and a lot of natural structures (like collagen for instance) exhibit strong SHG properties, so there is no need for probes or dyes in certain cases. SHG images can be collected simultaneously with standard microscopy and two-photon-excitation-fluorescence microscopy for membrane imaging (see, for instance, [43]).

The coherent nature of the SHG signal allows us to use nonlinear holography for measuring the complex two-dimensional (amplitude and phase) SHG signal [73, 116]. The idea is quite similar to conventional linear holography [52, 124]. A frequency doubling crystal is used to produce a coherent reference beam at the second-harmonic frequency, which allows to measure the phase of the one emitted from the reflector [72].

On the other hand, since only the dye/membrane produces the second-harmonic signal, SHG microscopy allows a precise imaging of the dye/membrane, clear from any scattering from the surrounding medium, contrary to the fundamental frequency image, where the signal measured is produced by both the reflector and the medium. As it will be shown in this chapter, this is the main feature which makes second-harmonic imaging very efficient when it is not possible to obtain an image of the medium without

the dye in order to filter the medium noise. In practical situations [72], it is not possible to get an image without the reflector. The main purpose of this work is to justify that the second-harmonic generation acts in such situations as a powerful contrast imaging approach.

More precisely, we study the case of a nanoparticle with non vanishing second-order susceptibility tensor $\chi^{(2)}$ embedded in a randomly heterogeneous medium illuminated by an incoming electromagnetic field at a fixed frequency ω. We give asymptotic formulas for the electromagnetic field diffracted by the particle and the medium at the fundamental frequency and at the second-harmonic frequency. Then we use a backpropagation algorithm in order to recover the position of the particle from boundary measurements of the fields. We study the images obtained by backpropagation both in terms of resolution and stability. In particular, we elucidate that the second-harmonic field provides a more stable image than that from fundamental frequency imaging, with respect to medium noise, and that the signal-to-noise ratio for the second-harmonic image does not depend neither on $\chi^{(2)}$ nor on the volume of the particle. The aforementioned are the main findings of this study.

The chapter is organized as follows. In section 5.2 we formulate the problem of SHG. In section 5.3, asymptotic expansions in terms of the size of the small reflector (the nanoparticle) of the scattered field at the fundamental frequency and the second-harmonic generated field are derived. In section 5.4, we introduce backpropagation imaging functions for localizing the point reflector using the scattered field at the fundamental frequency as well as the second-harmonic field. In section 5.5, we perform a stability and resolution analysis of the backpropagation imaging functions. We show that the medium noise affects the stability and resolution of the imaging functions in different ways. We prove that using the second-harmonic field renders enhanced stability for the reconstructed image. Our main findings are delineated by a few numerical examples in section 5.6. The chapter ends with a short discussion.

5.2 Problem formulation

In this chapter we consider a small electric reflector Ω_r with a non vanishing second-order susceptibility tensor χ embedded in a randomly heterogeneous medium. The reflector is illuminated by a plane electromagnetic wave. We assume that the plane wave is polarized in the transverse magnetic direction and the second-harmonic field is in the transverse electric mode. The polarization of the second-harmonic field is given by symmetry properties of the second-order susceptibility tensor. This transverse

magnetic–transverse electric polarization mode is known to be supported by a large class of optical nonlinear materials [127]. We choose this polarization mode so that the full Maxwell equations reduce to a Helmholtz equation in $\mathbb{R}^2$ and therefore, a two-dimensional study of the second harmonic generation with scalar fields would be possible. The results would be pretty similar in a general three-dimensional case for the full Maxwell equations, but the computations would be much elusive.

In order to describe the mathematical model, we assume that the medium has random fluctuations described by a given random process μ with Gaussian statistics and mean zero. Furthermore, we assume that μ has a small amplitude and is compactly supported in $\mathbb{R}^2$ and let $\Omega_\mu := \text{supp}(\mu)$. We refer to μ as the medium noise. We also assume that the refractive index of the background homogeneous medium $\mathbb{R}^2 \setminus \overline{\Omega_\mu}$ is 1. The medium is illuminated by a plane wave at frequency $\omega > 0$, intensity $U_I > 0$, and direction $\theta \in \mathbb{S}^1$:

$$U_0(x) = U_I e^{i\omega\theta\cdot x}, \tag{5.2.1}$$

with $\mathbb{S}^1$ being the unit circle.

The small-volume reflector Ω_r is in Ω_μ and has a refractive index given by

$$[\sigma_r - 1]\mathbf{1}_{\Omega_r}(x), \tag{5.2.2}$$

where σ_r is the refractive index contrast of the reflector, Ω_r is compactly supported in Ω_μ with volume $|\Omega_r|$, and $\mathbf{1}_{\Omega_r}$ is the characteristic function of Ω_r. The squared refractive index $n(x)$ in the whole space has then the following form:

$$\frac{1}{n(x)} = (1 + \mu(x) + [\sigma_r - 1]\mathbf{1}_{\Omega_r}(x)). \tag{5.2.3}$$

The scattered field u_s generated by the plane wave satisfies the Helmholtz equation:

$$\nabla \cdot (([\sigma_r - 1]\mathbf{1}_{\Omega_r} + \mu + 1)\nabla(u_s + U_0)) + \omega^2(u_s + U_0) = 0 \quad \text{in } \mathbb{R}^2, \tag{5.2.4}$$

together with the Sommerfeld radiation condition

$$\lim_{|x|\to\infty} \sqrt{|x|}(\frac{\partial u_s}{\partial |x|} - i\omega u_s) = 0. \tag{5.2.5}$$

The point reflector also scatters a second field v at frequency 2ω. Since

$$n(x) = \frac{(2\omega)^2}{[\sigma_r - 1]\mathbf{1}_{\Omega_r} + 1}(1 - \frac{\mu}{[\sigma_r - 1]\mathbf{1}_{\Omega_r} + 1}) + O(||\mu||^2_{L^\infty(\Omega_\mu)}),$$

the field v satisfies, up to $O(||\mu||^2_{L^\infty(\Omega_\mu)})$, the following Helmholtz equation [39, 68, 129]:

$$\left(\Delta + \frac{(2\omega)^2}{[\sigma_r - 1]\mathbf{1}_{\Omega_r} + 1}(1 - \frac{\mu}{[\sigma_r - 1]\mathbf{1}_{\Omega_r} + 1})\right) v = \sum_{k,l=1,2} \chi_{kl}\partial_{x_k} U \partial_{x_l} U \mathbf{1}_{\Omega_r} \quad \text{in } \mathbb{R}^2, \tag{5.2.6}$$

subject to the Sommerfeld radiation condition

$$\lim_{|x|\to\infty} \sqrt{|x|}\left(\frac{\partial v}{\partial |x|} - 2i\omega v\right) = 0, \tag{5.2.7}$$

where χ is the electric polarization of the reflector, and can be written as $\chi(x) = (\chi_{ij})_{i,j=1,2}\mathbf{1}_{\mathrm{r}}(x)$ and $U = u_s + U_0$ is the total field. The coupled problems (5.2.4)-(5.2.5) and (5.2.6)-(5.2.7) have been mathematically investigated in [31, 32, 35].

Let us consider Ω to be a domain large enough so that $\Omega_\mu = \mathrm{supp}(\mu) \Subset \Omega$ and measure the fields u_s and v on its boundary $\partial\Omega$. The goal of the imaging problem is to locate the reflector from the far-field measurements of the scattered field u_s at the fundamental frequency and/or the second-harmonic generated field v. It will be shown in this chapter that, in the presence of medium noise, the use of the second-harmonic field yields a better stability properties for imaging the small reflector Ω_r than the use of the scattered field at the fundamental frequency.

5.3 Small-volume expansions

In this section, we establish small-volume expansions for the solutions of problems (5.2.4)-(5.2.5) and (5.2.6)-(5.2.7). We assume that the reflector is of the form $\Omega_r = z_r + \delta B$, where its characteristic size δ is small, z_r is its location, and B is a smooth domain such that $B \subset B(0,1)$ with $B(0,1)$ being the ball of radius 1 and center the origin 0. We derive asymptotic expansions of u_s and v as δ goes to zero.

5.3.1 Fundamental frequency problem

Before deriving an asymptotic expansion of u_s as δ goes to zero, we first approximate the background solution, *i.e.*, the field that would be observed without the reflector in terms of the amplitude of the random process μ. We construct its first-order correction as a function of μ.

Let $U^{(\mu)} = u_s^{(\mu)} + U_0$ be the total field that would be observed in the absence of any reflector. The scattered field $u_s^{(\mu)}$ satisfies

$$\begin{cases} \nabla \cdot \Big((1+\mu)\nabla(u_s^{(\mu)} + U_0)\Big) + \omega^2(u_s^{(\mu)} + U_0) = 0 \quad \text{in } \mathbb{R}^2, \\ \lim\limits_{|x|\to\infty} \sqrt{|x|}(\dfrac{\partial u_s^{(\mu)}}{\partial |x|} - i\omega u_s^{(\mu)}) = 0. \end{cases} \tag{5.3.1}$$

Therefore,

$$\nabla \cdot (1+\mu)\nabla u_s^{(\mu)} + \omega^2 u_s^{(\mu)} = -\nabla \cdot \mu \nabla U_0 \quad \text{in } \mathbb{R}^2.$$

Since $\Omega_\mu \Subset \Omega$, the following estimate holds

$$||u_s^{(\mu)}||_{H^1(\Omega)} \leq C||\mu||_{L^\infty} \tag{5.3.2}$$

for some positive constant C independent of μ. Here, $H^1(\Omega)$ is the set of functions in $L^2(\Omega)$, whose weak derivatives are in $L^2(\Omega)$. We refer the reader to Appendix B.1 for a proof of (5.3.2), which uses the same arguments as those in [1, 2]. Actually, one can prove that

$$u_s^{(\mu)}(x) = -\int_{\Omega_\mu} \mu(y)\nabla U_0(y) \cdot \nabla G_\omega^{(0)}(x,y)dy + O(||\mu||_{L^\infty}^2), \quad x \in \Omega.$$

Moreover, writing

$$\nabla \cdot \Big((1+\mu)\nabla(u_s^{(\mu)} + U_0)\Big) = -\omega^2(u_s^{(\mu)} + U_0),$$

it follows by using Meyers' theorem [101] (see also [37, pp. 35-45]) that there exists $\eta > 0$ such that for all $0 \leq \eta' \leq \eta$,

$$\begin{aligned} ||\nabla u_s^{(\mu)}||_{L^{2+\eta'}(\Omega')} &\leq ||\nabla(u_s^{(\mu)} + U_0)||_{L^{2+\eta'}(\Omega)} + ||\nabla U_0||_{L^{2+\eta'}(\Omega)} \\ &\leq C||u_s^{(\mu)} + U_0||_{L^{2+\eta'}(\Omega)} + ||\nabla U_0||_{L^{2+\eta'}(\Omega)} \\ &\leq C||u_s^{(\mu)}||_{L^{2+\eta'}(\Omega)} + C' \end{aligned}$$

for some positive constants C and C', where $\Omega' \Subset \Omega$. From the continuous embedding of $H^1(\Omega)$ into $L^{2+\eta'}(\Omega)$ and (5.3.2) we obtain

$$||u_s^{(\mu)}||_{L^{2+\eta'}(\Omega)} \leq C'',$$

for some constant C'' independent of μ. Therefore,

$$||\nabla u_s^{(\mu)}||_{L^{2+\eta'}(\Omega')} \leq C \tag{5.3.3}$$

for some constant C independent of μ.

Now, we turn to the derivation of an asymptotic expansion of u_s as δ goes to zero. On one hand, by subtracting (5.2.4) from (5.3.1), we get

$$\nabla \cdot \Big(([\sigma_r - 1]\mathbf{1}_{\Omega_r} + \mu + 1)\nabla(u_s - u_s^{(\mu)})\Big) + \omega^2(u_s - u_s^{(\mu)}) = -\nabla \cdot [\sigma_r - 1]\mathbf{1}_{\Omega_r}\nabla U_0 - \nabla \cdot [\sigma_r - 1]\mathbf{1}_{\Omega_r}\nabla u_s^{(\mu)} \quad \text{in } \mathbb{R}^2. \tag{5.3.4}$$

On the other hand, we have

$$\begin{aligned} ||[\sigma_r - 1]\mathbf{1}_{\Omega_r}\nabla u_s^{(\mu)}||_{L^2(\Omega)} &\leq C|\Omega_r|^{\frac{\eta}{8+2\eta}}||\nabla u_s^{(\mu)}||_{L^{2+\frac{\eta}{2}}(\Omega)} \\ &\leq C|\Omega_r|^{\frac{\eta}{8+2\eta}}||\nabla u_s^{(\mu)}||_{L^2(\Omega)}^{\frac{1}{4+\eta}}||\nabla u_s^{(\mu)}||_{L^{2+\eta}(\Omega)}^{\frac{1}{4+\eta}}, \end{aligned}$$

and hence, by (5.3.2) and (5.3.3), we arrive at

$$||[\sigma_r - 1]\mathbf{1}_{\Omega_r}\nabla u_s^{(\mu)}||_{L^2(\Omega)} \leq C|\Omega_r|^{\frac{\eta}{8+2\eta}}||\mu||_{L^\infty}^{\frac{2}{4+\eta}}.$$

Therefore, we can neglect in (5.3.4) the term $\nabla \cdot [\sigma_r - 1]\mathbf{1}_{\Omega_r}\nabla u_s^{(\mu)}$ as $||\mu||_{L^\infty} \to 0$.

Let $w^{(\mu)}$ be defined by

$$\nabla \cdot (1 + \mu + [\sigma_r - 1]\mathbf{1}_{\Omega_r})\nabla w^{(\mu)} + \omega^2 w^{(\mu)} = \nabla \cdot [\sigma_r - 1]\mathbf{1}_{\Omega_r}\nabla(x - z_r) \quad \text{in } \mathbb{R}^2, \tag{5.3.5}$$

subject to the Sommerfeld radiation condition

$$\lim_{|x|\to\infty} \sqrt{|x|}\left(\frac{\partial w^{(\mu)}}{\partial |x|} - i\omega w^{(\mu)}\right) = 0.$$

Using the Taylor expansion

$$U_0(x) = U_0(z_r) + (x - z_r) \cdot \nabla U_0(z_r) + O(|x - z_r|^2),$$

one can derive the inner expansion

$$(u_s - u_s^{(\mu)})(x) = w^{(\mu)}(x) \cdot \nabla U_0(z_r) + O(\delta^2), \tag{5.3.6}$$

for x near z_r. The following estimate holds. We refer the reader to Appendix B.2 for its proof.

Proposition 5.3.1. *There exists a positive constant C independent of δ such that*

$$||u_s - u_s^{(\mu)} - w^{(\mu)}(x) \cdot \nabla U_0(z_r)||_{H^1(\Omega)} \leq C\delta^2.$$

Let $G_\omega^{(\mu)}$ be the outgoing Green function in the random medium, that is, the solution to

$$(\nabla \cdot (1+\mu)\nabla + \omega^2) G_\omega^{(\mu)}(., z) = -\delta_z \quad \text{in } \mathbb{R}^2, \tag{5.3.7}$$

subject to the Sommerfeld radiation condition

$$\lim_{|x|\to\infty} \sqrt{|x|}(\frac{\partial G_\omega^{(\mu)}}{\partial |x|} - i\omega G_\omega^{(\mu)}) = 0.$$

Here, δ_z is the Dirac mass at z. An important property satisfied by $G_\omega^{(\mu)}$ is the reciprocity property [20]:

$$G_\omega^{(\mu)}(x, z) = G_\omega^{(\mu)}(z, x), \qquad x \neq z. \tag{5.3.8}$$

Let us denote by $G_\omega^{(0)}$ the outgoing background Green function, that is, the solution to

$$(\Delta + \omega^2) G_\omega^{(0)}(., z) = -\delta_z \qquad \text{in } \mathbb{R}^2, \tag{5.3.9}$$

subject to the Sommerfeld radiation condition.

The Lippmann-Schwinger representation formula:

$$\begin{aligned}
(G_\omega^{(\mu)} - G_\omega^{(0)})(x, z_r) &= \int_{\Omega_\mu} \mu(y) \nabla G_\omega^{(\mu)}(y, z_r) \cdot \nabla G_\omega^{(0)}(x, y)\, dy \\
&= \int_{\Omega_\mu} \mu(y) \nabla G_\omega^{(0)}(y, z_r) \cdot \nabla G_\omega^{(0)}(x, y)\, dy \\
&\quad + \int_{\Omega_\mu} \mu(y) \nabla (G_\omega^{(\mu)} - G_\omega^{(0)})(y, z_r) \cdot \nabla G_\omega^{(0)}(x, y)\, dy
\end{aligned}$$

holds for $x \in \partial\Omega$. Since $\Omega_\mu \Subset \Omega$, we have

$$\left| (G_\omega^{(\mu)} - G_\omega^{(0)})(x, z_r) - \int_{\Omega_\mu} \mu(y) \nabla G_\omega^{(0)}(y, z_r) \cdot \nabla G_\omega^{(0)}(x, y)\, dy \right| \leq$$
$$||\mu||_{L^\infty} ||\nabla G_\omega^{(0)}(x, \cdot)||_{L^\infty(\Omega_\mu)} ||\nabla (G_\omega^{(\mu)} - G_\omega^{(0)})(\cdot, z_r)||_{L^2(\Omega_\mu)}.$$

Similarly to (5.3.2), one can prove that

$$||\nabla(G_\omega^{(\mu)} - G_\omega^{(0)})(\cdot, z_r)||_{L^2(\Omega_\mu)} \leq C||\mu||_{L^\infty}, \tag{5.3.10}$$

and hence, there exists a positive constant C independent of μ such that

$$\left|(G_\omega^{(\mu)} - G_\omega^{(0)})(x, z_r) - \int_{\Omega_\mu} \mu(y)\nabla G_\omega^{(0)}(y, z_r) \cdot \nabla G_\omega^{(0)}(x, y)\, dy\right| \leq C||\mu||_{L^\infty}^2, \tag{5.3.11}$$

uniformly in $x \in \partial\Omega$.

Since

$$||\nabla\nabla G_\omega^{(0)}(x, \cdot)||_{L^\infty(\Omega_\mu)} \leq C \tag{5.3.12}$$

uniformly in $x \in \partial\Omega$, the estimate

$$\left|\nabla(G_\omega^{(\mu)} - G_\omega^{(0)})(x, z_r) - \nabla\int_{\Omega_\mu} \mu(y)\nabla G_\omega^{(0)}(y, z_r) \cdot \nabla G_\omega^{(0)}(x, y)\, dy\right| \leq C||\mu||_{L^\infty}^2, \tag{5.3.13}$$

holds in exactly the same way as in (5.3.11). Therefore, the following Born approximation holds.

Proposition 5.3.2. *We have*

$$\begin{aligned} G_\omega^{(\mu)}(x, z_r) &= G_\omega^{(0)}(x, z_r) - \int_{\Omega_\mu} \mu(y)\nabla G_\omega^{(0)}(y, z_r) \cdot \nabla G_\omega^{(0)}(x, y)\, dy + O(||\mu||_{L^\infty}^2), \\ \nabla G_\omega^{(\mu)}(x, z_r) &= \nabla G_\omega^{(0)}(x, z_r) - \nabla\int_{\Omega_\mu} \mu(y)\nabla G_\omega^{(0)}(y, z_r) \cdot \nabla G_\omega^{(0)}(x, y)\, dy + O(||\mu||_{L^\infty}^2) \end{aligned}$$

uniformly in $x \in \partial\Omega$.

We now turn to an approximation formula for $w^{(\mu)}$ as $||\mu||_{L^\infty} \to 0$. By integrating by parts we get

$$w^{(\mu)}(x) = (1 - \sigma_r)\int_{\Omega_r} \nabla(w^{(\mu)}(y) - (y - z_r)) \cdot \nabla G_\omega^{(\mu)}(x, y)\, dy, \quad x \in \mathbb{R}^2.$$

Using (5.3.12) we have, for x away from Ω_r,

$$w^{(\mu)}(x) = (1 - \sigma_r)[\int_{\Omega_r} \nabla(w^{(\mu)}(y) - (y - z_r))\, dy] \cdot [\nabla G_\omega^{(\mu)}(x, z_r) + O(\delta)]. \tag{5.3.14}$$

Now let $\mathbf{1}_B$ denote the characteristic function of B. Let $\widetilde{w}$ be the solution to

$$\begin{cases} \nabla \cdot (1 + [\sigma_r - 1]\mathbf{1}_B)\nabla\widetilde{w} = 0 \quad \text{in } \mathbb{R}^2, \\ \widetilde{w}(\widetilde{x}) - \widetilde{x} \to 0 \quad \text{as } |\xi| \to +\infty. \end{cases} \tag{5.3.15}$$

The following result holds. We refer the reader to Appendix B.3 for its proof.

Proposition 5.3.3. *We have*

$$\nabla \Big(w^{(\mu)}(y) - (y - z_r) \Big) = \delta \nabla \widetilde{w}(\widetilde{y}) + O(\delta[||\mu||_{L^\infty} + (\delta\omega)^2]), \tag{5.3.16}$$

where the scaled variable

$$\widetilde{y} = \frac{y - z_r}{\delta}.$$

From (5.3.16), it follows that

$$\int_{\Omega_r} \nabla(w^{(\mu)}(y) - (y - z_r))\, dy = \delta^2 \int_B \nabla \widetilde{w}(\widetilde{x})\, d\widetilde{x} + O(\delta^3[||\mu||_{L^\infty} + (\delta\omega)^2]). \tag{5.3.17}$$

Define the polarization tensor associated to σ_r and B by (see [26])

$$M(\sigma_r, B) := (\sigma_r - 1) \int_B \nabla \widetilde{w}(\widetilde{x})\, d\widetilde{x},$$

where $\widetilde{w}$ is the solution to (5.3.15). The matrix $M(\sigma_r, B)$ is symmetric definite (positive if $\sigma_r > 1$ and negative if $\sigma_r < 1$). Moreover, if B is a disk, then $M(\sigma_r, B)$ takes the form [26]:

$$M(\sigma_r, B) = \frac{2(\sigma_r - 1)}{\sigma_r + 1} |B| I_2,$$

where I_2 is the identity matrix.

To obtain an asymptotic expansion of $u_s(x) - u_s^{(\mu)}(x)$ in terms of the characteristic size δ of the scatterer, we take the far-field expansion of (5.3.6). Plugging formula (5.3.17) into (5.3.14), we obtain the following small-volume asymptotic expansion.

Proposition 5.3.4. *We have*

$$u_s(x) = u_s^{(\mu)}(x) - \delta^2 M(\sigma_r, B) \nabla U_0(z_r) \cdot \nabla G_\omega^{(\mu)}(x, z_r) + O(\delta^3[1 + ||\mu||_{L^\infty} + (\delta\omega)^2]), \tag{5.3.18}$$

uniformly in $x \in \partial\Omega$.

Finally, using (5.3.13) we arrive at the following result.

Theorem 5.3.5. *We have as* δ *goes to zero*

$$\begin{aligned} (u_s - u_s^{(\mu)})(x) \;=\; & -\delta^2 M(\sigma_r, B) \nabla U_0(z_r) \cdot \left[\nabla G_\omega^{(0)}(x, z_r) + \nabla \int_{\Omega_\mu} \mu(y) \nabla G_\omega^{(0)}(y, z_r) \cdot \nabla G_\omega^{(0)}(x, y)\, dy \right] \\ & + O(\delta^3[1 + ||\mu||_{L^\infty} + (\delta\omega)^2] + \delta^2 ||\mu||_{L^\infty}^2), \end{aligned} \tag{5.3.19}$$

uniformly in $x \in \partial\Omega$.

Theorem 5.3.5 shows that the asymptotic expansion (5.3.19) is uniform with respect to ω and μ, provided that $\omega \leq C/\delta$ and $||\mu||_{L^\infty} \leq C'\sqrt{\delta}$ for two positive constants C and C'.

5.3.2 Second-harmonic problem

We apply similar arguments to derive a small-volume expansion for the second-harmonic field v at frequency 2ω. Here the derivation is simpler than before. It is based on Born approximations with respect to both the size of the reflector and the amplitude of the medium noise. It is worth emphasizing that the asymptotic expansion with respect to the size of the reflector does not involve the notion of polarization tensor.

Introduce $G_{2\omega}^{(\sigma_r,\mu)}(.,z)$ the outgoing solution of

$$\left(\Delta + \frac{(2\omega)^2}{[\sigma_r - 1]\mathbf{1}_{\Omega_r} + 1}(1 - \frac{\mu}{[\sigma_r - 1]\mathbf{1}_{\Omega_r} + 1})\right) G_{2\omega}^{(\sigma_r,\mu)}(.,z) = -\delta_z \qquad \text{in } \mathbb{R}^2.$$

Let $G_{2\omega}^{(0)}$ be the solution to (5.3.9) subject to the Sommerfeld radiation condition with ω replaced by 2ω.

Similarly to (5.3.19), an asymptotic expansion for $G_{2\omega}^{(\sigma_r,\mu)}$ in terms of δ can be derived. We have

$$(G_{2\omega}^{(\sigma_r,\mu)} - G_{2\omega}^{(\mu)})(x,z) = O(\delta^2)$$

for $x \neq z$ and x, z away from z_r. Here $G_{2\omega}^{(\mu)}$ is the solution to (5.3.7) with ω replaced by 2ω. Moreover, the Born approximation yields

$$(G_{2\omega}^{(\sigma_r,\mu)} - G_{2\omega}^{(0)})(x,z) \;=\; -(2\omega)^2 \int_{\Omega_\mu} \mu(y) G_{2\omega}^{(0)}(y,z) G_{2\omega}^{(0)}(x,y) dy + O(\delta^2 + ||\mu||_{L^\infty}^2)$$

for $x \neq z$ and x, z away from z_r. From the integral representation formula:

$$v(x) = -\int_{\Omega_r} \sum_{k,l=1,2} \chi_{kl} \partial_{x_k} U(y) \partial_{x_l} U(y) G_{2\omega}^{(\sigma_r,\mu)}(x,y) dy,$$

it follows that

$$v(x) = -\delta^2 |B| \left(\sum_{k,l} \chi_{kl} \partial_{x_k} U(z_r) \partial_{x_l} U(z_r) \right) G_{2\omega}^{(\sigma_r,\mu)}(x,z_r) + O(\delta^3),$$

where $|B|$ denotes the volume of B, and hence, keeping only the terms of first-order in μ and of second-order in δ:

$$v(x) = -\delta^2|B| \left(\sum_{k,l} \chi_{kl} \partial_{x_k} U(z_r) \partial_{x_l} U(z_r) \right) \left[G^{(0)}_{2\omega}(x, z_r) - 4\omega^2 \int_\Omega \mu(y) G^{(0)}_{2\omega}(x, y) G^{(0)}_{2\omega}(y, z_r) dy + O(||\mu||^2_{L^\infty}) \right] + O(\delta^3).$$

We denote by $(S)^\theta$ the source term (the source term strongly depends on the angle θ of the incoming plane wave):

$$(S)^\theta = \left(\sum_{k,l} \chi_{kl} \partial_{x_k} U(z_r) \partial_{x_l} U(z_r) \right).$$

Now, since

$$U(x) = U_I e^{i\omega\theta\cdot x} + \int_\Omega \mu(y) \nabla G^{(0)}_\omega(x, y) \cdot \nabla U_0(y) dy + O(||\mu||^2_{L^\infty} + \delta),$$

which follows by using the Born approximation and the inner expansion (5.3.6), we can give an expression for the partial derivatives of U. We have

$$\partial_{x_k} U(x) = i\omega\theta_k U_I e^{i\omega\theta\cdot x} - i\omega\theta \cdot \int_\Omega \nabla(\mu(y) e^{i\omega\theta\cdot y}) \partial_{x_k} G^{(0)}_\omega(x, y) dy + O(||\mu||^2_{L^\infty} + \delta).$$

We can rewrite the source term as

$$\begin{aligned} \left(\sum_{k,l} \chi_{k,l} \partial_{x_k} U(z_r) \partial_{x_l} U(z_r) \right) = -\omega^2 U_I^2 \sum_{k,l} \chi_{kl} \Big[& \theta_k \theta_l e^{i\omega\theta\cdot z_r} \\ & - \theta_k \theta \cdot \int_\Omega \nabla(\mu(y) e^{i\omega\theta\cdot y}) \partial_{x_l} G^{(0)}_\omega(z_r, y) dy - \theta_l \theta \cdot \int_\Omega \nabla(\mu(y) e^{i\omega\theta\cdot y}) \partial_{x_k} G^{(0)}_\omega(z_r, y) dy \\ & + \theta \cdot \int_\Omega \nabla(\mu(y) e^{i\omega\theta\cdot y}) \partial_{x_l} G^{(0)}_\omega(z_r, y) dy \theta \cdot \int_\Omega \nabla(\mu(y) e^{i\omega\theta\cdot y}) \partial_{x_k} G^{(0)}_\omega(z_r, y) dy \Big] \\ & + O(||\mu||^2_{L^\infty} + \delta). \end{aligned}$$

Assume that $\mu \in \mathcal{C}^{0,\alpha}$ for $0 < \alpha < 1/2$. From

$$\begin{aligned} \int_\Omega \nabla(\mu(y) e^{i\omega\theta\cdot y}) \partial_{x_l} G^{(0)}_\omega(z_r, y) dy &= \int_\Omega \nabla(\mu(y) e^{i\omega\theta\cdot y} - \mu(z_r) e^{i\omega\theta\cdot z_r}) \partial_{x_l} G^{(0)}_\omega(z_r, y) dy \\ &= -\int_\Omega \nabla \partial_{x_l} G^{(0)}_\omega(z_r, y) (\mu(y) e^{i\omega\theta\cdot y} - \mu(z_r) e^{i\omega\theta\cdot z_r}) dy \end{aligned} \tag{5.3.20}$$

one can show that, for $0 < \alpha' \leq \alpha$, we have [63]

$$\left|\theta \cdot \int_\Omega \nabla(\mu(y)e^{i\omega\theta\cdot y})\partial_{x_l} G_\omega^{(0)}(z_r, y)dy\theta \cdot \int_\Omega \nabla(\mu(y)e^{i\omega\theta\cdot y})\partial_{x_k} G_\omega^{(0)}(z_r, y)dy\right| \leq C||\mu||^2_{\mathcal{C}^{0,\alpha'}},$$

where C is a positive constant independent of μ.

So, if we split $(S)^\theta$ into a deterministic part and a random part:

$$(S)^\theta = (S)^\theta_{det} + (S)^\theta_{rand} + O(||\mu||^2_{\mathcal{C}^{0,\alpha}} + \delta),$$

we get

$$(S)^\theta_{det} = -\omega^2 U_I^2 e^{i2\omega\theta\cdot z_r} \sum_{k,l} \chi_{k,l}\theta_k\theta_l, \tag{5.3.21}$$

and

$$\begin{aligned}(S)^\theta_{rand} &= \omega^2 \sum_{k,l} \chi_{k,l}\Bigg[\theta_k\theta \cdot \int_\Omega \nabla(\mu(y)e^{i\omega\theta\cdot y})\partial_{x_l} G_\omega^{(0)}(z_r, y)dy \\ &\quad +\theta_l\theta \cdot \int_\Omega \nabla(\mu(y)e^{i\omega\theta\cdot y})\partial_{x_k} G_\omega^{(0)}(z_r, y)dy\Bigg].\end{aligned} \tag{5.3.22}$$

Finally, we obtain the following result.

Theorem 5.3.6. *Assume that $\mu \in \mathcal{C}^{0,\alpha}$ for $0 < \alpha < 1/2$. Let $0 < \alpha' \leq \alpha$. The following asymptotic expansion holds for v as δ goes to zero:*

$$\begin{aligned}v(x) = -\delta^2|B|\Bigg((S)^\theta_{det}\left[G_{2\omega}^{(0)}(x, z_r) - 4\omega^2 \int_\Omega \mu(y)G_{2\omega}^{(0)}(x, y)G_{2\omega}^{(0)}(y, z_r)dy\right] + (S)^\theta_{rand}G_{2\omega}^{(0)}(x, z_r)\Bigg) \\ + O(\delta^3 + \delta^2||\mu||^2_{\mathcal{C}^{0,\alpha'}})\end{aligned} \tag{5.3.23}$$

uniformly in $x \in \partial\Omega$.

5.4 Imaging functional

In this section, two imaging functionals are presented for locating small reflectors. For the sake of simplicity, we assume that B and Ω are disks centered at 0 with radius 1 and R, respectively.

5.4.1 The fundamental frequency case

We assume that we are in possession of the following data: $\{u_s(x),\ x \in \partial\Omega\}$. We introduce the backpropagation imaging functional (or time - reversal)

$$\forall z^S \in \Omega,\ I(z^S) = \int_{\partial\Omega\times\mathbb{S}^1} \frac{1}{i\omega} e^{-i\omega\theta\cdot z^S} \theta^\top \overline{\nabla G_\omega^{(0)}(x, z^S)} u_s(x) d\sigma(x) d\sigma(\theta), \tag{5.4.1}$$

where $\top$ denotes the transpose. Introduce the matrix:

$$R_\omega(z_1, z_2) = \int_{\partial\Omega} \overline{\nabla G_\omega^{(0)}(x, z_1)} \nabla G_\omega^{(0)}(x, z_2)^\top d\sigma(x), \qquad z_1, z_2 \in \Omega' \Subset \Omega. \tag{5.4.2}$$

Using (5.3.19), we have the following expansion for $I(z^S), z^S \in \Omega'$,

$$\begin{aligned} I(z^S) = \int_{\partial\Omega\times\mathbb{S}^1} \frac{1}{i\omega} e^{-i\omega\theta\cdot z^S} \theta^\top \overline{\nabla G_\omega^{(0)}(x, z^S)} u_s^{(\mu)}(x) d\sigma(x) d\sigma(\theta) \\ - \frac{2\pi\delta^2(\sigma_r - 1)}{\sigma_r + 1} U_I \int_{\mathbb{S}^1} e^{-i\omega\theta\cdot(z^S - z_r)} \theta^\top \Bigg[R_\omega(z^S, z_r) \\ + \int_{\partial\Omega} \overline{\nabla G_\omega^{(0)}(x, z^S)} \left(\nabla \int_{\Omega_\mu} \mu(y) \nabla G_\omega^{(0)}(y, z_r) \cdot \nabla G_\omega^{(0)}(x, y) dy \right)^\top d\sigma(x) \Bigg] \theta d\sigma(\theta) \\ + O(\delta^3 + \delta^2 ||\mu||_{L^\infty}^2). \end{aligned} \tag{5.4.3}$$

Note that

$$\begin{aligned} &\int_{\partial\Omega} \overline{\nabla G_\omega^{(0)}(x, z^S)} \left(\nabla \int_{\Omega_\mu} \mu(y) \nabla G_\omega^{(0)}(y, z_r) \cdot \nabla G_\omega^{(0)}(x, y) dy \right)^\top d\sigma(x) \\ &\quad = \int_{\Omega_\mu} \mu(y) \int_{\partial\Omega} \overline{\nabla G_\omega^{(0)}(x, z^S)} \left(\nabla \nabla G_\omega^{(0)}(x, y) \nabla G_\omega^{(0)}(y, z_r) \right)^\top d\sigma(x) dy. \end{aligned}$$

Remark 5.4.1. *Here, the fact that not only we backpropagate the boundary data but also we average it over all the possible illumination angles in $\mathbb{S}^1$ has two motivations. As will be shown later in section 5.5, the first reason is to increase the resolution and make the peak at the reflector's location isotropic. If we do not sum over equi-distributed illumination angles over the sphere, we get more of "8-shaped" spot, as shown in Figure 5.6.7. The second reason is that an average over multiple measurements increases the stability of the imaging functional with respect to measurement noise.*

Remark 5.4.2. *If we could take an image of the medium in the absence of reflector before taking the real image, we would be in possession of the boundary data $\{u_s - u_s^{(\mu)},\ x \in \partial\Omega\}$, and thus we would be able to detect the reflector in a very noisy*

background. But in some practical situations [72], it is not possible to get an image without the reflector. As it will be shown in section 5.5, second-harmonic generation can be seen as a powerful contrast imaging approach [72]. In fact, we will prove that the second harmonic image is much more stable with respect to the medium noise and to the volume of the particle than the fundamental frequency image.

5.4.2 Second-harmonic backpropagation

If we write a similar imaging functional for the second-harmonic field v, assuming that we are in possession of the boundary data $\{v(x),\ x \in \partial\Omega\}$, we get

$$\forall z^S \in \Omega,\ J_\theta(z^S) = \int_{\partial\Omega\times\mathbb{S}^1} v(x)\overline{G_{2\omega}^{(0)}(x,z^S)}e^{-2i\omega\theta\cdot z^S}d\sigma(x)d\sigma(\theta). \tag{5.4.4}$$

As before, using (5.3.23) we can expand J in terms of δ and μ. Considering first-order terms in δ and μ we get

$$\begin{aligned} J(z^S) = -\pi\delta^2 \int_{\mathbb{S}^1} e^{-2i\omega\theta\cdot z^S} \Bigg[(S)_{det}^\theta \Big(\int_{\partial\Omega} \overline{G_{2\omega}^{(0)}(x,z^S)} G_{2\omega}^{(0)}(x,z_r)d\sigma(x) \\ - 4\omega^2 \int_{\partial\Omega} \overline{G_{2\omega}^{(0)}(x,z^S)} \int_\Omega \mu(y) G_{2\omega}^{(0)}(y,x) G_{2\omega}^{(0)}(y,z_r)dyd\sigma(x) \Big) \\ + (S)_{rand}^\theta \int_{\partial\Omega} \overline{G_{2\omega}^{(0)}(x,z^S)} G_{2\omega}^{(0)}(x,z_r)d\sigma(x) \Bigg] d\sigma(\theta) + O(\delta^3 + \delta^2||\mu||^2_{\mathcal{C}^{0,\alpha'}}), \end{aligned}$$

where $0 < \alpha' \leq \alpha$. Now, if we define $Q_{2\omega}$ as

$$Q_{2\omega}(x,z) = \int_{\partial\Omega} G_{2\omega}^{(0)}(y,x)\overline{G_{2\omega}^{(0)}(y,z)}d\sigma(y). \tag{5.4.5}$$

We have

$$\begin{aligned} J(z^S) = -\pi\delta^2 \int_{\mathbb{S}^1} e^{-2i\omega\theta\cdot z^S} \Bigg[(S)_{det}^\theta \left(Q_{2\omega}(z_r,z^S) - 4\omega^2 \int_{\Omega_\mu} \mu(y) G_{2\omega}^{(0)}(y,z_r) Q_{2\omega}(y,z^S)dy \right) \\ + (S)_{rand}^\theta Q_{2\omega}(z_r,z^S) \Bigg] d\sigma(\theta) + O(\delta^3 + \delta^2||\mu||^2_{\mathcal{C}^{0,\alpha'}}). \end{aligned} \tag{5.4.6}$$

5.5 Statistical analysis

In this section, we perform a resolution and stability analysis of both functionals. Since the image we get is a superposition of a deterministic image and of a random field created by the medium noise, we can compute the expectation and the covariance

functions of those fields in order to estimate the signal-to-noise ratio. For the reader's convenience we give our main results in the following proposition.

Proposition 5.5.1. *Let l_μ and σ_μ be respectively the correlation length and the standard deviation of the process μ. Assume that l_μ is smaller than the wavelength $2\pi/\omega$. Let $(SNR)_I$ and $(SNR)_J$ be defined by*

$$(SNR)_I = \frac{\mathbb{E}[I(z_r)]}{(Var[I(z_r)])^{1/2}}, \tag{5.5.1}$$

and

$$(SNR)_J = \frac{\mathbb{E}[J(z_r)]}{(Var[J(z_r)])^{\frac{1}{2}}}. \tag{5.5.2}$$

We have

$$(SNR)_I \approx \frac{\sqrt{2}\pi^{3/2}\omega\delta^2 U_I}{\sigma_\mu l_\mu \sqrt{\omega\ diam\ \Omega_\mu}} \frac{|\sigma_r - 1|}{\sigma_r + 1}, \tag{5.5.3}$$

and

$$(SNR)_J \geq \frac{l_\mu^\alpha \left(\int_{\mathbb{S}^1} \left(\sum_{k,l} \chi_{k,l}\theta_k\theta_l \right) d\theta \right)}{\sqrt{C}\sigma_\mu \min(\omega^{-\alpha}, 1) \max_{k,l} |\chi_{k,l}| \sqrt{(\omega diam\ \Omega_\mu)^{3+2\alpha} + 1}}. \tag{5.5.4}$$

Here, diam denotes the diameter, α is the upper bound for Holder-regularity of the random process μ (see section 5.5.1).

5.5.1 Assumptions on the random process μ

Let $z(x)$, $x \in \mathbb{R}^2$ be a stationary random process with Gaussian statistics, zero mean, and a covariance function given by $R(|x-y|)$ satisfying $R(0) = \sigma_\mu^2$, $|R(0) - R(s)| \leq \sigma_\mu^2 \frac{s^{2\alpha}}{l_\mu^{2\alpha}}$ and R is decreasing. Then, z is a $\mathcal{C}^{0,\alpha'}$ process for any $\alpha' < \alpha$ ([3, Theorem 8.3.2]). Let F be a smooth odd bounded function, with derivative bounded by one. For example $F = \arctan$ is a suitable choice. Take

$$\mu(x) = F[z(x)].$$

Then μ is a bounded $\mathcal{C}^{0,\alpha'}$ stationary process with zero mean. We want to compute the expectation of its norm. Introduce

$$p(h) = \max_{\|x-y\| \leq \sqrt{2}h} \mathbb{E}|z(x) - z(y)|.$$

One can also write $p(u) = \sqrt{2}\sqrt{R(0) - R(\sqrt{2}u)}$. According to [3], for all $h, t \in \Omega_\mu$, almost surely,

$$|z(t+h) - z(t)| \leq 16\sqrt{2}[\log(B)]^{1/2} p(\frac{|h|}{l_\mu}) + 32\sqrt{2} \int_0^{\frac{|h|}{l_\mu}} (-\log u)^{1/2}\, dp(u),$$

where B is a positive random variable with $\mathbb{E}[B^n] \leq (4\sqrt{2})^n$ ([3, Formula 3.3.23]). We have that

$$p(|h|) \leq \sqrt{2}^{1+\alpha} \sigma_\mu \frac{|h|^\alpha}{l_\mu^\alpha}.$$

By integration by parts we find that

$$\int_0^{\frac{|h|}{l_\mu}} (-\log u)^{1/2}\, dp(u) = \Big[(-\log u)^{1/2} p(u)\Big]_0^{\frac{|h|}{l_\mu}} + \frac{1}{2} \int_0^{\frac{|h|}{l_\mu}} (-\log u)^{-1/2} u^{-1} p(u) du.$$

For any $\varepsilon > 0$, since $s^\varepsilon \sqrt{-\log s} \leq \frac{1}{\sqrt{\varepsilon}} e^{1/2}$ on $[0,1]$, we have, as $|h|$ goes to 0, that

$$\Big[(-\log u)^{1/2} p(u)\Big]_0^{\frac{|h|}{l_\mu}} \leq e^{\frac{1}{2}} \frac{\sqrt{2}^{1+\alpha} \sigma_\mu}{\sqrt{\varepsilon}} \frac{|h|^{\alpha-\varepsilon}}{l_\mu^\alpha}.$$

Similarly, when $|h| < \frac{1}{2e}$, for every $0 < u < |h|$,

$$(-\log u)^{-1/2} s^{-1} p(u) \leq \sqrt{2}^{1+\alpha} \sigma_\mu \frac{u^{\alpha-1}}{l_\mu^\alpha}.$$

So we get, when $|h|$ goes to 0, for every $\varepsilon > 0$,

$$\int_0^{\frac{|h|}{l_\mu}} (-\log u)^{1/2}\, dp(u) \leq \frac{e^{\frac{1}{2}} \sqrt{2}^{1+\alpha} \sigma_\mu}{\sqrt{\varepsilon}} \frac{|h|^{\alpha-\varepsilon}}{l_\mu^\alpha} + \frac{\sqrt{2}^{1+\alpha} \sigma_\mu}{\alpha} \frac{|h|^\alpha}{l_\mu^\alpha}.$$

Therefore, when $|h|$ goes to zero, we have for any $\varepsilon > 0$:

$$|z(t+h) - z(t)| \leq 32\sqrt{2}^\alpha \log(B)^{1/2} \sigma_\mu \frac{|h|^\alpha}{l_\mu^\alpha} + 64 e^{\frac{1}{2}} \sqrt{2}^\alpha \sigma_\mu \frac{1}{l_\mu^\alpha} \left[\frac{1}{\sqrt{\varepsilon}} |h|^{\alpha-\varepsilon} + \frac{1}{2}|h|^\alpha\right].$$

Since $F' \leq 1$, composing by F yields, for any $x, y \in \mathbb{R}^2$,

$$|\mu(x) - \mu(y)| \leq |z(x) - z(y)|.$$

We get the following estimate on $\|\mu\|_{\mathcal{C}^{0,\alpha'}}$, for any $\alpha' \in]0,\alpha[$, almost surely

$$\sup_{\substack{x,y\in\Omega_\mu \\ |x-y|\leq h}} \frac{|\mu(x)-\mu(y)|}{|x-y|^{\alpha'}} \leq 32\sqrt{2}^{\alpha}\log(B)^{1/2}\sigma_\mu \frac{h^{\alpha-\alpha'}}{l_\mu^\alpha} + 64e^{\frac{1}{2}}\sqrt{2}^{\alpha}\sigma_\mu \frac{1}{l_\mu^\alpha}\left[\frac{1}{\sqrt{\alpha-\alpha'}} + \frac{1}{2}h^{\alpha-\alpha'}\right]$$

$$\|\mu\|_{\mathcal{C}^{0,\alpha'}} \leq 64\sqrt{2}^{\alpha}\frac{e^{\frac{1}{2}}\left[\log(B)^{1/2}+1\right]}{\sqrt{\alpha-\alpha'}}\frac{\sigma_\mu}{l_\mu^\alpha},$$

which gives, since $\mathbb{E}[\log B] \leq \mathbb{E}[B] - 1 \leq 4\sqrt{2} - 1$

$$\mathbb{E}[\|\mu\|^2_{\mathcal{C}^{0,\alpha'}}] \leq 64^2 2^{4+\alpha}\frac{e}{\alpha-\alpha'}\frac{\sigma_\mu^2}{l_\mu^{2\alpha}}. \tag{5.5.5}$$

5.5.2 Standard backpropagation

Expectation

We use (5.4.3) and the fact that $\mathbb{E}(\mu)(x) = 0,\ \forall x \in \Omega$, to find that

$$\mathbb{E}[I(z^S)] = -2\pi\delta^2\frac{\sigma_r - 1}{\sigma_r + 1}U_I \int_{\mathbb{S}^1} e^{-i\omega\theta\cdot(z^S - z_r)}\theta^\top R_\omega(z^S, z_r)\theta d\theta. \tag{5.5.6}$$

We now use the Helmholtz-Kirchoff theorem . Since (see [20]):

$$\lim_{R\to\infty}\int_{|x|=R}\nabla G_\omega^{(0)}(x,y)\overline{\nabla G_\omega^{(0)}(z,y)}^\top dy = \frac{1}{\omega}\nabla_z\nabla_x\ \mathrm{Im}\left[G_\omega^{(0)}(x,z)\right]$$

and

$$\mathrm{Im}\left[G_\omega^{(0)}(x,z)\right] = \frac{1}{4}J_0(\omega|x-z|), \tag{5.5.7}$$

we can compute an approximation of R_ω.

$$\begin{aligned}\frac{1}{\omega}\nabla_z\nabla_x\ \mathrm{Im}\left[G_\omega^{(0)}(x,z)\right] = \frac{1}{4}\Bigg[&\omega J_0(\omega|x-z|)\left(\frac{(x-z)}{|x-z|}\frac{(x-z)^\top}{|x-z|}\right) \\ &- \frac{2J_1(\omega|x-z|)}{|x-z|}\left(\frac{(x-z)}{|x-z|}\frac{(x-z)^\top}{|x-z|}\right) \\ &+ \frac{J_1(\omega|x-z|)}{|x-z|}I_2\Bigg],\end{aligned} \tag{5.5.8}$$

where I_2 is the 2×2 identity matrix. We can see that R_ω decreases as $|z_r - z^S|^{-\frac{1}{2}}$. The imaging functional has a peak at location $z^S = z_r$. Evaluating R_ω at $z^S = z_r$ we get

$$R_\omega(z_r, z_r) = \frac{\omega}{8} I_2.$$

So we get the expectation of I at point z_r:

$$\mathbb{E}[I(z_r)] \approx -\frac{\pi^2(\sigma_r - 1)}{2(\sigma_r + 1)} \omega \delta^2 U_I. \tag{5.5.9}$$

Covariance

Let

$$\mathrm{Cov}\left(I(z^S), I(z^{S'})\right) = \mathbb{E}\Big[\left(I(z^S) - \mathbb{E}[I(z^S)]\right)\overline{\left(I(z^{S'}) - \mathbb{E}[I(z^{S'})]\right)}\Big]. \tag{5.5.10}$$

Define

$$\widetilde{R}_\omega(z^S, z_r, y) = \int_{\partial\Omega} \overline{\nabla G_\omega^{(0)}(x, z^S)} \left(\nabla\nabla G_\omega^{(0)}(x, y) \nabla G_\omega^{(0)}(y, z_r)\right)^\top d\sigma(x).$$

Using (5.4.3) and (5.5.9), we get

$$\begin{aligned} I(z^S) - \mathbb{E}[I(z^S)] = &\int_{\partial\Omega \times \mathbb{S}^1} \frac{1}{i\omega} e^{-i\omega\theta \cdot z^S} \theta^\top \overline{\nabla G_\omega^{(0)}(x, z^S)^\top} u_s^{(\mu)}(x) dx d\theta \\ &- 2\pi\delta^2 \frac{\sigma_r - 1}{\sigma_r + 1} U_I \int_{\mathbb{S}^1} e^{-i\omega\theta \cdot (z^S - z_r)} \left[\int_\Omega \mu(y) \theta^\top \widetilde{R}_\omega(z^S, z_r, y) \theta dy\right] d\theta. \end{aligned}$$

The computations are a bit tedious. For brevity, we write the quantity above as

$$I(z^S) - \mathbb{E}[I(z^S)] = A_I(z^S) + B_I(z^S),$$

with

$$A_I(z^S) = \int_{\partial\Omega \times \mathbb{S}^1} \frac{1}{i\omega} e^{-i\omega\theta \cdot z^S} \theta^\top \overline{\nabla G_\omega^{(0)}(x, z^S)} u_s^{(\mu)}(x) dx d\theta,$$

and

$$B_I(z^S) = -2\pi\delta^2 \frac{\sigma_r - 1}{\sigma_r + 1} U_I \int_{\mathbb{S}^1} e^{-i\omega\theta \cdot (z^S - z_r)} \left[\int_\Omega \mu(y) \theta^\top \widetilde{R}_\omega(z^S, z_r, y) \theta dy\right] d\theta.$$

We now compute each term of the product in (5.5.10) separately.

Main speckle term: We need to estimate the typical size of A_I. From (5.3.2), keeping only terms of first-order in μ yields

$$A_I(z^S) = -\int_{\partial\Omega\times\mathbb{S}^1} \frac{1}{i\omega} e^{-i\omega\theta\cdot z^S} \theta^\top \overline{\nabla G_\omega^{(0)}(x,z^S)} \int_\Omega \mu(y) \nabla G_\omega^{(0)}(x,y)\cdot\nabla U_0(y) dy dx d\theta + O(\|\mu\|_\infty^2),$$

so we have:

$$A_I(z^S) = -U_I \int_{\Omega\times\mathbb{S}^1} e^{-i\omega\theta\cdot(z^S-y)} \mu(y) \theta^\top R_\omega(z^S,y)\theta dy d\theta,$$

and hence,

$$A_I(z^S)\overline{A_I(z^{S'})} = U_I^2 \int_{\mathbb{S}^1} e^{-i\omega\theta\cdot(z^S-z^{S'})} \left[\int\int_{\Omega\times\Omega} e^{i\omega\theta\cdot(y-y')} \mu(y)\mu(y') \theta^\top R_\omega(z^S,y)\overline{R_\omega(z^{S'},y')}\theta dy dy'\right] d\theta.$$

We assume that the medium noise is localized and stationary on its support Ω_μ. We also assume that the correlation length l_μ is smaller than the wavelength. We note σ_μ the standard deviation of the process μ. We can then write:

$$\mathbb{E}\left[A_I(z^S)\overline{A_I(z^{S'})}\right] = U_I^2\sigma_\mu^2 l_\mu^2 \int_{\mathbb{S}^1} e^{i\omega\theta\cdot(z^S-z^{S'})} \int_{\Omega_\mu} \theta^\top R_\omega(z^S,y)\overline{R_\omega(z^{S'},y)}\theta dy d\theta.$$

We introduce

$$P_\omega(z^S,y,z^{S'}) := \int_{\mathbb{S}^1} e^{i\omega\theta\cdot(z^S-z^{S'})} \theta^\top R_\omega(z^S,y)\overline{R_\omega(z^{S'},y)}\theta d\theta, \tag{5.5.11}$$

where R_ω is defined by (5.4.2). Therefore, we have

$$\mathbb{E}\left[A_I(z^S)\overline{A_I(z^{S'})}\right] = U_I^2\sigma_\mu^2 l_\mu^2 \int_{\Omega_\mu} P_\omega(z^S,y,z^{S'}) dy. \tag{5.5.12}$$

Hence, A_I is a complex field with Gaussian statistics of mean zero and covariance given by (5.5.12). It is a speckle field and is not localized.

We compute its typical size at point $z^S = z^{S'} = z_r$, in order to get signal-to-noise estimates. Using (5.5.8), we get that for $|x-z| >> 1$:

$$\lim_{R\to\infty} \int_{|x|=R} \nabla G_\omega^{(0)}(x,y)\overline{\nabla G_\omega^{(0)}(z,y)}^\top dy = \frac{\omega}{4} J_0(\omega|x-z|) \left(\frac{(x-z)}{|x-z|}\frac{(x-z)^\top}{|x-z|}\right).$$

Since we have, for $|x-z| >> 1$,

$$J_0(\omega|x-z|) \sim \frac{\sqrt{2}\cos(\omega|x-z| - \frac{\pi}{4})}{\sqrt{\pi\omega|x-z|}},$$

we obtain that

$$R_\omega(x,z) \approx \frac{\sqrt{\omega}\cos(\omega|x-z| - \pi/4)}{2\sqrt{2\pi}}|x-z|^{-1/2}\left(\frac{(x-z)}{|x-z|}\frac{(x-z)^\top}{|x-z|}\right) \text{ for } |x-z| >> 1. \tag{5.5.13}$$

Now we can write

$$\mathbb{E}\left[A_I(z_r)\overline{A_I(z_r)}\right] \approx U_I^2\sigma_\mu^2 l_\mu^2 \int_{\Omega_\mu}\left(\frac{\sqrt{\omega}}{2\sqrt{2\pi}}\right)^2 \frac{1}{2}|y-z_r|^{-1}\int_{\mathbb{S}^1}\theta^\top\left(\frac{(y-z_r)}{|y-z_r|}\frac{(y-z_r)^\top}{|y-z_r|}\right)\theta d\theta dy.$$

If we compute the term:

$$\int_{\mathbb{S}^1}\theta^\top\left(\frac{(y-z_r)}{|y-z_r|}\frac{(y-z_r)^\top}{|y-z_r|}\right)\theta d\theta = \int_0^{2\pi}\left[\left(\frac{(y-z_r)_1}{|y-z_r|}\right)^2\cos^2\theta + \left(\frac{(y-z_r)_2}{|y-z_r|}\right)^2\sin^2\theta\right]d\theta,$$

then, after linearization and integration, we get

$$\int_{\mathbb{S}^1}\theta^\top\left(\frac{(y-z_r)}{|y-z_r|}\frac{(y-z_r)^\top}{|y-z_r|}\right)\theta d\theta = \pi.$$

So we have:

$$\mathbb{E}\left[A_I(z_r)\overline{A_I(z_r)}\right] \approx \pi U_I^2\sigma_\mu^2 l_\mu^2\int_{\Omega_\mu}\left(\frac{\sqrt{\omega}}{4\sqrt{\pi}}\right)^2|y-z_r|^{-1}dy,$$

and therefore,

$$\mathbb{E}\left[A_I(z_r)\overline{A_I(z_r)}\right] \approx \pi\frac{\omega}{8}U_I^2\sigma_\mu^2 l_\mu^2 \text{diam } \Omega_\mu. \tag{5.5.14}$$

Secondary speckle term: We have

$$B_I(z^S)\overline{B_I(z^{S'})} = \left(2\pi\delta^2\frac{\sigma_r - 1}{\sigma_r + 1}U_I\right)^2\int_{\mathbb{S}^1}e^{-i\omega\theta\cdot(z^S - z^{S'})} \left[\int_\Omega \mu(y)\mu(y')\theta^\top\widetilde{R}_\omega(z^S, z_r, y)\overline{\widetilde{R}_\omega(z^{S'}, z_r, y')}\theta dy dy'\right]d\theta.$$

So we get the expectation:

$$\mathbb{E}\left[B_I(z^S)\overline{B_I(z^{S'})}\right] = \left(2\pi\delta^2\frac{\sigma_r-1}{\sigma_r+1}U_I\right)^2\sigma_\mu^2 l_\mu^2 \int_{\mathbb{S}^1} e^{-i\omega\theta\cdot(z^S-z^{S'})}\theta^\top\left[\int_{\Omega_\mu}\widetilde{R}_\omega(z^S,z_r,y)\overline{\widetilde{R}_\omega(z^{S'},z_r,y)}dy\right]\theta d\theta.$$

This term also creates a speckle field on the image. As before, we compute the typical size of this term at point z_r. We first get an estimate on $\widetilde{R}_\omega$.

$$|\left(\widetilde{R}_\omega(z^S,z_r,y)\right)_{i,j}| \leq |\partial_j G_\omega^{(0)}(y,z_r)|| \sum_{k=1,2}\int_{\partial\Omega}\partial_{y_i}\overline{G_\omega^{(0)}(x,z^S)}\partial_{y_i}\partial_{y_k}G_\omega^{(0)}(x,y)d\sigma(x)|.$$

We recall the Helmholtz-Kirchoff theorem

$$\int_{\partial\Omega}\overline{G_\omega^{(0)}(x,y)}G_\omega^{(0)}(x,z)d\sigma(x) \sim \frac{1}{4\omega}J_0(\omega|y-z|) \quad \text{as } R\to\infty,$$

from which

$$\int_{\partial\Omega}\partial_{y_i}\overline{G_\omega^{(0)}(x,z^S)}\partial_{y_i}\partial_{y_k}G_\omega^{(0)}(x,y)d\sigma(x) = \frac{1}{4\omega}\left(\partial_i\partial_i\partial_k f\right)(z^S-y),$$

where f is defined by $f(x)=J_0(\omega|x|)$. We have

$$\partial_i\partial_j\partial_k f(x) = \omega\left(\frac{3\left(a_{i,j,k}(x)-b_{i,j,k}(x)\right)}{|x|^2}\left[J_0'(\omega|x|)-\omega|x|J_0''(\omega|x|)\right]+a_{i,j,k}(x)\omega^2 J_0^{(3)}(\omega|x|)\right),$$

where $a_{i,j,k}$ and $b_{i,j,k}$ are rational fractions in the coefficients of x bounded by 1. Now, recall the power series of J_0:

$$J_0(z) = \sum_k(-1)^k\frac{\left(\frac{1}{4}z^2\right)^k}{(k!)^2}.$$

We can write

$$J_0'(\omega|x|)-\omega|x|J_0''(\omega|x|) = -\frac{\omega^3}{4}|x|^3+o(|x|^3).$$

Hence, since $J_0^{(3)}(x)\sim\frac{3}{4}x$ when $x\to 0$, we can prove the following estimate for x around 0:

$$\frac{1}{4\omega}(\partial_i\partial_j\partial_k f)(x) \sim \frac{3b_{i,j,k}(x)}{16}\omega^3|x|.$$

In order to get the decay of $\widetilde{R}_\omega$ for large arguments we use the following formulas: $J_0' = -J_1$, $J_0'' = \frac{1}{x}J_1 - J_0$, and $J_0^{(3)} = J_1 - \frac{1}{x^2}J_1 + \frac{1}{x}J_0$. We get

$$\frac{1}{4\omega}|\partial_i\partial_j\partial_k f(x)| \leq \omega^2(\omega|x|)^{-1/2} \quad \text{as } x \to \infty.$$

We also have the following estimate:

$$|\nabla G_\omega^{(0)}(y, z_r)| \leq \left(\frac{2}{\pi}\right)^{1/2} \max\left(\frac{1}{|y - z_r|}, \frac{\omega}{\sqrt{\omega|y - z_r|}}\right).$$

We can now write the estimate on $\widetilde{R_{\omega i,j}}$

$$|\widetilde{R_\Omega}(z^S, z_r, y)_{i,j}| \leq \omega^2 \left(\frac{2}{\pi}\right)^{1/2} \min\left(\omega|y - z_r|, \frac{1}{\sqrt{\omega|y - z^S|}}\right) \max\left(\frac{1}{\omega|y - z_r|}, \frac{1}{\sqrt{\omega|y - z_r|}}\right).$$

We can now go back to estimating the term B_I. We split the domain of integration $\Omega_\mu = B(z_r, \omega^{-1}) \cup \Omega_\mu \backslash B(z_r, \omega^{-1})$ to get

$$\left|\mathbb{E}\left[B_I(z_r)\overline{B_I(z_r)}\right]\right| \leq \left(2\pi\delta^2\frac{\sigma_r - 1}{\sigma_r + 1}U_I\right)^2 \sigma_\mu^2 l_\mu^2 \\ 4\pi\omega^4\frac{2}{\pi}\left[\int_{\Omega_\mu \backslash B(z_r,\omega^{-1})} \frac{1}{|y - z_r|^2}dy + \int_{B(z_r,\omega^{-1})} \omega^2 dy\right].$$

Hence,

$$\left|\mathbb{E}\left[B_I(z_r)\overline{B_I(z_r)}\right]\right| \leq 8\left(2\pi\delta^2\frac{\sigma_r - 1}{\sigma_r + 1}U_I\right)^2 \omega^4\sigma_\mu^2 l_\mu^2 \log(\omega \text{ diam } \Omega_\mu). \tag{5.5.15}$$

Double products: The double products $A_I\overline{B_I}$ and $B_I\overline{A_I}$ have a typical amplitude that is the geometric mean of the typical amplitudes of A_I and B_I. So they are always smaller than one of the main terms $|A_I|^2$ or $|B_I|^2$.

Signal-to-noise ratio estimates

We can now give an estimate of the signal-to-noise ratio $(SNR)_I$ defined by (5.5.1). Using (5.5.9), (5.5.14), and (5.5.15) we get

$$(SNR)_I \approx \frac{\frac{\pi^2(\sigma_r - 1)}{2(\sigma_r + 1)}\omega\delta^2 U_I}{\sigma_\mu l_\mu \left(\pi\frac{\omega}{8} \text{ diam } \Omega_\mu + 8\left(2\pi\delta^2\frac{\sigma_r - 1}{\sigma_r + 1}U_I\right)^2 \omega^4 \log(\omega \text{ diam } \Omega_\mu)\right)^{1/2}}, \tag{5.5.16}$$

Since $\delta << \frac{2\pi}{\omega}$ we have that $\delta\omega << 1$, so we can estimate $(SNR)_I$ as follows

$$(SNR)_I \approx \frac{\sqrt{2}\pi^{3/2}\frac{\sigma_r-1}{\sigma_r+1}\omega\delta^2 U_I}{\sigma_\mu l_\mu \sqrt{\omega \text{ diam } \Omega_\mu}}. \tag{5.5.17}$$

The perturbation in the image I comes from different phenomena. The first one, and the most important is the fact that we image not only the field scattered by the reflector, but also the field scattered by the medium's random inhomogeneities. This is why the signal-to-noise ratio depends on the volume and the contrast of the particle we are trying to locate. It has to stand out from the background. The other terms in the estimate (5.5.16) of $(SNR)_I$ are due to the phase perturbation of the field scattered by the particle when it reaches the boundary of Ω which can be seen as a travel time fluctuation of the scattered wave by the reflector. Both the terms are much smaller than the first one. $(SNR)_I$ depends on the ratio ω/l_μ. If the medium noise has a shorter correlation length, then the perturbation induced in the phase of the fields will more likely self average.

5.5.3 Second-harmonic backpropagation

Expectation

We have:

$$\mathbb{E}[J(z^S)] = -\pi\delta^2 \int_{\mathbb{S}^1} e^{-2i\omega\theta\cdot z^S} \Bigg[(S)^\theta_{det} \int_{\partial\Omega} \overline{G^{(0)}_{2\omega}(x, z^S)} G^{(0)}_{2\omega}(x, z_r) dx + \mathbb{E}[(S)^\theta_{rand}] \int_{\partial\Omega} \overline{G^{(0)}_{2\omega}(x, z^S)} G^{(0)}_{2\omega}(x, z_r) dx \Bigg] d\theta. \tag{5.5.18}$$

Since $\mathbb{E}[(S)^\theta_{rand}] = 0$ we obtain by using (5.3.21) that

$$\mathbb{E}[J(z^S)] = \pi\delta^2\omega^2 U_I^2 \int_{\mathbb{S}^1} \left(\sum_{k,l} \chi_{k,l}\theta_k\theta_l \right) e^{2i\omega\theta\cdot(z_r - z^S)} d\theta \int_{\partial\Omega} \overline{G^{(0)}_{2\omega}(x, z^S)} G^{(0)}_{2\omega}(x, z_r) dx. \tag{5.5.19}$$

If we define $\widetilde{Q}_{2\omega}$ as

$$\widetilde{Q}_{2\omega}(x, y) = \int_{\mathbb{S}^1} \left(\sum_{k,l} \chi_{k,l}\theta_k\theta_l \right) e^{2i\omega\theta\cdot(x-y)} d\theta, \tag{5.5.20}$$

then it follows that

$$\mathbb{E}[J(z^S)] = \delta^2\omega^2 U_I^2 \widetilde{Q}_{2\omega}(z_r, z^S) Q_{2\omega}(z_r, z^S),$$

where $Q_{2\omega}$ is given by (5.4.5). To get the typical size of this term we first use the Helmholtz-Kirchhoff theorem [20]:

$$Q_{2\omega}(z_r, z^S) \sim \frac{1}{2\omega} \operatorname{Im}\left(G^{(0)}_{2\omega}(z_r, z^S)\right). \tag{5.5.21}$$

Therefore, we obtain that

$$\mathbb{E}[J(z_r)] = \frac{\pi}{8}\delta^2\omega U_I^2 \int_{\mathbb{S}^1} \left(\sum_{k,l} \chi_{k,l}\theta_k\theta_l\right) d\theta. \tag{5.5.22}$$

Covariance

We have:

$$J(z^S) - \mathbb{E}[J](z^S) = \pi\delta^2 \int_{\mathbb{S}^1} e^{-2i\omega\theta\cdot z^S} \Big[(S)^\theta_{det} 4\omega^2 \int_\Omega G^{(0)}_{2\omega}(s, z_r)\mu(s)Q_{2\omega}(s, z^S)ds \\ - (S)^\theta_{rand} Q_{2\omega}(z_r, z^S)\Big] d\theta.$$

Denote by

$$A_J(z^S) = 4\pi\delta^2\omega^2 \int_{\mathbb{S}^1} e^{-2i\omega\theta\cdot z^S} (S)^\theta_{det} \int_\Omega G^{(0)}_{2\omega}(s, z_r)\mu(s)Q_{2\omega}(s, z^S)ds d\theta,$$

and

$$B_J(z^S) = \pi\delta^2 \int_{\mathbb{S}^1} e^{-2i\omega\theta\cdot z^S} (S)^\theta_{rand} Q_{2\omega}(z_r, z^S) d\theta.$$

Then we can write the covariance function,

$$\operatorname{Cov}\left(J(z^S), J(z^{S'})\right) = \mathbb{E}\Big[\left(J(z^S) - \mathbb{E}[J(z^S)]\right)\overline{(J(z^{S'}) - \mathbb{E}[J(z^{S'})])}\Big],$$

in the form

$$\operatorname{Cov}\left(J(z^S), J(z^{S'})\right) = \mathbb{E}\Big[A(z^S)\overline{A(z^{S'})} + B(z^S)\overline{B_J(z^{S'})} + A_J(z^S)\overline{B_J(z^{S'})} + \overline{A_J(z^S)}B_J(z^{S'})\Big].$$

We will now compute the first two terms separately and then we deal with the double products.

The speckle term $A_J\overline{A_J}$: From

$$A_J(z^S)\overline{A_J(z^{S'})} = 16\pi^2\delta^4\omega^4 \int_{\mathbb{S}^1} e^{-2i\omega\theta\cdot(z^S-z^{S'})}|(S)^\theta_{det}|^2 \int\int_{\Omega\times\Omega} G^{(0)}_{2\omega}(s,z_r)\overline{G^{(0)}_{2\omega}(s',z_r)}\mu(s)\overline{\mu(s')}Q_{2\omega}(s,z^S)\overline{Q_{2\omega}(s',z^{S'})}dsds'd\theta,$$

it follows by using (5.3.21) that

$$A_J(z^S)\overline{A_J(z^{S'})} = 16\pi^2\delta^4\omega^8U_I^4 \int_{\mathbb{S}^1} e^{-2i\omega\theta\cdot(z^S-z^{S'})}|\sum_{k,l}\chi_{k,l}\theta_k\theta_l|^2d\theta \int\int_{\Omega\times\Omega} G^{(0)}_{2\omega}(s,z_r)\overline{G^{(0)}_{2\omega}(s',z_r)}\mu(s)\overline{\mu(s')}Q_{2\omega}(s,z^S)\overline{Q_{2\omega}(s',z^{S'})}dsds'.$$

If we write $C_\mu(s,s') = \mathbb{E}[\mu(s)\mu(s')]$, then we find that

$$\mathbb{E}[A_J(z^S)\overline{A_J(z^{S'})}] = 16\pi^2\delta^4\omega^8U_I^4 \int_{\mathbb{S}^1} e^{-2i\omega\theta\cdot(z^S-z^{S'})}|\sum_{k,l}\chi_{k,l}\theta_k\theta_l|^2d\theta \int\int_{\Omega\times\Omega} G^{(0)}_{2\omega}(s,z_r)\overline{G^{(0)}_{2\omega}(s',z_r)}C_\mu(s,s')Q_{2\omega}(s,z^S)\overline{Q_{2\omega}(s',z^{S'})}dsds',$$

since μ is real.

As previously, we assume that the medium noise is localized and stationary on its support (which is Ω_μ). We note σ_μ the standard deviation of the process μ and l_μ its correlation length. We can then write

$$\mathbb{E}[A_J(z^S)\overline{A_J(z^{S'})}] = 16\pi^2\delta^4\omega^8U_I^4\sigma_\mu^2l_\mu^2 \int_{\mathbb{S}^1} e^{-2i\omega\theta\cdot(z^S-z^{S'})}|\sum_{k,l}\chi_{k,l}\theta_k\theta_l|^2d\theta \int_{\Omega_\mu} |G^{(0)}_{2\omega}(s,z_r)|^2Q_{2\omega}(s,z^S)\overline{Q_{2\omega}(s,z^{S'})}ds.$$

The term $\mathbb{E}[A_J(z^S)\overline{A_J(z^{S'})}]$ shows the generation of a non localized speckle image, creating random secondary peaks. We will later estimate the size of those peaks in order to find the signal-to-noise ratio. We compute the typical size of this term. We get, using (5.5.21):

$$\mathbb{E}[A_J(z^S)\overline{A_J(z^{S'})}] \approx 4\pi^2U_I^4\delta^4\omega^6\sigma_\mu^2l_\mu^2 \int_{\mathbb{S}^1}|\sum_{k,l}\chi_{k,l}\theta_k\theta_l|^2d\theta \int_{\Omega_\mu}|G^{(0)}_{2\omega}(s,z_r)|^2 \text{ Im } G^{(0)}_{2\omega}(s,z^S) \text{ Im } G^{(0)}_{2\omega}(s,z^{S'})ds. \quad (5.5.23)$$

Then we use the facts that

$$|G^{(0)}_{2\omega}(x,y)| \approx \frac{1}{4\sqrt{\pi 2\omega}}|x-y|^{-1/2}$$

and

$$\text{Im } G^{(0)}_{2\omega}(x,y) = \frac{1}{4}J_0(2\omega|x-y|) \approx \frac{\cos\left(2\omega|x-y|-\pi/4\right)}{4\sqrt{\pi\omega}}|x-y|^{-1/2}$$

if $|x-y| >> 1$. Then, as previously, we write $\Omega_\mu = \Omega_\mu \backslash B(z_r,\omega^{-1}) \cup B(z_r,\omega^{-1})$. Using (5.5.23), we arrive at

$$\mathbb{E}[A_J(z_r)\overline{A_J(z_r)}] \approx 4\pi^2 U_I^4\delta^4\omega^6\sigma_\mu^2 l_\mu^2 \int_{\mathbb{S}^1} |\sum_{k,l}\chi_{k,l}\theta_k\theta_l|^2 d\theta$$

$$\left(\frac{1}{512\pi^2\omega^2}\int_{\Omega_\mu\backslash B(z_r,\omega^{-1})}\frac{\cos^2\left(2\omega|s-z_r|-\pi/4\right)}{|s-z_r|^2}ds + \frac{1}{16}\int_{B(z_r,\omega^{-1})}|G^{(0)}_{2\omega}(s,z_r)|^2 J_0(2\omega|s-z_r|)^2 ds\right),$$

which yields

$$\mathbb{E}[A_J(z_r)\overline{A_J(z_r)}] \approx \frac{\pi}{128}U_I^4\delta^4\omega^4\sigma_\mu^2 l_\mu^2 \log(\omega \text{ diam } \Omega_\mu)\int_{\mathbb{S}^1}|\sum_{k,l}\chi_{k,l}\theta_k\theta_l|^2 d\theta. \qquad (5.5.24)$$

The localized term $B_J\overline{B_J}$: We have

$$B_J(z^S)\overline{B_J(z^{S'})} = \pi^2\delta^4 Q_{2\omega}(z_r,z^S)\overline{Q_{2\omega}(z_r,z^{S'})}\int_{\mathbb{S}^1} e^{-2i\omega\theta\cdot(z^S-z^{S'})}|(S)^\theta_{rand}|^2 d\theta.$$

Using (5.3.22) and (5.3.20) we have that $(S)^\theta_{rand}$ can be re-written as

$$(S)^\theta_{rand} = -\omega^2 U_I^2\int_\Omega \left(\mu(y)e^{i\omega\theta\cdot y} - \mu(z_r)e^{i\omega\theta\cdot z_r}\right) \left[\sum_{k,l}\chi_{k,l}\left(\theta_k\theta\cdot\nabla\partial_{x_l}G^{(0)}_\omega(z_r,y) + \theta_l\theta\cdot\nabla\partial_{x_k}G^{(0)}_\omega(z_r,y)\right)\right]dy.$$

We need to get an estimate on S^θ_{rand}'s variance. As in section 5.2 we have the following estimate for any $0<\alpha'<1/2$:

$$\frac{1}{4}|y-z_r|^{\alpha'}\left|\partial_{x_k}\partial_{x_l}H_0^1(\omega|y-z_r|)\right| \le \frac{1}{2}\min\left(1,\sqrt{\frac{2}{\pi}}\omega^{3/2}|y-z_r|^{\alpha'-1/2}\right)\max\left(1,|y-z_r|^{\alpha'-2}\right).$$

We get, for any $\alpha' < \min(\alpha, \frac{1}{2})$,

$$|S^{\theta}_{rand}| \leq \omega^2 U_I^2 \|\mu\|_{\mathcal{C}^{0,\alpha'}} \max_{k,l} |\chi_{k,l}| \, \omega^{2-2\alpha'} \left[\frac{8\sqrt{2\pi}}{3/2+\alpha'} \left(\omega \text{diam } \Omega_\mu\right)^{3/2+\alpha'} + \frac{\pi}{\alpha'} \right],$$

and

$$\left| \mathbb{E}[B_J(z^S)\overline{B_J(z^{S'})}] \right| \leq \frac{128\pi^3}{(3/2+\alpha')^2} \omega^{4-2\alpha'} \delta^4 U_I^4 \max_{k,l} |\chi_{k,l}|^2 \, \mathbb{E}\left[\|\mu\|^2_{\mathcal{C}^{0,\alpha'}} \right] \left[\left(\omega \text{diam } \Omega_\mu\right)^{3+2\alpha'} + \frac{1}{\alpha'} \right] Q_{2\omega}(z_r, z^S) \overline{Q_{2\omega}(z_r, z^{S'})}.$$

Note that $Q_{2\omega}(z_r, z^S)$, defined in (5.4.5), behaves like $\frac{1}{8\omega} J_0(2\omega|z_r - z^S|)$ which decreases like $|z_r - z^S|^{-1/2}$ as $|z_r - z^S|$ becomes large. The term B_J is localized around z_r. It may shift, lower or blur the main peak but it will not contribute to the speckle field on the image. We still need to estimate its typical size at point z_r in order to get the signal-to-noise ratio at point z_r. Using (5.5.21) and (5.5.5) we get

$$\mathbb{E}[B_J(z_r)\overline{B_J(z_r)}] \leq \frac{2^{17+\alpha}\pi^3}{(3/2+\alpha')^2} \frac{e}{\alpha - \alpha'} \omega^{2-2\alpha'} \delta^4 U_I^4 \max_{k,l} |\chi_{k,l}|^2 \left[\left(\omega \text{diam } \Omega_\mu\right)^{3+2\alpha'} + \frac{1}{\alpha'} \right] \frac{\sigma_\mu^2}{l_\mu^{2\alpha}}.$$

We can write $\left(\omega \text{diam } \Omega_\mu\right)^{3+2\alpha'} \leq \left(\omega \text{diam } \Omega_\mu\right)^{3+2\alpha} + 1$. We can take $\alpha' = \frac{\alpha}{2}$. Let $C = \frac{2^{18+1/2}\pi^3 e}{(3/2)^2}$. We get that

$$\mathbb{E}[B_J(z_r)\overline{B_J(z_r)}] \leq C\omega^2 \min\left(\omega^{-2\alpha}, 1\right) \delta^4 U_I^4 \max_{k,l} |\chi_{k,l}|^2 \, \frac{\sigma_\mu^2}{l_\mu^{2\alpha}} \left[\left(\omega \text{diam } \Omega_\mu\right)^{3+2\alpha} + 1 \right]. \tag{5.5.25}$$

Remark 5.5.2. *We note that even though the term B_J is localized, meaning it would not create too much of a speckle far away from the reflector, it is still the dominant term of the speckle field around the reflector's location.*

The double products $A_J\overline{B_J}$ and $\overline{A_J}B_J$: This third term has the size of the geometric mean of the first two terms A_J and B_J. So we only need to concentrate on the first two terms. Also this term is still localized because of $Q(z_r, z^S)$ that decreases as $|z_r - z^S|^{-1/2}$.

Signal-to-noise ratio

As before, we define the signal-to-noise ratio $(SNR)_J$ by (5.5.2). Using (5.5.22), (5.5.24) and (5.5.25),

$$\frac{\mathbb{E}[J(z_r)]}{(Var(J(z_r))^{\frac{1}{2}}} \geq \frac{l_\mu^\alpha \left(\int_{\mathbb{S}^1} \left(\sum_{k,l} \chi_{k,l} \theta_k \theta_l \right) d\theta \right)}{\sqrt{C}\sigma_\mu \min(\omega^{-\alpha}, 1) \max_{k,l} |\chi_{k,l}| \sqrt{(\omega \text{diam } \Omega_\mu)^{3+2\alpha} + 1}}.$$

The difference here with the standard backpropagation is that the (SNR) does not depend on neither the dielectric contrast of the particle, the nonlinear susceptibility nor even the particle's volume. All the background noise created by the propagation of the illuminating wave in the medium is filtered because the small inhomogeneities only scatter waves at frequency ω. The nanoparticle is the only source at frequency 2ω so it does not need to stand out from the background. The perturbations seen on the image J are due to travel time fluctuations of the wave scattered by the nanoparticle (for the speckle field) and to the perturbations of the source field at the localization of the reflector (for the localized perturbation). The second-harmonic image is more resolved than the fundamental frequency image.

5.5.4 Stability with respect to measurement noise

We now compute the signal-to-noise ratio in the presence of measurement noise without any medium noise ($\mu = 0$). The signal u_s and v are corrupted by an additive noise $\nu(x)$ on $\partial\Omega$. In real situations it is of course impossible to achieve measurements for an infinity of plane waves illuminations. So in this part we assume that the functional J is calculated as an average over n different illuminations, uniformly distributed in $\mathbb{S}^1$. We consider, for each $j \in [0, n]$, an independent and identically distributed random process $\nu^{(j)}(x),\ x \in \partial\Omega$ representing the measurement noise. We use the model of [21]: if we assume that the surface of Ω is covered with sensors half a wavelength apart and that the additive noise has variance σ and is independent from one sensor to another one, we can model the additive noise process by a Gaussian white noise with covariance function:

$$\mathbb{E}(\nu(x)\overline{\nu(x')}) = \sigma_\nu^2 \delta(x - x'),$$

where $\sigma_\nu = \sigma^2 \frac{\lambda}{2}$.

Standard backpropagation

We write, for each $j \in [0, n]$, $u_s^{(j)}$ as

$$u_s^{(j)}(x) = -2\pi\delta^2 \frac{\sigma_r - 1}{\sigma_r + 1} U_I e^{i\omega\theta^{(j)}\cdot z_r} \nabla G_\omega^{(0)}(x, z_r) \cdot (i\omega\theta^{(j)}) + o(\delta^2) + \nu^{(j)}(x),$$

where $\nu^{(j)}$ is the measurement noise associated with the j-th illumination. We can write I as

$$I(z^S) = \frac{1}{n} \sum_{j=1}^{n} \int_{\partial\Omega} \frac{1}{i\omega} e^{-i\omega\theta^{(j)}\cdot z^S} (\theta^{(j)})^\top \overline{\nabla G_\omega^{(0)}(x, z^S)} u_s(x) dx,$$

Further,

$$I(z^S) = -2\pi\delta^2 \frac{\sigma_r - 1}{\sigma_r + 1} U_I \frac{1}{n} \sum_{j=1}^{n} e^{i\omega\theta^{(j)}\cdot(z_r - z^S)} (\theta^{(j)})^\top R_\omega(z_r, z^S)\theta^{(j)} + \frac{1}{n} \sum_{j=1}^{n} \int_{\partial\Omega} \frac{1}{i\omega} e^{-i\omega\theta^{(j)}\cdot z^S} (\theta^{(j)})^\top \overline{\nabla G_\omega^{(0)}(x, z^S)} \nu^{(j)}(x) dx.$$

We get that

$$\mathbb{E}[I(z^S)] = -2\pi\delta^2 \frac{\sigma_r - 1}{\sigma_r + 1} U_I \frac{1}{n} \sum_{j=1}^{n} e^{i\omega\theta^{(j)}\cdot(z_r - z^S)} (\theta^{(j)})^\top R_\omega(z_r, z^S)\theta^{(j)},$$

so that, using (5.5.8) and (5.5.7)

$$\mathbb{E}[I(z_r)] \sim -\frac{\pi(\sigma_r - 1)}{4(\sigma_r + 1)} \omega\delta^2 U_I. \tag{5.5.26}$$

We compute the covariance

$$Cov(I(z^S), I(z^{S'})) = \mathbb{E}\left[\frac{1}{n^2} \left(\sum_{j=1}^{n} \frac{1}{i\omega} e^{-i\omega\theta^{(j)}\cdot z^S} \int_{\partial\Omega} \nu^{(j)}(x) (\theta^{(j)})^\top \overline{\nabla G_\omega^{(0)}(x, z^S)} dx \right) \left(\sum_{l=1}^{n} \frac{-1}{i\omega} e^{i\omega\theta^{(l)}\cdot z^{S'}} \int_{\partial\Omega} \nu^{(l)}(x') (\theta^{(l)})^\top \nabla G_\omega^{(0)}(x', z^{S'}) dx' \right) \right],$$

and obtain that

$$Cov(I(z^S), I(z^{S'})) = \sigma^2 \frac{\lambda}{2} \frac{1}{\omega^2 n^2} \sum_{j=1}^{n} e^{-i\omega\theta^{(j)}\cdot(z^S - z^{S'})} (\theta^{(j)})^\top R_\omega(z^S, z^{S'})\theta^{(j)}.$$

The signal-to-noise ratio is given by

$$(SNR)_I = \frac{\mathbb{E}[I(z_r)]}{(Var(I(z_r))^{\frac{1}{2}}}.$$

If we compute

$$Var(I(z_r)) \sim \sigma^2 \frac{\pi}{8\omega^2 n},$$

then $(SNR)_I$ can be expressed as

$$(SNR)_I = \frac{\sqrt{\pi n}\delta^2\omega^2[\sigma_r - 1]U_I}{[\sigma_r + 1]\sigma}.$$

The backpropagation functional is very stable with respect to measurement noise. Of course, the number of measurements increases the stability because the measurement noise is averaged out. We will see in the following that the second-harmonic imaging is also pretty stable with respect to measurement noise.

Second-harmonic backpropagation

We write, for each $j \in [0, n]$, v_j as

$$v^{(j)}(x) = -\delta^2(2\omega)^2 \left(\sum_{k,l} \chi_{k,l} \partial_{x_k} U^{(j)}(z_r) \partial_{x_l} U^{(j)}(z_r) \right) G^{(0)}_{2\omega}(x, z_r) + \nu^{(j)}(x),$$

where ν_j is the measurement noise at the j-th measurement. Without any medium noise the source term (S) can be written as

$$(S)^{\theta^{(j)}} = \sum_{k,l} \chi_{k,l} \partial_{x_k} U^{(j)}(z_r) \partial_{x_l} U^{(j)}(z_r) = -\omega^2 U_I^2 e^{2i\omega\theta^{(j)}\cdot z_r} \sum_{k,l} \chi_{k,l} \theta^{(j)}_k \theta^{(j)}_l.$$

So we can write J as

$$J(z^S) = \frac{1}{n} \sum_{j=1}^{n} \int_{\partial\Omega} v^{(j)}(x) \overline{G^{(0)}_{2\omega}(x, z^S)} e^{-2i\omega\theta^{(j)}\cdot z^S} dx,$$

or equivalently,

$$J(z^S) = -\delta^2(2\omega)^2 \frac{1}{n} \sum_{j=1}^{n} (S)^{\theta^{(j)}} \int_{\partial\Omega} G^{(0)}_{2\omega}(x, z_r) \overline{G^{(0)}_{2\omega}(x, z^S)} e^{-2i\omega\theta^{(j)}\cdot z^S} dx$$
$$+ \frac{1}{n} \sum_{j=1}^{n} \int_{\partial\Omega} \nu^{(j)}(x) \overline{G^{(0)}_{2\omega}(x, z^S)} e^{-2i\omega\theta^{(j)}\cdot z^S} dx.$$

We get that

$$\mathbb{E}[J(z^S)] = -\delta^2(2\omega)^2\frac{1}{n}\sum_{j=1}^{n}(S)^{\theta^{(j)}}e^{-2i\omega\theta^{(j)}\cdot z^S}Q_{2\omega}(z_r, z^S),$$

so that, using (5.5.21):

$$\mathbb{E}[J(z_r)] \sim \delta^2 U_I^2\frac{\omega^3}{2n}\sum_{k,l,j}\chi_{k,l}\theta_k^{(j)}\theta_l^{(j)}.$$

We can compute the covariance

$$Cov(J(z^S), J(z^{S'})) = \mathbb{E}\Bigg[\frac{1}{n^2}\left(\sum_{j=1}^{n}e^{-2i\omega\theta^{(j)}\cdot z^S}\int_{\partial\Omega}\nu^{(j)}(x)\overline{G_{2\omega}^{(0)}(x, z^S)}dx\right)$$
$$\left(\sum_{l=1}^{n}e^{2i\omega\theta^{(l)}\cdot z^{S'}}\int_{\partial\Omega}\nu^{(l)}(x)G_{2\omega}^{(0)}(x', z^{S'})dx'\right)\Bigg],$$

which yields

$$Cov(J(z^S), J(z^{S'})) = \sigma^2\frac{\lambda}{2}Q_{2\omega}(z^{S'}, z^S)\frac{1}{n^2}\sum_{j=1}^{n}e^{-2i\omega\theta^{(j)}\cdot(z^S - z^{S'})}.$$

Now we have

$$Var(J(z_r))^{1/2} \sim \frac{\sigma}{2\omega}\sqrt{\frac{\pi}{2n}}.$$

The signal-to-noise ratio,

$$(SNR)_J = \frac{\mathbb{E}[J(z_r)]}{(Var(J(z_r))^{\frac{1}{2}}},$$

is given by

$$(SNR)_J = \frac{2\delta^2\omega^2 U_I\left(\sum_j\sum_{k,l}\chi_{k,l}\theta_k^{(j)}\theta_l^{(j)}\right)}{\pi\sigma\sqrt{n}}.$$

Even though it appears that the (SNR) is proportional to $\frac{1}{\sqrt{n}}$, the term $\sum_j\theta_k^{(j)}\theta_l^{(j)}$ is actually much bigger. In fact, if we pick $\theta^{(j)} = \frac{2j\pi}{n}$ we get that

$$\sum_{k,l}\chi_{k,l}\sum_j\theta_k^{(j)}\theta_l^{(j)} = \sum_{j=1}^{n}\left(\chi_{1,1}\cos^2\frac{2j\pi}{n} + \chi_{2,2}\sin^2\frac{2j\pi}{n} + 2\chi_{1,2}\sin\frac{2j\pi}{n}\cos\frac{2j\pi}{n}\right),$$

and hence,

$$\sum_{k,l}\chi_{k,l}\sum_j\theta_k^{(j)}\theta_l^{(j)} \sim \frac{n}{2}\max[\chi_{1,1}, \chi_{2,2}].$$

Therefore, we can conclude that

$$(SNR)_J = \frac{\delta^2 \omega^2 U_I^2 \sqrt{n} \max[\chi_{1,1}, \chi_{2,2}]}{\pi \sigma_\nu}.$$

The signal-to-noise ratio is very similar to the one seen in the classic backpropagation case. So the sensitivity with respect to relative measurement noise should be similar. It is noteworthy that in reality, due to very small size of the (SHG) signal (χ has a typical size of 10^{-12} m/V), the measurement noise levels will be higher for the second-harmonic signal.

5.6 Numerical results

5.6.1 The direct problem

We consider the medium to be the square $[-1, 1]^2$. The medium has an average propagation speed of 1, with random fluctuations with Gaussian statistics (see Figure 5.6.2). To simulate μ we use the algorithm described in [21] which generates random Gaussian fields with Gaussian covariance function and take a standard deviation equal to 0.02 and a correlation length equal to 0.25. We consider a small reflector in the medium $\Omega_r = z_r + \delta B(0, 1)$ with $z_r = (-0.2, 0.5)$ and $\delta = 0.004/\pi$, represented on Figure 5.6.1. The contrast of the reflector is $\sigma_r = 2$. We fix the frequency to be $\omega = 8$. We get the boundary data u_s when the medium is illuminated by the plane wave $U_I(x) = e^{i\omega\theta \cdot x}$. The correlation length of the medium noise was picked so that it has a similar size as the wavelength of the illuminating plane wave. We get the boundary data by using an integral representation for the field $u_{s,\theta}$. We also compute the boundary data for the second-harmonic field v. We compute the imaging functions I and J respectively defined in (5.4.1) and (5.4.4), averaged over two different lightning settings. (see Figures 5.6.7 and 5.6.8 for instance).

5.6.2 The imaging functionals and the effects of the number of plane wave illuminations

We compute the imaging functionals I and J respectively defined in (5.4.1) and (5.4.4), averaged over four different illuminations settings. We fix the noise level ($\sigma_\mu = 0, 02$), the volume of the particle ($v_r = 10^{-2}$) and the contrast $\sigma_r = 2$. In Figures 5.6.7 and 5.6.8 the image is obtained after backpropagating the boundary data from one

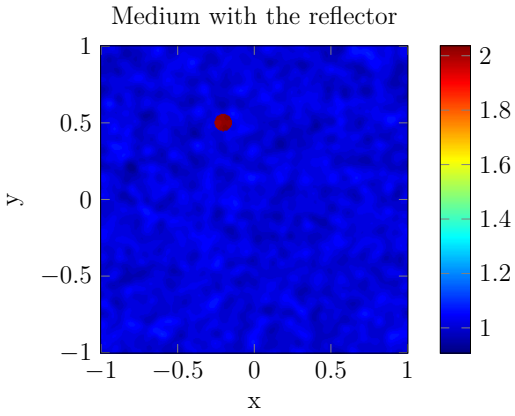

Figure 5.6.1

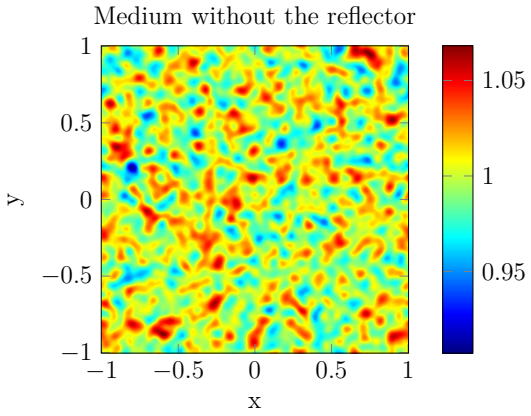

Figure 5.6.2

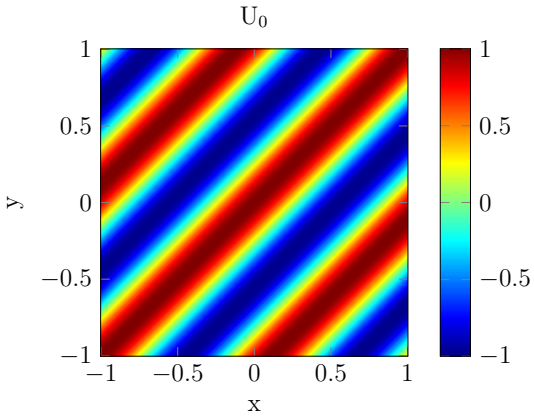

Figure 5.6.3 Incoming field U_I.

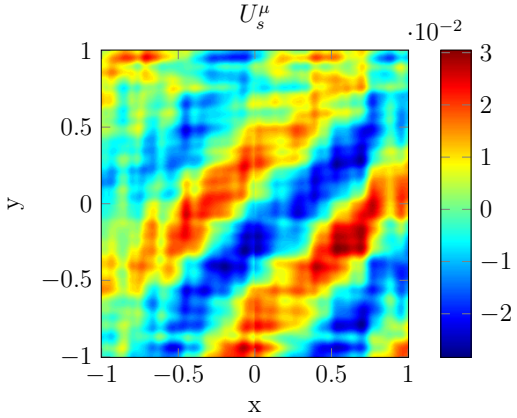

Figure 5.6.4

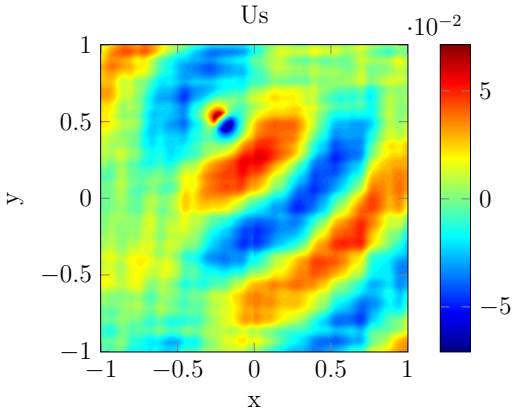

Figure 5.6.5

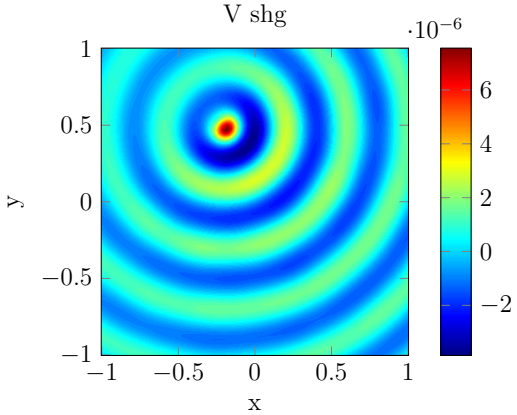

Figure 5.6.6

illumination ($\theta = 0$). On the following graphs, we average over several illumination angles:

- 4 uniformly distributed angles for Figures 5.6.9 and 5.6.10.
- 8 uniformly distributed angles for Figures 5.6.11 and 5.6.12.
- 32 uniformly distributed angles for Figures 5.6.13 and 5.6.14.

As predicted, the shape of the spot on the fundamental frequency imaging is very dependant on the illumination angles, whereas with second-harmonic imaging we get an acceptable image with only one illumination. In applications, averaging over different illumination is useful because it increases the stability with respect to measurement noise. It is noteworthy that, as expected, the resolution of the second-harmonic image is twice higher than the regular imaging one.

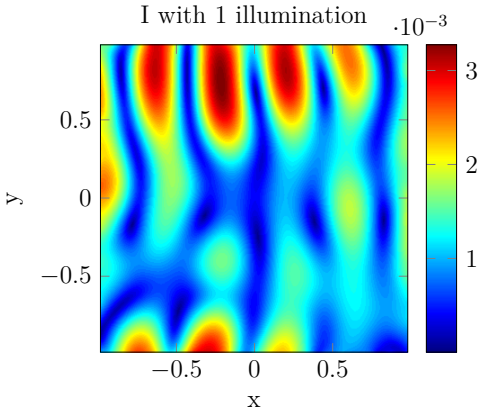

Figure 5.6.7

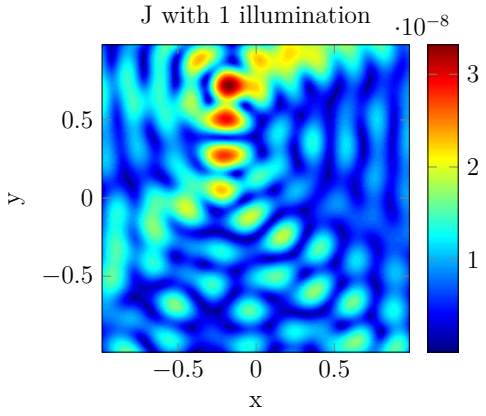

Figure 5.6.8

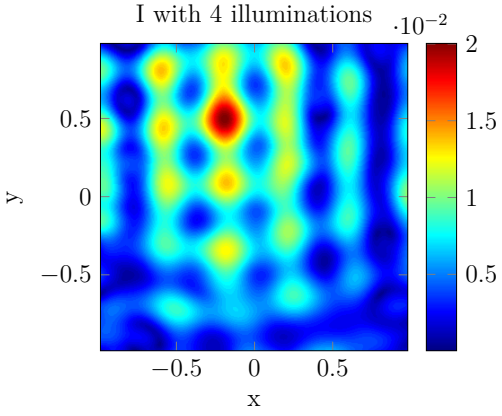

Figure 5.6.9

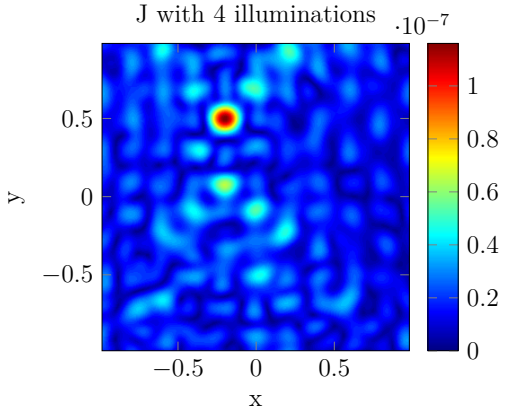

Figure 5.6.10

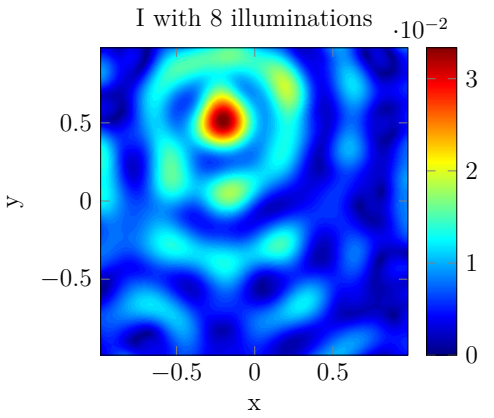

Figure 5.6.11

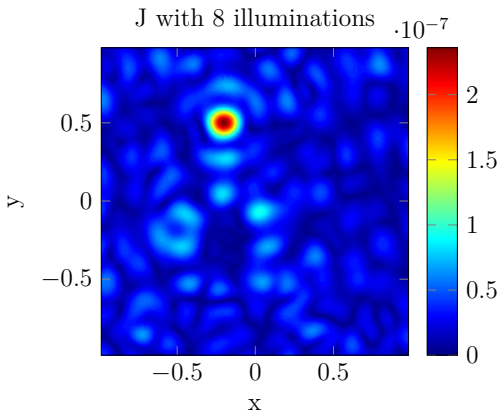

Figure 5.6.12

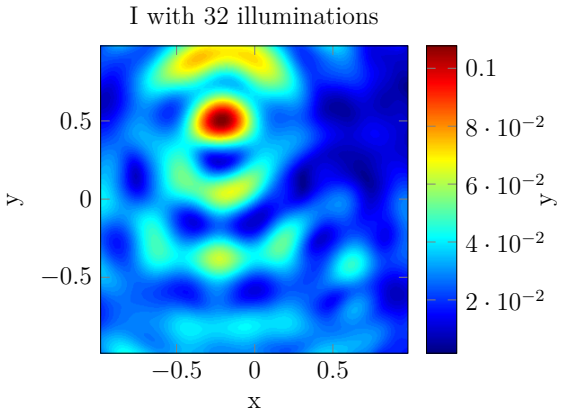

Figure 5.6.13

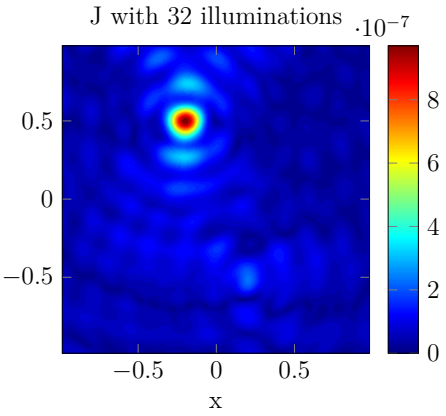

Figure 5.6.14

5.6.3 Statistical analysis

Stability with respect to medium noise

Here we show numerically that the second-harmonic imaging is more stable with respect to medium noise. In Figure 5.6.15, we plot the standard deviation of the error $|z_{est} - z_r|$ where z_{est} is the estimated location of the reflector. For each level of medium noise we compute the error over 120 realizations of the medium, using the same parameters, as above. The functional imaging J is clearly more robust than earlier.

Effect of the volume of the particle

We show numerically that the quality of the second-harmonic image does not depend on the volume of the particle. We fix the medium noise level ($\sigma_\mu = 0.02$) and plot the standard deviation of the error with respect to the volume of the particle (Figure 5.6.16).

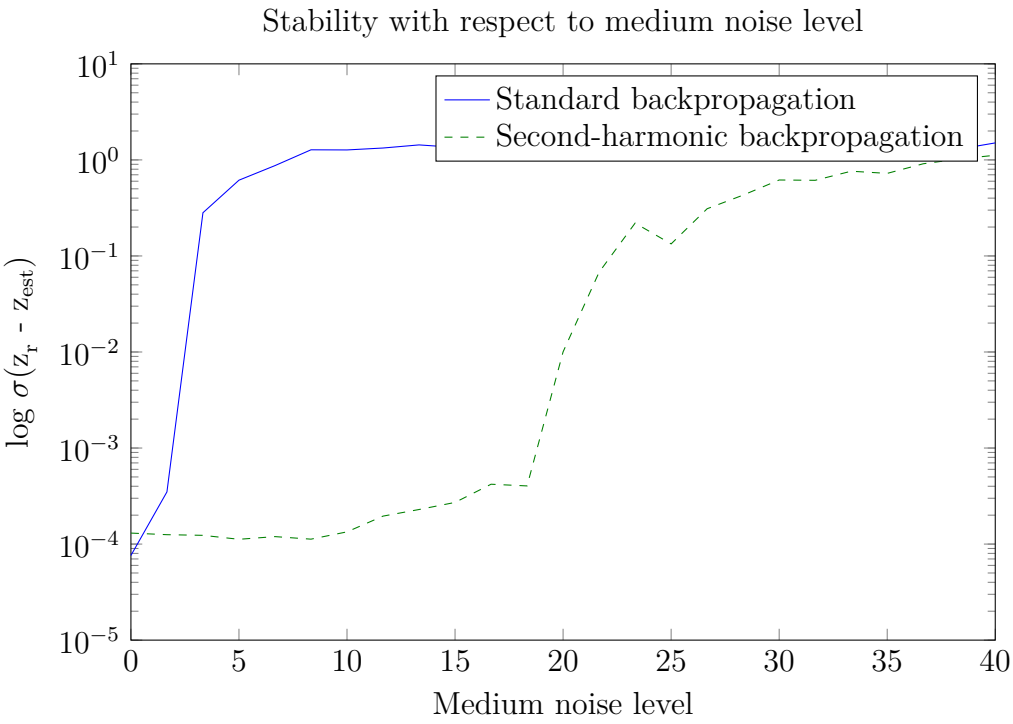

Figure 5.6.15 Standard deviation of the localization error with respect to the medium noise level for standard backpropagation (top) and second-harmonic image (bottom).

We can see that if the particle is too small, the fundamental backpropagation algorithm cannot differentiate the reflector from the medium and the main peak gets buried in the speckle field. The volume of the particle does not have much influence on the second-harmonic image quality.

Stability with respect to measurement noise

We compute the imaging functionals with a set of data obtained without any medium noise and perturbed with a Gaussian white noise for each of 8 different illuminations. For each noise level, we average the results over 100 images. Figure 5.6.17 shows that both functionals have similar behaviors.

As mentioned before, in applications, the weakness of the SHG signal will induce a much higher relative measurement noise than in the fundamental data. Since the model we use for measurement noise has a zero expectation, averaging measurements over different illuminations can improve the stability significantly as shown in Figure 5.6.18, where the images have been obtained with 16 illuminations instead of 8.

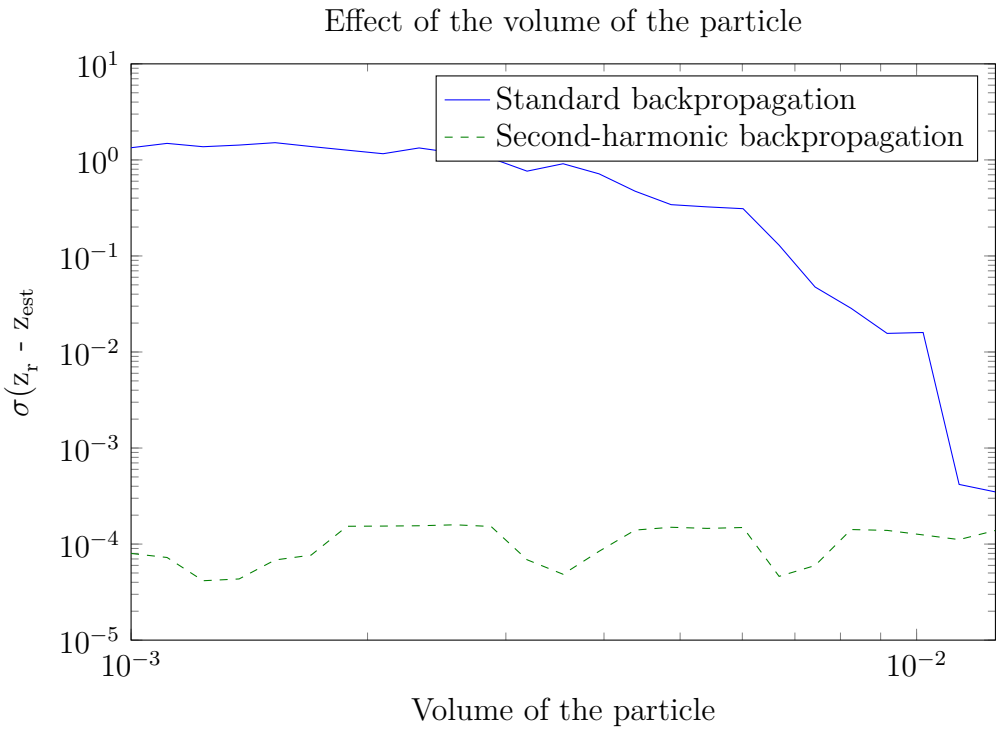

Figure 5.6.16 Standard deviation of the localization error with respect to the reflector's volume (log scale) for standard backpropagation (top) and second-harmonic image (bottom).

5.7 Concluding remarks

We have studied how second-harmonic imaging can be used to locate a small reflector in a noisy medium, gave asymptotic formulas for the second-harmonic field, and investigated statistically the behavior of the classic and second-harmonic backpropagation functionals. We have proved that the backpropagation algorithm is more stable with respect to medium noise. Our results can also be extended to the case of multiple scatterers as long as they are well-separated.

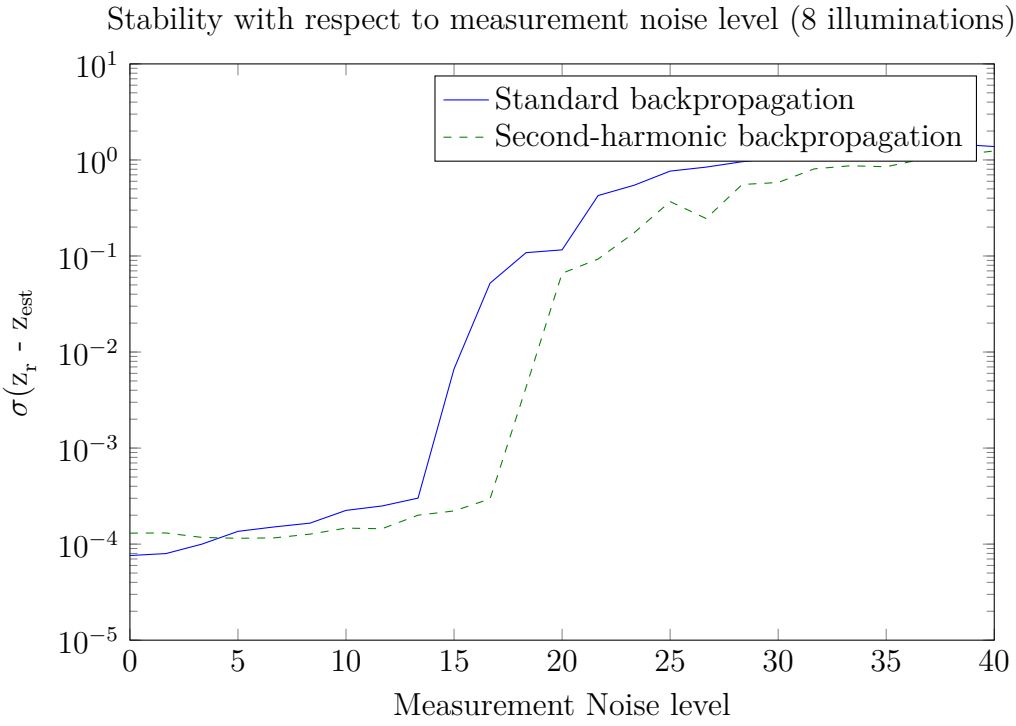

Figure 5.6.17 Standard deviation of the localization error with respect to measurement noise level for standard backpropagation (top) and second-harmonic image (bottom).

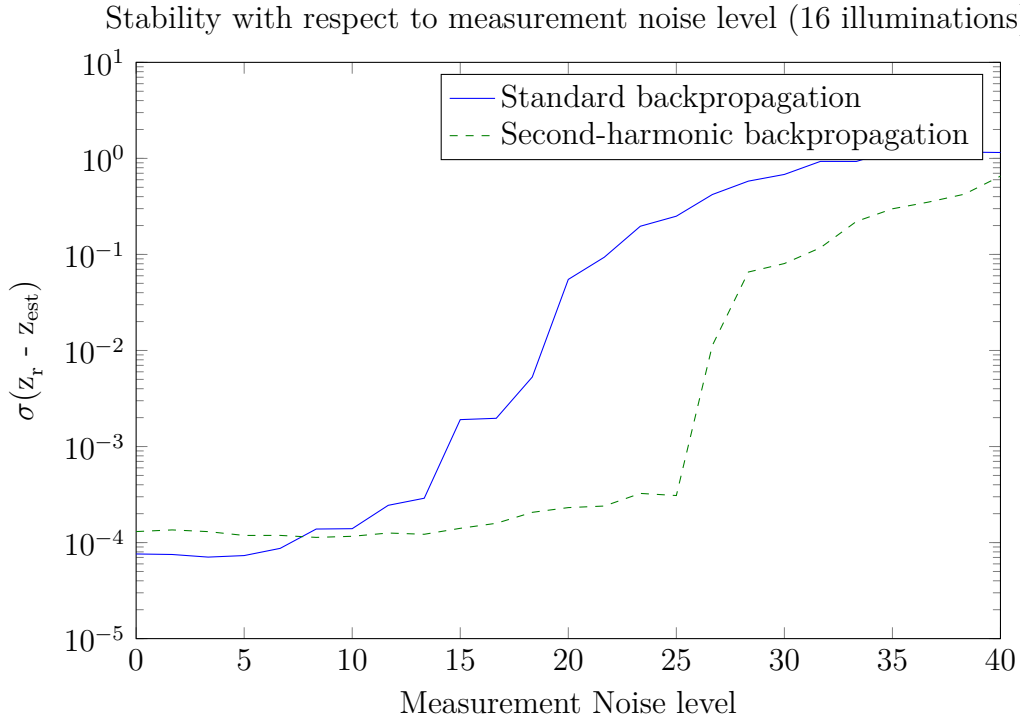

Figure 5.6.18 Standard deviation of the localization error with respect to measurement noise level, when averaged over 16 illuminations of angles uniformly distributed between 0 and 2π for standard backpropagation (top) and second-harmonic image (bottom).

Conclusion

This thesis is divided in two parts: some mathematical modeling of new hybrid imaging techniques, and a theoretical study of nanoparticle imaging using wave equations.

In the first part we showed how hybrid techniques allowed the recovery of high-resolution images from internal data, as opposed to boundary data for "single-wave" classical imaging processes. A new class of inverse problems arises from these new methods. We adapted some classical methods to this new class of problems - such as the optimal control least square approach - and we also introduced a new direct stable reconstruction method, called the viscosity method, for recovering the electrical conductivity from an internal current. The viscosity method is an evolution in conductivity imaging as it provides a fast and stable reconstruction of the electrical conductivity. In the first chapter, we were able to prove that the reconstruction converges for a broad class of discontinuous coefficients that model well the regularity of the coefficients one can expect *in vivo*. In the second chapter we proved the convergence for a class of smoother coefficients and different boundary conditions. We expect it can be adapted to different boundary conditions modeling different experiments. These new hybrid imaging techniques have a great potential and the knowledge of internal data opens the way to imaging anisotropic quantities such as conductivity tensors or elasticity tensors.

Regarding surface plasmons, recovering the resonance of the far field from Maxwell's equations is only the first step. The final goal is to be able to quantitatively understand the phenomenon and to be able to predict the behavior of one or many particles without solving the full $3D$ Maxwell system. The small volume approximation done in Chapter 4 erases the size dependence of the eigen value problem: it becomes only shape dependent. The next step is to recover the size dependance that has been observed experimentally as well as the higher order multipolar moments. For instance, for larger particles ($\sim 100\,nm$) a quadrupole moment can be measured [89]. An understanding of the near field would allow the computation of the temperature field in a radius of a few nanometers around the particle where temperature measurements are very challenging.

This is a crucial step for the development of fluence measurement techniques [115] and photothermal therapy [74], one of the most promising cancer therapy method.

In our study of second harmonic generation, we quantified the efficiency of a backpropagation algorithm in the presence of medium noise when the data satisfies the Helmholtz equation. These algorithms are currently being used in the next generation of ultrasound imaging in order to obtain a very high number of image per second [59]. The computations done here contribute to quantifying the numerical efficiency of backpropagation algorithms in the electromagnetic case and can be extended to similar cases in acoustics.

Appendix A

Proof of the jump formula for the curl of $\mathcal{A}_D$

We want to prove the jump formula (4.4.8) for $\boldsymbol{\nu} \times \nabla \times \mathcal{A}_D$. The continuity of $\mathcal{A}_D^k[\boldsymbol{\phi}]$ is a consequence of the continuity of single layer potentials. Assume that $\boldsymbol{\phi}$ is a continuous tangential field. We first prove the jump relation for $k = 0$. For $z \in \mathbb{R}^3 \setminus \partial D$,

$$\nabla \times \mathcal{A}_D[\boldsymbol{\phi}](z) = \int_{\partial D} \nabla_z \times (\boldsymbol{\phi}(y)\Gamma(z,y))\, d\sigma(y).$$

So if $x \in \partial D$ and $z = x + h\boldsymbol{\nu}(x)$, then by using vector calculus we have:

$$\boldsymbol{\nu}(x) \times \nabla \times \mathcal{A}_D[\boldsymbol{\phi}](z) = \int_{\partial D} \Big[(\boldsymbol{\phi}(y) \cdot \boldsymbol{\nu}(x))\, \nabla_z \Gamma(z,y) - (\nabla_z \Gamma(z,y) \cdot \boldsymbol{\nu}(x))\, \boldsymbol{\phi}(y) \Big] d\sigma(y).$$

Since $\boldsymbol{\phi}$ is tangential, we have $\forall y \in \partial D, \boldsymbol{\nu}(y) \cdot \boldsymbol{\phi}(y) = 0$, so we can write

$$\boldsymbol{\nu}(x) \times \nabla \times \mathcal{A}_D[\boldsymbol{\phi}](z) = \int_{\partial D} \Big[(\boldsymbol{\phi}(y) \cdot [\boldsymbol{\nu}(x) - \boldsymbol{\nu}(y)])\, \nabla_z \Gamma(z,y) - (\nabla_z \Gamma(z,y) \cdot \boldsymbol{\nu}(x))\, \boldsymbol{\phi}(y) \Big] d\sigma(y).$$

Here, following the same idea as the one in the proof of the jump of the double layer potential in [51], we introduce

$$\mathcal{D}_D[1](z) = \int_{\partial D} \frac{\partial \Gamma}{\partial \boldsymbol{\nu}(y)}(z,y) d\sigma(y), \quad z \in \mathbb{R}^3 \setminus \partial D,$$

which takes the following values ([51, p. 48]):

$$\mathcal{D}_D[1](z) = \begin{cases} 0 \quad \text{if} \qquad z \in \mathbb{R}^3 \setminus \overline{D}, \\ -\dfrac{1}{2} \quad \text{if} \qquad z \in \partial D, \\ -1 \quad \text{if} \qquad z \in D. \end{cases} \tag{A.0.1}$$

We write

$$\boldsymbol{\nu}(x) \times \nabla \times \mathcal{A}_D[\boldsymbol{\phi}](z) = \boldsymbol{\phi}(x)\mathcal{D}_D[1](z) + f(z)$$

with

$$f(z) = \int_{\partial D} \Big[(\boldsymbol{\phi}(y) \cdot [\boldsymbol{\nu}(x) - \boldsymbol{\nu}(y)]) \nabla_z \Gamma(z,y)$$
$$-(\nabla_z \Gamma(z,y) \cdot [\boldsymbol{\nu}(x) - \boldsymbol{\nu}(y)])\, \boldsymbol{\phi}(y) - (\nabla_z \Gamma(z,y) \cdot \boldsymbol{\nu}(y))\, \boldsymbol{\phi}(y) - \frac{\partial \Gamma}{\partial \boldsymbol{\nu}(y)}(z,y) \boldsymbol{\phi}(x) \Big] d\sigma(y).$$

Using the fact that $\nabla_z \Gamma(z,y) = -\nabla_y \Gamma(z,y)$ we get

$$f(z) = \int_{\partial D} \Big[(\boldsymbol{\phi}(y) \cdot [\boldsymbol{\nu}(x) - \boldsymbol{\nu}(y)]) \nabla_z \Gamma(z,y)$$
$$- (\nabla_z \Gamma(z,y) \cdot [\boldsymbol{\nu}(x) - \boldsymbol{\nu}(y)])\, \boldsymbol{\phi}(y) + \frac{\partial \Gamma}{\partial \boldsymbol{\nu}(y)}(z,y)\, (\boldsymbol{\phi}(y) - \boldsymbol{\phi}(x)) \Big] d\sigma(y). \quad \text{(A.0.2)}$$

Now, we have only to prove that f is continuous across ∂D, i.e., when $t \to 0$, $f(z) = f(x + t\boldsymbol{\nu}(x)) \longrightarrow f(x)$. If we assume that it is true, then we can write for $z \in \mathbb{R}^3 \setminus \overline{D}$,

$$\boldsymbol{\nu}(x) \times \nabla \times \mathcal{A}_D[\boldsymbol{\phi}](z) = \Big[\boldsymbol{\phi}(x) \mathcal{D}_D[1](z) - \boldsymbol{\phi}(x) \mathcal{D}_D[1](x) + f(z) \Big] - \frac{\phi}{2}(x),$$

since $\mathcal{D}_D[1](x) = -1/2$. So, when $t \to 0^+$, we get

$$\boldsymbol{\nu}(x) \times \nabla \times \mathcal{A}_D[\boldsymbol{\phi}](x)\Big|_+ = \Big[-\boldsymbol{\phi}(x) \mathcal{D}_D[1](x) + f(x) \Big] - \frac{\phi}{2}(x).$$

Now we see that since $\boldsymbol{\phi}(y) \cdot \boldsymbol{\nu}(y) = 0, \quad \forall y \in \partial D$

$$-\boldsymbol{\phi}(x) \mathcal{D}_D[1](x) + f(x) = -\int_{\partial D} \frac{\partial \Gamma}{\partial \boldsymbol{\nu}(y)}(x,y) \boldsymbol{\phi}(x) d\sigma(y)$$
$$+ \int_{\partial D} \Big[(\boldsymbol{\phi}(y) \cdot \boldsymbol{\nu}(x)) \nabla_x \Gamma(x,y) - (\nabla_x \Gamma(x,y) \cdot \boldsymbol{\nu}(x)) + \frac{\partial \Gamma}{\partial \nu(y)}(x,y) \boldsymbol{\phi}(x) \Big] d\sigma(y),$$

which is exactly

$$-\boldsymbol{\phi}(x) \mathcal{D}_D[1](x) + f(x) = \int_{\partial D} \boldsymbol{\nu}(x) \times \nabla_x \times [\Gamma(x,y) \boldsymbol{\phi}(y)]\, d\sigma(y).$$

So the limit can be expressed as

$$\boldsymbol{\nu}(x) \times \nabla \times \mathcal{A}_D[\boldsymbol{\phi}](x)\Big|_+ = \int_{\partial D} \boldsymbol{\nu}(x) \times \nabla_x \times [\Gamma(x,y) \boldsymbol{\phi}(y)]\, d\sigma(y) - \frac{\phi}{2}(x).$$

The limit when $t \to 0^-$ is computed similarly and we find (4.4.8) for $k = 0$. The extension to $k > 0$ can be done because the difference between the double layer potential with kernel Γ^k and Γ is continuous; see, for instance, [51, p.47].

Now, we go back to the continuity of f defined by (A.0.2). We apply several results from [51] to get the continuity. The following lemma, which we state here for the sake of completeness, can be found in [51].

Lemma A.0.1. *Assume that the kernel K is continuous for all x in a neighborhood D_h of ∂D, $y \in \partial D$ and $x \neq y$. Assume that there exists $M > 0$ such that*

$$|K(x,y)| \leq M|x-y|^{-2}$$

and assume that there exists $m \in \mathbb{N}$ such that

$$|K(x_1,y) - K(x_2,y)| \leq M \sum_{j=1}^{m} |x_1 - y|^{-2-j} |x_1 - x_2|^j$$

for all $x_1, x_2 \in D_h$, $y \in \partial D$ with $2|x_1 - x_2| \leq |x_1 - y|$ and that

$$\left| \int_{\partial D \setminus S_{x,r}} K(z,y) d\sigma(y) \right| \leq M$$

for all $x \in \partial D$ and $z = x + h\boldsymbol{\nu}(x) \in D_h$ and all $0 < r < R$. Then,

$$u(z) = \int_{\partial D} K(z,y)[\phi(y) - \phi(x)] d\sigma(y)$$

belongs to $\mathcal{C}^{0,\alpha}(D_h)$ if $\phi \in \mathcal{C}^{0,\alpha}(\partial D)$.

It can be shown that

$$\left| \frac{\partial \Gamma(x,y)}{\partial \boldsymbol{\nu}(y)} - \frac{\partial \Gamma(z,y)}{\partial \boldsymbol{\nu}(y)} \right| \leq C \frac{|x-z|}{|z-y|^3}.$$

Using the above lemma with $m = 1$ and the kernel associated with the double layer potential gives

$$\int_{\partial D} \frac{\partial \Gamma}{\partial \boldsymbol{\nu}(y)}(z,y) \left[\boldsymbol{\phi}(y) - \boldsymbol{\phi}(x)\right] d\sigma(y) \longrightarrow \int_{\partial D} \frac{\partial \Gamma}{\partial \boldsymbol{\nu}(y)}(x,y) \left[\boldsymbol{\phi}(y) - \boldsymbol{\phi}(x)\right] d\sigma(y)$$

as $z \to x \in \partial D$.

We now make use of the following lemma from [51].

Lemma A.0.2. *Assume that the kernel $K(x,y)$ is continuous for all x in a closed domain Ω containing ∂D in its interior, $y \in \partial D$ and $x \neq y$. Assume that there exists $M > 0$ and $\alpha \in]0,2]$ such that*

$$|K(x,y)| \leq M|x-y|^{\alpha-2}$$

and assume that there exists $m \in \mathbb{N}$ such that

$$|K(x_1,y) - K(x_2,y)| \leq M \sum_{j=1}^{m} |x_1 - y|^{\alpha-2-j} |x_1 - x_2|^j$$

for all $x_1, x_2 \in D_h$, $y \in \partial D$ with $2|x_1 - x_2| \leq |x_1 - y|$. Then

$$u(x) = \int_{\partial D} K(x,y)\phi(y) d\sigma(y), \quad x \in \Omega$$

belongs to $\mathcal{C}^{0,\beta}(\Omega)$ *if* $\phi \in \mathcal{C}^{0,\alpha}(\partial D)$. $\beta \in]0,\alpha]$ *if* $\alpha \in]0,1[$, $\beta \in]0,1[$ *if* $\alpha = 1$ *and* $\beta \in]0,1]$ *if* $\alpha \in]1,2[$.

Using the fact that ∂D is of class $\mathcal{C}^2$, we have

$$|\boldsymbol{\nu}(x) - \boldsymbol{\nu}(y)| \leq |x - y|, \quad \forall x, y \in \partial D.$$

We can apply Lemma A.0.2 with $\alpha = 1$ and $m = 1$ to the second and third terms of f and get the continuity of

$$\int_{\partial D} \left[(\boldsymbol{\phi}(y) \cdot [\boldsymbol{\nu}(x) - \boldsymbol{\nu}(y)]) \nabla_z \Gamma(z,y) - (\nabla_z \Gamma(z,y) \cdot [\boldsymbol{\nu}(x) - \boldsymbol{\nu}(y)]) \boldsymbol{\phi}(y) \right] d\sigma(y) \tag{A.0.3}$$

when $z \to x \in \partial D$, which conclude the proof for a continuous tangential field ϕ. The formula can be extended to L^2_T by a density argument .

Appendix B

Proofs of some estimates in Chapter 5

B.1 Proof of (5.3.2)

Let R be large enough so that $\Omega_\mu \Subset B_R$, where B_R is the ball of radius R and center 0. Let $S_R = \partial B_R$ be the sphere of radius R, and introduce the Dirichlet-to-Neumann operator $\mathcal{T}$ on S_R:

$$\begin{aligned} \mathcal{T} \ : \ H^{1/2}(S_R) &\longrightarrow H^{-1/2}(S_R) \\ u &\longmapsto \mathcal{T}[u]. \end{aligned} \tag{B.1.1}$$

According to [110], $\mathcal{T}$ is continuous and satisfies

$$-\text{Re } \langle \mathcal{T}[u], u\rangle \geq \frac{1}{2R}\|u\|^2_{L^2(S_R)}, \quad \forall u \in H^{1/2}(S_R), \tag{B.1.2}$$

and

$$\text{Im } \langle \mathcal{T}[u], u\rangle > 0 \text{ if } u \neq 0. \tag{B.1.3}$$

Here, $\langle \, , \, \rangle$ denotes the duality pair between $H^{1/2}(S_R)$ and $H^{-1/2}(S_R)$. Now introduce the continuous bilinear form a:

$$\begin{aligned} H^1(B_R) \times H^1(B_R) &\longrightarrow \mathbb{C} \\ (u,v) &\longmapsto a(u,v) = \int_{B_R} (1+\mu)\nabla u \cdot \overline{\nabla v} - \omega^2 \int_{B_R} u\overline{v} - \langle \mathcal{T}[u], v\rangle \, , \end{aligned} \tag{B.1.4}$$

as well as the continuous bilinear form b:

$$\begin{aligned} H^1(B_R) &\longrightarrow \mathbb{C} \\ v &\longmapsto b(v) = \int_{B_R} \mu \nabla U_0 \cdot \overline{\nabla v}. \end{aligned} \tag{B.1.5}$$

Problem (5.2.4)-(5.2.5) has the following variational formulation: Find $u \in H^1(B_R)$ such that

$$a(u,v) = b(v) \ \ \forall v \in H^1(B_R). \tag{B.1.6}$$

With (B.1.2) one can show that

$$\text{Re } a(u,u) \geq C_1 \|\nabla u\|^2_{L^2(B_R)} - C_2 \|u\|^2_{L^2(B_R)}, \tag{B.1.7}$$

so that a is weakly coercive with respect to the pair $(H^1(B_R), L^2(B_R))$. Since the imbedding of $H^1(B_R)$ into $L^2(B_R)$ is compact we can apply Fredholm's alternative to problem (B.1.6). Hence, we deduce existence of a solution from uniqueness of a solution which easily follows by using identity (B.1.3).

Now we want to prove that if u is the solution of (B.1.6) then

$$\|u\|_{H^1(B_R)} \leq \|\mu\|_\infty. \tag{B.1.8}$$

We proceed by contradiction. Assume that $\forall n \in \mathbb{N}$, there exists $\mu_n \in L^\infty(B_R)$ compactly supported and $u_n \in H^1(B_R)$ solution of (B.1.6) such that

$$\|v_n\|_{H^1(B_R)} = 1, \quad \|\mu_n\|_\infty \longrightarrow 0.$$

$(v_n)_{n\in\mathbb{N}}$ is bounded in $H^1(B_R)$ so there exists a subsequence still denoted by v_n and $v^* \in H^1(B_R)$ such that $v_n \rightharpoonup v^*$ in $H^1(B_R)$ and $v_n \to v^*$ in $L^2(B_R)$. We want to prove that v_n converges strongly in $H^1(B_R)$ to v^* and that $v^* = 0$. This will contradict the fact that $\forall n,\ \|v_n\|_{H^1(B_R)} = 1$. Now since v_n is a solution of (B.1.6), we have

$$\int_{B_R} (1+\mu_n)\nabla v_n \cdot \overline{\nabla v_n} - \omega^2 \int_{B_R} v_n \overline{v_n} - \langle \mathcal{T} v_n, v_n \rangle = \int_{B_R} \mu_n \nabla U_0 \cdot \overline{\nabla v_n}.$$

We can write

$$\widetilde{a}(v_n, v_n) \longrightarrow 0,$$

where

$$\widetilde{a}(u,v) = \int_{B_R} \nabla u \cdot \overline{\nabla v} - \omega^2 \int_{B_R} u\overline{v} - \langle \mathcal{T} u, v \rangle, \quad \forall (u,v) \in H^1(B_r).$$

Since $v_n \rightharpoonup v^*$ in $H^1(B_R)$, $\widetilde{a}(v_n, v^*) \longrightarrow \widetilde{a}(v^*, v^*)$. Using (B.1.6) we get

$$\widetilde{a}(v_n, v^*) = \int_{B_R} \mu_n \left[\nabla U_0 \cdot \overline{\nabla v^*} - \nabla v_n \cdot \overline{\nabla v^*} \right] \longrightarrow 0 \quad (n \to \infty).$$

hence

$$\widetilde{a}(v^*, v^*) = 0.$$

We can also write

$$\widetilde{a}(v_n - v^*, v_n - v^*) = \widetilde{a}(v_n, v_n) - \widetilde{a}(v_n, v^*) - \widetilde{a}(v^*, v_n) + \widetilde{a}(v^*, v^*).$$

Since $\widetilde{a}$ is strongly continous on $H^(B_R)$, $\widetilde{a}(v_n, v^*) \longrightarrow \widetilde{a}(v^*, v^*) = 0$ $(n \to \infty)$ and $\widetilde{a}(v_n, v_n) \longrightarrow 0$. So,

$$\widetilde{a}(v_n - v^*, v_n - v^*) \longrightarrow 0.$$

Now we decompose $\widetilde{a} = \widetilde{a_c} + \widetilde{a_w}$ into a coercive part

$$\widetilde{a_c}(u,v) = \int_{B_R} \nabla u \cdot \overline{\nabla v} - \langle \mathcal{T} u, v \rangle$$

and a weakly continuous part:

$$\widetilde{a_w}(u,v) = -\omega^2 \int_{B_R} u\overline{v}.$$

Since $\widetilde{a_w}$ is weakly continuous, $\widetilde{a_w}(v_n - v^*, v_n - v^*) \longrightarrow 0$. Hence

$$\widetilde{a_c}(v_n - v^*, v_n - v^*) = \widetilde{a}(v_n - v^*, v_n - v^*) - \widetilde{a_w}(v_n - v^*, v_n - v^*) \longrightarrow 0, \quad (n \to \infty). \tag{B.1.9}$$

Using equation (B.1.9) together with the coercivity of $\widetilde{a_c}$ we get the strong convergence of v_n in $H^1(B_R)$:

$$\|v_n - v^*\|_{H^1(B_R)} \longrightarrow 0 \quad (n \to \infty).$$

Using the fact that $\widetilde{a}$ is weakly coercive with respect to the pair $(H^1(B_R), L^2(B_R))$ together with (B.1.3) we can show that

$$\widetilde{a}(v^*, v^*) = 0 \Rightarrow v^* = 0.$$

Hence the contradiction: $\|v_n\|_{H^1(B_R)} = 1$ and $v_n \longrightarrow 0$ strongly in $H^1(B_R)$.

B.2 Proof of Proposition (5.3.1)

Denote $V = u_s - u_s^{(\mu)} - w^{(\mu)} \cdot \nabla U_0(z_r)$. V is a solution on $\mathbb{R}^2$ of

$$\nabla \cdot (1 + \mu + [\sigma_r - 1]\mathbf{1}_{\Omega_r})\nabla V + \omega^2 V = -\nabla \cdot [\sigma_r - 1]\mathbf{1}_{\Omega_r} \nabla \left[U_0 - \nabla(x - z_r) \cdot \nabla U_0(z_r)\right] \tag{B.2.1}$$

subject to the Sommerfeld radiation condition. Now, define V_0 as the solution on $\mathbb{R}^2$ of:

$$\nabla \cdot (1 + \mu + [\sigma_r - 1]\mathbf{1}_{\Omega_r})\nabla V_0 = -\nabla \cdot [\sigma_r - 1]\mathbf{1}_{\Omega_r} \nabla \left[U_0 - \nabla(x - z_r) \cdot \nabla U_0(z_r)\right]. \tag{B.2.2}$$

with the condition $V_0(x) \longrightarrow 0$ $(x \to \infty)$.

From [7, Lemma A.1], there exist three positive constants C, $\widetilde{C}$ and κ independent of μ and δ such that

$$\|\nabla V_0\|_{L^2(B_R)} \leq C\delta \|\nabla \left[U_0 - \nabla(x - z_r) \cdot \nabla U_0(z_r)\right] \|_{L^\infty(\Omega_r)}, \tag{B.2.3}$$

and

$$\|V_0\|_{L^2(B_R)} \leq \widetilde{C}\delta^{1+\kappa} \|\nabla \left[U_0 - \nabla(x - z_r) \cdot \nabla U_0(z_r)\right] \|_{L^\infty(\Omega_r)}. \tag{B.2.4}$$

If we write $W = V - V_0$, we have that W solves:

$$\nabla \cdot (1 + \mu + [\sigma_r - 1]\mathbf{1}_{\Omega_r})\nabla W + \omega^2 W = -\omega^2 V_0, \tag{B.2.5}$$

with the boundary condition $\frac{\partial W}{\partial \nu} - \mathcal{T}_\omega(W) = \mathcal{T}_\omega(V) - \mathcal{T}_0(V_0)$ on ∂B_R, where $\mathcal{T}_\omega$ is the Dirichlet-to-Neumann map on S_R defined in (B.1.1) associated with the frequency ω. The condition can be re-written : $\frac{\partial W}{\partial \nu} - \mathcal{T}_\omega(W) = (\mathcal{T}_\omega - \mathcal{T}_0)(V_0)$. So, based on the well posedness of (B.2.5), there exist a constant C' independent of μ and δ such that

$$\|W\|_{H^1(B_R)} \leq C' \left(\|V_0\|_{L^2(B_R)} + \| \left[\mathcal{T}_\omega - \mathcal{T}_0\right](V_0) \|_{L^2(\partial B)} \right). \tag{B.2.6}$$

Now, we can write that, for some constant still denoted C independent of μ and δ:

$$\|V\|_{H^1(B_R)} \leq C \left(\|V_0\|_{H^1(B_R)} + \|V_0\|_{L^2(B_R)} \right). \tag{B.2.7}$$

Since $\delta < 1$, using (B.2.3) and (B.2.4) we get

$$\|V\|_{H^1(B_R)} \leq C\delta^2. \tag{B.2.8}$$

B.3 Proof of Proposition 5.3.3

Denote ϕ: $y \longrightarrow \widetilde{y} = \phi(y) = \frac{y - z_r}{\delta}$. If we define $\forall \widetilde{y} \in B(0,1)$: $\widetilde{w}^{(\mu)}(\widetilde{y}) = \frac{1}{\delta} w^{(\mu)}(\phi^{-1}(\widetilde{y}))$, we want to prove the following:

$$\|\widetilde{w}^{(\mu)}(\widetilde{y}) - \widetilde{y} - \widetilde{w}(\widetilde{y})\|_{H^1(B(0,1))} \leq C \left(\|\mu\|_\infty + \delta\omega^2 \right). \tag{B.3.1}$$

Now, using (5.3.5), one can see that $\widetilde{w}^{(\mu)}$ satisfies the following equation:

$$\nabla \cdot (1 + [\sigma_r - 1]\mathbf{1}_B + \widetilde{\mu}) \nabla \widetilde{w}^{(\mu)} + \omega^2 \delta \widetilde{w}^{(\mu)} = \nabla \cdot ([\sigma_r - 1]\mathbf{1}_B \nabla \widetilde{y}), \tag{B.3.2}$$

where $\widetilde{\mu} = \mu \circ \phi^{-1}$, equipped with the Sommerfeld radiation condition. Using equation (5.3.15) we get that

$$\nabla \cdot (1 + [\sigma_r - 1]\mathbf{1}_B + \widetilde{\mu}) \nabla \left(\widetilde{w}^{(\mu)} - \widetilde{y} - \widetilde{w} \right) = -\nabla \cdot \left(\widetilde{\mu} \nabla \widetilde{w}^{(\mu)} \right) - \omega^2 \delta \widetilde{w}^{(\mu)}, \tag{B.3.3}$$

Now, using Meyer's theorem [101], we get the following estimate:

$$\|\nabla \left(\widetilde{w}^{(\mu)}(\widetilde{y}) - \widetilde{y} - \widetilde{w}(\widetilde{y}) \right) \|_{L^2(B)} \leq C \left(\|\widetilde{\mu} \nabla \widetilde{w}^{(\mu)}\|_{L^2(B)} + \omega\delta^2 \|\widetilde{w}^{(\mu)}\|_{L^2(B)} \right). \tag{B.3.4}$$

We need to estimate $\|\widetilde{w}^{(\mu)}\|_{H^1(B(0,1))}$. Introduce $\widetilde{w}_0^{(\mu)}$ as the solution of

$$\nabla \cdot (1 + [\sigma_r - 1]\mathbf{1}_B + \widetilde{\mu}) \nabla \widetilde{w}_0^{(\mu)} = \nabla \cdot ([\sigma_r - 1]\mathbf{1}_B \nabla \widetilde{y}). \tag{B.3.5}$$

with the condition $\widetilde{w}_0^{(\mu)}(\widetilde{y}) \longrightarrow 0$ as $\widetilde{y} \to \infty$. Meyers theorem gives:

$$\|\widetilde{w}_0^{(\mu)}\|_{H^1(B(0,1))} \leq C \|[\sigma_r - 1]\nabla \widetilde{y}\|_{L^2(B(0,1))}. \tag{B.3.6}$$

We can see that $\widetilde{w}^{(\mu)} - \widetilde{w}_0^{(\mu)}$ is a solution of

$$\nabla \cdot (1 + [\sigma_r - 1]\mathbf{1}_B + \widetilde{\mu}) \nabla \left(\widetilde{w}^{(\mu)} - \widetilde{w}_0^{(\mu)} \right) + \omega^2 \delta \left(\widetilde{w}^{(\mu)} - \widetilde{w}_0^{(\mu)} \right) = -\omega^2 \delta \widetilde{w}_0^{(\mu)}. \tag{B.3.7}$$

We get that

$$\|\widetilde{w}^{(\mu)} - \widetilde{w}_0^{(\mu)}\|_{H^1(B(0,1))} \leq C\omega^2 \delta \|\widetilde{w}_0^{(\mu)}\|_{L^2(B(0,1))}.$$

So, using (B.3.6) we get

$$\|\widetilde{w}^{(\mu)}\|_{H^1(B(0,1))} \leq C \left(1 + \omega^2 \delta \right). \tag{B.3.8}$$

Since $\|\widetilde{\mu}\nabla\widetilde{w}^{(\mu)}\|_{L^2(B(0,1))} \leq \|\widetilde{\mu}\|_{L^\infty(B(0,1))}\|\widetilde{w}^{(\mu)}\|_{H^1(B(0,1))}$ and $\|\widetilde{\mu}\|_{L^\infty(B(0,1))} \leq \|\mu\|_\infty$, using (B.3.4) and (B.3.6) we get

$$\|\nabla\left(\widetilde{w}^{(\mu)}(\widetilde{y}) - \widetilde{y} - \widetilde{w}(\widetilde{y})\right)\|_{L^2(B(0,1))} \leq C\left(\|\mu\|_\infty + \delta\omega^2(1 + \|\mu\|_\infty + \delta\omega^2)\right),$$

which is exactly, as $\|\mu\|_\infty \to 0$ and $\delta \to 0$, for $y \in \Omega_r$

$$\nabla\left(w^{(\mu)}(y) - (y - z_r)\right) = \delta\nabla\widetilde{w}(\frac{y - z_r}{\delta}) + O\left(\delta\|\mu\|_\infty + (\delta\omega)^2\right). \tag{B.3.9}$$

Bibliography

[1] Abboud, T. and Ammari, H. (1996a). Diffraction at a curved grating: Approximation by an infinite plane grating. *J. Math. Anal. Appl.*, 202:1076–1100.

[2] Abboud, T. and Ammari, H. (1996b). Diffraction at a curved grating: Tm and te cases, homogenization. *J. Math. Anal. Appl.*, 202:995–1026.

[3] Adler, R. (2010). *The Geometry of Random Fields*. Society for Industrial and Applied Mathematics, Philadelphia,.

[4] Aliroteh, M., Scott, G., and Arbabian, A. (2014). Frequency-modulated magneto-acoustic detection and imaging.

[5] Ambrosio, L., Fusco, N., and Pallara, D. (2000). *Functions of bounded variation and free discontinuity problems*, volume 254. Clarendon Press Oxford.

[6] Ammari, H. (2008). *An introduction to mathematics of emerging biomedical imaging*, volume 62. Springer.

[7] Ammari, H., Bonnetier, E., Capdeboscq, Y., Tanter, M., and Fink, F. (2008a). Electrical impedance tomography by elastic deformation. *SIAM J. Appl. Math.*, 68:1557–1573.

[8] Ammari, H., Bonnetier, E., Capdeboscq, Y., Tanter, M., Fink, M., et al. (2008b). Electrical impedance tomography by elastic deformation. *SIAM Journal on Applied Mathematics*, 68(6):1557–1573.

[9] Ammari, H., Boulier, S., and Millien, P. (2015). A mathematical and numerical framework for magnetoacoustic tomography with magnetic induction. *arXiv preprint arXiv:1501.04803*.

[10] Ammari, H., Bretin, E., Garnier, J., Kang, H., Lee, H., and Wahab, A. (2014a). Mathematical methods in elasticity imaging. *Princeton University Press, Princeton*, 1(4):13.

[11] Ammari, H., Bretin, E., Millien, P., Seppecher, L., and Seo, J.-K. (To appear). Mathematical modeling in full-field optical coherence elastography. *SIAM. Journal on Applied Mathematics*.

[12] Ammari, H., Capdeboscq, Y., Kang, H., and Kozhemyak, A. (2009). Mathematical models and reconstruction methods in magneto-acoustic imaging. *European Journal of Applied Mathematics*, 20(03):303–317.

[13] Ammari, H., Chow, Y. T., Liu, K., and Zou, J. (2013a). Optimal shape design by partial spectral data. *arXiv preprint arXiv:1310.6098*.

[14] Ammari, H., Ciraolo, G., Kang, H., Lee, H., and Yun, K. (2012a). Spectral analysis of the neumann-poincar\'e operator and characterization of the gradient blow-up. *arXiv preprint arXiv:1206.2074*.

[15] Ammari, H., Deng, Y., and Millien, P. (2014b). Surface plasmon resonance of nanoparticles and applications in imaging. *arXiv preprint arXiv:1412.3656*.

[16] Ammari, H., Garapon, P., Kang, H., and Lee, H. (2008c). A method of biological tissues elasticity reconstruction using magnetic resonance elastography measurements. *Quarterly of Applied Mathematics*, 66(1):139–176.

[17] Ammari, H., Garnier, J., Giovangigli, L., Jing, W., and Seo, J.-K. (2013b). Spectroscopic imaging of a dilute cell suspension. *arXiv preprint arXiv:1310.1292*.

[18] Ammari, H., Garnier, J., and Jing, W. (2012b). Resolution and stability analysis in acousto-electric imaging. *Inverse Problems*, 28(8):084005.

[19] Ammari, H., Garnier, J., Jing, W., Kang, H., Lim, M., Sølna, K., and Wang, H. (2013c). *Mathematical and statistical methods for multistatic imaging*. Springer.

[20] Ammari, H., Garnier, J., Jing, W., Kang, H., Lim, M., Wang, H., and SØlna., K. (2013d). *Mathematical and Statistical Methods for Multistatic Imaging*, volume 2098 of *Lecture Notes in Mathematics*. Springer-Verlag, Berlin.

[21] Ammari, H., Garnier, J., Jugnon, V., and Kang, H. (2012c). Stability and resolution analysis for a topological derivative based imaging functionnal. *SIAM J. Control Optim.*, 50(1):48–76.

[22] Ammari, H., Garnier, J., and Millien, P. (2014c). Backpropagation imaging in nonlinear harmonic holography in the presence of measurement and medium noises. *SIAM Journal on Imaging Sciences*, 7(1):239–276.

[23] Ammari, H., Giovangigli, L., Nguyen, L. H., and Seo, J.-K. (2014d). Admittivity imaging from multi-frequency micro-electrical impedance tomography. *arXiv preprint arXiv:1403.5708*.

[24] Ammari, H., Grasland-Mongrain, P., Millien, P., Seppecher, L., and Seo, J.-K. (2014e). A mathematical and numerical framework for ultrasonically-induced lorentz force electrical impedance tomography. *Journal de Mathématiques Pures et Appliquées*.

[25] Ammari, H., Iakovleva, E., Lesselier, D., and Perrusson, G. (2007). Music-type electromagnetic imaging of a collection of small three-dimensional inclusions. *SIAM Journal on Scientific Computing*, 29(2):674–709.

[26] Ammari, H. and Kang, H. (2004). *Reconstruction of Small Inhomogeneities from Boundary Measurements*, volume 1864 of *Lecture Notes in Mathematics*. Springer-Verlag, Berlin.

[27] Ammari, H. and Kang, H. (2007). *Polarization and moment tensors: with applications to inverse problems and effective medium theory*, volume 162. Springer.

[28] Ammari, H., Kwon, O., Seo, J. K., and Woo, E. J. (2004). T-scan electrical impedance imaging system for anomaly detection. *SIAM Journal on Applied Mathematics*, 65(1):252–266.

[29] Ammari, H., Seo, J. K., and Zhou, L. (2014). Viscoelastic modulus reconstruction using time harmonic vibrations. *ArXiv e-prints*.

[30] Ammari, H., Waters, A., and Zhang, H. (2014). Stability analysis for magnetic resonance elastography. *arXiv preprint arXiv:1409.5138*.

[31] Bao, G. and Dobson, D. (1994). Second harmonic generation in nonlinear optical films. *J. Math. Phys.*, 35(4):1622–1633.

[32] Bao, G., Li, Y., and Zhou, Z. (2008). l^p estimates of time-harmonic maxwell's equations in a bounded domain. *J. Diff. Equat.*, 245(12):3674–3686.

[33] Bao, G., Lin, J., and Triki, F. (2010). A multi-frequency inverse source problem. *Journal of Differential Equations*, 249(12):3443–3465.

[34] Bao, G., Lin, J., Triki, F., et al. (2011). Numerical solution of the inverse source problem for the helmholtz equation with multiple frequency data.

[35] Bao, G., Minut, A., and Zhou, Z. (2007). l^p estimates for maxwell's equations with source term. *Comm. Part. Diff. Equat.*, 32(7-9):1449–1471.

[36] Basford, A. T., Basford, J. R., Kugel, J., and Ehman, R. L. (2005). Lorentz-force-induced motion in conductive media. *Magnetic resonance imaging*, 23(5):647–651.

[37] Bensoussan, A., Lions, J., and Papanicolaou, G. (1978). *Asymptotic Analysis for Periodic Structures*. North-Holland Publishing Co., Amsterdam-New York.

[38] Bercoff, J., Tanter, M., and Fink, M. (2004). Supersonic shear imaging: a new technique for soft tissue elasticity mapping. *Ultrasonics, Ferroelectrics, and Frequency Control, IEEE Transactions on*, 51(4):396–409.

[39] Bloembergen, N. and Pershan, P. (1962). Light wave at the boundary of nonlinear media. *Phys. Rev.*, 128(2).

[40] Bressan, A. and Shen, W. (1998). On discontinuous differential equations. *Differential inclusions and optimal control*, pages 73–87.

[41] Brown, E. and McKee, T. (2003). Dynamic imaging of collagen and its modulation in tumors in vivo using second-harmonic generation. *Nature medicine*, 9(6):796–800.

[42] Buffa, A., Costabel, M., and Sheen, D. (2002). On traces for h (curl, ω) in lipschitz domains. *Journal of Mathematical Analysis and Applications*, 276(2):845–867.

[43] Campagnola, P. and Loew, L. (2003). Second-harmonic imaging microscopy for visualizing biomolecular arrays in cells, tissues and organisms. *Nature Biotech.*, 21(11):1356–1360.

[44] Canny, J. (1986). A computational approach to edge detection. *Pattern Analysis and Machine Intelligence, IEEE Transactions on*, (6):679–698.

[45] Capdeboscq, Y., Fehrenbach, J., de Gournay, F., and Kavian, O. (2009). Imaging by modification: numerical reconstruction of local conductivities from corresponding power density measurements. *SIAM Journal on Imaging Sciences*, 2:1003.

[46] Chen, Y.-Z. and Wu, L.-C. (1998). *Second order elliptic equations and elliptic systems*, volume 174. American Mathematical Soc.

[47] Cheney, M., Isaacson, D., and Newell, J. C. (1999). Electrical impedance tomography. *SIAM review*, 41(1):85–101.

[48] Choy, M. and Byer, R. (1976). Accurate second-order susceptibility measurements of visible and infrared nonlinear crystals. *Phys. Rev. B*, 14(4):1693.

[49] Clarke, F. H. (1998). *Nonsmooth analysis and control theory*, volume 178. Springer.

[50] Colton, D. and Kress, R. (2012). *Inverse acoustic and electromagnetic scattering theory*, volume 93. Springer.

[51] Colton, D. and Kress, R. (2013). *Integral equation methods in scattering theory*, volume 72. SIAM.

[52] Cuche, E., Bevilacqua, F., and Depeursinge, C. (1999). Digital holography for quantitative phase-contrast imaging. *Optics Lett.*, 24(5):291–293.

[53] Dubois, A. and Boccara, A.-C. (2008). Full-field optical coherence tomography. In *Optical Coherence Tomography*, pages 565–591. Springer.

[54] Dubois, A., Grieve, K., Moneron, G., Lecaque, R., Vabre, L., and Boccara, C. (2004). Ultrahigh-resolution full-field optical coherence tomography. *Applied Optics*, 43(14):2874–2883.

[55] El-Brolossy, T., Abdallah, T., Mohamed, M. B., Abdallah, S., Easawi, K., Negm, S., and Talaat, H. (2008). Shape and size dependence of the surface plasmon resonance of gold nanoparticles studied by photoacoustic technique. *The European Physical Journal-Special Topics*, 153(1):361–364.

[56] Elbau, P., Mindrinos, L., and Scherzer, O. (2014). Mathematical modelling of optical coherence tomography. *arXiv preprint arXiv:1403.0726*.

[57] Evans, L. (2010). *Partial Differential Equations*. Graduate studies in mathematics. American Mathematical Society.

[58] Foster, K. R. and Schwan, H. P. (1988). Dielectric properties of tissues and biological materials: a critical review. *Critical reviews in biomedical engineering*, 17(1):25–104.

[59] Gateau, J., Aubry, J.-F., Pernot, M., Fink, M., and Tanter, M. (2011). Combined passive detection and ultrafast active imaging of cavitation events induced by short pulses of high-intensity ultrasound. *Ultrasonics, Ferroelectrics, and Frequency Control, IEEE Transactions on*, 58(3):517–532.

[60] Gebauer, B. and Scherzer, O. (2008). Impedance-acoustic tomography. *SIAM Journal on Applied Mathematics*, 69(2):565–576.

[61] Giaquinta, M. and Martinazzi, L. (2012). *An introduction to the regularity theory for elliptic systems, harmonic maps and minimal graphs*. Springer.

[62] Gil, M. I. (1995). *Norm Estimations for Operator Valued Functions and Applications*, volume 192. CRC Press.

[63] Gilbarg, D. and Trudinger, N. (1977). *Elliptic Partial Differential Equations of Second Order*.

[64] Goss, S., Johnston, R., and Dunn, F. (1978). Comprehensive compilation of empirical ultrasonic properties of mammalian tissues. *The Journal of the Acoustical Society of America*, 64(2):423–457.

[65] Grasland-Mongrain, P., Mari, J.-M., Chapelon, J.-Y., and Lafon, C. (2013). Lorentz force electrical impedance tomography. *IRBM*, 34(4):357–360.

[66] Grieser, D. (2014). The plasmonic eigenvalue problem. *Reviews in Mathematical Physics*, 26(03).

[67] Griesmaier, R. (2008). An asymptotic factorization method for inverse electromagnetic scattering in layered media. *SIAM Journal on Applied Mathematics*, 68(5):1378–1403.

[68] Guyot-Sionnest, P., Chen, W., and Shen, Y. (1986). General consideration on optical second-harmonic generation from surfaces and interfaces. *Phys. Rev. B*, 33(12).

[69] Hao, F., Nehl, C. L., Hafner, J. H., and Nordlander, P. (2007). Plasmon resonances of a gold nanostar. *Nano letters*, 7(3):729–732.

[70] Heinz, T. (1991). Second-order nonlinear optical effects at surfaces and interfaces. In *Nonlinear Surface Electromagnetic Phenomena*, pages 353–416. Elsevier, Amsterdam.

[71] Horn, B. K. and Schunck, B. G. (1981). Determining optical flow. In *1981 Technical Symposium East*, pages 319–331. International Society for Optics and Photonics.

[72] Hsieh, C.-L. (2011). *Imaging with Second-Harmonic Generation Nanoparticles*. PhD thesis, California Institute of Technology.

[73] Hsieh, C.-L., Grange, R., Pu, Y., and Psaltis, D. (2009). Three-dimensional harmonic holographic microcopy using nanoparticles as probes for cell imaging. *Optics Express*, 17(4):2880–2891.

[74] Huang, X., El-Sayed, I. H., Qian, W., and El-Sayed, M. A. (2006). Cancer cell imaging and photothermal therapy in the near-infrared region by using gold nanorods. *Journal of the American Chemical Society*, 128(6):2115–2120.

[75] Hui, P., Xu, C., and Stroud, D. (2004). Second-harmonic generation for a dilute suspension of coated particles. *Phys. Rev. B*, 69(1):014203.

[76] Jain, P. K., Lee, K. S., El-Sayed, I. H., and El-Sayed, M. A. (2006). Calculated absorption and scattering properties of gold nanoparticles of different size, shape, and composition: applications in biological imaging and biomedicine. *The Journal of Physical Chemistry B*, 110(14):7238–7248.

[77] Ji, L. and McLaughlin, J. (2004). Recovery of the lamé parameter μ in biological tissues. *Inverse Problems*, 20(1):1.

[78] Kang, H. and Seo, J. K. (1999). Inverse conductivity problem with one measurement: Uniqueness of balls in \bbbrˆ3. *SIAM Journal on Applied Mathematics*, 59(5):1533–1539.

[79] Kellogg, O. (1953). Foundations of potential theory.

[80] Khavinson, D., Putinar, M., and Shapiro, H. S. (2007). Poincaré's variational problem in potential theory. *Archive for rational mechanics and analysis*, 185(1):143–184.

[81] Kim, B. S., Ryu, H. S., Kang, K. H., and Park, S. J. (2013). Intrathyroidal parathyroid hyperplasia in tertiary hyperparathyroidism. *Journal of surgical case reports*, 2013(5):rjt034.

[82] Kunyansky, L. (2012). A mathematical model and inversion procedure for magneto-acousto-electric tomography. *Inverse Problems*, 28(3):035002.

[83] Larsson, J. (2007). Electromagnetics from a quasistatic perspective. *American Journal of Physics*, 75(3):230–239.

[84] Lembo, D. and Cavalli, R. (2010). Nanoparticulate delivery systems for antiviral drugs. *Antivir Chem Chemother*, 21(2):53–70.

[85] Li, X. and He, B. (2010). Multi-excitation magnetoacoustic tomography with magnetic induction for bioimpedance imaging. *Medical Imaging, IEEE Transactions on*, 29(10):1759–1767.

[86] Li, X., Xu, Y., and He, B. (2007). Imaging electrical impedance from acoustic measurements by means of magnetoacoustic tomography with magnetic induction (mat-mi). *Biomedical Engineering, IEEE Transactions on*, 54(2):323–330.

[87] Li, Y. and Nirenberg, L. (2003). Estimates for elliptic systems from composite material. *Communications on pure and applied mathematics*, 56(7):892–925.

[88] Liang, X., Crecea, V., and Boppart, S. A. (2010). Dynamic optical coherence elastography: a review. *Journal of innovative optical health sciences*, 3(04):221–233.

[89] Link, S. and El-Sayed, M. A. (1999). Size and temperature dependence of the plasmon absorption of colloidal gold nanoparticles. *The Journal of Physical Chemistry B*, 103(21):4212–4217.

[90] Maeda, H., Wu, J., Sawa, T., Matsumura, Y., and Hori, K. (2000). Tumor vascular permeability and the epr effect in macromolecular therapeutics: a review. *Journal of controlled release*, 65(1):271–284.

[91] Mallat, S. (2008). *A wavelet tour of signal processing: the sparse way*. Academic press.

[92] Manduca, A., Oliphant, T. E., Dresner, M., Mahowald, J., Kruse, S., Amromin, E., Felmlee, J. P., Greenleaf, J. F., and Ehman, R. L. (2001). Magnetic resonance elastography: non-invasive mapping of tissue elasticity. *Medical image analysis*, 5(4):237–254.

[93] Mantegazza, G. A.-C. (1997). A note on the theory of sbv functions. *Boll. Un. Mat. Ital*, pages 375–382.

[94] Mariappan, L. and He, B. (2013). Magnetoacoustic tomography with magnetic induction: Bioimepedance reconstruction through vector source imaging. *IEEE transactions on medical imaging*, 32(3).

[95] Mariappan, L., Hu, G., and He, B. (2014). Magnetoacoustic tomography imaging of biological tissues with magnetic induction under the static field of mri scanner. In *Biomedical Imaging (ISBI), 2014 IEEE 11th International Symposium on*, pages 149–152. IEEE.

[96] Mayergoyz, I. D., Fredkin, D. R., and Zhang, Z. (2005). Electrostatic (plasmon) resonances in nanoparticles. *Physical Review B*, 72(15):155412.

[97] Mayergoyz, I. D. and Zhang, Z. (2006). Numerical analysis of plasmon resonances in nanoparticles. *IEEE transactions on magnetics*, 42(4):759–762.

[98] McLaughlin, J. R. and Yoon, J.-R. (2004). Unique identifiability of elastic parameters from time-dependent interior displacement measurement. *Inverse Problems*, 20(1):25.

[99] McLaughlin, J. R., Zhang, N., and Manduca, A. (2010). Calculating tissue shear modulus and pressure by 2d log-elastographic methods. *Inverse Problems*, 26(8):085007.

[100] Mertz, J. (2004). Nonlinear microscopy: new techniques and applications. *Current Opinion in Neurobiology*, 14(5):610–616.

[101] Meyers, N. (1963). An l^p-estimate for the gradient of solutions of second order elliptic divergence equations. *Ann. Scuola Norm. Sup. Pisa*, 3:189–206.

[102] Miller, R. (1964). Optical second harmonic generation in piezoelectric crystals. *Appl. Phys. Lett.*, 5(1):17–19.

[103] Mitrea, D., Mitrea, M., and Pipher, J. (1996). Vector potential theory on nonsmooth domains in r3 and applications to electromagnetic scattering. *Journal of Fourier Analysis and Applications*, 3(2):131–192.

[104] Montalibet, A. (2002). *Etude du couplage acousto-magnétique: détection des gradients de conductivité électrique en vue de la caractérisation tissulaire*. PhD thesis, Villeurbanne, INSA.

[105] Moreaux, L., Sandre, O., and Mertz, J. (2000). Membrane imaging by second-harmonic generation microscopy. *J. Opt. Soc. Am. B*, 17(10):1685–1694.

[106] Morimoto, T., Kimura, S., Konishi, Y., Komaki, K., Uyama, T., Monden, Y., Kinouchi, D. Y., and Iritani, D. T. (1993). A study of the electrical bio-impedance of tumors. *Investigative Surgery*, 6(1):25–32.

[107] Muthupillai, R. and Ehman, R. L. (1996). Magnetic resonance elastography. *Nature medicine*, 2(5):601–603.

[108] Naetar, W. and Scherzer, O. (2014). Quantitative photoacoustic tomography with piecewise constant material parameters. *arXiv preprint arXiv:1403.2620*.

[109] Nahas, A., Bauer, M., Roux, S., and Boccara, A. C. (2013). 3d static elastography at the micrometer scale using full field oct. *Biomedical optics express*, 4(10):2138–2149.

[110] Nédélec, J. (1992). Quelques propriétés des dérivées logaritmiques des fonctions de hankel. *C.R. Acad. Sci. Paris*, 1(314):507–510.

[111] Nguyen, H.-M. and Vogelius, M. S. (2009). A representation formula for the voltage perturbations caused by diametrically small conductivity inhomogeneities. proof of uniform validity. In *Annales de l'Institut Henri Poincare (C) Non Linear Analysis*, volume 26, pages 2283–2315. Elsevier.

[112] O'Neal, D. P., Hirsch, L. R., Halas, N. J., Payne, J. D., and West, J. L. (2004). Photo-thermal tumor ablation in mice using near infrared-absorbing nanoparticles. *Cancer letters*, 209(2):171–176.

[113] Oraevsky, A. and Karabutov, A. (2003). Optoacoustic tomography. *Biomedical photonics handbook*, 34:1–34.

[114] Pride, S. (1994). Governing equations for the coupled electromagnetics and acoustics of porous media. *Physical Review B*, 50(21):15678.

[115] Prost, A. and Bossy, E. (2015). Photoacoustic generation by a gold nanosphere: from the linear to the nonlinear thermoelastic regime. *arXiv preprint arXiv:1501.04871*.

[116] Pu, Y., Centurion, M., and Psaltis, D. (2008). Harmonic holography: a new holographic principle. *Appl. Optics*, 47(4):A103–A110.

[117] Razani, M., Mariampillai, A., Sun, C., Yang, V. X., and Kolios, M. C. (2012). Biomechanical properties of soft tissue measurement using optical coherence elastography. In *SPIE BiOS*, pages 820758–820758. International Society for Optics and Photonics.

[118] Rogowska, J., Patel, N., Fujimoto, J., and Brezinski, M. (2004). Optical coherence tomographic elastography technique for measuring deformation and strain of atherosclerotic tissues. *Heart*, 90(5):556–562.

[119] Roth, B. J. (2011). The role of magnetic forces in biology and medicine. *Experimental Biology and Medicine*, 236(2):132–137.

[120] Roth, B. J. and Schalte, K. (2009). Ultrasonically-induced lorentz force tomography. *Medical & biological engineering & computing*, 47(6):573–577.

[121] Sarid, D. and Challener, W. (2010). *Modern introduction to surface plasmons: theory, Mathematica modeling, and applications*. Cambridge University Press.

[122] Scherzer, O. (2011). *Handbook of Mathematical Methods in Imaging: Vol. 1*. Springer.

[123] Schmitt, J. (1998). Oct elastography: imaging microscopic deformation and strain of tissue. *Optics express*, 3(6):199–211.

[124] Schnars, U. and Jüptner, W. (1994). Direct recording of holograms by a ccd target and numerical reconstruction. *Appl. Optics*, 33(2):179–181.

[125] Seo, J. and Woo, E. (2012). *Nonlinear Inverse Problems in Imaging*. Wiley.

[126] Seo, J. K. and Woo, E. J. (2011). Magnetic resonance electrical impedance tomography (mreit). *SIAM review*, 53(1):40–68.

[127] Shen, Y. (1984). *The Principles of Nonlinear Optics*. Wiley-Interscience, New York.

[128] Sohr, H. (2012). *The Navier-Stokes equations: An elementary functional analytic approach*. Springer.

[129] Soussi, S. (2005). Second-harmonic generation in the undepleted-pump approximation. *Multiscale Model. Simul.*, 4(1):115–148.

[130] Torres, R. H. (1998). Maxwell's equations and dielectric obstacles with lipschitz boundaries. *Journal of the London Mathematical Society*, 57(01):157–169.

[131] Tseng, N. and Roth, B. J. (2008). The potential induced in anisotropic tissue by the ultrasonically-induced lorentz force. *Medical & biological engineering & computing*, 46(2):195–197.

[132] Vu, X. H., Levy, M., Barroca, T., Tran, H. N., and Fort, E. (2013). Gold nanocrescents for remotely measuring and controlling local temperature. *Nanotechnology*, 24(32):325501.

[133] Wang, L. V. and Yang, X. (2007). Boundary conditions in photoacoustic tomography and image reconstruction. *Journal of biomedical optics*, 12(1):014027–014027.

[134] Wen, H., Shah, J., and Balaban, R. S. (1998). Hall effect imaging. *Biomedical Engineering, IEEE Transactions on*, 45(1):119–124.

[135] Widlak, T. and Scherzer, O. (2012). Hybrid tomography for conductivity imaging. *Inverse Problems*, 28(8):084008.

[136] Widlak, T. and Scherzer, O. (2014). Stability in the linearized problem of quantitative elastography. *arXiv preprint arXiv:1406.0291*.

[137] Xu, Y. and He, B. (2005). Magnetoacoustic tomography with magnetic induction (mat-mi). *Physics in medicine and biology*, 50(21):5175.

[138] Zavelani-Rossi, M., Celebrano, M., Biagioni, P., Polli, D., Finazzi, M., Duò, L., Cerullo, G., Labardi, M., Allegrini, M., and Grand, J. (2008). Near-field second-harmonic generation in single gold nanoparticles. *Appl. Phys. Lett.*, 92(9):093119–093119.

[139] Zhou, L., Zhu, S., and He, B. (2014). A reconstruction algorithm of magnetoacoustic tomography with magnetic induction for an acoustically inhomogeneous tissue. *IEEE transactions on bio-medical engineering*, 61(6):1739–1746.

List of Figures

List of Tables

Index